

Visualization of the cellular uptake of nanoparticles

Rosemary Adsley MPharm

Thesis submitted to the University of Nottingham
for the degree of Doctor of Philosophy

December 2013

Abstract

The effect of nanoparticle surface charge and conjugation to the cell penetrating peptide Tat on the uptake of nanoparticles into MRC-5 fibroblasts was investigated using a range of advanced imaging techniques including atomic force microscopy (AFM), scanning ion conductance microscopy (SICM) and fluorescence microscopy. New technologies are required to investigate the uptake of nanoparticles into cells since although many studies have examined their ultimate destination within cells, very little work has been done to look at the initial interaction between the nanoparticles and cell which also plays an important role in their uptake.

Polyacrylamide nanoparticles (40-50nm) showed a clear correlation between increased positive charge and cellular uptake. Uptake was particularly enhanced for nanoparticles with a charge $>15\text{mV}$. These results obtained using fluorescence microscopy correlated well with those observed using AFM. Nanoparticles with low levels of positive charge (6.9mV) caused minor effects on bilayer structure such as fusion of holes in the bilayer, whilst negatively charged nanoparticles had no effect on the bilayer. Polyacrylamide nanoparticles conjugated to the cell penetrating peptide Tat, with a charge of 5.2mV, displayed greater cell uptake and increased effects on the bilayer depth and coverage than the similarly charged nanoparticles alone. This indicated that the peptide leads to enhanced uptake by additional mechanisms other than just the presence of a positive charge.

In contrast, silica nanoparticles (300nm), with high levels of positive (27mV) and negative charge (-25mV), entered cells to a similar extent. However, when the interaction with the cell membrane was imaged using Scanning Surface Confocal Microscopy (SSCM), there appeared to be some differences. Silica nanoparticles possessing a negative charge were often found to be associated with extensions of the membrane. Positively charged particles were also found associated with membrane extensions in some cases but were also frequently observed isolated on the membrane. Both caused the formation of defects in the cell membrane although these were larger and more widespread for the positively charged particles. The results highlight the importance of using multiple imaging techniques to investigate cellular interaction and uptake in order to provide a complete picture of all the processes involved.

List of publications

- Welsler K, Adsley R, Moore BM, Chan WC, Aylott JW. Protease sensing with nanoparticle based platforms. *Analyst*, 2001; 136: 29-41.

List of posters/presentations

Oral Presentations

- SICM Workshop, Imperial College London. 2011. Visualization of the cellular interaction and uptake of nanoparticles using AFM and SICM.
- Nottingham Nanocentre and Nanoscience Centre Researchers Forum on particle sizing. 2011. Particle sizing through differential centrifugation, The CPS Disc Centrifuge.
- Bionanotechnology III, Cambridge 2012. Visualization of the interaction and cellular uptake of nanosensors.

Posters

- AstraZeneca PhD Review Day 2012. Visualization of the cellular uptake of nanoparticles using Atomic Force Microscopy and Scanning Ion Conductance Microscopy. Awarded Best Science Prize.
- Bionanotechnology III, Cambridge 2012. Visualization of the interaction and cellular uptake of nanoparticles.

Acknowledgements

Thanks to my supervisors Dr Jon Aylott, Dr Stephanie Allen, Dr Weng Chan and Dr Kathryn Hill for their guidance and support over the last few years. Also all the technicians and others I have worked with especially Dr Emma King and Ian Ward for help with fluorescence microscopy, Giovanna De Filippi at Ionscope Ltd and Professor Yuri Korchev and Dr Pavel Novak for help with SICM and the use of the SSCM at Imperial College. Finally, Xinyong Chen, Kasia Nursynska and Delyan Ivanov for their help with the AFM work in this thesis.

I'd also like to thank all those involved with the DTC especially Chris Grindon, Claudia Matz and all the DTC students in A03 along with all the other students in various lab groups I have worked in, especially those in D38 – Helen, Veeren, Arpan and Andrea.

To all my friends and colleagues who have helped me to escape the lab and get through the past few years with copious amounts of tea, coffee and cake especially Rachel Doidge, Samantha Waite and Leigh-Anne Carroll, and all my friends from various orchestras, St Mary's and Manor Pharmacy.

Finally to Mum, Dad and Phil, for your constant love, support and encouragement and all the opportunities you have given me to get to where I am today, thank you.

Contents

List of Figures	4
List of abbreviations	11
Chapter 1 – Introduction	13
1.1 <i>Imaging the interaction and uptake of nanoparticles</i>	13
1.2 <i>Cellular uptake of nanoparticles</i>	14
1.2.1 <i>Phagocytosis</i>	17
1.2.2 <i>Clathrin mediated endocytosis</i>	17
1.2.3 <i>Caveolae mediated endocytosis</i>	19
1.2.4 <i>Flotillin dependent endocytosis</i>	20
1.2.5 <i>Macropinocytosis</i>	21
1.2.6 <i>Direct translocation</i>	22
1.3 <i>Factors affecting cellular uptake of nanoparticles</i>	23
1.3.1 <i>Size</i>	26
1.3.2 <i>Charge</i>	29
1.3.3 <i>Cell Penetrating Peptides (CPPs)</i>	32
1.4 <i>MRC-5 cells</i>	35
1.5 <i>Advanced imaging techniques</i>	36
1.5.1 <i>Fluorescence microscopy</i>	37
1.5.2 <i>Atomic Force Microscopy (AFM)</i>	42
1.5.3 <i>Scanning Ion Conductance Microscopy (SICM)</i>	46
1.5.4 <i>Scanning surface confocal microscopy (SSCM)</i>	48
1.6 <i>Aims and Thesis outline</i>	49
Chapter 2 – Materials, Methods and Instrumentation	50
2.1 <i>Materials</i>	50
2.2 <i>Instrumentation</i>	50
2.2.1 <i>Dynamic Light Scattering</i>	50
2.2.2 <i>Zeta potential</i>	52
2.2.3 <i>Disc Centrifuge</i>	54
2.2.4 <i>Fluorescence</i>	59
2.3 <i>Methods -Nanoparticle synthesis</i>	61

2.3.1 Polyacrylamide nanoparticles	61
2.3.2 Tat peptide conjugation	62
2.3.3 Silica nanoparticles.....	64
2.4 Characterization methods	65
2.4.1 Zeta potential.....	65
2.4.2 Size	65
2.4.3 Fluorescence	65
2.5 Cell culture methods.....	66
2.6 Sample preparation.....	66
2.6.1 Atomic Force Microscopy.....	66
2.6.2 Scanning Ion Conductance Microscopy	68
2.6.3 Fluorescence Microscopy.....	69
Chapter 3 - Nanoparticle characterisation	71
3.1 Introduction	71
3.1.1 Polyacrylamide nanoparticles	71
3.1.2 Silica nanoparticles.....	72
3.2 Results and Discussion.....	75
3.2.1 Nanoparticle charge.....	75
3.2.2 Nanoparticle size.....	79
3.2.3 Calculating nanoparticle density using the CPS disc centrifuge	91
3.2.4 Fluorescence	94
3.3 Conclusion.....	98
Chapter 4 - Scanning Probe Microscopy.....	100
Atomic Force Microscopy and Scanning Ion Conductance Microscopy	100
4.1 Introduction	100
4.1.1 Cell membranes.....	101
4.1.2 Supported lipid bilayers	102
4.1.3 Atomic Force Microscopy.....	102
4.1.4 Scanning Ion Conductance Microscopy	107
4.1.5 Comparison between AFM and SICM	109
4.2 Results and Discussion.....	111
4.2.1 AFM results	111

4.2.2 SICM Results.....	126
4.3 Conclusion.....	135
Chapter 5 - Fluorescence microscopy	137
5.1 Fluorescence microscopy and nanoparticle uptake	137
5.1.1 Imaging nanoparticle uptake with fluorescence.....	137
5.1.2 Cellular uptake of polyacrylamide nanoparticles.....	137
5.1.3 Cellular uptake of silica nanoparticles.....	140
5.2 Results and Discussion.....	144
5.2.1 Polyacrylamide nanoparticles	144
5.2.2 Tat conjugated polyacrylamide nanoparticles.....	150
5.2.3 Silica nanoparticles.....	154
5.3 Conclusion.....	159
Chapter 6 – Conclusions and Future Perspectives	161
6.1 Conclusion.....	161
6.2 Technical limitations of equipment and future advances	163
6.2.1 Scanning Ion Conductance Microscopy	163
6.2.2 Advances in Atomic Force Microscopy	164
6.2.3 Fluorescence microscopy	166
6.3 Future work	171
Chapter 7 - References	174

List of Figures

Figure 1.1: Diagram showing the major pathways of endocytosis, subsequent intracellular trafficking and final destination within cells. Inside the boxes are listed some of the main molecules involved in each pathway. CCP (clathrin coated pit), CDC42 (cell division cycle 42), CLIC-D (dynamin dependent clathrin independent carriers), CLIC-DI (dynamin and clathrin-independent carriers), EPS15 (epidermal growth factor receptor substrate 15), ER (endoplasmic reticulum), LE (late endosome), mono-Ub (mono-ubiquitylation), MVB (multi-vesicular body), PKC (protein kinase C), RE (recycling endosomes), TGN (trans-Golgi network), TK (tyrosine kinase) ¹⁶	16
Figure 1.2: The cellular uptake of nanoparticles depends on a number of factors including the properties of the nanoparticle, how it interacts with the medium it is in and the biological surfaces that it encounters.....	27
Figure 1.3: B16-F10 cells incubated with nanoparticles of (A) 50nm for one hour, (B) 200nm for three hours and (C) 500nm for three hours. Insets are the corresponding phase contrast images.....	29
Figure 1.4: Amine functionalised cationic 50nm silica nanoparticles caused defect formation in model lipid bilayers (a) Schematic of an amine functionalised silica nanoparticle, (b) DMPC lipid bilayer, (c) addition of the nanoparticles caused defect formation ⁹⁷	31
Table 1.1: Table listing some of the commonly used CPPs along with their structure, sequence and proposed uptake mechanism. Table adapted from ^{103,106}	33
Figure 1.5: Tat peptide conjugated to Oregon Green accumulates in endosomes.....	35
Figure 1.6: Jablonski diagram showing the movement of electrons between the different energy levels involved in fluorescence	38
Figure 1.7: Basic set up of a filter cube indicating the excitation and emission filters and the dichromatic mirror	39
Figure 1.8: A-C are images of 6µm fluorescent beads obtained using a widefield microscope. (A) Fluorescent beads mounted in PBS with minimal background fluorescence, (B) shows the same beads mounted in PBS containing a fluorophore with the same spectral characteristics as the fluorophore in the bead to show effects of increased background and (C) shows image (B) after background subtraction	40
Figure 1.9: Representation of the scattered light in the z plane from a point shaped object.....	41
Figure 1.10: Basic principle of AFM	44
Figure 1.11: Layout of typical SICM equipment adapted from ¹⁶⁵ . An A6 monolayer is grown on a membrane filter which is mounted on a 3D piezo stage controlled by the scan control and feedback systems. The modulated glass pipette scans the monolayer to produce images of the topography of the membrane.....	46

Figure 1.12: Schematic representation of the hopping mode of SICM	47
Figure 1.13: (A) SSCM set up, (B) Dotted line shows position where optical fluorescent image obtained as pipette moves over sample in SSCM, (C) Dotted line shows fluorescence image from same sample when using confocal alone	48
Figure 2.1: Typical setup of the Zetasizer Nano ZS for size determination using NIBS at 173° to measure particle diameter ¹⁷⁹	52
Figure 2.2: Typical setup of a Zetasizer for measuring zeta potential ¹⁸⁰	54
Figure 2.3: The design of the CPS Disc Centrifuge.....	55
Figure 2.4: Differential sedimentation.....	56
Figure 2.5: The low density disc.	59
Figure 2.6: Structure of Alexa 488.	60
Figure 2.7: Structure of 3-(acrylamidopropyl)-trimethylammonium chloride (ACTA). ...	62
Figure 2.8: Structure of N-acryloxysuccinimide.	62
Figure 2.9: Conjugation of Tat peptide to nanoparticles via SMCC. Adapted from ¹⁸⁹	63
Figure 3.1: Increasing nanoparticle charge with increasing ACTA incorporation in PBS and serum free DMEM.	75
Figure 3.2: Decrease in nanoparticle charge caused by the incorporation of 5% N-acryloxysuccinimide.	76
Figure 3.3: Zeta potential of Tat conjugated polyacrylamide nanoparticles compared to unfunctionalised polyacrylamide nanoparticles.	76
Figure 3.4: Zeta potential of negative and positively charged silica nanoparticles.	77
Figure 3.5: Zeta potential of polyacrylamide (A) and silica (B) nanoparticles in serum containing DMEM.....	78
Figure 3.6: Intensity and volume distributions of (A) unfunctionalised (Intensity 54nm, Volume: 37nm) and (B) 15% ACTA (Intensity: 59nm, Volume: 42nm) polyacrylamide nanoparticle diameter in PBS.....	80
Figure 3.7: Diameter of polyacrylamide nanoparticles with increasing proportion of ACTA in PBS and serum free DMEM.....	80
Figure 3.8: Intensity and volume distributions of polyacrylamide nanoparticle diameter containing 5% N-acryloxysuccinimide (Intensity 76nm, Volume 39nm).	81
Figure 3.9: Diameter of unfunctionalised and 5% N-acryloxysuccinimide polyacrylamide nanoparticles in PBS and serum free DMEM.	81
Figure 3.10: Intensity and volume distributions of Tat conjugated polyacrylamide nanoparticles in serum free DMEM.	82

Figure 3.11: Polyacrylamide nanoparticle diameter (A) unfunctionalised (33.8nm) and (B) 15% ACTA (33.2nm).....	83
Figure 3.12: Polyacrylamide nanoparticle diameter in PBS and serum free DMEM on disc centrifuge.....	84
Figure 3.13: (A) Negatively charged (290nm) and (B) positively charged (292nm) silica nanoparticle diameter in PBS.....	86
Figure 3.14: Comparison of size of negative and positively charged silica nanoparticles in PBS and serum free DMEM.....	87
Figure 3.15: Representative traces of (A) negative and (B) positively charged silica nanoparticle diameter in PBS measured using the CPS disc centrifuge.	88
Figure 3.16: Comparison of negatively charged and positively charged silica nanoparticle diameter in PBS and serum free DMEM.	89
Figure 3.17: (A) Negatively charged and (B) positively charged silica nanoparticle diameter after three hours in serum free DMEM.	90
Figure 3.18: Diameter of silica nanoparticles in water and D ₂ O calculated at different densities: (A) 1.3g/cm ³ , (B) 1.6g/cm ³ , (C) 2.0g/cm ³	92
Figure 3.19: Diameter of polyacrylamide nanoparticles in water and D ₂ O calculated at different densities (A) 1.3g/cm ³ , (B) 1.7g/cm ³ , (C) 2.0g/cm ³ and (D) 2.3g/cm ³	93
Figure 3.20: Fluorescence intensity of polyacrylamide nanoparticles with different charge measured on fluorimeter.	95
Figure 3.21: Fluorescence intensity of polyacrylamide nanoparticles on widefield microscope.....	95
Figure 3.22: Fluorescence intensity of silica nanoparticles on fluorimeter.....	96
Figure 3.23: Fluorescence intensity of silica nanoparticles on widefield fluorescent microscope.....	97
Table 3.1: Summary table of polyacrylamide and silica nanoparticle diameter (nm) in PBS and serum free DMEM (SF DMEM) measured using Dynamic Light Scattering (DLS) and the CPS Disc Centrifuge. (-) indicates batches of nanoparticles not measured using the CPS Disc Centrifuge.	98
Table 3.2: Summary table of the zeta potential (mV) of polyacrylamide and silica nanoparticles in PBS, DMEM and serum free DMEM (SF DMEM).	98
Figure 4.1: The effect of the cationic polymer poly-L-lysine on a DMPC supported lipid bilayer. The addition of the polymer caused the appearance of defects in the bilayer which are indicated by the white arrows ²³⁴	103

Figure 4.2: (a) Space filling model of Tat, (b) DMPC bilayer before addition of Tat, (c) and (d) are subsequent images taken over 20mins showing the formation and expansion of defects in the bilayer	106
Figure 4.3: COS-7 cells exposed to virus like particles (green fluorescence) showing uptake of the particles over a four hour time period. The red star indicates the beginning of the scanning for fluorescence and VLPs indicates when the fluorescent virus like particles (VLPs) were added	108
Figure 4.4: Diameter of DPPC liposomes obtained using the low density disc.....	111
Figure 4.5: (A) DPPC bilayer, (B) cross section of DPPC bilayer as indicated by white line in (A). Bilayer height is 6.3nm.	112
Figure 4.6: AFM image of 100µg/ml suspension of positively charged polyacrylamide nanoparticles in water on a mica surface. Scan size 2 x 2 µm.	113
Figure 4.7: AFM images of a DPPC lipid bilayer exposed to increasing concentrations of positively charged polyacrylamide nanoparticles. (A) The DPPC bilayer was relatively stable over time and when exposed to 20µl of HPLC grade water (B). Images C to F show the effect of exposure to increasing concentrations of positively charged nanoparticles (C) 1µg/ml, (D) 10µg/ml and (E) 25µg/ml. (F) was taken 30 minutes after (E). Scan size 5 x 5 µm.	114
Figure 4.8: Cross sections of DPPC bilayer exposed to positively charged nanoparticles demonstrate the nanoparticle addition had no effect on bilayer thickness. (A) DPPC bilayer before particle addition, height is 4.8nm. (B) DPPC bilayer following the addition of 25µg/ml positively charged nanoparticles, height is 5.0nm.. Scan size 5µm x 5µm.	115
Figure 4.9: Enlarged area of Figure 4.8B to show detail of positively charged polyacrylamide nanoparticles associated with the edge of membrane defects and mica. Scan size 2 x 2 µm.....	116
Figure 4.10: AFM images of the effects of Tat peptide on a lipid bilayer. (A) DPPC bilayer and (B) following addition of 20µl HPLC grade water shows some mobility but few changes in bilayer structure. Images C to F show the bilayer following exposure to increasing concentrations of Tat peptide. (C) 1µM, (D) 2.5µM, (E) 5µM and (F) 10µM. The formation of higher domains is observed around the edge of bilayer defects. Scan size 5 x 5µm.....	117
Figure 4.11: AFM images of a smaller area of the same DPPC bilayer as in Figure 4.10. (A) DPPC bilayer, (B) following addition of 20µl HPLC grade water, (C) 1µM Tat, (D) 2.5µM Tat, (E) 5µM Tat showing raised domains around edge of defect. (F) 10µM Tat with further coverage of raised domains. White arrows indicate the same defect in the bilayer which gradually expands along with the merging of other defects. Scan size 2 x 2µm.	118

Figure 4.12: Cross sections of DPPC before (A) and after exposure (B) to 5 μ M Tat peptide. Original height of bilayer is 3.6nm, in B1, bilayer height is 4.6nm and the height of the bilayer where Tat peptide acts is 5.7nm, approximately 1nm higher. Scan size 2 x 2 μ m. 119

Figure 4.13: AFM images of the interaction between Tat conjugated polyacrylamide nanoparticles and a DPPC lipid bilayer. (A) DPPC, (B) following addition of 20 μ l HPLC grade water, (C) 1 μ g/ml Tat conjugated nanoparticles, (D) 10 μ g Tat conjugated nanoparticles caused the appearance of small holes in the bilayer and exposure to higher concentrations such as 25 μ g/ml (E) led to the formation of new defects and solubilisation of the bilayer over time. Image (F) was taken one hour after (E) Scan size 5 x 5 μ m. 122

Figure 4.14: (A) DPPC bilayer before exposure to Tat conjugated nanoparticles, (A1) cross section indicated by white line on (A). (B) DPPC bilayer following exposure to 25 μ g/ml Tat conjugated nanoparticles, (B1) Cross section indicated by white line on (B) showing particles and changes in bilayer height. Original bilayer height in (A) is 5.7nm and following exposure to Tat peptide conjugated nanoparticles, bilayer height reduces to 4.8nm and particle height is 21.5nm (B1). 123

Figure 4.15: AFM images of the interaction between Tat conjugated polyacrylamide nanoparticles and a DPPC lipid bilayer. (A) DPPC, (B) following addition of 20 μ l HPLC grade water, (C) 1 μ g/ml Tat conjugated nanoparticles, (D) 10 μ g Tat conjugated nanoparticles caused the appearance of small holes in the bilayer and exposure to higher concentrations such as 25 μ g/ml (E) led to the formation of new defects and solubilisation of the bilayer over time. Image (F) was taken one hour after (E) Scan size 2 x 2 μ m. 124

Figure 4.16: MRC-5 cells control samples (A) large area of multiple MRC-5 cells and (B) a smaller area both showing relatively flat membrane. The cytoskeleton can be observed in (A). 127

Figure 4.17: (A) Topography image of MRC-5 cell exposed to negatively charged silica nanoparticles, (B) Corresponding fluorescence images showing nanoparticles and aggregates of nanoparticles (green). (C) Overlaid image of fluorescence and topography..... 128

Figure 4.18: Smaller area scan of MRC-5 cell exposed to negatively charged silica nanoparticles (A) Topography, (B) corresponding fluorescence and (C) overlaid image of fluorescence and topography showing multiple negatively charged silica nanoparticles (green) associated with the cell membrane. 130

Figure 4.19: A topography image that indicates the interaction of a single negatively charged silica nanoparticle with the cell membrane. The nanoparticle is indicated by the arrow. 131

Figure 4.20: Effect of 1.3 μ m silica nanoparticles on MRC-5 cells. This image was taken using hopping mode only at Nottingham. The arrow indicates the damaged area of the cell membrane. 132

Figure 4.21: (A) Topography image of MRC-5 cells exposed to positively charged silica nanoparticles, (B) corresponding fluorescence image. (C) is the overlaid image showing holes visible in the cell membrane plus diffuse fluorescence from positively charged silica nanoparticles. 133

Figure 4.22: Positively charged silica nanoparticle (indicated by the arrow) partially embedded in membrane and also associated with a region of the membrane. 134

Figure 4.23: Isolated positively charged silica nanoparticle partially embedded in the cell membrane. 135

Figure 5.1: 80nm silica nanoparticles in human dermal fibroblasts cells (A) bright field, (B) RITC-silica nanoparticles (red) (C) Merge of RITC-silica particles and LysoTracker Green, (D) Merge of RITC-silica particles and DAPI (blue) 141

Figure 5.2: Representative images showing polyacrylamide nanoparticles (green) with increasing positive charge in MRC-5 cells. Images are shown in pairs of green fluorescence alone beside the green fluorescence and brightfield merged images. (A) Control, (B) Unfunctionalised (-3.3mV), (C) 2% ACTA (1.8mV), (D) 5% ACTA (6.9mV), (E) 10% ACTA (13.2mV), (F) 15% ACTA (17.6mV) (G) 20% ACTA (18.6mV)..... 145

Figure 5.3: Example images of MRC-5 cells exposed to polyacrylamide nanoparticles to show perinuclear, punctate distributions of nanoparticles (green) indicating an endocytic route of uptake. (A) 5% ACTA containing polyacrylamide particles and (B) enlarged area from white box in (A). (C) 20% ACTA containing polyacrylamide nanoparticles and (D) enlarged area from white box in (C). 146

Figure 5.4: Increase in cellular uptake of polyacrylamide nanoparticles with increasing charge 147

Figure 5.5: (A) Green fluorescence from Alexa 488 containing nanoparticles within MRC-5 cells, (B) Brightfield and green fluorescence overlaid image showing intracellular localization of polyacrylamide nanoparticles containing 5% N-acryloxysuccinimide. ... 149

Figure 5.6: Comparison of the green fluorescence intensity of 5% N-acryloxysuccinimide (NAS) polyacrylamide nanoparticles (-5.5mV) and unfunctionalised polyacrylamide nanoparticles (-3.3mV) in MRC-5 cells. 150

Figure 5.7: Representative image of MRC-5 cells containing Tat conjugated polyacrylamide nanoparticles (5.2mV)..... 151

Figure 5.8: (A) MRC-5 cells with Tat conjugated nanoparticles and (B) enlarged area from (A) to show intracellular distribution of nanoparticles close to the nucleus. 151

Figure 5.9: Comparison of the green fluorescence intensity in cells after exposure to nanoparticles containing increasing amounts of ACTA or conjugated to Tat peptide.

Unfunctionalised (-3.3mV), 15% ACTA (17.6mV), 20% ACTA (18.6mV), Tat peptide conjugated (5.2mV).	152
Figure 5.10: (A) Pair of images showing green fluorescence from negatively charged silica nanoparticles (-25mV) in MRC-5 cells and the merged green fluorescence and brightfield image. (B) Green fluorescence from positively charged silica nanoparticles (27mV) in MRC-5 cells and merged green fluorescence and brightfield image.	155
Figure 5.11: Images showing in greater detail the intracellular localization of silica nanoparticles in MRC-5 cells. (A) Negative silica nanoparticles and (B) enlarged image of region in (A) showing perinuclear localization of nanoparticles. (C) Positive nanoparticles and (D) enlarged region of (C) again showing a perinuclear distribution.	156
Figure 5.12 Green fluorescence intensity within cells incubated with negative and positively charged silica nanoparticles. N=45	157
Figure 5.13: Confocal microscope images of (A) negatively charged phosphate functionalised and (B) positively charged quaternary ammonium functionalised silica nanoparticles in HeLa cells showing the nanoparticles (containing FITC and RITC), FM4-64 is a marker for endosomes and the merged image shows colocalization of the negatively charged but not the positively charged nanoparticles with endosomes ⁹⁸ ...	158
Figure 6.1: Resolution of different microscopy techniques.	167
Figure 6.2: Diagram to show basic principle of STED ¹³⁶	168
Figure 6.3: HeLa cells stained with antibodies against the nuclear pore complex protein Nup153 and secondary antibodies conjugated with ATT0647N on a standard confocal (CLSM) and a TCS STED Confocal microscope (Leica)	169
Figure 6.4: Diagram of the basic principle of STORM	170
Figure 6.5: TdEosFP-Pallaxin expressed in Hep G2 cells to label adhesion complexes on lower surface using TIRF and TIRF/STORM combined	170

List of abbreviations

- ACTA – 3-(acrylamidopropyl)-trimethylammonium chloride
- AFM – Atomic Force Microscopy
- AMPA – N-(3-aminopropyl) methacrylamide hydrochloride
- APS – Ammonium persulfate
- APTES - Aminopropyltriethoxysilane
- CLSM – Confocal Laser Scanning Microscopy
- CPP – Cell Penetrating Peptides
- DLS – Dynamic Light Scattering
- DMEM – Dulbecco’s Modified Eagle Medium
- DPPC - Dipalmitoylphosphatidylcholine
- FACS – Fluorescence Activated Cell Sorting
- FCS – Fetal Calf Serum
- F-PALM – Fluorescence Photoactivated Localization Microscopy
- HPICM – Hopping Probe Ion Conductance Microscopy
- LDV – Laser Doppler Velocimetry
- NAS – N-acryloxysuccinimide
- NC AFM – Non Contact Atomic Force Microscopy
- NIBS – Non Invasive Back Scatter
- NSOM – Near-field Scanning Optical Microscopy
- PALM – Photoactivated Localization Microscopy
- PALS – Phase Analysis Light Scattering
- PEBBLE – Probes Encapsulated by Biologically Localized Embedding
- PEG – Polyethylene glycol
- PBS – Phosphate Buffered Saline
- PSF – Point Source Function

SEM – Scanning Electron Microscopy

SICM – Scanning Ion Conductance Microscopy

SMCC – Sulfo-succinimidyl-4-(N-maleimidomethyl)cyclohexane-1-carboxylate

SLB – Supported Lipid Bilayer

STED – Stimulated Emission Depletion Microscopy

STORM – Stochastic Optical Reconstruction Microscopy

SSCM – Scanning Surface Confocal Microscopy

Tat - Transactivator of transcription

TEM – Transmission Electron Microscopy

TEMED – Tetramethylethylenediamine

TEOS – Tetraethyl orthosilicate

TIRF – Total internal reflectance microscopy

TMAC – N-trimethoxysilylpropyl-N,N,N-trimethylammonium chloride

Chapter 1 – Introduction

1.1 Imaging the interaction and uptake of nanoparticles

It has been repeatedly demonstrated that many different types of nanoparticles will enter cells, but it is often unclear by which route this uptake occurs. Learning more about the uptake processes involved will provide a greater degree of understanding and may help in experimental and formulation design, aiding the production of more efficient cellular delivery systems. This could, for example, include nanoparticles that may target a certain route of uptake in order to avoid potentially disruptive subcellular compartments such as endosomes and lysosomes.

Visual information about the interaction of nanoparticles with cell membranes on the nanoscale has been difficult to obtain in the past. This is due to limitations in the resolution of imaging techniques, and the complex nature and relatively rapid speed of the uptake processes. Imaging of the intracellular localization of nanoparticles following uptake has generally been performed using fluorescence microscopy, which has a limited maximum resolution of approximately 200nm. However, imaging technology has improved and it is now possible to obtain some of this information using a combination of advanced imaging techniques. These include scanning probe microscopy techniques such as Atomic Force Microscopy (AFM), which can be used to obtain nanoscale images of the interaction of nanoparticles with small regions of model cell membranes and increasingly, cells. In addition, multiple new fluorescence microscopy techniques such as confocal microscopy and stimulated emission depletion microscopy enable the larger scale tracking of nanoparticles within multiple cells at high resolution. Another technique, Scanning Ion Conductance Microscopy (SICM), is a scanning probe technique that works in a non contact manner. It can also be used to obtain nanometre and micron scale resolution images of the interactions of nanoparticles with cell membranes and some advanced systems allow this process to be imaged in real time on live cells. Another advantage of SICM is that it can be combined with confocal microscopy in a technique known as Scanning Surface Confocal Microscopy (SSCM). This allows the uptake of nanoparticles into cells to be tracked using both topography and fluorescence imaging simultaneously.

1.2 Cellular uptake of nanoparticles

Cells have the ability to internalize a range of substances, from small, single molecules through to larger particles such as bacteria. This uptake can occur through a number of different pathways which are all important and work together in order to maintain life, allow cell signalling and migration and protect the cell from infectious agents. Some of these routes of uptake are also exploited by nanoparticles. Investigations into the internalization of nanoparticles into cells are important because of the human health effects of exposure to nanoparticles of various different shapes, sizes and compositions through, for example, air pollution and cosmetics^{1, 2}. Nanoparticles are also being used in an increasing range of applications including diagnostics, measurement of intracellular analytes such as calcium and oxygen, imaging, phototherapy and gene and small molecule drug delivery³⁻⁸. Nanoparticles have unique properties due to their size and they often behave very differently to a bulk amount of the same material⁹. Their small size, ranging from a few nanometres up to several hundred nanometres, enables them to be present inside cells with minimal disturbance of the cell itself. Nanoparticles therefore have great potential for a variety of biological applications due to their ability to enter cells but this ability is also a potential risk since relatively little is known about the toxicity of some nanoparticles².

Methods of delivering nanoparticles to cells include gene gun, pico-injection, electroporation, liposomal delivery and conjugation to cell penetrating peptides and other targeting moieties¹⁰⁻¹². Some of these techniques, such as liposomal delivery and the use of cell penetrating peptides have been shown to be efficient and biocompatible. However, others display low efficiency and reproducibility and may cause irreversible damage to the cell. For example, picoinjection can only be performed on one cell at a time and causes more cell perturbation than the internalization of multiple nanoparticles¹⁰. However, these delivery techniques are not always required. Multiple studies have shown that nanoparticles can enter cells without the need for any delivery vehicle^{6, 8, 11, 12}. The size of nanoparticles means that they can usually not freely diffuse into cells as single molecules and ions can, instead, they need to engage with some form of cellular machinery in order to enter the cell¹².

Different pathways of cellular uptake enable cells to maintain life via the internalization of molecules required for many cellular processes including development, neurotransmission, cell-cell communication and signalling. Small molecules and ions do not require a carrier system, they can diffuse or cross the membrane using protein pumps and channels in the bilayer. Larger molecules, greater than a few nanometres in size in general do not have this ability, therefore they need to be transported into the cell in a different way. This transport can occur via a number of different endocytic pathways including phagocytosis, clathrin mediated endocytosis, caveolae mediated endocytosis and macropinocytosis. These pathways are often distinct in the molecules they transport into the cell and they are highly regulated by a number of proteins. However, they have the potential to be upregulated depending on the cellular environment, inhibition of one of the other endocytic pathways, and the needs of the cell¹³. Phagocytosis, macropinocytosis, clathrin and caveolae mediated endocytosis have all been implicated in the energy dependent uptake of nanoparticles into cells (Figure 1.1)^{2,14}.

The route of uptake that is used by nanoparticles to enter cells is important because it can influence their subsequent intracellular trafficking and final destination within the cell⁹. In some cases, where nanoparticles are used as drug delivery tools, or for the imaging of specific analytes or processes within cells, targeting of the nanoparticle to a specific internalization route or intracellular organelle may be beneficial. In addition to the targeting of certain uptake routes, learning more about the mechanisms by which to avoid other routes may also be of use. For instance, phagocytosis is a destructive mechanism usually used for the removal of infectious agents such as bacteria, and large, micron sized particles have been shown to be cleared from the body by this process. Other uptake routes, for instance clathrin mediated endocytosis, direct nanoparticles via the degradative endolysosomal pathway therefore this route should be avoided for certain, sensitive molecules such as DNA and proteins.

There are a number of different ways that the different endocytic routes have been classified in the past but as more is discovered about the pathways and the molecules involved in regulating them, it can become difficult to separate them completely. This is because there is often some degree of overlap in the molecules

involved and the cargos that are transported, since most cargos can enter cells by several pathways¹⁵. The improvement of imaging techniques such as fluorescence and electron microscopy has enabled the visualization of the final intracellular destination of drugs or conjugates within cells, but little is known about the initial stages of this interaction and what can be done to influence it. The major uptake routes are discussed below but since this work focussed mainly on the initial stages of the interaction rather than the complicated downstream processes, the reader is referred to a review by Doherty et al which discusses in greater detail many of the proteins and processes involved¹⁵.

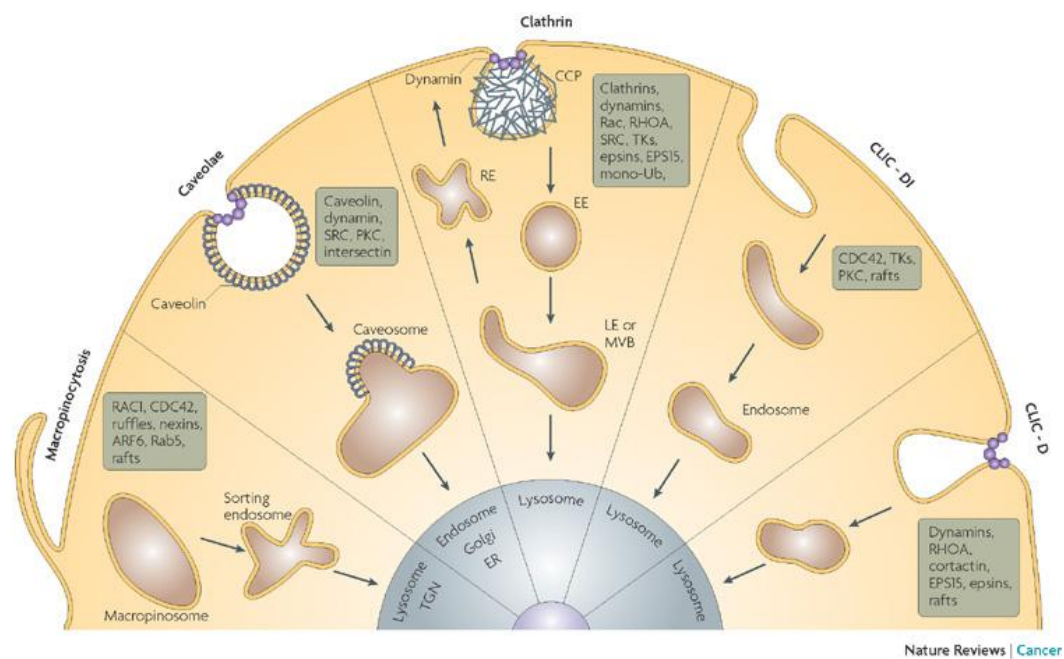


Figure 1.1: Diagram showing the major pathways of endocytosis, subsequent intracellular trafficking and final destination within cells. Inside the boxes are listed some of the main molecules involved in each pathway. CCP (clathrin coated pit), CDC42 (cell division cycle 42), CLIC-D (dynamine dependent clathrin independent carriers), CLIC-DI (dynamine and clathrin-independent carriers), EPS15 (epidermal growth factor receptor substrate 15), ER (endoplasmic reticulum), LE (late endosome), mono-Ub (mono-ubiquitylation), MVB (multi-vesicular body), PKC (protein kinase C), RE (recycling endosomes), TGN (trans-Golgi network), TK (tyrosine kinase)¹⁶.

1.2.1 Phagocytosis

Phagocytosis only occurs in specialised cells such as macrophages because it is primarily used for the protection of the cell from agents such as bacteria and viruses, along with clearance of apoptotic cells from the body. When specialized phagocytic cells such as macrophages, monocytes or neutrophils are exposed to nanoparticles coated with protein (opsonins) in the bloodstream, they will be engulfed into these phagocytic cells^{13, 15, 17}. The phagocytic route of uptake is generally a destructive one since it enables cells to kill bacteria. It is also important in the immune response of the body to infection since the destruction of bacteria within the cell leads to the appearance of bacterial peptides on the surface of phagocytic cells, provoking an immune response. However, the use of biodegradable nanoparticles such as PLGA exploits the enzymatic degradation and hydrolysis that occurs within these cells, since this allows the nanoparticles to be broken down releasing, for example, a drug^{13, 18}.

The other routes of cell uptake are known as the non-phagocytic pathways and they occur to some extent in most cells. These pathways are clathrin mediated endocytosis, caveolae mediated endocytosis, macropinocytosis, and clathrin and caveolae independent endocytosis.

1.2.2 Clathrin mediated endocytosis

Clathrin mediated endocytosis occurs via the uptake of molecules into clathrin coated pits and it is the most common and well described route of uptake. It can be receptor or non-receptor mediated but most types of clathrin mediated endocytosis progress through a series of steps that lead to the endolysosomal pathway¹⁵. It occurs when clathrin proteins polymerise to form a basket like structure on the cell membrane. These are referred to as clathrin coated pits although they consist of several cytosolic proteins but with clathrin as the main unit¹⁷. Clathrin coated vesicles can also be formed from intracellular compartments using a range of different adaptor and accessory proteins which can subsequently influence the range of molecules that are transported within the vesicle^{15, 17}.

Other proteins are involved in the formation of clathrin coated pits and vesicles and one of the major proteins identified to play an important role is adaptor protein 2 (AP2) which has been shown to be important for the formation of clathrin coated

pits and vesicles generated from the cell membrane^{15, 17}. Adaptor proteins such as AP2 help to coordinate the nucleation of clathrin in regions of the cell membrane that will subsequently be internalized. CLASPs (Clathrin associated sorting proteins) are involved in recognising cargo and sorting signals¹⁷. Adaptor proteins including AP2 and accessory proteins such as SNX9, containing the N-BAR or BAR domains are important for producing deformation and the formation of a curved structure within the membrane. This is formed from the three legged clathrin structure that is assembled into 'triskelions', a curved polygonal web, which results in vesicle formation via their binding to clathrin and AP2 and their role in recruiting dynamin^{15, 17, 19}. A vesicle with a diameter of around 100nm is formed when the large GTPase protein dynamin cleaves the vesicle structure from the membrane, forming a clathrin coated vesicle. Dynamin forms a helical polymer around the neck of the vesicle and following hydrolysis of GTP, detachment of the vesicle from the membrane occurs^{15, 20}. The diameter of the vesicle limits the size of molecules that can be internalized into cells by this route. Once cleaved from the cell membrane, intracellular trafficking of the vesicle begins, and the clathrin coat is removed by the ATP dependent protein Hsc70 along with cofactors such as auxilin and cyclin-G-associated kinase^{15, 21, 22}. This vesicle may eventually fuse with and deliver its contents to endosomes which mature and acidify into late endosomes and lysosomes¹⁷.

Low density lipoprotein (LDL), transferrin and epidermal growth factor (EGF) have all been shown to be ligands for the receptor mediated form of clathrin mediated endocytosis^{13, 15, 17}. The transferrin receptor is widely regarded as the classical marker for clathrin mediated endocytosis. It contains a tyrosine based YTRF motif and these motifs along with di-leucine (LL) motifs have been shown to direct molecules towards endosomes and lysosomes. The motif is recognised by sites on AP2 proteins which can subsequently interact with clathrin leading to internalization via this route^{15, 23, 24}. Clathrin coated pits can interact with a range of different adaptor and accessory proteins, enabling the internalization of a number of different cargos within one vesicle^{15, 17, 19}.

Clathrin mediated endocytosis has been demonstrated to be involved in the internalization of a number of different types of nanoparticles including PLGA and

silica based systems^{25, 26}. In receptor independent clathrin mediated endocytosis, which may be exploited by some nanoparticles, substances interact non-specifically with the area of membrane containing clathrin leading to their uptake by this route^{18, 27}.

1.2.3 Caveolae mediated endocytosis

Caveolae mediated endocytosis is another major endocytic pathway and is one of the most well characterised non clathrin mediated pathways²⁸. It involves the formation of flask shaped structures in the cell surface membrane formed from caveolin 1 and 2, which generally have a size of around 50-100nm. However, fluorescent labelling of the protein caveolin 1 has enabled the observation of the joining of these flask shaped structures together and incomplete detachment from the cell membrane^{15, 17, 29}. It is also known as lipid raft endocytosis since the vesicles are formed from areas of the membrane rich in phospholipids, sphingolipids and cholesterol^{25, 27}. This process most commonly occurs in endothelial cells, adipocytes, fibroblasts and smooth muscle cells^{15, 29, 30}. There are three mammalian caveolin proteins. Caveolin 3 is only found in muscle cells whilst both caveolin 1 and 2 are found in non muscle cells^{31, 32}. The only cells that appear to lack caveolin of any kind are neurons and leukocytes. Caveolin 1 is believed to be necessary and possibly sufficient alone to produce caveolae. It has been demonstrated that overexpression of caveolin 1 in caveolae deficient cells can lead to the production of the flask shaped invaginations characteristic of caveolae^{15, 31}. Caveolin 1 polymerises and binds to fatty acid tails of the glycosphingolipid GM1^{15, 33}. It can colocalize with GM1 and another glycosphingolipid, Gb3, both of which are found, along with their ligands cholera toxin and shiga toxin on the outer leaflet of the cell membrane^{15, 29, 34}. In contrast, caveolin 1 is found on the inner, cytoplasmic leaflet of the membrane but it forms a hairpin like structure that is embedded in the membrane³¹. This allows it to interact with these molecules whilst both the N and C terminus remain in the cytoplasm^{15, 17}. Caveolae are initially formed in the Golgi body where they are associated with cholesterol which is then involved in the deposition and inducement of mobility of caveolin 1 in the membrane³¹. The morphology of vesicles associated with caveolae uptake appears to be highly variable and has been shown to include large pH neutral vesicles known as caveosomes, along with smaller vesicles and tubules, many of which do not appear

to fully dissociate from the membrane^{15, 32}. As well as the formation of traditional vesicles, caveolin proteins have also been implicated in the transcytosis across endothelial barriers of non enveloped viruses and serum components^{15,17}.

A number of different cargo have been shown to be internalized by caveolae mediated endocytosis including SV40 virions, cholera toxin B subunit and glycosylphosphatidylinositol (GPI) linked proteins^{15, 32, 35}. In addition, caveolae mediated endocytosis has been shown to be particularly important for the transport of cholesterol. Along with clathrin mediated endocytosis, it also depends on the protein, dynamin, which is involved in the scission of the coated vesicles from the cell membrane. Unlike phagocytosis and clathrin mediated endocytosis, it has been suggested that caveolae mediated endocytosis is not generally a destructive uptake route since it often avoids endosomes and lysosomes and is therefore exploited by some bacteria and viruses. However this has been challenged recently and it has been shown that caveolae can fuse with endosomes using RAB5 and can be recycled, returning to the cell membrane^{25, 32, 35}. Caveolae mediated endocytosis has also been proposed as an uptake route that could be targeted when trying to deliver sensitive molecules such as proteins, RNA and DNA. This targeting could be achieved by using molecules which are known to target the caveolae mediated endocytosis pathway including folic acid, albumin and cholesterol^{13, 18}.

1.2.4 Flotillin dependent endocytosis

Flotillin dependent endocytosis appears to have similarities to caveolae mediated endocytosis since investigations using fluorescence and electron microscopy appear to show similar flask shaped invaginations of the cell membrane. However, unlike caveolae, overexpression of flotillin does not induce the formation of these structures as in the case of overexpression of caveolin 1^{15, 36}. There is a high degree of structural similarity between flotillin and caveolin 1 and they also form a hairpin structure within the cell membrane^{15, 17}. This suggests that flotillin may also play a role in the ordering and stabilising of lipid raft structure formation within the membrane in a similar way to caveolin 1^{15, 37}. It is therefore thought that flotillin dependent endocytosis may be a stand alone pathway or it may play a role in other clathrin or caveolae independent pathways³⁸. Flotillin 1 has been shown to be involved in the dynamin dependent but clathrin and caveolin 1 independent uptake

of cell surface proteoglycans which are found to be trafficked to late endosomes in structures that are positively labelled for flotillin 1^{15,17,39}.

1.2.5 Macropinocytosis

Macropinocytosis occurs in most cells to some extent but it can be induced by exposure to growth factors such as platelet derived growth factor that trigger receptor tyrosine kinases in the cell membrane^{13, 40}. It involves the ruffling of the cell surface membrane which is driven by the cytoskeletal protein, actin. These ruffles form projections that then collapse onto each other or rejoin the membrane. When they fuse the projections encapsulate extracellular fluid which can contain a variety of substances including nanoparticles^{15 25, 40}. Unlike clathrin and caveolae mediated endocytosis it is not induced via ligand binding¹⁷. Macropinocytosis has been identified to be dependent on the proteins rac1 and actin, which are linked to an ability to form membrane ruffles¹⁵. Despite it being a well recognised process, the details of many of the molecules involved in the mechanism and regulation of macropinocytosis are either unknown or poorly characterised. The kinase PAK1 has been identified to be important for macropinocytosis and it is required to induce the process via binding and activation of GTP-bound Rac which triggers the formation of membrane ruffles⁴⁰⁻⁴². Other proteins believed to be important in macropinocytosis are PI3K, Ras family GTPases, Arf6 and src whilst N-WASP and SNX9 are involved in ruffle formation via their effects on actin^{15, 40, 41, 43}.

Macropinocytosis is known to be a cholesterol dependent process since cholesterol is required for the recruitment of activated rac1¹⁵. Macropinocytosis results in the formation of large (1-5 μ m), heterogeneous uncoated vesicles known as macropinosomes, which are filled with extracellular fluid⁴⁰. The fate of these vesicles varies between cell types but in most cases they are observed to acidify and decrease in size, and in some cases they fuse with lysosomes. It is a particularly prominent route of uptake in macrophages, and has been suggested as the likely route of uptake for the cell penetrating peptide Tat⁴⁴. Macropinocytosis is a relatively non specific route of uptake and therefore has the potential to transport many different types of nanoparticles into cells. Even those particles with no specific targeting mechanism may be internalized since if they are located near, and interact to some extent with the cell membrane, there is a chance that they may be

encapsulated by the membrane projection, and taken into the cell along with the extracellular fluid surrounding them^{13, 18, 27}.

1.2.6 Direct translocation

Finally, one mechanism of nanoparticle entry into cells that does not involve endocytic pathways is that of direct translocation, also known as transcellular transport. It has been suggested as a route for the uptake of some types of nanoparticles, especially those of a very small size containing amine groups and cationic moieties. Additionally, it has also been identified as a potential route for the uptake of cell penetrating peptides including Tat and CADY^{45, 46}. It occurs when nanoparticles enter cells by crossing the cell membrane without using any of the uptake routes mentioned above. Small, positively charged entities may enter cells in this way by causing transient defects in the bilayer structure. This can increase the permeability of the cell membrane, enabling them to traverse the bilayer^{8, 47, 48}. Since the lipid bilayer is fluid, and molecules can move around, the pores in the membrane are usually quickly repaired by the cell which may explain why it is not always a cytotoxic process. However, at high concentrations it may become irreparable, leading to loss of intracellular fluid and cell death⁴⁶. This kind of transport has been observed for antimicrobial peptides that can form pores in the membrane of bacteria leading to their translocation across the membrane⁴⁸.

Inhibition studies have frequently been performed in order to try and selectively inhibit endocytic pathways and to discover more about the factors that influence them and the molecules that are involved. However, as previously mentioned, there can be a high degree of overlap between pathways and inhibition of a molecule can affect more than one pathway despite the high level of characterisation of some of the pathways. In addition, inhibition may lead to upregulation of another pathway by the cell and the effects of inhibitors can be highly cell line dependent, further complicating the results²⁸. One example is that of cholesterol depletion which is commonly performed when investigating caveolae mediated endocytosis. Cholesterol depletion can be achieved using a number of different molecules including methyl β cyclodextran (M β CD), filipin and nystatin. However, the removal of cholesterol has multiple effects including a decrease in the number of caveolae in the membrane as well as effects on clathrin mediated endocytosis leading to a

decrease in the uptake of transferrin. In addition, cholesterol depletion also results in a decrease in membrane ruffling which consequently affects macropinocytosis¹⁵. There are numerous examples of how chemical inhibitors designed to be specific for certain pathways can have effects on other uptake routes and also on cell morphology and viability. For example, M β CD is used as an inhibitor of caveolae mediated endocytosis via sequestration of cholesterol, but has been found to inhibit the uptake of transferrin, a marker of clathrin dependent endocytosis and has also been found to lead to changes in cell morphology at concentrations used for inhibition studies^{28, 49}. Statins have also been used to inhibit caveolae mediated endocytosis but the large decrease in cholesterol that they produce has non specific inhibitory effects on clathrin, macropinocytosis and phagocytosis⁴⁹. Both chlorpromazine and K⁺ depletion have been used as inhibitors of clathrin mediated endocytosis, but K⁺ depletion has also been found to inhibit clathrin independent pathways such as caveolae, whilst chlorpromazine can reduce cell viability²⁸. Both have also been shown to lead to reduced uptake of fluid phase markers used to identify macropinocytosis⁴⁹. Many of the chemical inhibitors used have effects on the actin cytoskeleton including filipin and nystatin, used to inhibit caveolae mediated endocytosis, and amiloride and nystatin used to inhibit macropinocytosis. These global effects on actin filaments can have non-specific effects on other routes of endocytosis since actin is a key component in many pathways⁴⁹. In an effort to produce more specific inhibition of uptake routes, techniques such as RNA interference to silence genes, and the introduction of dominant negative proteins to inactivate proteins have been used. These lead to more specific inhibition of a certain uptake pathway and have been exploited to try and design inhibitors that interact with specific proteins without affecting others^{28, 50}. However, it remains extremely difficult to isolate the effect of these inhibitory molecules to only one pathway because of the inevitable overlap between pathways and the desire of the cell to maintain life by upregulating pathways in order to gain what it needs²⁸.

1.3 Factors affecting cellular uptake of nanoparticles

Nanoparticles are of great interest in the field of drug delivery since they have unique properties compared to bulk amounts of the same materials. They are being investigated as tools that can be used to increase the efficiency of drug delivery via the use of new formulations, and their chemistry often means they can be easily

modified to include targeting moieties^{27, 51}. The interfacial properties of nanoparticles affect their interactions with their environment and these properties have been shown to affect the rate and extent to which nanoparticles enter cells^{17, 52}. These effects are highly variable between different nanoparticles and cell types and depend on how the nanoparticles interact with constituents of the extracellular fluid and components of the cell membrane including proteins and lipids^{53, 54}. Improving the understanding of these interactions may help in the design of more efficient, targeted delivery systems.

A number of factors have been identified that influence the uptake of nanoparticles into cells and these include cell type, membrane composition²⁸, nanoparticle material^{27, 55}, charge^{27, 56}, size^{2, 57}, shape^{58, 59} and surface chemistry⁵⁷ along with the extracellular environment that uptake occurs in. For instance, if one uptake route is blocked for any reason, another can be upregulated so that uptake still occurs and this ability helps cells to maintain life²⁸. In addition, the presence of any conjugated molecules such as polymers or peptides can affect the rate and route of uptake⁶⁰⁻⁶⁵.

The interactions of nanoparticles with components of the cell membrane can lead to a variety of possible interactions including the formation of protein coronas around particles, wrapping of the particle in the cell membrane and potentially some biocatalytic processes⁶⁶. How nanoparticles interact with their environment is influenced not only by their own characteristics such as size and charge which will be discussed in detail later, but also through the molecules that adsorb to the nanoparticle surface, forming what is known as the corona. The formation of a biomolecular corona, a layer around the nanoparticle surface often composed of lipids or proteins, can have significant effects on the interaction of the nanoparticle with the cell membrane and this is often different to the interaction of the bare nanoparticle⁶⁷⁻⁶⁹. The corona is a dynamic structure that changes depending on the environment. It consists of a tightly bound 'hard layer' and a more loosely associated 'soft' layer where molecules exchange rapidly⁷⁰. The presence of the corona drastically reduces the surface energy of the nanoparticle^{67, 69-71}. However, although the surface energy is reduced, the presence of the protein, lipids and other biomolecules in the layer can lead to enhanced and sometimes specific interactions

with the membrane causing increased uptake and could potentially can be exploited to provide targeting of nanoparticle delivery *in vivo*^{67, 71, 69}

Once they have been internalized into the cell, most nanoparticles will then move through intracellular compartments such as early and late endosomes, lysosomes, Golgi bodies and rough endoplasmic reticulum and their trafficking and retention within these compartments can be influenced by the interaction of nanoparticle surface groups with intracellular molecules⁷². Once inside the endolysosomal system, the nanoparticles generally cannot escape into the cytoplasm unless they are specifically designed for endosomal escape via the use of additional molecules. For instance, it has been suggested that some cationic molecules have the ability to escape the destructive environment of the endolysosomal pathway enabling their release into the cytoplasm, which may have potential in the design of more efficient drug delivery systems^{52, 61}.

When performing experiments to study nanoparticle uptake, it is important to note that that the physicochemical properties of nanoparticles vary depending on the media in which they are suspended. Cell culture media contains proteins such as albumin which can adsorb to the surface of some nanoparticles leading to aggregation and reversal of a positive surface charge⁵⁴. The pH and ionic strength of the medium also affect the zeta potential of the particles and dispersion stability^{52, 73}.

Since so many factors have the potential to influence cellular uptake of nanoparticles, many studies have been performed in order to try and identify which factors may be of greatest importance. Many groups have looked at the effect of one, or a combination of these factors, but there is a great deal of variety in both the way the studies are performed (e.g. cell type, nanoparticle type and experimental conditions), and in their outcomes. This makes it very difficult to draw any definitive conclusions, and it is impossible to say that one parameter will always affect cellular uptake in a certain way. It is highly likely that a combination of many different factors is involved, and that the contribution of these different parameters varies between different nanoparticles and cell types⁵⁴.

1.3.1 Size

Nanoparticle size is a key parameter that affects their properties and it is their size that can impart different properties to that of the bulk material. Size can influence both the route of cellular uptake and the extent and rate of uptake^{55, 74}. Smaller particles may be internalized by pinocytosis mechanism such as clathrin or caveolae mediated endocytosis, whilst larger particles are generally shown to be internalized via macropinocytosis and/or phagocytosis in specialized cells. This is thought to be because the size of the vesicles produced during clathrin and caveolae mediated endocytosis are limited in size, generally to particles less than 200nm³⁰. In contrast, the mechanism by which cells internalize extracellular fluid and other substances by macropinocytosis means that much larger particles can be internalized into cells via this route^{17, 25, 57, 75, 76}.

The size of nanoparticles has also been shown to influence their final location within an organism. For instance, small nanoparticles with a diameter of less than 100nm can escape blood vessels and this is of particular interest when considering targeted delivery to tumours since blood vessels in tumours are often more permeable which in turn leads to accumulation of nanoparticles within tumours. In contrast, particles on the micron scale, with a similar size to bacteria for example, are often cleared rapidly from the body by macrophages via phagocytosis, consequently their potential for use as drug delivery tools may be limited⁷⁷. Control of size is therefore a key parameter in the design of nanoparticles for use as drug delivery and diagnostic or imaging tools. A small size is often desirable in the latter case since this means the nanoparticles have a high surface area to volume ratio and a fast response time to changes in the environment⁷⁸.

The first step in the cellular uptake of nanoparticles involves their interaction with the cell membrane and this interaction is partially dependent on the size of the nanoparticle because a large particle interacting with a cell surface experiences the average effects of a variety of heterogeneous regions of the membrane whilst smaller nanoparticles can interact with one homogenous patch at a time (Figure 1.2). Cell membranes are not uniform and contain regions rich in molecules required for clathrin and caveolae mediated uptake therefore the interaction of nanoparticles with different areas of a membrane due to its size may affect uptake to some extent⁵².

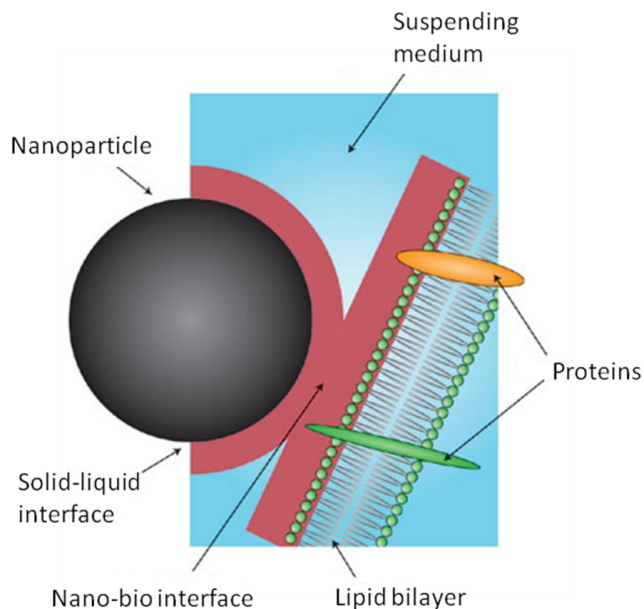


Figure 1.2: The cellular uptake of nanoparticles depends on a number of factors including the properties of the nanoparticle, how it interacts with the medium it is in and the biological surfaces that it encounters⁵².

Nanoparticle size also impacts on the ability of the nanoparticle to interact with membrane proteins and receptors, and the process of membrane wrapping, which is involved in many forms of endocytosis. In addition, the size of the nanoparticles may change during uptake as the nanoparticle encounters different environments both within and outside the cell, and aggregation of nanoparticles is a common problem observed in biological systems^{2, 17, 79}.

A number of studies have investigated the effect of nanoparticle size on uptake but the experimental conditions vary greatly, making it difficult to compare the results. The group of Rejman, in a detailed study, have shown that all sizes of fluorescent latex nanoparticles (up to 500nm) were eventually taken up by B16 cells, with smaller particles found in perinuclear regions and larger ones found at the periphery of the cell (Figure 1.3). No internalization of particles was seen at 4°C indicating that an energy dependent uptake mechanism was being used. Once the particles had entered cells, further trafficking appeared to be microtubule dependent since treatment of the cells with nocodazole, which disrupts microtubules, prevented intracellular trafficking of particles from early to late endosomes. Nocodazole affected the uptake of the smaller particles to a greater

extent than the larger particles, suggesting that a different route was used for differently sized particles. Another method of investigating uptake routes is to use cholesterol depletion which inhibits many of the routes of uptake including clathrin and caveolae mediated endocytosis and macropinocytosis. In this study it was shown to cause a decrease in uptake as particle size increased^{15, 17, 57}. Both potassium depletion and treatment with chlorpromazine, which block clathrin mediated endocytosis, caused inhibition of the uptake of smaller particles to a greater extent than larger particles suggesting smaller particles (up to 200nm) were internalized by clathrin dependent endocytosis⁵⁷.

A number of reports from different groups investigating the uptake of many different types of nanoparticles into cells have frequently concluded that smaller nanoparticles are often shown to enter cells at a faster rate and to a greater extent than larger nanoparticles. However, very small nanoparticles (<20nm) have been found to have a lesser degree of uptake, possibly due to an increased rate of dissociation from the cell membrane, which results in less chance of uptake occurring⁸⁰⁻⁸⁴.

The studies reviewed here are just some of the examples of the literature available regarding nanoparticle uptake into cells. It is impossible to definitively say that a certain size of nanoparticle will be taken up exclusively by certain routes, since although size plays an important role in uptake, it is also dependent on the other factors discussed earlier. A particular pattern of size dependent uptake that is observed in one cell type may not be repeated in another, since the effect of nanoparticle size on uptake appears to be highly cell line dependent⁸⁰. This could be explained by the different contributions of the various endocytic pathways to overall cellular uptake, since not all cells use the same routes to the same extent. Although it is difficult to draw firm conclusions about the effect of size on cellular uptake of nanoparticles, the examples discussed serve to demonstrate the complex nature of investigating these processes and some of the possible techniques by which information can be obtained.

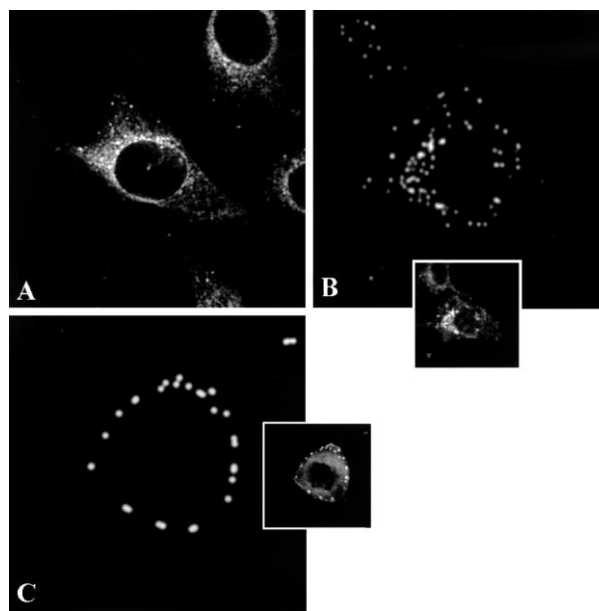


Figure 1.3: B16-F10 cells incubated with nanoparticles of (A) 50nm for one hour, (B) 200nm for three hours and (C) 500nm for three hours. Insets are the corresponding phase contrast images⁵⁷.

1.3.2 Charge

It has been reported by many groups that both anionic and cationic entities including liposomes, polymers and nanoparticles will enter cells in the absence of any delivery vehicle, despite the seemingly unfavourable interaction between the charge on anionic nanoparticles and the cell membrane^{2, 14, 55, 85-89}. However, although both anionic and cationic nanoparticles have been shown to enter cells, there can be differences in the extent and rate to which this occurs. For instance in a number of studies, cationic nanoparticles and polymer complexes have been found to be more extensively taken up by cells than the anionic versions^{47, 90, 91}. In contrast, other studies have suggested that in some cases, the anionic particles display enhanced uptake compared to neutral particles. The presence of a neutral charge or ligand, e.g. polyethylene glycol, has been shown to limit the uptake of nanoparticles^{11, 90}. A neutral charge is sometimes desirable if the nanoparticles are required to have minimal interaction with their biological environment. When considering the effect of charge, the functional groups present that impart the charge to the nanoparticles should also be taken into consideration. These groups influence other properties of the nanoparticles such as solubility and interactions

with the surrounding environment, and a change in the surface functionality without a change in charge can affect internalization^{11,92}.

Literature reports suggest that positive charge is in itself a delivery mechanism for cellular uptake of entities such as nanoparticles, peptides and polymer complexes^{60,93}. Positive charge is exploited by a variety of commercial products such as Lipofectamine, as a means of delivering molecules into cells¹². A number of suggestions have been made about how positive charge leads to cell uptake but it probably begins with electrostatic interactions of the positively charged vector with regions or groups (e.g. sialic acid and proteoglycans) in the cell membrane which often has a slightly negative overall charge. Positively charged molecules therefore may interact more strongly with the cell membrane than neutral or negatively charged versions. This increased association and interaction may subsequently increase the chance of the particles being internalized into cells by some form of endocytosis^{11,17,27,79}.

A number of groups have shown that positively charged materials such as cationic nanoparticles exploit this ionic interaction, causing a temporary disruption in the cell membrane. This means that they may subsequently cross the cell membrane by generating transient holes in the bilayer^{62,94,95}. This interaction has also been demonstrated using AFM, where it has been observed that cationic nanoparticles induce the formation and growth of nanoscale holes in supported lipid bilayers. Complementary studies looking at cell membrane leakage of cytosolic lactate dehydrogenase at non toxic nanoparticle concentrations also indicate the formation of nanoscale holes in the membrane⁸⁶. However, many reports suggest that these positively charged species often display some degree of cytotoxicity due to their membrane effects, therefore future applications may be limited²⁷.

Other uptake routes have been suggested for cationic nanoparticles including clathrin and caveolae mediated endocytosis and macropinocytosis. In most studies, the uptake of nanoparticles is considered to be an active process, requiring energy from the cell for the uptake of both anionic and cationic particles. Once inside the cell, intracellular processing of nanoparticles is important in determining their fate and it has also been suggested that cationic nanoparticles have the ability to escape

endosomes thereby evading the degradative lysosomal pathway which has implications for improved drug delivery^{13,85,96}.

Positively charged nanoparticles can be produced by a variety of methods. Schulz *et al.* demonstrated that positively charged ammonium moieties can be incorporated into nanoparticles and these can associate with negatively charged biological membranes, leading to enhanced internalization of these substances into cells¹². The functionalisation of nanoparticles with amine groups can also provide a positive surface charge, and amine functionalised nanoparticles have been shown to cause the formation of defects in membranes, both on live and fixed cells and also on a model artificial membrane (Figure 1.4)²⁷.

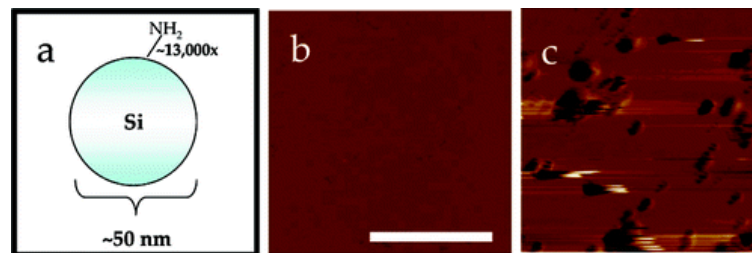


Figure 1.4: Amine functionalised cationic 50nm silica nanoparticles caused defect formation in model lipid bilayers (a) Schematic of an amine functionalised silica nanoparticle, (b) DMPC lipid bilayer, (c) addition of the nanoparticles caused defect formation⁹⁷.

As explained above, there are therefore a number of possible explanations for the enhanced uptake of positively charged nanoparticles. However, a significant number of studies also demonstrate that negatively charged nanoparticles can enter cells without any additional delivery vehicles, and that this uptake is greater than that of unfunctionalised nanoparticles with a neutral charge^{27, 98}. Negative surface charge can be introduced onto particles via a number of methods that frequently include the incorporation of carboxyl groups into the nanoparticle matrix or conjugation onto the surface of the nanoparticles. The increased uptake of negatively charged nanoparticles is more difficult to explain but it must occur as a result of an interaction between the nanoparticles and molecules on the surface of the cell, for example proteins, that lead to uptake^{17, 27, 55}. In addition, the

nanoparticles may interact with cationic regions of the cell membrane which are small but significant in number¹¹. The negatively charged nanoparticles may then be internalized following non specific binding^{91, 99}. Some uptake mechanisms, e.g. macropinocytosis are non specific. If the nanoparticles associate and interact with the membrane to some extent and are therefore located close to the cell surface, this increases the chances that they may be encapsulated into a vesicle formed by cell membrane ruffling during macropinocytosis and enter cells by this route. In studies of negatively charged silica nanoparticle uptake, this has been termed a pinocytosis related non-specific adsorptive endocytosis mechanism¹⁰⁰. Caveolae mediated endocytosis has also been suggested as a route of uptake for many negatively charged species²⁵.

Functionalisation of nanoparticles with a surface charge, especially a positive charge, therefore seems to improve their internalization into cells. Another method by which a positive charge can be imparted to nanoparticles is via conjugation to cationic molecules. One of the classic examples of these molecules are the cell penetrating peptides, which have been extensively investigated in recent years due to their ability to cross cell membranes.

1.3.3 Cell Penetrating Peptides (CPPs)

The improved uptake of various different cargo including nanoparticles, drugs, proteins and liposomes when conjugated to CPPs has been reported by many different groups^{44, 101, 102}. In addition to enhanced delivery of molecules into cells, they may also promote endosomal escape allowing for the delivery of molecules such as drugs to the cytosol, and from there to a variety of intracellular organelles including mitochondria and the nucleus¹⁰³. CPPs are also in clinical development for the targeted delivery of a number of different therapeutic agents for multiple conditions¹⁰⁴. CPPs are a family of molecules that include antennapedia, transportan, HSV-1, VP22 and HIV-1 Tat peptide that demonstrate an ability to efficiently cross cell membranes with minimal disruption, whilst also delivering their cargo¹⁰⁵. However, although many studies have been carried out investigating the entry of CPPs into cells, the precise mechanism of uptake has been a subject of some controversy. A number of different pathways have been suggested to be involved in CPP entry into cells including clathrin, macropinocytosis and direct

translocation across the membrane¹⁰⁶. Many groups have investigated the uptake of CPPs but in a similar way to the investigation into the uptake route of nanoparticles discussed previously, results are significantly influenced by cell line and experimental conditions. This makes comparison of results and the assigning of uptake mechanisms difficult^{50, 107}.

Most CPPs are characterized by a high proportion of positively charged amino acids, especially arginine and lysine. It is believed that this abundance of positive charge aids their internalization, particularly because there is little structural or sequence homology between different peptides^{44, 105, 108}. However, a number of CPPs contain a series of alternating cationic and hydrophobic residues which means they can adopt an α -helix conformation, enabling them to penetrate membranes. In addition, some CPPs are amphipathic which also appears to aid their cellular uptake^{103, 106}.

Cell Penetrating Peptide	Origin	Structure	Sequence	Proposed mechanism	References
Tat	HIV-1 transcriptional activator	Random coil/ PPII helix	GRKKRRQRRRQ	Direct penetration, pore formation, multiple endocytic routes	50, 109
Penetratin (pAntp)₍₄₃₋₆₈₎	<i>Antennapedia Drosophila melanogaster</i>	Amphipathic α -helical/ β -sheet	RQIKIWFQNRRMKWKK	Direct penetration, endocytosis	110
Octarginine	Model peptide (chimeric)	Random coil α -helical	RRRRRRRR	Direct penetration, endocytosis	111
pVEC	Murine vascular endothelial cadherin	Amphipathic, β -sheet	LLIILRRIRKQAHASK	Direct penetration, transporter-mediated	112
Pep-1	Chimeric	Amphipathic, α -helical	KETWWETWWTEWSQPKKRRKV	Direct penetration, pore formation	106 113
Transportan	Galanin-mastoparan neuropeptide	Amphipathic, α -helical	GWTLNSAGYLLGKINLKALAALAKKIL	Endocytosis, direct penetration	104, 106
MAP	Model amphipathic peptides (chimeric)	Amphipathic, α -helical	KLALKLALKALKAAKKA	Multiple mechanisms	114
MPG	HIV gp41	Amphipathic, β -sheet	GALFLGFLFAAGSTMGAWSQPKKRRKV	Direct penetration	113
CADY	PPTG1 peptide derived	Amphipathic, α -helical	GLWRALWRLRLSLWRLWRA	Multiple endosomal routes	115

Table 1.1: Table listing some of the commonly used CPPs along with their structure, sequence and proposed uptake mechanism. Table adapted from ^{103, 106}.

The positive charge on the peptide leads to an electrostatic attraction between the peptide and components of the cell membrane such as phospholipid head groups, glycosaminoglycans or heparan sulphate proteoglycans (HSPG) ^{45, 105, 106, 116-118}. HSPGs have been shown to be important for the uptake of some CPPs but in other cases have been suggested to sequester cationic CPPs, reducing their uptake¹⁰³. The

consensus opinion now appears to be that CPPs can use both direct translocation across the cell membrane along with a number of different endocytic routes including macropinocytosis, clathrin and caveolae mediated endocytosis depending on the peptide, cell type and any associated cargo^{25, 44, 50, 106}. The contribution of an endocytic mechanism is supported by a number of studies demonstrating reduced uptake of CPPs at 4°C, suggesting an active uptake mechanism is involved. It is further supported by the ability of CPPs to modify the actin cytoskeleton and show increased uptake of markers of macropinocytosis such as dextran. A number of studies have identified reduced uptake of CPPs in the presence of amiloride and cytochalasin D which inhibit macropinocytosis^{50, 101}. CPPs have been shown to accumulate in lysosomes but cytoplasmic labelling has also been observed, which may result from the escape of the peptide from endosomes or from direct translocation across the membrane¹⁰³.

Fluorescence microscopy is commonly used as an investigative tool for examining endocytosis of CPPs but care must be taken when choosing a suitable dye since it can modify the properties of the peptide. In addition, the high affinity of the peptide for the plasma membrane and proteins in tissue culture media must also be considered in the experimental design. The positive charge on many CPPs means that they will associate with negatively charged proteins in tissue culture media, reducing the proportion of free peptide that is available for cellular uptake¹⁰³. CPPs such as Tat have been found to strongly adhere to the cell surface membrane and they cannot be removed by simple washing procedures. Instead, washes must be undertaken with heparin, and trypsinization performed in order to remove the portion of the peptide that is firmly bound to the cell surface membrane¹⁰³. Omission of these important steps has led to inaccurate measurements of peptide uptake by techniques such as FACS, which does not distinguish fluorescence from membrane bound peptide from that of peptide within cells⁴⁴. In addition, it was thought for a number of years that CPPs localized to the nucleus following cellular uptake but this has since been shown to be due to fixation artefacts⁴⁴.

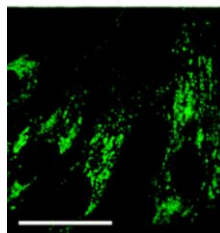


Figure 1.5: Tat peptide conjugated to Oregon Green accumulates in endosomes¹¹⁹.

1.4 MRC-5 cells

MRC-5 cells are human lung fibroblasts derived from normal human male foetal lung. They were used in this work since they are a human lung fibroblast and therefore have potential to be exposed to nanoparticles from the environment via inhalation⁷⁹. Inhalation of nanoparticles is an important consideration since subsequent intracellular trafficking of the nanoparticles could lead to systemic exposure, and the characteristics of the nanoparticles can be an important factor in determining their potential for entry to the body by this route^{120, 121}.

Very few studies have been performed using MRC-5 cells to investigate endocytosis of nanoparticles, but the few studies that have been performed have indicated that they have the potential to spontaneously internalize cationic particles formed of lipopolyamines¹²². In addition, it has been suggested that they can perform phagocytosis even though they are not professional phagocytic cells via a study investigating the internalization of *Encephalitozoon cuniculi*, a spore forming parasite. The spores were internalized by an actin dependent mechanism into an intracellular vesicle which was positive for the lysosomal membrane marker LAMP-1¹²³.

Most of the studies into MRC-5 cell endocytosis have used electron rather than fluorescence microscopy to discover the intracellular localization of nanoparticles. Ng et al used TEM to demonstrate the uptake and subcellular localization of 20nm gold and polystyrene nanoparticles within MRC-5 cells. The nanoparticles were spontaneously internalized when added to culture media and the majority of gold nanoparticles were found to be located within intracellular vesicles with some found in the cytosol. In contrast, more of the polystyrene nanoparticles were found located in the cytosol¹²⁴. The same group, in a paper by Li, again showed that 20nm

gold nanoparticles were internalized into cellular vesicles within MRC-5 cells located close to the nucleus. The nanoparticles caused damage to DNA and inhibited cell proliferation indicating potential cytotoxicity of these nanoparticles¹²⁵. The uptake of carbon black and titanium dioxide nanoparticles into MRC-5 cells has also been investigated using TEM and they were found to accumulate within intracellular vesicles but were excluded from intracellular organelles such as the nucleus and mitochondria. The internalization into vesicles suggests an endocytic route of uptake and in this study it was suggested that macropinocytosis may be the primary uptake mechanism¹²⁶.

Radu et al investigated the effects of 40-60nm hematite (iron oxide) nanoparticles on MRC-5 cells. The uptake and intracellular localization of the nanoparticles was not investigated but it was found that exposure of the cells to these nanoparticles led to a decrease in intracellular glutathione and an increase in lipid peroxidation due to oxidative stress and the production of reactive oxygen species in the cell by the nanoparticles¹²⁷. The same group also found that exposure of MRC-5 cells to very small, <20nm silica nanoparticles led to changes in cell morphology and again, an increase in lipid peroxidation¹²⁸.

The internalization of the cell penetrating peptide Tat, conjugated to streptavidin has also been investigated in MRC-5 cells using fluorescence microscopy. It was found that the conjugate, which was designed as a potential delivery vector, was located within intracellular, perinuclear vesicles¹²⁹.

However, when considering the results of these studies, it is important to bear in mind that they are generally stand alone studies and may not have been subjected to the greatest degree of peer review and scrutiny.

1.5 Advanced imaging techniques

A wide range of techniques are available that enable visualization of the interaction and uptake of nanoparticles into cells both on *in vitro* and model systems. These include microscopy techniques ranging from electron microscopy, such as TEM that can image intracellular structures, through to live cell fluorescence imaging. In addition, the scanning probe techniques of AFM and SICM have proven to be valuable tools for studying these interactions on the nanoscale. Few studies

however have combined both fluorescence and scanning probe techniques in order to provide an overview of the interactions and uptake occurring on both the nano and micron scales.

1.5.1 Fluorescence microscopy

There are several forms of luminescence which differ in the way the system is excited. For example, in electroluminescence, the system is excited via an electric current; chemiluminescence occurs due to a chemical reaction and photoluminescence results from excitation via photons. Photoluminescence can be divided into two sub groups, fluorescence and phosphorescence. The main difference between fluorescence and phosphorescence is the duration of their luminescence. Fluorescence ends immediately when the illumination is stopped whilst phosphorescence can last for longer after the excitation has ended. Stokes first described fluorescence in 1852 and noted that fluorescence emission always occurs at a longer wavelength than that of the excitation light. In the 1930's the use of fluorophores was investigated in biological specimens for the first time.

Since there are many vibrational states in organic molecules, a number of energy bands exist, causing broad absorbance and emission spectra that are produced by the movement of electrons between these energy bands. Electrons can exist in different energy states, the ground state being a stable and low energy state. When light of a certain wavelength, known as the excitation wavelength, hits a molecule, the photons are absorbed by the electrons in the molecule. This causes the electrons to move from their ground state (S_0) to a higher energy level, the excited state (S_1) (Figure 1.6). Electrons only remain at this higher energy level for a very short period of time and some of the energy of the electron is lost by thermal processes such as non radiative heat loss. The electrons then leave this excited state and lose the remaining energy absorbed, returning to the ground state. This energy is emitted as fluorescent light and it has less energy, and therefore a longer wavelength than the excitation light. This change in wavelength is known as Stokes shift and as the Stokes shift value increases, it become easier to separate excitation from emission light through the use of fluorescence filter combinations. The absorption and emission of energy can be seen as specific characteristics of a molecule^{130, 131}.

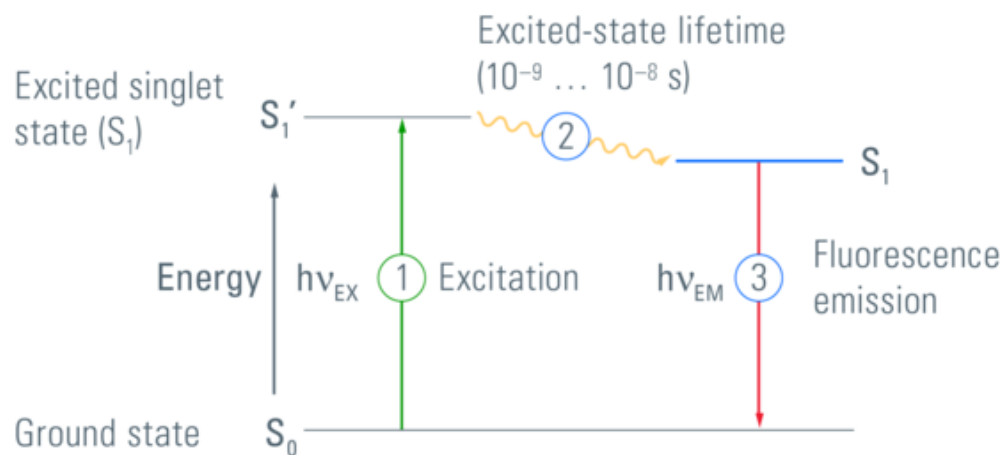


Figure 1.6: Jablonski diagram showing the movement of electrons between the different energy levels involved in fluorescence.

Fluorescence imaging can be used qualitatively and quantitatively, and several different fluorophores can be used simultaneously, as long as they vary in their excitation and emission wavelengths. In addition, colocalization and interaction studies can be performed using fluorescence, along with measurements of ion concentrations and observation of cellular processes.

Fluorophores are molecules that when excited by specific wavelengths of light will emit light of another wavelength. The likelihood of a particular fluorophore absorbing a photon of the excitation light is known as the extinction coefficient. Larger extinction coefficients indicate that the absorption of a photon in a given wavelength region is more likely. The quantum yield denotes the ratio of the number of photons emitted compared to those absorbed (usually 0.1-1)¹³¹. Quantum yield values are always below one due to the loss of energy through non-radiative pathways, such as heat or a photochemical reaction, rather than the re-radiative pathway of fluorescence. Extinction coefficient, quantum yield, intensity of the light source and fluorescence lifetime are all important factors that contribute to the fluorescence emission. The development of brighter, more stable fluorophores has contributed to the widespread use of fluorescence microscopy for the study of cells and cellular processes^{131, 132}.

In a fluorescent microscope, light is provided either by a laser as a monochromatic light, or from a bright and powerful light source such as a mercury-vapour or xenon arc lamp. The light passes through a fluorescence filter cube containing three main

components, the excitation filter, dichromatic mirror and emission filter. The excitation filter is usually a short pass filter that transmits short wavelengths of light, or a band pass filter that transmits a band of wavelengths and blocks longer and shorter wavelengths. This selects the wavelength of light which can excite the fluorophore in the sample. Narrower band pass filters are useful to help to separate fluorophores with similar characteristics¹³⁰. The dichromatic mirror is usually a long pass filter that transmits long wavelengths and reflects short wavelengths of light towards the sample. The mirror is tilted at 45° with respect to the incoming excitation light and reflects the light through the objective and onto the sample. Excitation light that is reflected by the specimen is of a short wavelength and is not transmitted through the dichromatic mirror so will be blocked. The emission filter is used when emitted light from fluorophores in the sample is gathered by the objective. The emission filter only allows light of a certain wavelength to transmit, i.e. the light emitted by the sample. Since fluorophores emit light of a longer wavelength than the excitation light, the emitted light passes through the dichromatic mirror and towards the detector. In most microscopes, the excitation and emission filters and dichromatic mirror are incorporated into an optical cube which is mounted on a revolving mechanism so that multiple cubes are available to enable a range of fluorophores to be studied in one sample (Figure 1.7)¹³³.

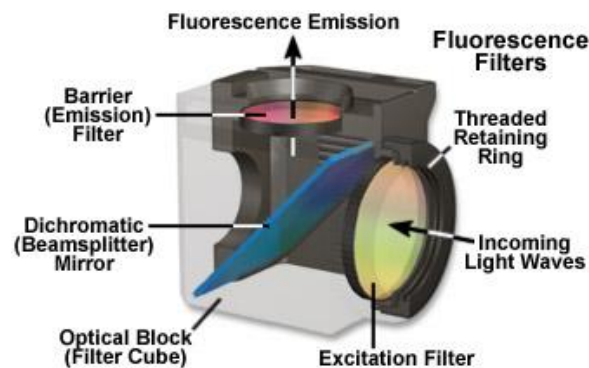


Figure 1.7: Basic set up of a filter cube indicating the excitation and emission filters and the dichromatic mirror¹³³.

The quality of the detector used is one of the key parameters in obtaining the highest resolution image possible since the resolution partly depends on the number of photons detected. Widefield microscopes usually use a charge coupled

detector (CCD) which can collect photons from the whole image, whilst confocal systems use photomultiplier tubes. This is because the pinhole restriction used to obtain high resolution images in confocal microscopy limits the number of photons that can be detected. The sensitivity of the detector depends on the detection limit and the quantum efficiency, which is the percentage of photons collected by the detector^{131, 134}. Improving the signal to noise ratio, i.e. increasing the number of photons detected above background noise helps to improve image quality and increases the precision of any measurements performed^{131, 135}. Figure 1.8 shows fluorescent beads in a low background (A) and a high background (B) and indicates that when fewer photons are collected above the background level, the image produced (C) is of a lower quality and contrast and measurements of fluorescence intensity are less precise¹³⁵.

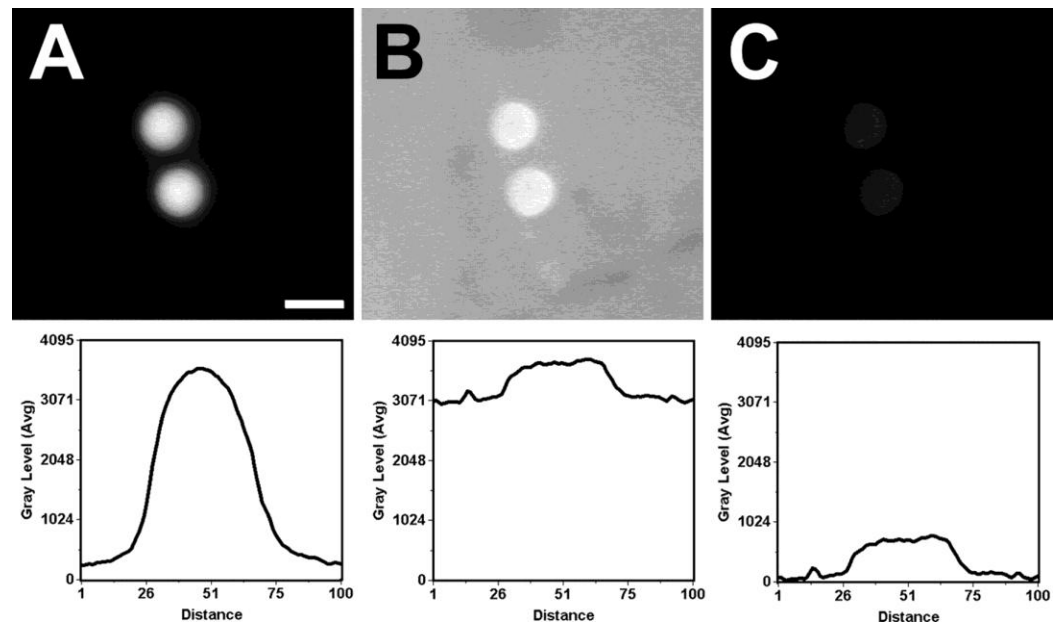


Figure 1.8: A-C are images of 6 μ m fluorescent beads obtained using a widefield microscope. (A) Fluorescent beads mounted in PBS with minimal background fluorescence, (B) shows the same beads mounted in PBS containing a fluorophore with the same spectral characteristics as the fluorophore in the bead to show effects of increased background and (C) shows image (B) after background subtraction¹³⁵.

A wide range of fluorescent microscopes have been developed beginning with simple widefield systems and advancing through to confocal systems that help improve image quality by excluding out of focus light using pinholes. Finally, more recently, the development of super resolution microscopy techniques has overcome

limits imposed by the diffraction barrier of light, thereby further increasing resolution and these are introduced in detail in Chapter 6. In addition to improvements in microscope technology, other advances have been made in the post image acquisition analysis techniques such as deconvolution¹³¹.

1.5.1.1 Deconvolution

Every light source used in fluorescence microscopy will emit scattered light above and below the plane of the object itself (Figure 1.9)^{130, 135}. Deconvolution is a technique that is used to remove this out of focus fluorescence information and therefore to produce higher quality images with a better contrast. It is the process of applying mathematical algorithms to the data and using these to reassign out of focus fluorescence to the most likely point of source^{131, 136}.

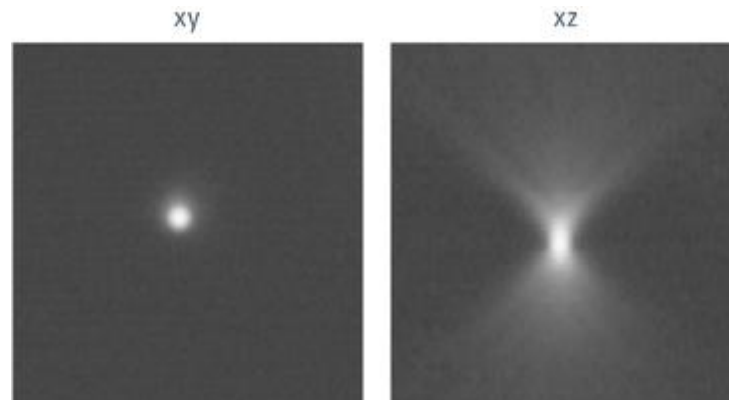


Figure 1.9: Representation of the scattered light in the z plane from a point shaped object¹³⁷.

Instead of the computational processing that is required using deconvolution for images obtained using widefield microscopes, confocal laser scanning microscopy (CLSM) uses pinholes to exclude out of focus fluorescence¹³⁰. However, a high light intensity is required due to the small confocal volume needed to obtain the highest resolution¹³⁶. The benefit of this sharper image that can be achieved using CLSM is therefore offset by a considerable disadvantage due to the high energy from the laser light source which can lead to fluorescence bleaching and cell damage (phototoxicity). Conventional widefield fluorescence microscope systems have advantages over CLSM since with the use of a lower intensity light, cells may be less damaged and photobleaching is less of an issue, however the resolution is worse.

Deconvolution is therefore useful when applied to widefield microscopy since it provides a convenient and fast method by which to improve the image contrast.

There are two main approaches to deconvolution, known as iterative restoration and nearest neighbour deconvolution. Iterative restoration is more time consuming since it reassigns out of focus fluorescence information to the point of source but it retains all of the image information. Nearest neighbour deconvolution is a subtractive technique which can lead to a loss of signal^{130, 134}. Both forms of deconvolution require the use of point spread functions (PSFs). These describe how the light from the point shaped object is spread out in the optical path. They are the result of all the influences that distort the imaging of a single sphere which, when imaged will not produce a perfect representative image due to the problem of scattered light and limits of the microscope. These influences include the wavelength of light, the objective and its numerical aperture and immersion media amongst others^{130, 132, 137}. PSFs can be measured or calculated for each wavelength and objective combination. Each different wavelength requires a separate PSF since light of different wavelengths spreads differently. These PSFs can then be applied to the images obtained to reassign the out of focus information resulting in a clearer image.

1.5.2 Atomic Force Microscopy (AFM)

Advanced scanning probe techniques such as AFM and SICM have only been developed since the 1980s. The field of scanning probe microscopy began with a stylus profiler developed by Schmalz in 1929 which, in a similar way to AFM consisted of a probe on the end of a cantilever which was used to generate an image of the profile of a surface¹³⁸. In the 1970s, Young developed a non contact mode of this technique introducing the use of piezoelectric ceramics to the field in order to provide control over the tip-sample distance. A major advance was the development of the scanning tunnelling microscope by Binnig and Rohrer in 1981, which used a metal wire tip to image the surface of a sample. However, it was limited to the use of conducting samples¹³⁸⁻¹⁴¹. Binnig and others went on to develop AFM which led to a widespread increase in the use of scanning probe microscopy since it is not limited to conducting samples. Further advances in different modes of imaging have increased the range of samples that can be

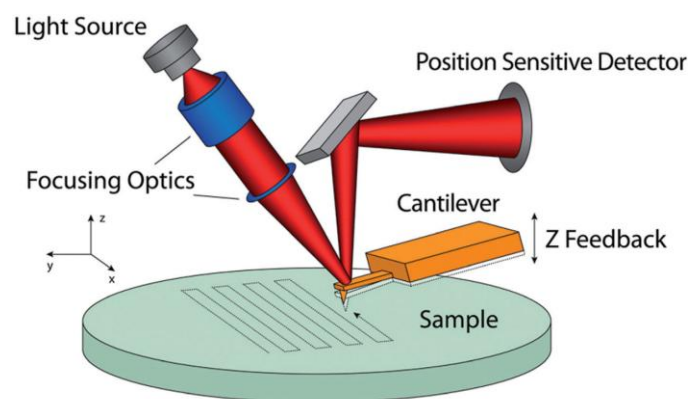
visualized using AFM^{138, 142, 143}. Finally, SICM was first introduced by Hansma in 1989 and major developments in the technique have been achieved by the Korchev and Klenerman groups at Imperial College London and Cambridge University. Although it is not as widely used as AFM, it has certain advantages that are discussed later and is increasing in popularity due to the production of commercially available systems^{144, 145}.

AFM is a scanning probe technique that uses the force between the tip and the sample to produce an image. It has many different applications including imaging of a wide range of samples such as supported lipid bilayers¹⁴⁶, polymers films¹⁴⁷, and the imaging of individual molecules such as proteins and DNA on the nanoscale¹⁴⁸. In addition, it can be used to investigate the forces of interaction between molecules via the use of functionalised tips coated with a certain material, for example ligands and receptors¹⁴⁹. AFM has the potential for molecular and atomic level resolution imaging of some samples and it can also be used to investigate the characteristics of the materials in the sample¹⁵⁰. There are a number of different modes that can be used when applying AFM to the imaging of a sample surface. These include contact mode, where the tip is raster scanned over the surface of a sample, and tapping mode where the tip is oscillated at a resonant frequency above the sample surface and the tip then gently taps the sample, reducing damage to the sample and tip^{151, 152}. Another benefit of AFM is that samples can be imaged in different environments, for example air, vacuum or liquid. This ability to image in the liquid environment gives AFM an advantage over other nanoscale microscopy techniques, for example electron microscopy such as SEM and TEM, which cannot be used for imaging of biological samples in their native environments¹⁵³. One of the main limitations of AFM is the difficulty in imaging very rough samples since the shape of the tip can hinder its ability to fit in between rough areas on the sample surface¹⁵⁰.

In AFM, a cantilever, with a sharp probe on the end, usually made of silicon or silicon nitride traces over the surface of the sample, providing a topography image of the sample surface. A laser shines onto the back of the cantilever where the tip is located, and as the tip moves over the surface, a change in the height of the sample causes the cantilever to deflect, changing the position of the reflected laser beam on a photodiode consisting of four quadrants^{150, 153-155}. The use of a reflected laser

beam helps to amplify the signal and the vertical movement in the cantilever is calculated by measuring the difference in voltage between the upper and lower quadrants of the photodiode, whilst any lateral movement of the tip is measured as the difference between the left and right quadrants^{138, 150, 153}. These measurements in x, y and z are combined in order to produce an image of the surface of the sample¹⁵⁰.

The sharpness and shape of the tip is one of the key parameters in achieving a high resolution AFM image. This is a common problem with all scanning probe techniques since the AFM tip or, for example, the glass pipette used in SICM, cannot be infinitely sharp. The size of the tip is usually large compared to many of the features being imaged, therefore it may not be able to reach and image the surface of a sample located in between or close to high regions of the sample. This is due to inhibition of the lateral movement of the tip close to a tall feature in the sample. The cantilever generally has a low spring constant, enabling fine control of the force between the tip and sample. Positioning of the cantilever and tip is controlled by ceramic piezoelectric transducers which have the ability to control positioning with an extremely high degree of accuracy by virtue of their ability to change shape when a potential difference is applied to opposite faces of the crystal. The deflection of the cantilever is influenced by Van der Waals forces between the tip and the sample and as the tip touches the sample surface, repulsive forces dominate. The tip is kept in contact with the sample and topography images are obtained via these close range repulsive interactions^{138, 150, 153-155}.



Unrestricted Optical Access from Below the Sample Plane

Figure 1.10: Basic principle of AFM¹⁵⁵.

Scanning of soft samples such as lipid bilayers can be performed in a liquid environment using the tapping mode technique of AFM. In this mode, the sample is gently tapped with the AFM tip rather than the tip being raster scanned across the sample surface as in contact mode. In tapping mode AFM, the cantilever is oscillated at or near its resonant frequency using a piezoelectric crystal. As the tip moves over the sample surface, changes in oscillation occur. As the tip approaches the surface of the sample, the amplitude of oscillation is decreased due to the interaction forces such as Van der Waals between the sample and tip. These changes in the oscillation amplitude are measured and feedback mechanisms are used to adjust the separation between the tip and the sample in order to maintain a constant amplitude and force and to produce the image of the sample^{138, 155}. Tapping mode AFM applies a low force from the tip onto the sample. In addition, since tapping mode AFM does not 'drag' the tip over the surface, this can prevent the tip sticking to the sample, reducing the effect of frictional and adhesive forces. In tapping mode AFM in liquid, the cantilevers normal resonant frequency is reduced. The entire fluid cell is oscillated in order to lead to oscillation of the cantilever¹⁵⁵.

By employing a liquid environment and the tapping mode technique, very low forces can be used during imaging in order to avoid damaging samples and it also enables hydrated bilayers, used as models of the cell membrane, to be imaged¹⁵⁶⁻¹⁵⁹. AFM has been used to image cells but with limited success for a number of reasons. Cells are relatively high when considering movement in the z direction of the cantilever, compared to some other samples such as polymer films and lipid bilayers so it can be difficult to image the entire cell and there is a high chance of tip contamination^{150, 160}. The other main problem is that since the tip exerts a force on the cell, it can lead to cell membrane deformation and rupture leading to reduced resolution and distorted images^{150, 161}. However, one benefit of this is that it has been used to image features below the cell membrane such as the cytoskeleton and other subcellular structures^{150, 162}.

1.5.3 Scanning Ion Conductance Microscopy (SICM)

SICM is a non contact scanning probe technique that uses changes in the ion current flowing through a nanopipette to track sample topography^{142, 163}. It is useful especially in the imaging of soft biological samples such as cells because they can be imaged in a non contact manner in a suitable medium to maintain cell survival. An electrolyte solution such as PBS is used to fill a hollow glass pipette and also to cover the sample (e.g. a cell monolayer). A bias voltage is applied through a silver chloride electrode in the pipette holder, creating an ion current between the solution in the pipette tip and the solution that the sample is contained in. As the pipette tip approaches the sample surface, the flow of ions through the pipette is partially blocked, leading to a reduction in the ion flow. The feedback control mechanism withdraws the pipette from the sample to maintain a constant current. Therefore, measurement of this ion current provides the non-contact element of SICM since the set point for pipette withdrawal is reached before the pipette touches the sample (Figure 1.11). In the first mode of SICM that was developed, automatic feedback control moved the pipette up or down in order to keep the current flowing through the pipette constant and a constant tip-sample distance was maintained¹⁶⁴.

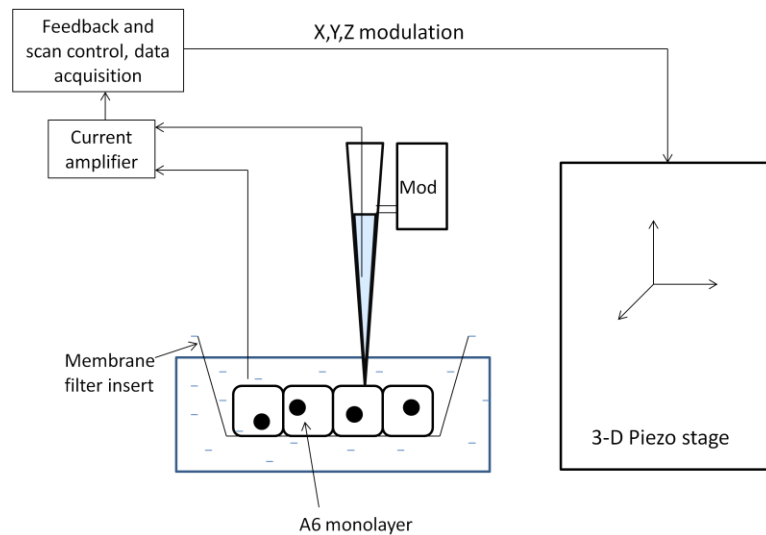


Figure 1.11: Layout of typical SICM equipment adapted from¹⁶⁵. An A6 monolayer is grown on a membrane filter which is mounted on a 3D piezo stage controlled by the scan control and feedback systems. The modulated glass pipette scans the monolayer to produce images of the topography of the membrane.

Hopping probe ion conductance microscopy (HPICM) is a technique that increases the height of the sample that can be imaged and it can be used to image samples containing significant height differences. The pipette tip is withdrawn to a point high above the sample surface and it approaches the sample from above, avoiding any problems caused by the tip colliding sideways with the sample (Figure 1.12)¹⁶⁴. When the pipette is far away from the sample, ion flow through the pipette is uninterrupted and the ion current is measured at its maximum. When the tip approaches the sample, the ion current flow reduces due to obstruction of the pipette by the sample, and when it reaches a given threshold (usually 0.25-1%), the tip withdraws from the sample before touching it¹⁶⁶⁻¹⁶⁹. The position of the z dimension actuator is recorded as the height of the sample at that point, creating a topography image of the sample surface¹⁶³. The decrease in ion current can be detected when the pipette tip is approximately one radius distance away from the sample surface and the resolution of SICM is therefore roughly equal to the internal radius of the pipette opening^{142, 170}. HPICM has been shown to have the ability to image fine cellular processes such as axons without causing damage to the cell. It has also enabled the development of a fast pre scan mode where the image is divided up into squares and the corners of each square are measured for roughness to determine what resolution to scan the square at. This enables an increase in the imaging speed since flat, featureless areas can be scanned quickly¹⁶⁴.

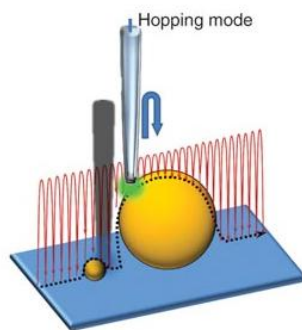


Figure 1.12: Schematic representation of the hopping mode of SICM¹⁶⁴.

In addition to topography imaging, SICM can also be used for investigation of cellular functions. This has been achieved in a number of different ways including using the tip to deliver molecules,¹⁷¹⁻¹⁷³ and combining it with an electrode enabling measurement of chemical changes on a membrane (e.g. ion channels)¹⁷⁴.

1.5.4 Scanning surface confocal microscopy (SSCM)

SICM has been combined with a number of other techniques including AFM¹⁷⁵, patch-clamp recording¹⁷⁶, and confocal microscopy¹⁷⁷. SSCM is a combination of SICM and confocal microscopy which allows the simultaneous acquisition of a topography image plus a fluorescence image that is in focus at the pipette tip. This enables identification of fluorescent structures on the cell surface e.g. labelled clathrin and caveolin endocytic pits, which can be linked to indentations in the membrane observed using topography imaging¹⁷⁸. It has also been used to look at the endocytosis of various nanoparticles and virus like particles into cells¹⁷⁷.

In SSCM, a confocal microscope is combined with the scanning pipette system^{1, 177}. The sample stage moves up and down in the z direction and the pipette is scanned in x and y. The laser is passed up a high numerical aperture objective (100x, 1.3N.A) so that it is focussed at the tip of the nanopipette and a pinhole is positioned at the image plane so that the confocal volume is just below the pipette. The 100x objective is mounted on a piezo and this allows the laser to track the pipette tip as it moves up and down over the sample so that wherever the pipette tip is in the z direction, the fluorescence image will be in focus at that point (Figure 1.13)¹⁷⁸.

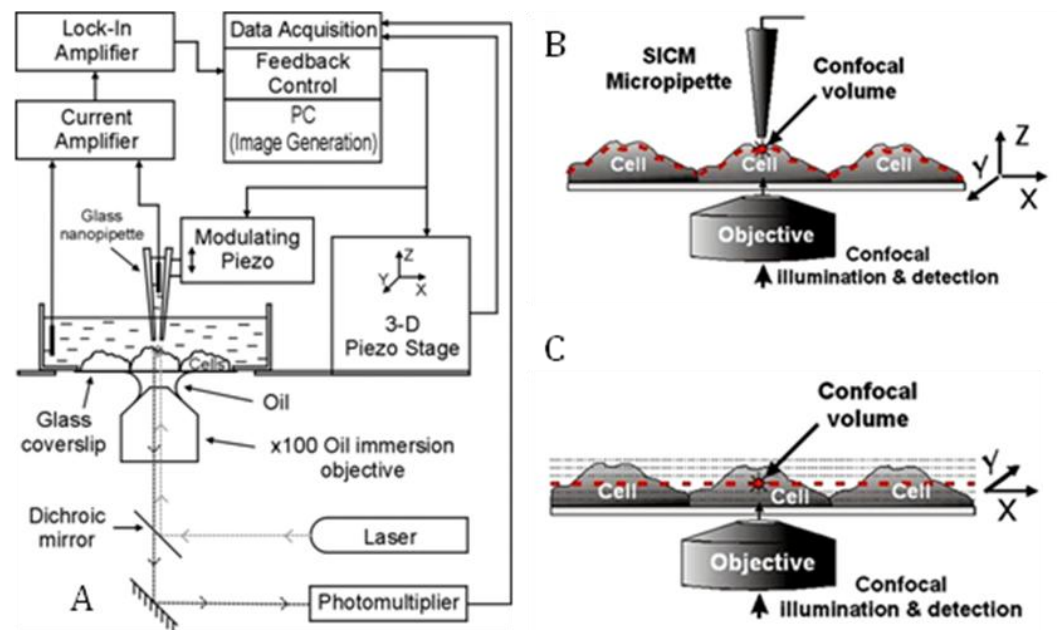


Figure 1.13: (A) SSCM set up, (B) Dotted line shows position where optical fluorescent image obtained as pipette moves over sample in SSCM, (C) Dotted line shows fluorescence image from same sample when using confocal alone¹⁷⁷.

1.6 Aims and Thesis outline

The huge diversity of nanoparticles that can be produced makes it difficult to definitively link a certain parameter to an effect on cellular uptake, especially because effect is likely to vary between cell line and environment. However, some parameters, especially charge, do seem to have broadly similar effects on many cell lines and this work aimed to further investigate this area via the production of nanoparticles with varying charge. In addition, the effect of nanoparticle conjugation to the cationic cell penetrating peptide Tat, was used to investigate the role of the peptide structure and conformation in the uptake of nanoparticles versus the effect of a positive charge alone.

AFM was used to investigate the interaction of polyacrylamide nanoparticles with a supported lipid bilayer and SICM/SSCM were used to visualize the interaction of silica nanoparticles with the membrane of MRC-5 cells. Uptake into MRC-5 cells for both types of nanoparticle was investigated using widefield fluorescence microscopy to identify the subcellular localization and to perform quantitative measurements of uptake. Chapters 2 and 3 introduce the synthesis routes and characterization of the nanoparticles. Chapter 4 investigates the interaction of polyacrylamide nanoparticles with a positive and negative charge or conjugated to Tat peptide, with a model cell membrane using AFM. It then goes on to visualize the interaction of positive and negatively charged silica nanoparticles with the cell membrane of MRC-5 cells using SICM and SSCM. The effect of charge and peptide conjugation on cellular uptake is further discussed in Chapter 5 through the use of fluorescence microscopy to visualize the intracellular location and to quantify the uptake of the nanoparticles. In the final chapter, the current limitations of the techniques used and future potential in imaging the cellular uptake of nanoparticles is discussed.

Chapter 2 – Materials, Methods and Instrumentation

2.1 Materials

Acrylamide, Dulbecco's Modified Eagle Medium (DMEM), 10x trypsin, dioctyl sulfosuccinate, N,N,N',N'-tetramethylethylenediamine (TEMED), 3-(acrylamidopropyl)-trimethylammonium chloride (ACTA), Ammonium persulfate (APS), tetraethylorthosilicate (TEOS), aminopropyltriethoxysilane (APTES), magnesium chloride, 28% Ammonia water and Tris buffer were obtained from Sigma Aldrich. N,N-methylene bisacrylamide and Brij 30 were obtained from Fluka Analytical. Sulfo-succinimidyl-4-(N-maleimidomethyl) cyclohexane-1-carboxylate (Sulfo-SMCC) was obtained from Calbiochem. Hexane and absolute ethanol were obtained from Fisher Scientific. Dipalmitoyl phosphatidylcholine (DPPC) was obtained from Avanti Polar Lipids. Tat peptide modified with a cysteine residue at the N terminus and with a C terminal acid group (CGRKKRRQRRR-COOH) with a purity of >95% was synthesised by Cambridge Research Biochemicals. 10kDa Alexa 488 dextran and Alexa 488 succinimidyl ester were obtained from Invitrogen. N-trimethoxysilylpropyl-N,N,N-trimethylammonium chloride (TMAC) was obtained from Gelest. N-(3-aminopropyl) methacrylamide hydrochloride (AMPA) was obtained from Polysciences Inc.

2.2 Instrumentation

2.2.1 Dynamic Light Scattering

Dynamic light scattering (DLS) is a particle sizing technique that has a wide range of detection in the nanometre size region, in some cases as low as 1nm. It is therefore well suited to the measurement of nanoparticle size and provides rapid, high throughput measurements.

DLS measurements are based on the light scattered from particles as they diffuse under Brownian motion. Brownian motion is induced by the bombardment of the particles by solvent molecules that are moving due to their thermal energy. Light scattering is wavelength dependent so the light source used is a laser. A constant temperature is also required in order to remove the effects of convection currents that could lead to non random motion. When the laser is shone through the suspension of particles, the light is scattered by the particles and the intensity of the

scattered light fluctuates at a rate that is dependent on the size of the particles. Small particles cause the light to fluctuate faster than larger particles. DLS measures these time dependent fluctuations in scattering intensity and uses it to determine the translational diffusion coefficient which is converted to particle size using the Stokes-Einstein equation¹⁷⁹.

The particle size reported is that of a sphere that scatters light identically and has the same translational diffusion coefficient to the observed particle. The size reported is also known as the hydrodynamic diameter since it refers to the size of the particle in a fluid. This often differs from the particle size obtained using techniques such as electron microscopy since it is affected by the presence of any surface structures, along with the concentration and type of ions in the suspension medium. Ions in the suspension medium and the total ionic concentration can affect the particle diffusion speed by changing the thickness of the electric double layer. A low conductivity medium produces an extended double layer of ions around the particle which reduces diffusion speed leading to a larger apparent hydrodynamic diameter. Higher conductivity medium suppresses the electrical double layer and therefore decreases the measured hydrodynamic diameter.

The Zetasizer Nano ZS uses a technology known as Non-Invasive Back-scatter (NIBS) where the detector that receives intensity fluctuation information is located at a 173° angle from the sample cuvette. NIBS provides a higher degree of sensitivity of measurement and allows analysis of samples with a higher concentration than for typical DLS arrangements, where the detector is placed at 90°. When using backscatter detection, the laser does not pass through the whole sample and this reduces the effect of multiple scattering, where light scattered by a particle is also scattered by others. It also means that the effect of large contaminants such as dust is removed because they scatter light mainly in the forward direction.

The instrument consists of a laser used to illuminate the sample contained in a cuvette and a detector that measures the scattered light at 173°. The intensity of scattered light must be within a specific range for the detector to successfully measure it. If too much light is detected, the detector becomes saturated. An attenuator is used to reduce the intensity of the laser source and therefore the

intensity of scattering if required, or to increase it if particles are very small or sample concentration is low. To measure particle size, the scattering intensity signal from the detector is passed to the correlator which compares scattering intensity at successive time intervals to derive the rate at which the intensity is varying. This information is passed to the computer where the data is analysed and size information is determined. The size distribution obtained is a plot of the relative intensity of light scattered by particles of different diameters, therefore it is known as the intensity distribution. The intensity distribution can be skewed by the presence of larger particles, for instance, a 50nm particle scatters light to an extent one million times larger than a 5nm particle. Therefore, while intensity distributions are useful for identifying the different populations of particles present in the sample, a number or volume distribution is used to look at the relative importance of each of these populations.

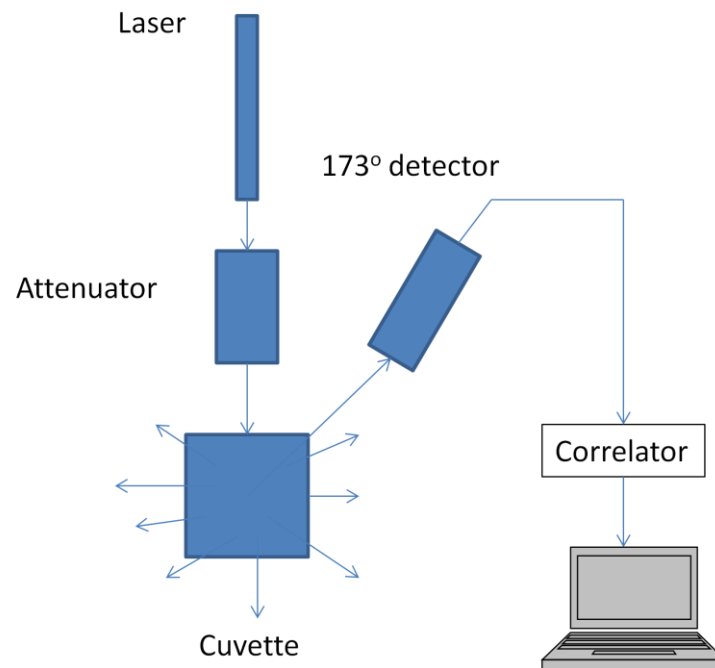


Figure 2.1: Typical setup of the Zetasizer Nano ZS for size determination using NIBS at 173° to measure particle diameter¹⁷⁹.

2.2.2 Zeta potential

The stability of colloidal systems is determined by the balance of repulsive and attractive forces. Zeta potential is the overall charge a particle acquires in a particular medium and depends on the surface chemistry of the particle and the

dispersant. Surface charge can arise from ionisation, ion adsorption and ion dissolution. In terms of the dispersant, a change in pH or ionic strength of the dispersing medium will affect zeta potential. The magnitude of the zeta potential gives an indication of the potential stability of the system and suspensions are stable when they have a zeta potential of greater than $\pm 30\text{mV}$ since particles tend to repel each other¹⁸⁰.

The layer surrounding a particle dispersed in liquid consists of two parts. These are an inner region, known as the Stern layer, where ions associate strongly with the particle. The second, outer layer is a region where they are less firmly associated. Within this second, diffuse, layer, there is a notional boundary inside which the strongly associated ions and the particle form a stable entity. This means that when the particle moves, the associated ions also move. The ions that are beyond this boundary remain with the bulk liquid phase. The potential at this boundary is the zeta potential.

During zeta potential measurements, an electric field is applied across a sample in a sample holder consisting of gold plated electrodes in a folded capillary cell. When subjected to an electric field, the velocity of the particles is determined by the charge associated with the particle, the viscosity of the medium and the applied field. Charged particles suspended in the liquid move towards the electrode of opposite charge with a velocity dependent on a number of factors including zeta potential. The velocity is measured using a technique known as M3-PALS (Phase Analysis Light Scattering) which allows calculation of electrophoretic mobility and from this, zeta potential. PALS is a variation of laser Doppler velocimetry (LDV) which measures the particle mobility generated when a potential is applied, using the frequency shift of light caused by particles moving in the cell^{180, 181}.

In zeta potential instruments, a single laser beam is split to provide an incident and reference beam. The incident beam passes through the sample and the scattered light is detected at 13° , while the reference beam is diverted around the cell. When an electric field is applied to the cell, any particles moving through the capillary cell cause the intensity of light detected to fluctuate with a frequency proportional to the particle speed and this information is passed to a digital signal processor. The scattered light from the incident beam is combined with the reference beam to

create the intensity variations. The software produces a frequency spectrum from which the electrophoretic mobility and the zeta potential are calculated. The intensity of the detected, scattered light must be within a specific range for the detector to successfully measure it. This is achieved using an attenuator, which adjusts the intensity of light reaching the sample. To correct for any difference in the cell wall thickness and dispersant refraction, compensation optics are installed to maintain alignment^{180, 181}.

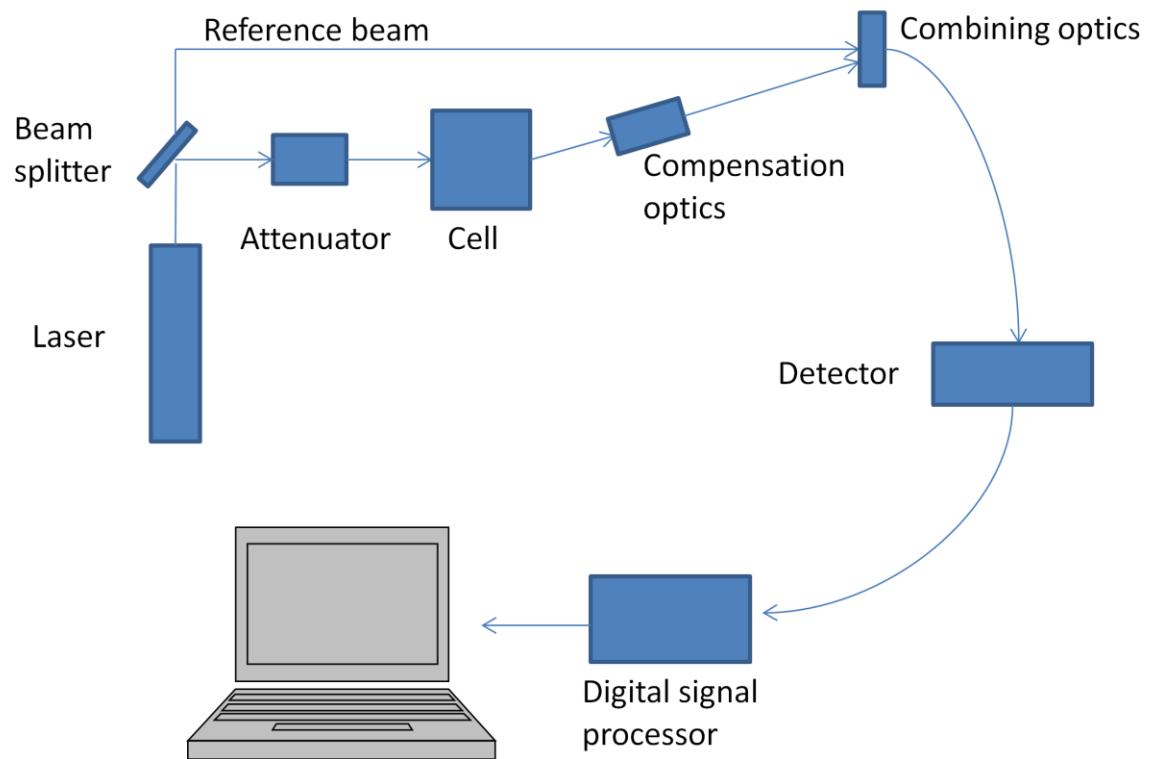


Figure 2.2: Typical setup of a Zetasizer for measuring zeta potential¹⁸⁰.

2.2.3 Disc Centrifuge

The CPS disc centrifuge is a particle sizing tool that can be used to size particles ranging from 3nm to 75 μ m. It is based on the principle of differential centrifugal sedimentation. In addition to the measurement of the size of particles with a density greater than that of water, for example gold or iron, the disc centrifuge can also be used to determine the size of particles such as liposomes that have a density similar to, or less than that of water, using the low density disc¹⁸².

It consists of a hollow, optically clear disc and a short wavelength monochromatic light of 405nm. Particle size is determined based on the time taken for the particles

to sediment through a sucrose gradient in the disc and to pass the light beam and detector located on the outside edge of the disc (Figure 2.3). When a sample is injected into the disc, it strikes the back of the disc and forms a thin film which spreads as it accelerates radially toward the surface of the fluid. When the sample reaches the surface of the fluid within the disc, it spreads over the surface and because of its lower density it initially floats on the higher density fluid. While the dispersion media for the sample then remains on the surface of the gradient, the sample particles begin to sediment through the gradient within the disc at a rate that is dependent on a number of factors including their size and density, as well as the density of the gradient fluid¹⁸².

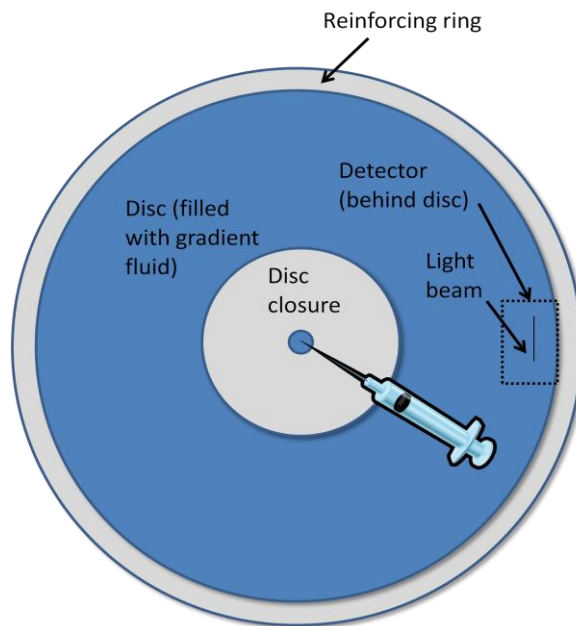


Figure 2.3: The design of the CPS Disc Centrifuge.

2.2.3.1 Differential Sedimentation

Sedimentation is the settling of particles under the influence of gravitational or centrifugal forces. It is a well known and reliable method of particle size analysis, and the disc centrifuge uses centrifugal sedimentation to size particles. Particles settle in a fluid under a gravitational field according to Stokes Law, at a rate that is proportional to the square of the particle diameter. Particles that differ in size by only a few percent will therefore sediment at significantly different rates. The time taken to reach the detector is used to calculate the size of the particles after

calibration with a standard of a known size. The technique is known as differential sedimentation because only a small part of the sample is being measured at any one time. Mie theory light scattering calculations are used to convert the intensity readings into a mass distribution¹⁸³.

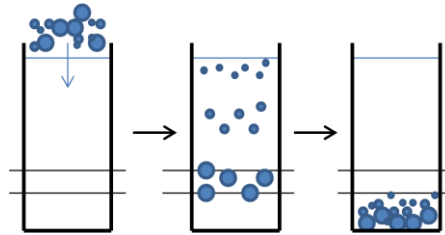


Figure 2.4: Differential sedimentation.

2.2.3.2 Stokes law of sedimentation

Stokes law of sedimentation determines the rate of sedimentation of spherical particles through a viscous medium in a gravitational field. In the disc centrifuge, gravitational acceleration is replaced with centrifugal acceleration which allows for the faster sedimentation of small particles. It describes how the drag force on a spherical particle moving through a fluid depends on the particle size, the difference in density between the particles and the gradient fluid, the viscosity of the fluid, and the strength of the centrifugal field, which is determined by rotational speed. In the disc centrifuge, Stokes law is used to determine the size of spherical particles by measuring the time required for the particles to settle a known distance in a fluid of known viscosity and density¹⁸³.

Stokes showed that when particles settle in a gravitational field under a certain set of conditions, the forces acting on the particle are in perfect balance and the particle immediately attains a constant velocity for the duration of the fall. The required conditions are:

1. The particle must be smooth, spherical and rigid enough not to deform due to the forces acting on it.
2. The particle must be small compared to the container of the fluid.
3. The particles in the fluid must be much smaller than the sample particle so the fluid is essentially homogenous in how it acts on the particle. If this

condition is not met, Brownian motion of small particles in the fluid can cause problems with analysis.

4. The settling speed must be slow enough that all viscous forces come from non turbulent flow.

The Stokes equation (1) shows that the sedimentation rate of the particle is proportional to the square of the particle diameter, the difference in density between the particles and fluid, the gravitational acceleration, and inversely proportional to fluid viscosity.

$$V = \frac{(D^2(\rho_p - \rho_f)g)}{18\eta} \quad (1)$$

Where:

V = sedimentation rate (cm/s)

η = fluid viscosity (poises)

ρ_p and ρ_f are the densities of the particle and the fluid respectively (g/cm^3)

g = gravitational constant (980 cm/sec^2)

D = particle diameter (cm)

Rearranging Stokes equation shows that the diameter of a particle can be determined by measuring the time (t) required to sediment a known distance (X):

$$\text{Since } t = \frac{X}{V}$$

Equation (1) becomes:

$$D = \frac{X18\eta}{(t(\rho_p - \rho_f)g)^{\frac{1}{2}}} \quad (2)$$

For a centrifuge running at constant speed and temperature, all of the parameters except time are constant during the analysis and (2) can be restated as:

$$D = \frac{K}{t^{\frac{1}{2}}} \quad (3)$$

where K is a combination of constants (density, viscosity and gravitational acceleration).

The disc centrifuge software uses the sedimentation time for a calibration standard of known diameter to determine the value of the constant, K. Each time a sample is analysed, a calibration standard run is used to determine a new value for K¹⁸³.

Inside the disc centrifuge, centrifugal acceleration replaces the gravitational field. The centrifugal acceleration increases as the particles move from the surface of the liquid towards the outside edge of the disc chamber, because the radius of rotation increases as the particles move outwards. Even though conditions within the disc centrifuge are different from sedimentation under gravity, the same equation (3) can be used to describe both processes.

2.2.3.3 Density determination

Particle density is the most critical parameter for accurate measurement of particle size using the disc centrifuge, and is a term in Stokes equation. If the density of the particle is close to that of the liquid in which it will be dispersed then it is even more important to get an accurate value of particle density. The disc centrifuge can be used to determine the density of the particles by running the sample on two different gradients e.g. a sucrose gradient in water and deuterium oxide (D₂O) which differ in density by 0.11g/cm³. The density can be changed in the procedure definition for the experiment and the files recalculated in order to get a new size distribution for each density value. The two distributions will overlap each other when the assumed particle density is correct¹⁸⁴.

2.2.3.4 Low density disc

The low density disc allows measurement of samples that have a density of approximately 1.0 g/cm³ or lower. A D₂O based gradient is used which can measure particle size down to 40nm. Unlike the normal disc, where the sample floats on the surface before sedimentation occurs, the sample is delivered to the outside edge of the disc using a special injection port into a V shaped groove in the front of the disc. In the base of this groove there are four capillary channels which lead to the outside edge of the disc chamber. When the sample reaches the bottom of the disc it spreads over the outside edge of the disc and forms a band of particles. The particles then float toward the surface during the analysis since they have a density lower than that of the gradient fluid. The particles still follow the same equations of

sedimentation but with a negative value for motion. The light source and detector are moved slightly more towards the centre of the disc for the analysis¹⁸².

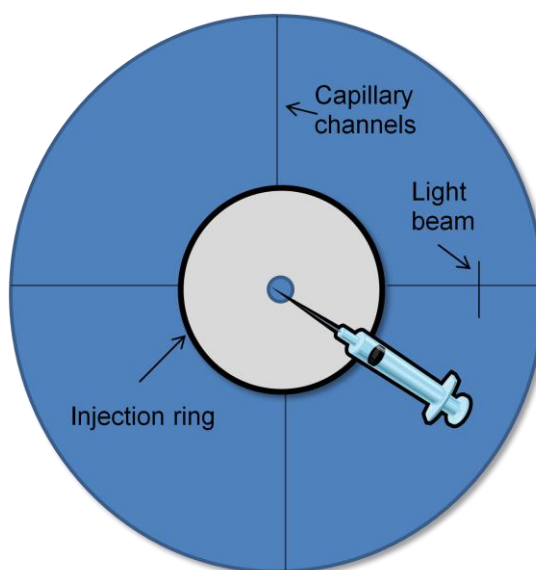


Figure 2.5: The low density disc.

2.2.4 Fluorescence

In order to enable the visualization of the nanoparticles during the uptake process and within cells following uptake, a fluorescent dye was incorporated into the nanoparticle matrix which could be visualized using fluorescent spectroscopy and microscopy. Alexa 488 conjugated to 10kDa dextran was trapped within the matrix of polyacrylamide nanoparticles. This conjugate is too large to escape the small pores in the nanoparticle matrix therefore remains within the particle, protecting the cell from any effects of the dye. For silica nanoparticles, the succinimidyl ester form of Alexa 488 was conjugated to APTES and this was incorporated into the nanoparticles as they formed. APTES is an amine functionalised silane monomer which can polymerise with other silane monomers such as TEOS so that the covalently bound dye is incorporated into the nanoparticle as it forms.

The dye used in these experiments was Alexa 488 which has a fluorescence emission wavelength of 520nm therefore emits in the green region. It was chosen because it is a bright, stable dye and the fluorescence emission intensity is not affected by pH over the range (pH 4-10) that may be encountered during cellular uptake. Alex Fluor dyes are generally hydrophilic and negatively charged, and they

have good quantum yields and long fluorescence lifetimes which helps to increase the ease of imaging and reduces problems associated with, for example, photobleaching, when attempting quantitative measurements¹⁸⁵.

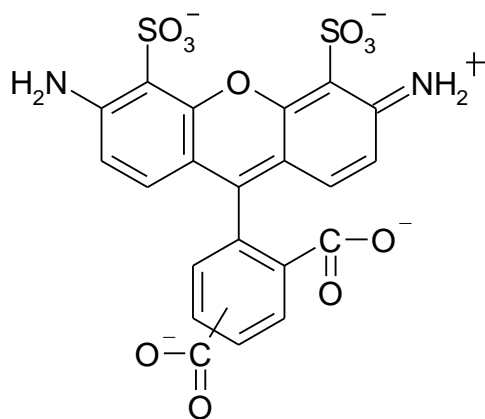


Figure 2.6: Structure of Alexa 488.

2.3 Methods -Nanoparticle synthesis

2.3.1 Polyacrylamide nanoparticles

Polyacrylamide nanoparticles were synthesised by the free radical polymerisation of acrylamide using a reverse microemulsion technique. Hexane was deoxygenated for at least 30 mins with argon. A water in oil microemulsion was prepared by dissolving the surfactants polyoxyethylene(4) lauryl ether (Brij 30) (3.08g) and dioctyl sulfosuccinate (1.59g) in deoxygenated hexane (42 ml) under argon in a round bottomed glass flask and adding the prepared aqueous phase containing the monomers. The monomer solution consisted of acrylamide (0.54g) and N,N'-methylene bisacrylamide (0.16g) in 2ml distilled water. The solution was warmed and sonicated in a water bath to dissolve the monomers. 1.975ml of this monomer solution was combined with 25 μ l of a 5mg/ml solution of Alexa 488 dextran to make a total aqueous phase volume of 2ml.

Polymerisation was initiated by the addition of 10% w/v APS, (30 μ l) and TEMED (15 μ l). The reaction proceeded for two hours under argon, after which time the hexane was removed by rotary evaporation leaving an opaque viscous residue. To remove excess reagents and dye, absolute ethanol was added and the nanoparticles were collected by centrifugation at 6000rpm/7750rcf for seven minutes. The washing procedure was repeated six times and the nanoparticles were then resuspended in ethanol which was removed using rotary evaporation to leave a powder which was stored in the fridge¹⁸⁶.

2.3.1.1 Positively charged polyacrylamide nanoparticles

To prepare positively charged polyacrylamide nanoparticles, increasing amounts of acrylamide were replaced with the positively charged monomer ACTA to produce nanoparticles containing 2, 5, 10, 15 and 20% ACTA. For example, nanoparticles containing 10% ACTA were made by combining 486.2mg acrylamide, 154mg N,N'-methylene bisacrylamide and 157.1mg ACTA which was measured out by weight since it was a viscous solution after taking into account the density of the solution¹⁸⁷.

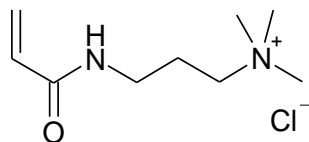


Figure 2.7: Structure of 3-(acrylamidopropyl)-trimethylammonium chloride (ACTA).

2.3.1.2 Negatively charged polyacrylamide nanoparticles

Negatively charged polyacrylamide nanoparticles were prepared via the use of N-acryloxysuccinimide. 5% of the acrylamide in the monomer solution was replaced with N-acryloxysuccinimide (56.2mg) and was incorporated into the nanoparticle matrix (473mg acrylamide and 160mg N,N-methylene bisacrylamide). Polymerisation was performed as described previously in section 2.3.1.

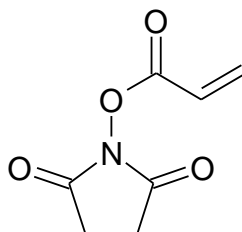


Figure 2.8: Structure of N-acryloxysuccinimide.

2.3.1.3 Amine functionalised polyacrylamide

Nanoparticles with an amine functionalisation for Tat conjugation were prepared by incorporating AMPA into the nanoparticle matrix. The monomer solution consisted of acrylamide (0.5295g), N,N'-methylene bisacrylamide (0.16g) and AMPA (27.2mg). The polymerisation was carried out in the same way as for unfunctionalised polyacrylamide nanoparticles. The amine functionalised particles were subsequently stored under argon at -20°C in order to reduce aggregation¹⁰.

2.3.2 Tat peptide conjugation

Tat peptide was conjugated to polyacrylamide nanoparticles via the heterobifunctional crosslinker Sulfo-SMCC. Crosslinkers such as SMCC contain an amine reactive NHS (N-hydroxysuccinimide) ester on one end and a sulf-hydryl-

reactive maleimide group on the other. Sulfo SMCC is a water soluble analogue of SMCC that possesses a negatively charged sulphonate group on the NHS ring, providing water solubility of at least 10mg/ml at room temperature. It is generally used to produce antibody enzyme conjugates but in this case, by modifying the peptide to include a cysteine group, and incorporating an amine group on the surface of the nanoparticle, conjugation of the peptide to the nanoparticle could be achieved. The reaction occurs in the pH range 6.5-7.5¹⁸⁸.

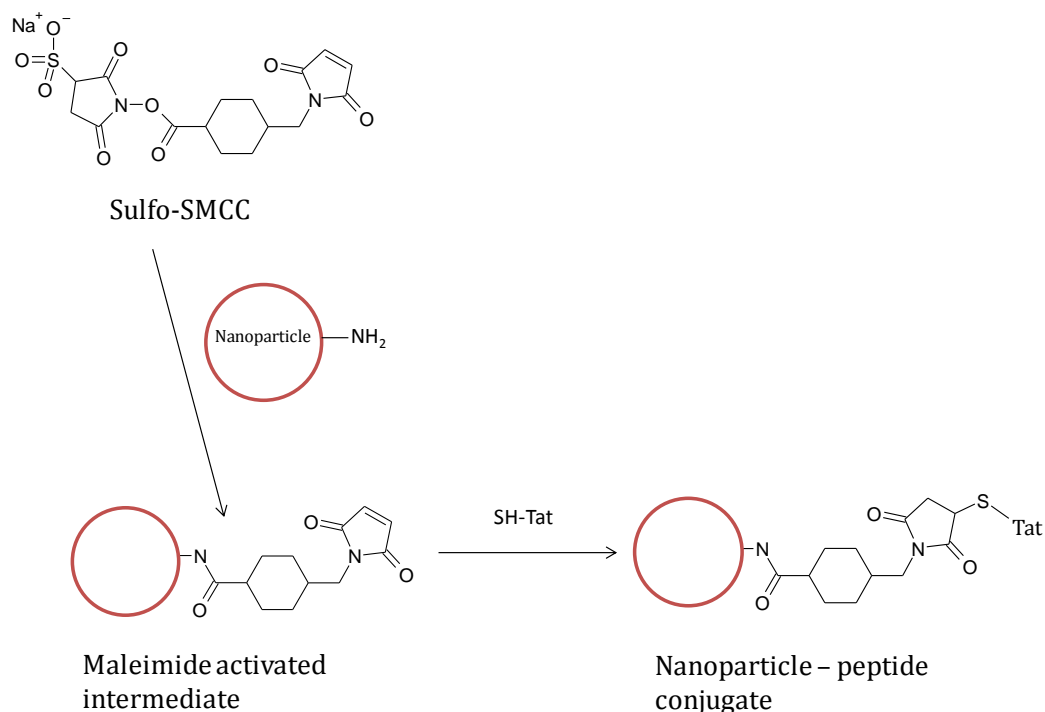


Figure 2.9: Conjugation of Tat peptide to nanoparticles via SMCC. Adapted from¹⁸⁹.

To synthesize Tat conjugated polyacrylamide nanoparticles, 100mg of amine functionalised nanoparticles were resuspended in 5ml of a 2mM solution of Sulfo-SMCC in PBS pH 7.4. The suspension was stirred at room temperature for one hour then precipitated with 7ml absolute ethanol and centrifuged at 6000rpm/7750rcf for five minutes. The supernatant was discarded and the nanoparticles were resuspended in 4ml PBS and 1ml of a 5mg/ml solution of Tat peptide (sequence CGRKKRRQRRR-COOH) in PBS. The suspension was stirred for one hour at room temperature and then overnight at 4°C. The nanoparticles were washed with 7ml

absolute ethanol and centrifuged (6000rpm/7750rcf for 5mins). The supernatant was discarded and the Tat conjugated nanoparticles were dried and stored at -20°C.

2.3.3 Silica nanoparticles

Silica nanoparticles were synthesised via a modification of the Stober method^{190, 191}.

1mg of dye (Alexa 488 succinimidyl ester) was dissolved in 90µl DMSO which was then stirred with 2ml absolute ethanol and 15µl APTES for 45 mins at room temperature.

0.15ml TEOS, 0.4ml APTES conjugated dye, 21.5ml absolute ethanol, 8.47ml water and 1.335ml 30% ammonia water were stirred together for one hour at room temperature in a small glass conical flask. To synthesize negatively charged particles, 1.35ml TEOS was added and the suspension was stirred for five hours. To synthesize positively charged particles, 1ml of TEOS was added and then after an additional 30 mins, 0.35ml of TMAC, (50% in methanol) was added and the suspension was stirred for five hours.

Nanoparticles were collected by centrifugation using a Hermle Z300 Universal Laboratory centrifuge at 6000rpm/7750rcf for 30 mins and the supernatant was discarded. The pellet was resuspended in absolute ethanol and this process was repeated twice and the nanoparticles were then left to dry fully overnight in a dessicator, then stored as a dry powder at 4°C.

2.4 Characterization methods

2.4.1 Zeta potential

Nanoparticle charge was measured using the Zetasizer Nano ZS (Malvern Instruments). Zeta potential was measured for a 2.5mg/ml suspension of polyacrylamide and a 0.25mg/ml suspension of silica in PBS, DMEM and serum free DMEM. Nanoparticles were sonicated for 15 mins prior to measurement to ensure adequate resuspension.

2.4.2 Size

2.4.2.1 Dynamic Light Scattering

Nanoparticles were sized using the Zetasizer Nano ZS. A 2.5mg/ml suspension of polyacrylamide and a 0.25mg/ml suspension of silica nanoparticles were prepared in PBS and serum free DMEM. 1ml of solution was placed in a DLS cuvette and a minimum of 12 readings were obtained. Particle suspensions were filtered using a 0.2 μ m syringe filter (polyacrylamide nanoparticles) or a 0.45 μ m filter (silica nanoparticles) before use.

2.4.2.2 CPS Disc Centrifuge

Polyacrylamide nanoparticles were prepared in a 5mg/ml solution and filtered through a 0.2 μ m syringe filter before use. Particle size was measured using a 4-12% sucrose in water gradient. Silica nanoparticles were prepared in a 0.5mg/ml suspension and filtered through a 0.45 μ m syringe filter before use. The nanoparticles were sized using an 8 – 24% sucrose in water gradient.

2.4.2.3 Statistical tests

Statistical tests performed to investigate the significance of differences between populations of nanoparticles were done using a two tailed T test with a 95% confidence interval using Microsoft Excel.

2.4.3 Fluorescence

Fluorescence intensity measurements of solutions used for DLS were taken using an excitation of 495nm for polyacrylamide (0.83mg/ml) and silica nanoparticles (0.025mg/ml) on a fluorimeter. Fluorescence emission was measured between 505nm and 550nm. In preparation for the measurement of the cellular uptake of

the nanoparticles, fluorescence intensity of both polyacrylamide (2.5mg/ml) and silica nanoparticles (0.025mg/ml) was also measured on the widefield Leica DMIRE2 microscope used for imaging cellular uptake of the nanoparticles so that any differences in particle fluorescence could be accounted for when quantifying the uptake of the different nanoparticles.

2.5 Cell culture methods

MRC-5 fibroblasts were cultured and passaged in DMEM supplemented with L-Glutamine, Penicillin, Streptomycin and 10% FCS (all obtained from Sigma, Poole, Dorset, UK) in T75 flasks (Corning Costar, Nottingham). 10x Trypsin was also obtained from Sigma and was diluted to a 1x concentration in PBS and stored in aliquots at -20°C. All reagents were purchased sterile or were sterilised before use via filtration through a 0.22µm Whatman sterile syringe filter. Cells were passaged only when 100% confluent in order to maintain an adequate growth rate when replated. When confluency was reached, the media was removed and replaced with 3 ml of trypsin at 37°C to detach the cells. After 5 minutes, cells were dislodged from the flask by gentle tapping and 7ml of DMEM was added. The cell suspension was transferred to a falcon tube and spun at 200g at room temperature for 5 mins. The supernatant was removed and the resulting cell pellet was resuspended in an appropriate volume of DMEM depending on the future use. To maintain the culture, cells were split 1:3 into new T75 flasks and if required for imaging, 0.5ml of cell suspension was added to a 35mm glass bottomed dish with 1.5ml DMEM.

2.6 Sample preparation

2.6.1 Atomic Force Microscopy

Supported lipid bilayers were formed via the vesicle fusion technique¹⁹². 1ml of DPPC, dissolved in chloroform was evaporated and resuspended in 10mM Tris HCl buffer pH 7.4. The resulting suspension was subjected to ten freeze-thaw cycles using liquid nitrogen and lukewarm water. Vesicles were formed using 21 passes through a small volume extrusion apparatus containing a 100nm polycarbonate filter¹⁹³. DPPC (T_m 41°C) was extruded at a higher than ambient temperature since it was in the gel phase at room temperature, which made it much more difficult to pass through the apparatus. The resulting vesicles were sized using dynamic light scattering and the CPS disc centrifuge.

In preparation for AFM imaging, the suspension was first diluted to 1mg/ml using 10mM Tris buffer and 100mM MgCl₂. 30µl was added to freshly cleaved muscovite mica and left for not less than four hours at ambient room temperature to form bilayers. The resulting lipid bilayers were imaged in 10mM MgCl₂ in Tris buffer (Sigma, Poole, Dorset, UK) in tapping mode using a Multimode AFM, with Nanoscope IIIa or V controller and liquid cell (Veeco, Santa Barbara, CA). Silicon nitride V-shaped AFM cantilevers with nominal spring constants of 0.58 N/m were employed (DNP cantilevers, Veeco). Typical set point was 0.6-0.7V, drive frequency 200-500mV, and scan rate 1Hz. All solutions were made with HPLC grade water and filtered through a 0.2 µm syringe filter prior to use.

Increasing concentrations of Tat peptide, 500nm-10µM, were added through the liquid cell before imaging following removal of the existing buffer solution.

Polyacrylamide nanoparticle suspensions were prepared at concentrations of 1, 10, 25 and 100µg/ml. All suspensions were made using HPLC grade water and were sonicated for at least 15 minutes before use. Before addition to the bilayer, suspensions were filtered through a 0.2µm syringe filter.

Before any analysis was performed on the images, all images were flattened (first order) using the Nanoscope Analysis software. Following this, section analysis was performed by drawing a line across certain features of interest in order to obtain a cross-section of the area of interest. This was used to gain quantitative information about changes in bilayer height following exposure to nanoparticles and peptides.

Further quantitative analysis was then performed using the bearing analysis function. This provided information about changes in the bilayer coverage following exposure to the peptide and nanoparticles. Bearing analysis is a method of plotting and analyzing the distribution of surface height over a sample. It reveals how much of a surface lies above or below a given height, therefore by selecting a threshold just above the mica surface; it is possible to measure the percentage of the image formed by the bilayer. It is also possible to remove the small percentage contributed by the nanoparticles by excluding very high features from the analysis. It is a better technique to use than surface roughness because that only represents the statistical deviation from an average height.

2.6.2 Scanning Ion Conductance Microscopy

Cells were washed twice with serum free DMEM (Sigma, Poole, Dorset, UK) and left for one hour at 37°C. 100µg of silica nanoparticles was added to the cells in serum free DMEM and incubated for 30mins at 37°C. The cells were washed three times with PBS and fixed using 100% ice cold methanol (Fisher Scientific, Loughborough, UK) at -20°C for 10 minutes before being washed with PBS and stored in the fridge before imaging. Nanoparticles were filtered through 0.45µm syringe filters before use.

Nanopipettes of approximately 50nm internal diameter were pulled from borosilicate glass capillaries of outer diameter 1mm and inner diameter 0.5mm (Intracell) using a laser based Brown-Flaming puller (P-2000, Sutter Instruments). The nanopipettes were filled with PBS filtered through PVDF 4mm, 0.22µm pore size Millex syringe filter (Millipore) using a Microfil 34AWG pipette filler (World Precision Instruments). The fixed cell samples were immersed in sterile filtered PBS. The pipettes displayed resistances of ~400MΩ.

Initially, SICM studies using HIPCM were performed to investigate whether it was a viable technique to use to look at the uptake of silica nanoparticles into live MRC-5 cells via topography. However, it was found that mobile membrane features interfered with imaging and cells could not be kept alive for long enough to get suitable images. In addition, MRC-5 cells have a number of membrane components that are a similar size to the nanoparticles being investigated which made it difficult to identify the nanoparticles. Further work therefore involved imaging cells that had been fixed following exposure to nanoparticles and a SSCM at Imperial College London was used in order to identify nanoparticles by their fluorescence. Spots of fluorescence could be seen relating to nanoparticles while more diffuse, out of focus fluorescence, was attributed to particles that had already been taken up by the cells. After locating the particles using fluorescence, high resolution topography imaging was then performed to investigate the effect of the particle charge on the membrane. Fluorescence was not used at this point since the resolution was too low.

2.6.3 Fluorescence Microscopy

2.6.3.1 Polyacrylamide nanoparticles

Cells were washed twice with serum free DMEM and left for one hour. 2.5mg of polyacrylamide nanoparticles were added to the cells in serum free DMEM after filtering through a 0.2µm syringe filter, and incubated for six hours at 37°C. The cells were washed three times with PBS and then fixed using 4% paraformaldehyde for 15 mins. Incubation time for all types of nanoparticle was chosen based on experience in the group and previous literature reports^{10,98}.

2.6.3.2 Tat conjugated polyacrylamide nanoparticles

Experiments to investigate the uptake of Tat conjugated polyacrylamide nanoparticles were carried out as described above except that nanoparticle suspensions were not filtered before use due to the aggregation of the nanoparticles.

2.6.3.3 Silica nanoparticles

Cells were grown to form a monolayer on a six well plate and the cells were washed twice with serum free DMEM and left for one hour. 50µg of particles were added to each well after filtering through a 0.45µm syringe filter, and incubated for three hours at 37°C. Initial experiments that involved seeding the cells directly onto glass bottomed dishes demonstrated that the silica nanoparticles adhered to multiple surfaces including the glass bottom of the dish and they could not be removed by repeated washing with PBS. To improve the images obtained in order to allow reliable measurement of intracellular fluorescence, the cells were seeded into six well plates and subjected to trypsinization following incubation with the nanoparticles. The resulting cell and nanoparticle suspension was centrifuged at 200g and the supernatant containing the excess nanoparticles was removed. The cells were replated onto individual glass bottomed dishes, left for 24 hours to adhere and then fixed with 4% paraformaldehyde for 15 mins before imaging.

2.6.3.4 Imaging

Uptake of nanoparticles into MRC-5 cells was investigated using a Leica DMIRE2 timelapse widefield fluorescent microscope with full stage incubation (37°C) and a Hammamatsu OrcaER monochrome camera and Leica CTR MIC camera controller.

Cells on glass bottomed dishes were imaged using a 63x oil objective. An XBO 75 xenon arc lamp was used with an ebx 75 electronic transformer to provide the light source. An S484/15x FITC filter with a bandwidth between 469 and 499nm was used in conjunction with a Chroma Custom 62000 dichroic filter cube. Excitation time was kept constant throughout the experiments to enable comparison of results (500ms). The uptake experiments were repeated three times and the number of cells (referred to as the N number in Chapter 5), is the total from all three experiments.

Images were deconvoluted using the Volocity 6.0 software (Perkin Elmer) with measured point source functions (PSFs) for the 63x objective in oil. Measurements of the uptake of the nanoparticles were performed by measuring the green fluorescence intensity from Alexa488 within cells. Individual cells were highlighted by drawing around the shape of the cell and the mean green fluorescence intensity from the nanoparticles for each cell was measured using Volocity 6.0 and recorded in Microsoft Excel. The background level of fluorescence in the control samples was measured and subtracted from the measurements for each sample. This was repeated for all the cells imaged and the minimum number of samples was thirty cells. An average (mean) measurement for all the cells was then taken and the standard deviation was calculated and the background fluorescence recorded from the control sample was subtracted. This value was then corrected for the difference in the fluorescence emission intensity of the nanoparticles themselves to provide the final measurement of uptake. This was done by measuring the fluorescence emission intensity of a suspension of nanoparticles in a glass bottomed dish on the Leica DMIRE2 microscope used for cellular imaging. The intensity was recorded ten times for each set of nanoparticles and the mean emission intensity was calculated. The emission intensity was then normalized to the most fluorescent set of nanoparticles and the fluorescence emission recorded from the cells was multiplied by this value to obtain a final measurement of fluorescence.

Chapter 3 - Nanoparticle characterisation

3.1 Introduction

Polyacrylamide and silica nanoparticles were chosen for this work because they have previously been shown to enter cells without causing cell death^{186, 191}. They are particularly suitable for this work because the method of synthesis allows their chemistry to be easily modified in order to either change the functional groups on the surface that interact with the cellular environment, or to impart a charge to the nanoparticle matrix.

3.1.1 Polyacrylamide nanoparticles

Polyacrylamide nanoparticles are small, hydrophilic and biocompatible nanoparticles. They were first developed as a sensing tool by the Kopelman group in the 1990s from fibre optic sensors. These encapsulated fluorescent dyes within a polymer matrix and were used for intracellular sensing. Despite advances in the miniaturisation of these probes, there were significant limitations associated with their use. These included the high skill of the operator and a lack of ability to do multiple and repeated measurements. It was identified that only the tip of the probe was actually required as the sensing element and this led to the development of a nanoparticle sized polymer matrix based on acrylamide which could encapsulate the dyes. These particles were termed PEBBLEs (Probe Encapsulated By Biologically Localized Embedding)¹⁹⁴⁻¹⁹⁶. The reduced size of the nanoparticles compared to the probes means that polyacrylamide nanoparticles can therefore occupy only 1ppb of a cell, causing negligible biological effects¹⁹⁴.

Polyacrylamide nanoparticles were developed as diagnostic tools for detecting analytes such as H⁺, Ca²⁺, Mg²⁺ and glucose via the encapsulation of fluorescent dyes. Their development has enabled both measurement and also visualization of the uptake process of the nanoparticles and their intracellular location. They are being investigated because their tuneable properties mean that they can be designed so they can target a particular intracellular pathway or location, enable measurement of analytes within a cell or deliver a therapeutic to a specific intracellular organelle^{197, 198}. They are porous, hydrophilic, inert, biocompatible nanoparticles with a size of less than 70nm, meaning they cause minimal cell perturbation. The

fluorescent dyes used for sensing can be trapped within the nanoparticle matrix by virtue of their conjugation to components of the nanoparticle or to a large molecule e.g. 10,000MW dextran, that is trapped within the matrix. This protects the cell from any effects of the dye, and also protects the dye from any cell components that may affect it, for example, enzymes^{76, 83, 199}. The porous nature of the matrix allows the diffusion of molecules and ions through the particles and their small size means that when used for measurement of intracellular analytes, response time is fast. Polyacrylamide nanoparticles can be easily modified during the synthesis process by the incorporation of different molecules into the matrix in order to provide a wide range of surface chemistries and functionalities. They can also be conjugated to other molecules such as cell penetrating peptides, oligonucleotides and aptamers following synthesis of nanoparticles with the required surface functionality^{10, 76, 200}.

Polyacrylamide nanoparticles are produced in a reverse microemulsion technique via the polymerisation of acrylamide and bisacrylamide within water droplets in an oil phase. The size of these water droplets and therefore the nanoparticle size distribution can be tightly controlled¹⁹⁸. Nanoparticles without any further modification have a slightly negative zeta potential but they can be easily modified via the incorporation of a positive monomer, 3-acrylamidopropyl trimethylammonium chloride (ACTA), to produce nanoparticles with varying degrees of positive charge¹⁸⁷. Alternatively, via incorporation of a monomer containing an amine group, other molecules such as cell penetrating peptides can be conjugated to the nanoparticles via a heterobifunctional crosslinker (SMCC)¹⁰.

3.1.2 Silica nanoparticles

Silica is used in a variety of forms in many different industrial applications including ceramics, catalysis and high tech industry such as computing^{201, 202}. The production of silica nanoparticles furthered the range of possible applications and their properties, including a high surface area to volume ratio, large pore size and biocompatibility mean that they can be applied to fields such as drug delivery, imaging and diagnostics²⁰³. Silica (or sol gel) nanoparticles are produced using a modification of the Stober method, published in 1968, and can be used to produce nanoparticles with a wide range of sizes depending on the reaction conditions¹⁹⁰. Similarly to polyacrylamide nanoparticles, silica nanoparticles synthesised with no

modifications have a negative zeta potential^{190, 204}. They can also be produced using a microemulsion technique²⁰⁵. Both of these techniques provide the opportunity to easily modify a number of properties of the nanoparticles by incorporation of different reagents that may affect size, charge or surface chemistry as well as adding functional groups in order to conjugate molecules to the surface of the nanoparticle^{73, 128, 206}.

The Stober synthesis is the ammonia catalysed reaction of tetraethylorthosilicate (TEOS) with water in low molecular weight alcohol, such as methanol or ethanol, to produce monodisperse spherical silica nanoparticles^{201, 207}. Nanoparticles are formed by hydrolysis of TEOS and subsequent condensation of silicic acid in ethanol (Equations 1 and 2)²⁰⁸. The rates of hydrolysis and condensation affect the size of the particles produced and a monodisperse population will generally be produced if the hydrolysed monomers produced in (1) react faster than they are produced²⁰².



Two main theories have been presented regarding how nanoparticles form during the Stober process. These are monomer addition and controlled aggregation. The monomer addition theory divides the Stober process into an initial stage of nucleation which is then followed by particle growth via the addition of the hydrolysed monomer to the particle surface. The rate of particle growth is limited by the hydrolysis of the monomers²⁰⁸⁻²¹¹. The second theory is known as controlled aggregation and is a single stage process where nucleation occurs continuously and the nuclei aggregate to form the particles^{201, 208, 212, 213}. It is unclear whether one theory is correct or whether combinations of both may occur to different extents depending on the reaction conditions.

A number of parameters are important in the preparation of silica nanoparticles. These include water and ammonia concentrations, pH, rate of hydrolysis and rate of condensation⁷⁴. These have been shown to influence properties of the nanoparticles such as pore size and shape, particle size and morphology. Water and ammonia

concentrations are particularly important and the rate of condensation is influenced by the amount of water. Increasing the concentration of water produces larger particles. Ammonia is required to produce spherical particles and increasing ammonia concentration has also been shown to produce larger particles^{190, 202}. However, for both water and ammonia, at very high concentrations, particle size sometimes decreases²⁰². Particles produced in ethanol are double the size of those produced in methanol and the use of higher molecular weight alcohols tends to produce particles with a wider size distribution^{190, 201}. The rate of addition of TEOS also has an effect on the final size and polydispersity of the particles. Particle size is a decreasing function of the rate of addition of TEOS which can be explained by a reduction of the nucleation period and better control of the reaction speed therefore particle size decreases as the rate of TEOS addition increases²⁰⁷.

Silica nanoparticles have a negative surface charge due to ionisation of surface silanol and hydroxyl groups but this can be modified via the addition of various functional groups such as trimethylammonium which imparts a positive charge to the nanoparticles^{73, 128, 214}. Silica nanoparticles with covalently attached amine surface functionalities have been developed and they carry a net positive surface charge but often demonstrate colloidal instability. The incorporation of increasing amounts of cationic trialkyloxysilanes has been shown to result in the formation of larger nanoparticles with a disrupted pore structure^{73, 215, 216}.

3.2 Results and Discussion

Nanoparticle uptake into cells is dependent on a number of factors, many of which relate to the physicochemical properties of the nanoparticles including size, shape, charge and surface chemistry. It was therefore crucial to have well characterised nanoparticles in order to enable reliable comparisons between the effects of these different parameters on nanoparticle uptake into cells. Nanoparticles were characterised in terms of their size and charge using a variety of different techniques including dynamic light scattering, the CPS disc centrifuge and zeta potential.

3.2.1 Nanoparticle charge

3.2.1.1 Polyacrylamide nanoparticle charge

The presence of ACTA in the nanoparticle matrix increased the zeta potential from approximately -7mV for unfunctionalised polyacrylamide nanoparticles to 19mV for the most positively charged version containing 20% ACTA (Figure 3.1).

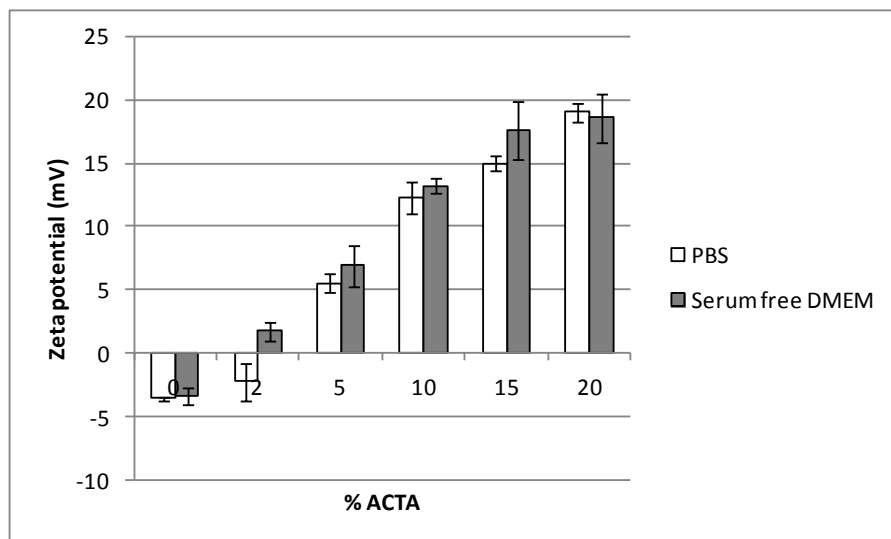


Figure 3.1: Increasing nanoparticle charge with increasing ACTA incorporation in PBS and serum free DMEM.

Incorporation of 5% N-acryloxysuccinimide produced nanoparticles with a charge of -11mV in PBS and -5.5mV in serum free DMEM (Figure 3.2).

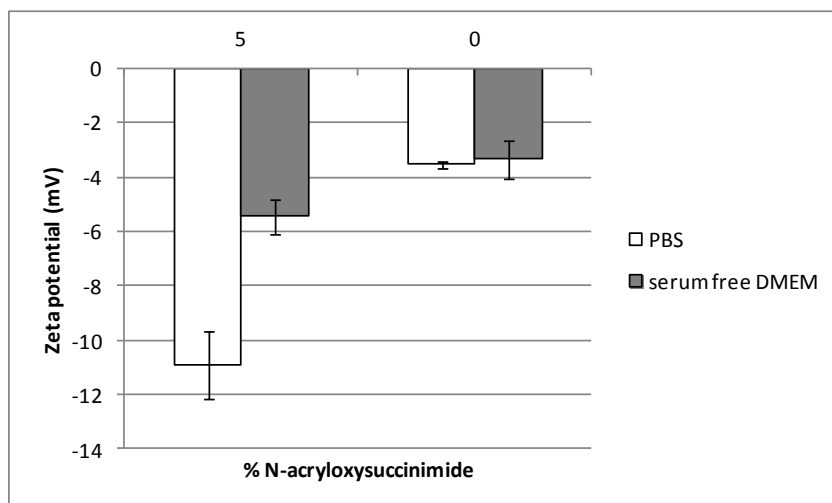


Figure 3.2: Decrease in nanoparticle charge caused by the incorporation of 5% N-acryloxysuccinimide.

Resuspension of unfunctionalised, ACTA and N-acryloxysuccinimide containing polyacrylamide nanoparticles in serum free DMEM as opposed to PBS often increased the zeta potential of the nanoparticles.

3.2.1.2 *Tat peptide conjugated polyacrylamide nanoparticle charge*

Amine functionalised polyacrylamide nanoparticles conjugated to Tat peptide had a positive zeta potential of 6.3mV in PBS and 5.2mV in serum free DMEM (Figure 3.3).

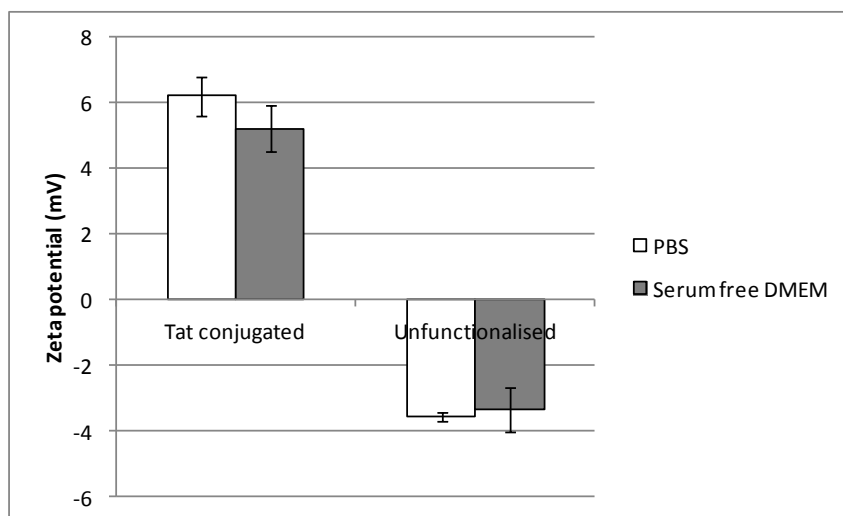


Figure 3.3: Zeta potential of Tat conjugated polyacrylamide nanoparticles compared to unfunctionalised polyacrylamide nanoparticles.

3.2.1.3 Silica nanoparticle charge

Negatively charged silica nanoparticles had a negative zeta potential of -29.4mV in PBS and -25mV in serum free DMEM. In contrast, nanoparticles containing TMAC had a positive zeta potential of 25.4mV in PBS. In serum free DMEM, the zeta potential was similar (26.5mV) (Figure 3.4)

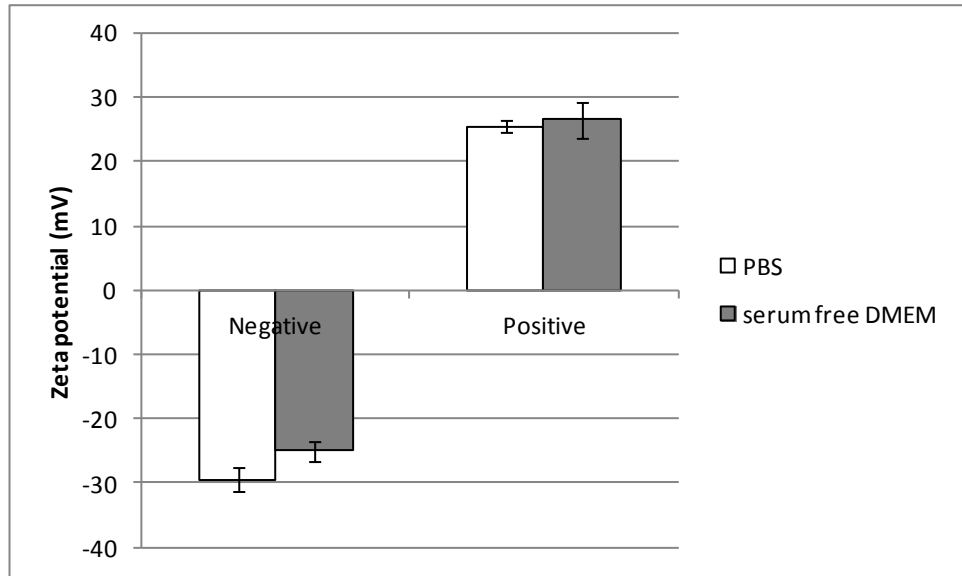


Figure 3.4: Zeta potential of negative and positively charged silica nanoparticles.

3.2.1.4 Effect of serum on nanoparticle charge

Both polyacrylamide and silica nanoparticle charge was measured in DMEM cell culture medium containing 10% serum proteins. The presence of these proteins caused a significant suppression of the positive charge on the nanoparticles compared to the zeta potential when measured in PBS or serum free DMEM. Both types of silica nanoparticles displayed a similar negative zeta potential in serum containing DMEM. For polyacrylamide nanoparticles, although the nanoparticles with 10% ACTA and above retained a positive charge, it was significantly suppressed compared to the zeta potential of the same particles in PBS and serum free DMEM (Figure 3.5). It has been suggested that this suppression in surface charge is due to the adsorption of proteins to the surface of the nanoparticle forming a layer that masks the charge. All uptake experiments were therefore performed in the absence of serum^{120, 217}.

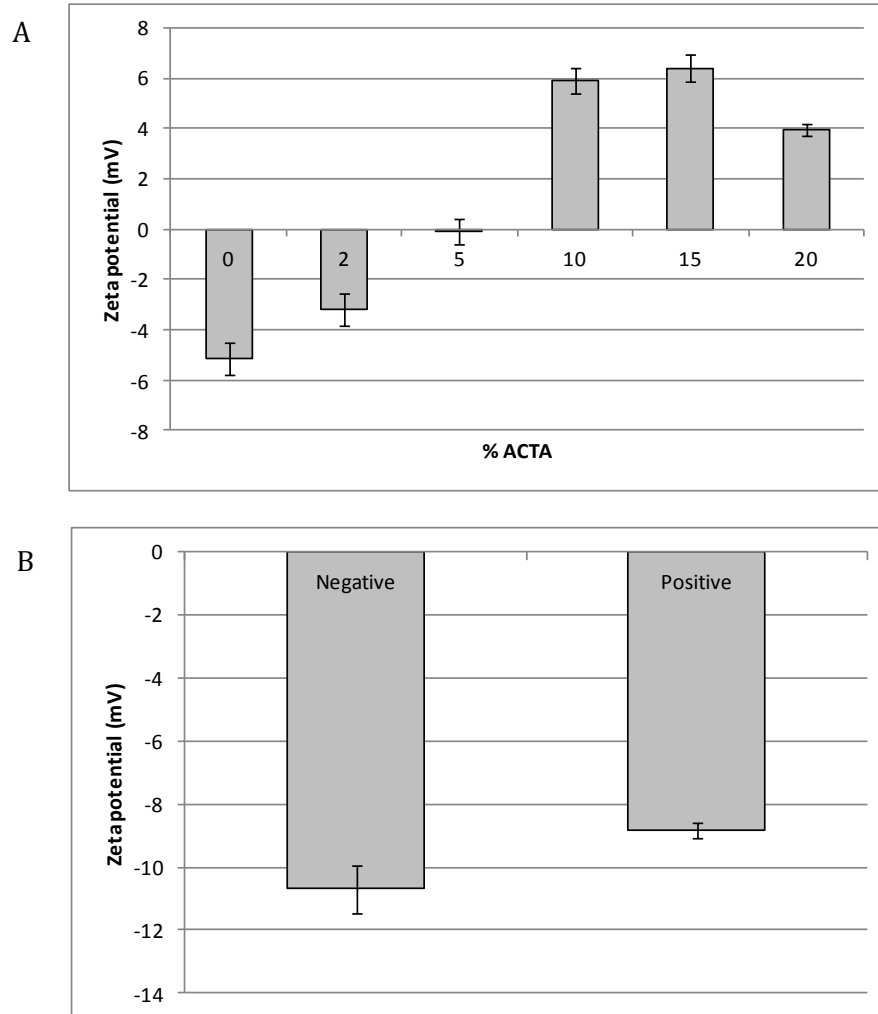


Figure 3.5: Zeta potential of polyacrylamide (A) and silica (B) nanoparticles in serum containing DMEM.

3.2.2 Nanoparticle size

Nanoparticle size distributions for polyacrylamide and silica nanoparticles were obtained using two different techniques – dynamic light scattering (DLS) and the CPS disc centrifuge.

3.2.2.1 Polyacrylamide - Dynamic Light Scattering

For all types of polyacrylamide nanoparticle produced, regardless of charge, a monodisperse population of particles was observed. Both intensity and volume plots for nanoparticle size are presented since whilst the intensity plot is most suitable when investigating how many populations of nanoparticles are present in the sample, it can be distorted due to the much greater amount of light that is scattered by the presence of a few larger particles. In the case of polyacrylamide nanoparticles, this was not a significant problem since only one population of nanoparticles with a size of between 37-54nm was observed following filtration. Intensity plots are therefore presented to show the monodisperse nature of the particles whilst the diameter of the particle is reported from the volume distribution (Figure 3.6).

Unfunctionalised polyacrylamide nanoparticles had a diameter of $37.4 \pm 0.4\text{nm}$ in PBS. The incorporation of increasing amounts of ACTA into the nanoparticles led to an overall trend of a small but significant increase in nanoparticle size when the maximum amount of ACTA was incorporated (Figure 3.7). Polyacrylamide nanoparticles containing 10% ACTA had a diameter of $39.3 \pm 1.3\text{nm}$ which was not significantly different to that of the unfunctionalised nanoparticles ($P > 0.05$) whilst the nanoparticles containing 15% and 20% ACTA had a diameter of $41.2 \pm 0.9\text{nm}$ and $53.4 \pm 1.5\text{nm}$ respectively which both differed significantly from the unfunctionalised nanoparticles ($P < 0.05$).

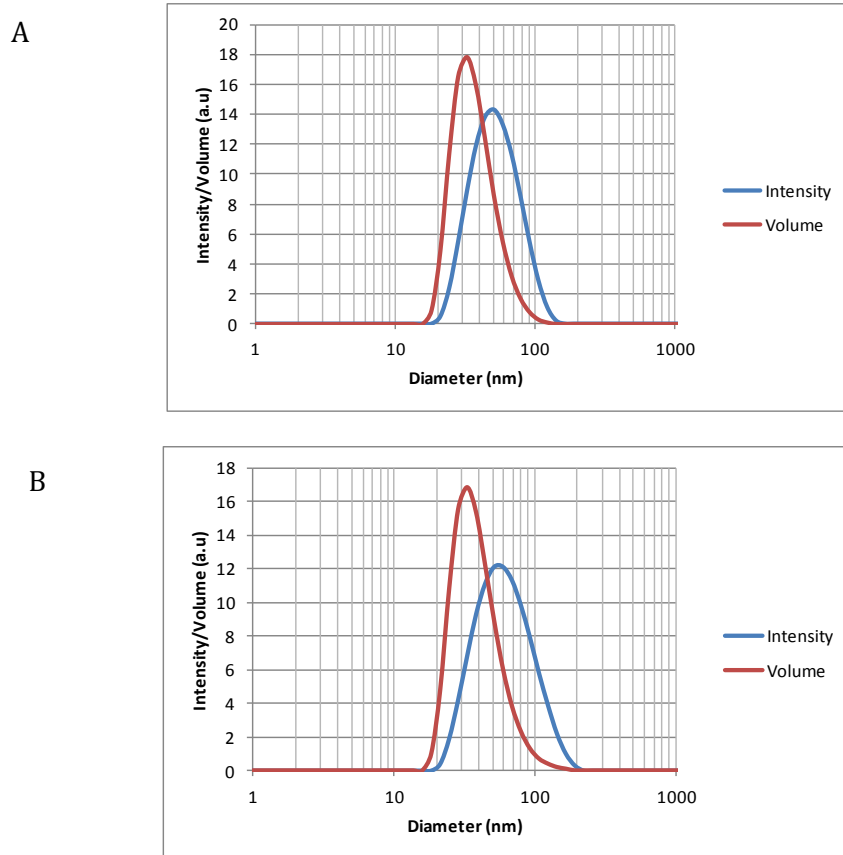


Figure 3.6: Intensity and volume distributions of (A) unfunctionalised (Intensity 54nm, Volume: 37nm) and (B) 15% ACTA (Intensity: 59nm, Volume: 42nm) polyacrylamide nanoparticle diameter in PBS.

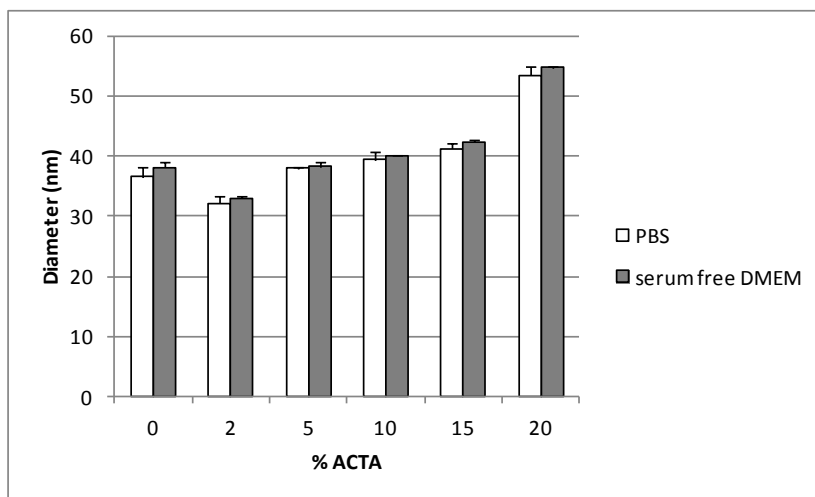


Figure 3.7: Diameter of polyacrylamide nanoparticles with increasing proportion of ACTA in PBS and serum free DMEM.

Negatively charged polyacrylamide nanoparticles containing 5% N-acryloxysuccinimide had a diameter of $40.3 \pm 1.7\text{nm}$ in PBS and $39.2 \pm 1\text{nm}$ in serum free DMEM (Figures 3.8 and 3.9).

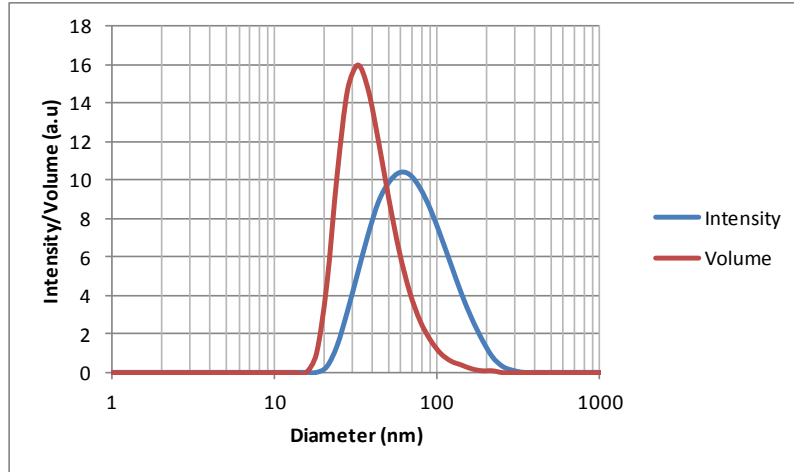


Figure 3.8: Intensity and volume distributions of polyacrylamide nanoparticle diameter containing 5% N-acryloxysuccinimide (Intensity 76nm, Volume 39nm).

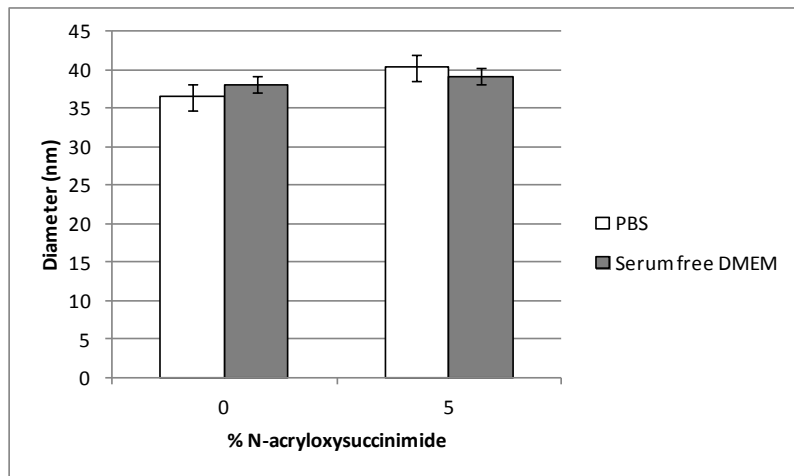


Figure 3.9: Diameter of unfunctionalised and 5% N-acryloxysuccinimide polyacrylamide nanoparticles in PBS and serum free DMEM.

The diameter of polyacrylamide nanoparticles did not change when resuspended in serum free DMEM compared to PBS for all types of particle (Figures 3.7 and 3.9).

3.2.2.2 Tat conjugated polyacrylamide – Dynamic Light Scattering

Tat peptide conjugated nanoparticles aggregated in both PBS and serum free DMEM and multiple populations of particles could be observed. In serum free DMEM, one population had a diameter of approximately 40-50nm, which is typical of the polyacrylamide nanoparticles produced in this work. There was a second, larger, population of particles with a size of 500-600nm, representing aggregates of nanoparticles. Finally, there was another small population of particles with a size of approximately 5000nm (Figure 3.10).

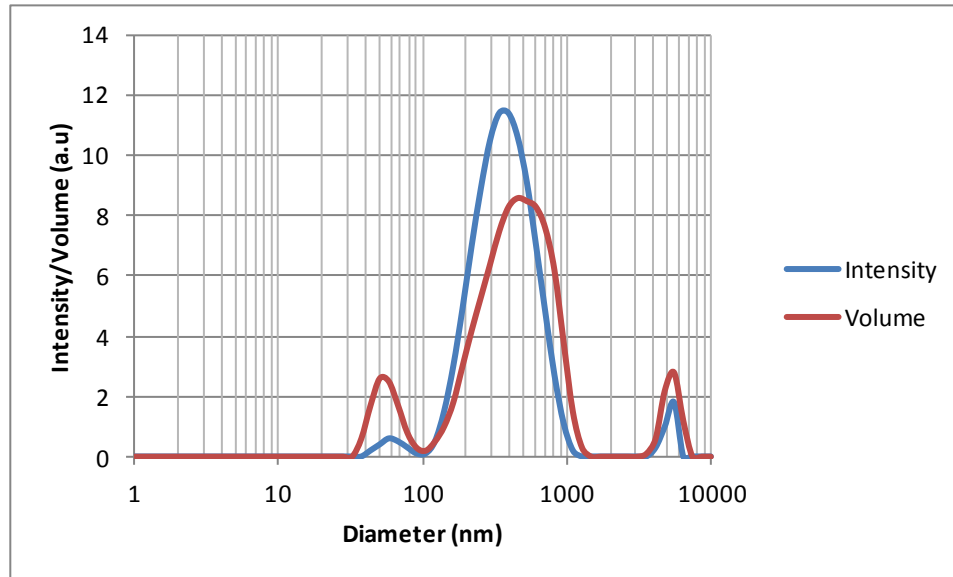


Figure 3.10: Intensity and volume distributions of Tat conjugated polyacrylamide nanoparticles in serum free DMEM.

3.2.2.3 Polyacrylamide - CPS Disc Centrifuge

The CPS disc centrifuge was also used to measure the size of polyacrylamide nanoparticles. A similar trend was observed to the DLS data, where particles containing up to 15% ACTA had a similar size to unfunctionalised polyacrylamide nanoparticles which had a diameter of 33nm (Figure 3.11). Nanoparticles containing 15% ACTA also had a diameter of 33nm whilst nanoparticles containing 20% ACTA tended to have a larger diameter of 40nm, although this was not significant ($P>0.05$).

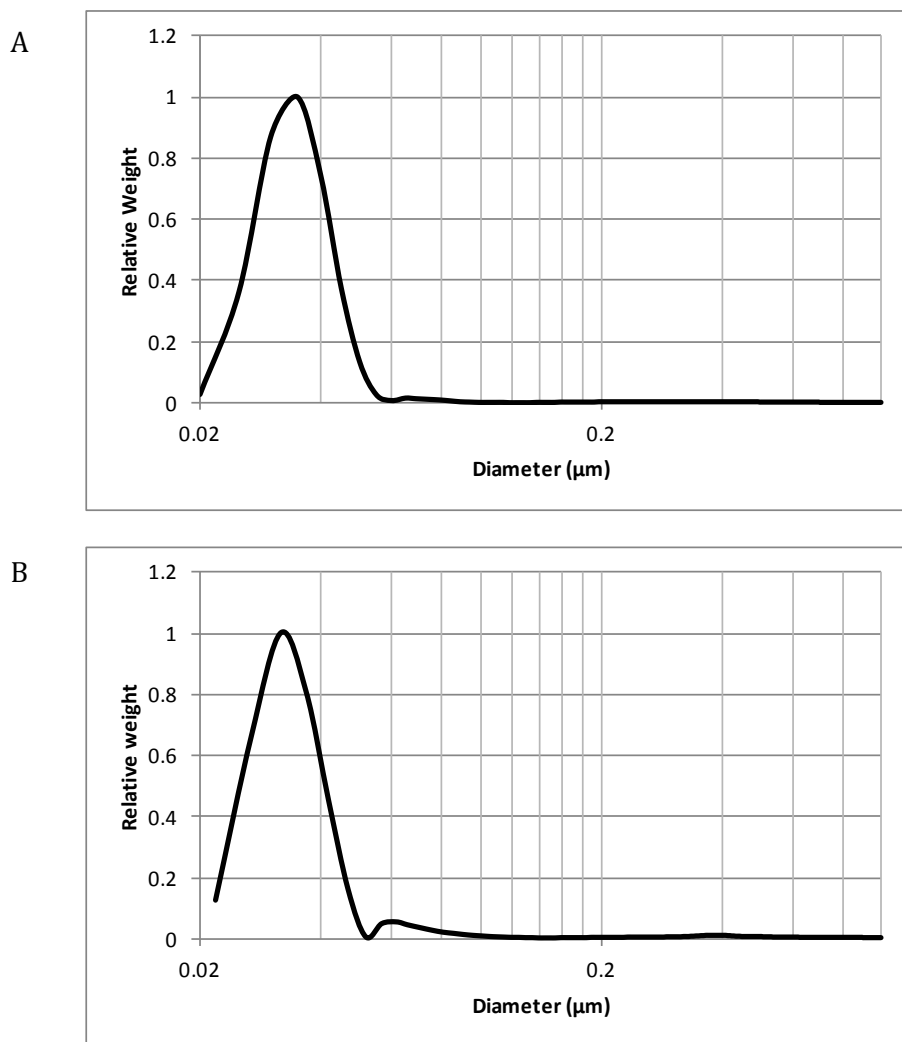


Figure 3.11: Polyacrylamide nanoparticle diameter (A) unfunctionalised (33.8nm) and (B) 15% ACTA (33.2nm).

The diameter of unfunctionalised polyacrylamide nanoparticles was reported to be similar using both techniques, 37nm via DLS versus 33nm on the disc centrifuge but for nanoparticles containing 15% ACTA, the reported size was lower using the disc centrifuge (33nm vs 41nm on DLS).

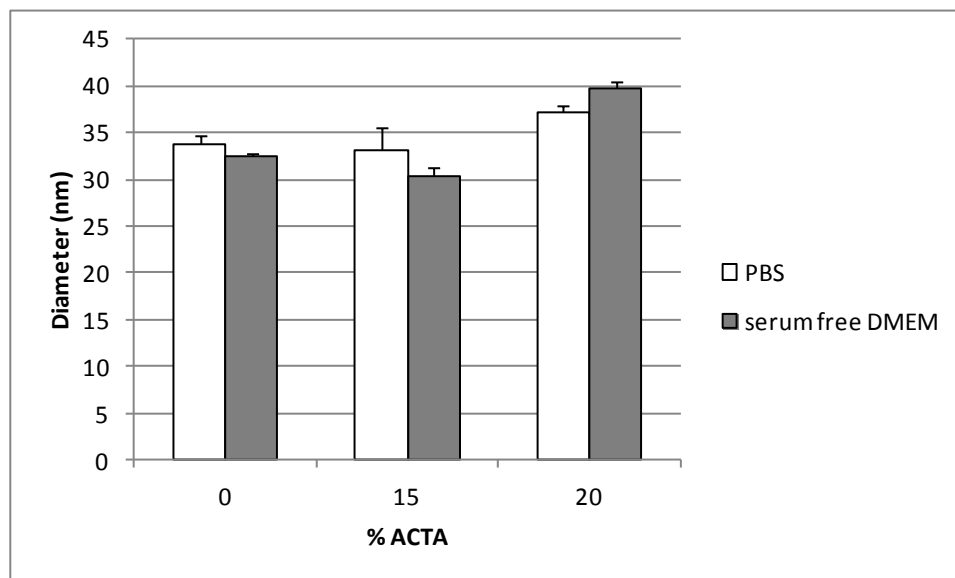


Figure 3.12: Polyacrylamide nanoparticle diameter in PBS and serum free DMEM on disc centrifuge.

3.2.2.4 Aggregation of polyacrylamide nanoparticles

During cell uptake experiments, nanoparticles were incubated with cells for six hours in serum free DMEM at 37°C. Some literature reports suggest that nanoparticles may aggregate during prolonged exposure to cell culture medium^{17, 120}. To investigate whether this affected particle size, aggregation studies were performed to investigate the size of nanoparticles over time using the CPS disc centrifuge. Polyacrylamide nanoparticles were left for six hours at 37°C in serum free DMEM and then sized using the disc centrifuge to see if aggregation had occurred.

For unfunctionalised polyacrylamide nanoparticles, after six hours in serum free DMEM, a monodisperse population of particles was observed with a diameter of 32nm. This was similar to the particle size measured directly after sonication indicating that aggregation did not occur. Polyacrylamide nanoparticles containing

15% ACTA also showed a similar distribution to the original, with a single peak at 33nm after six hours in serum free DMEM.

3.2.2.5 Silica – Dynamic Light Scattering

Reliable, repeatable production of silica nanoparticles with the required size and surface charge proved to be difficult. The nanoparticles produced tended to vary greatly in their size and morphology therefore a number of different synthesis routes were attempted in order to achieve nanoparticles with opposite charges but with a similar diameter. This was important since the diameter of the particles needed to be similar in order to be able to fully investigate the effect of charge on the interaction and uptake of the nanoparticles. It was found the use of a small conical flask with a high stirring rate and a rapid rate of addition of TEOS led to the production of roughly 300nm silica nanoparticles. The incorporation of TMAC into the basic silica nanoparticle matrix after thirty minutes of synthesis did not subsequently affect particle diameter, and nanoparticles were produced with an average size of $290 \pm 5.4\text{nm}$ for negatively charged silica nanoparticles and $292 \pm 2.9\text{nm}$ for positive silica nanoparticles (Figure 3.13).

It has been demonstrated previously by other groups that a rapid rate of TEOS addition can lead to the production of smaller nanoparticles, possibly due to the production of a large number of smaller nuclei onto which the TMAC can then add to in order to impart a positive charge. The presence of the ammonia is required in order to produce spherical particles and the use of ethanol also helps to produce smaller particles.

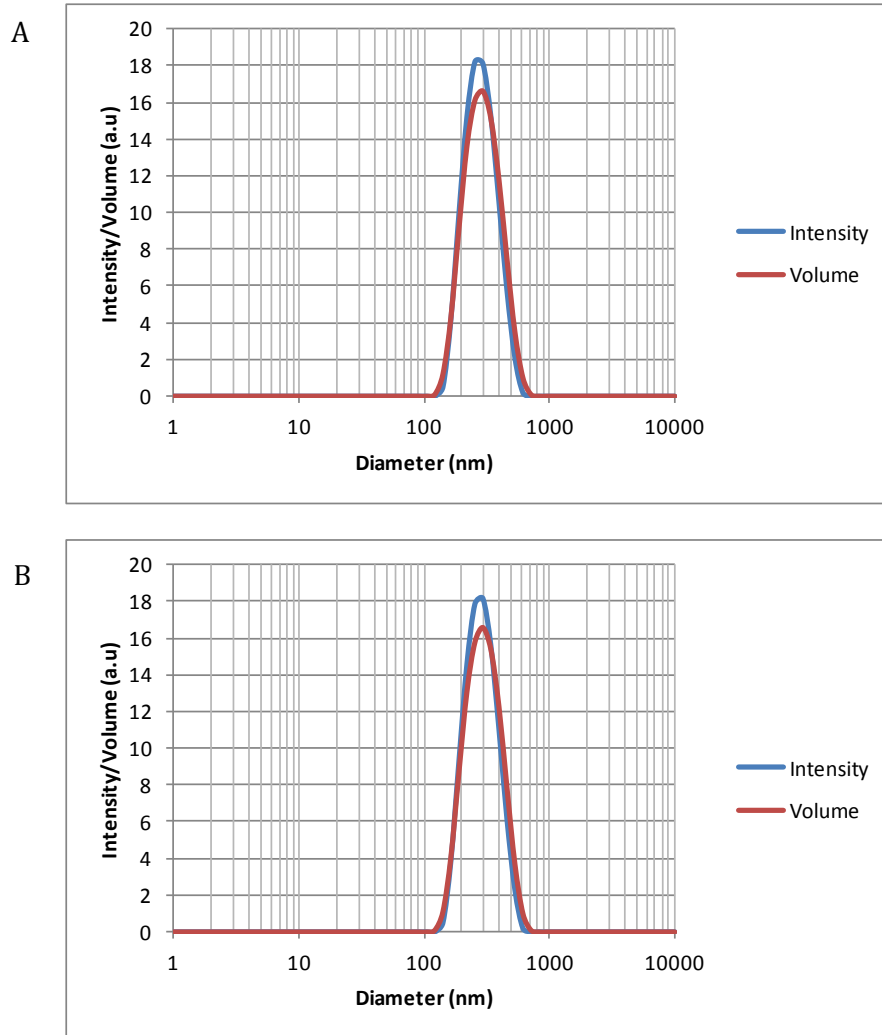


Figure 3.13: (A) Negatively charged (290nm) and (B) positively charged (292nm) silica nanoparticle diameter in PBS.

Resuspension of silica nanoparticles in serum free DMEM as opposed to PBS did not affect particle diameter (Figure 3.14).

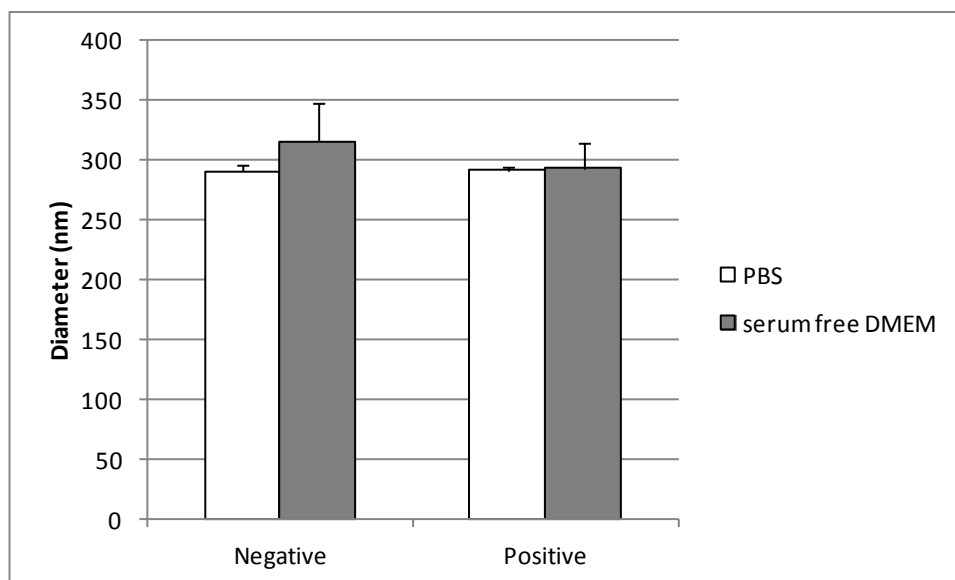


Figure 3.14: Comparison of size of negative and positively charged silica nanoparticles in PBS and serum free DMEM.

3.2.2.6 Silica - CPS Disc Centrifuge

Relative weight distributions for negatively charged silica nanoparticles showed one main population with a size of 361nm with an additional small peak at 426nm. Positively charged silica nanoparticles displayed a polydisperse population of particles with peaks at 325, 291 and 242 nm. Both negative and positively charged silica nanoparticle distributions displayed additional peaks compared to the DLS distributions. These peaks may have been present in the DLS samples but the disc centrifuge is much better at resolving populations of similarly sized particles which may account for their appearance in the disc centrifuge results (Figure 3.15 B). This is because as particles sediment in the disc centrifuge, they sediment at a rate that is proportional to the square of the particle diameter, therefore particles that differ in size by only a few percent will settle at significantly different rates.

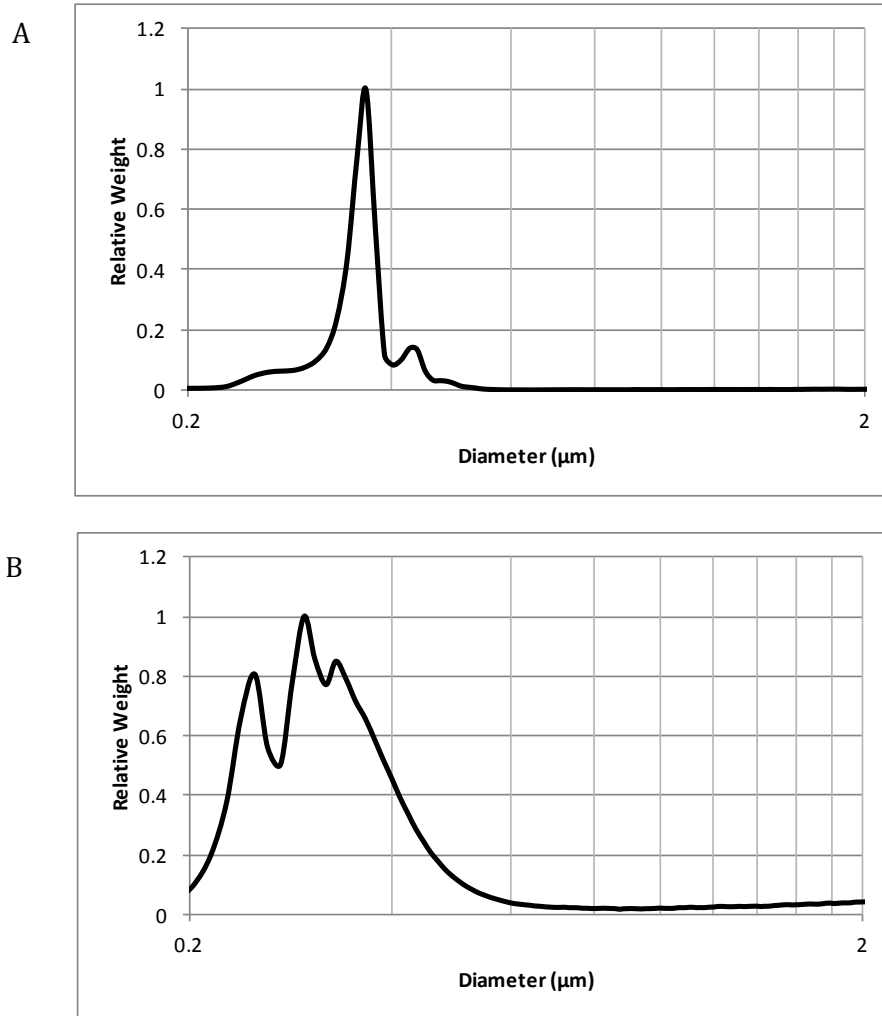


Figure 3.15: Representative traces of (A) negative and (B) positively charged silica nanoparticle diameter in PBS measured using the CPS disc centrifuge.

Using the disc centrifuge it was again shown that resuspension of the particles in serum free DMEM did not affect size (Figure 3.16).

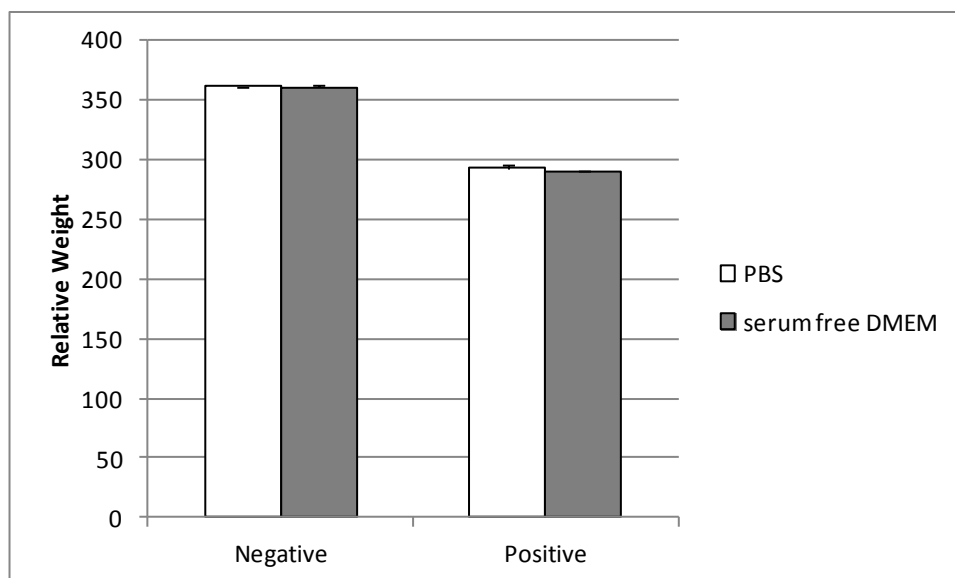


Figure 3.16: Comparison of negatively charged and positively charged silica nanoparticle diameter in PBS and serum free DMEM.

The diameter reported for negatively charged silica nanoparticles was larger (361nm) on the disc centrifuge than that from DLS (290nm). The main peak for the positively charged silica particles (291nm) correlated well with the diameter obtained using DLS (292nm).

3.2.2.7 Aggregation of silica nanoparticles

The aggregation of silica nanoparticles after three hours in serum free DMEM was assessed using the disc centrifuge. After three hours at 37°C, negatively charged silica nanoparticles did not aggregate and remained at a similar size (356nm). Positively charged nanoparticles displayed a change in the number and size of populations of nanoparticles, with two main peaks at 355nm and 419nm (Figure 3.17).

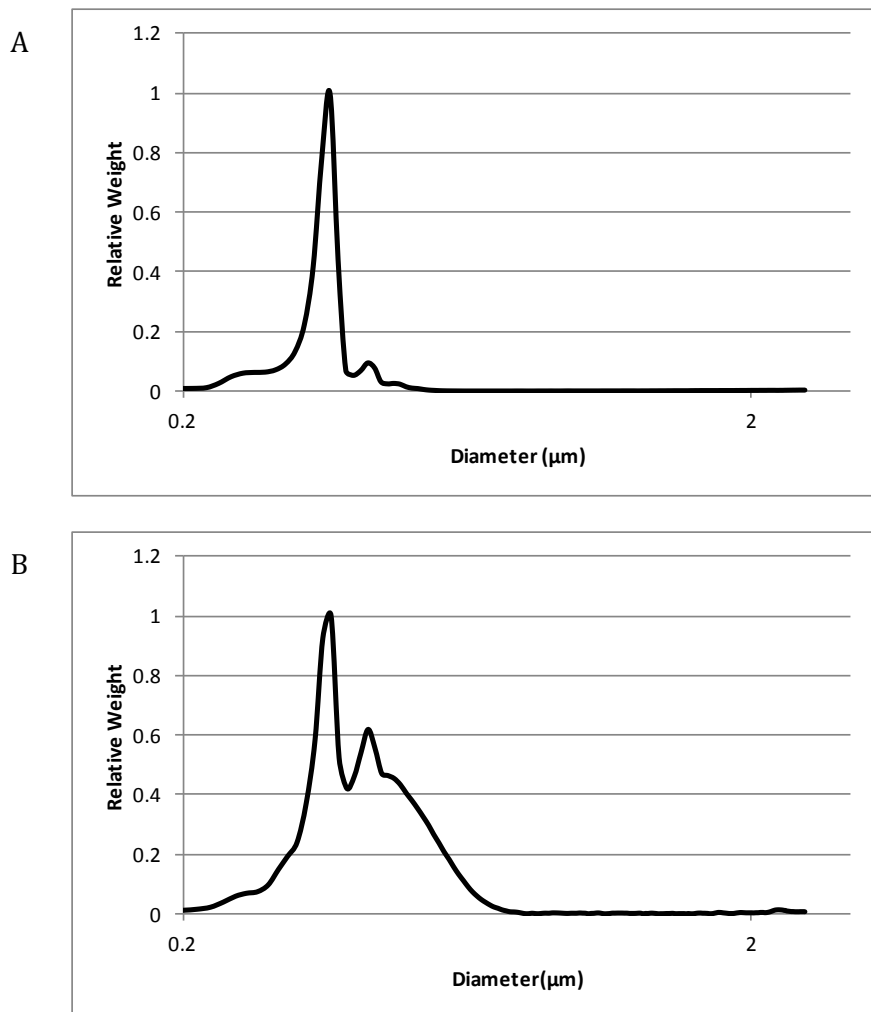


Figure 3.17: (A) Negatively charged and (B) positively charged silica nanoparticle diameter after three hours in serum free DMEM.

3.2.3 Calculating nanoparticle density using the CPS disc centrifuge

When measuring nanoparticle size using the CPS disc centrifuge, one of the most important parameters for accurate sizing is the density of the nanoparticle. This is because density is one of the factors that determine how quickly the particles settle in the gradient and it is a parameter in Stokes law of sedimentation:

$$t = \frac{X}{V} = \frac{(X18\eta)}{(D^2(\rho_p - \rho_f)g)}$$

The density of the nanoparticle therefore influences the size distribution obtained using the disc centrifuge, so the density of both silica and polyacrylamide nanoparticles was calculated in order to gain accurate size distributions. The density of nanoparticles can be calculated using the disc centrifuge by obtaining a particle size distribution in gradient fluids of two different densities. The two reported size distributions will only overlay exactly when the assumed density of the particle is correct and the distributions can be recalculated at different densities until they do. In these experiments, particles were analysed on both water based and deuterium oxide (D₂O) based 8-24% sucrose gradients which differ in density by approximately 0.11g/cm³.

In A, B and C in Figure 3.18, the particles are the same and measured on a water (blue) and D₂O based gradient (red), but because different densities are assumed, the reported size distributions are different. If a lower density (1.3g/cm³, Figure 3.18 A) than the actual density is used, the particles sediment faster than expected so the size appears to be larger (size is inversely proportional to the time taken to sediment). Conversely, if a higher density (2.0g/cm³, Figure 3.18 C) is used, the particles sediment slower than expected so the size appears to be smaller. Only at 1.6g/cm³ do the reported distributions in water and D₂O overlay exactly indicating that the density of the particles is 1.6g/cm³.

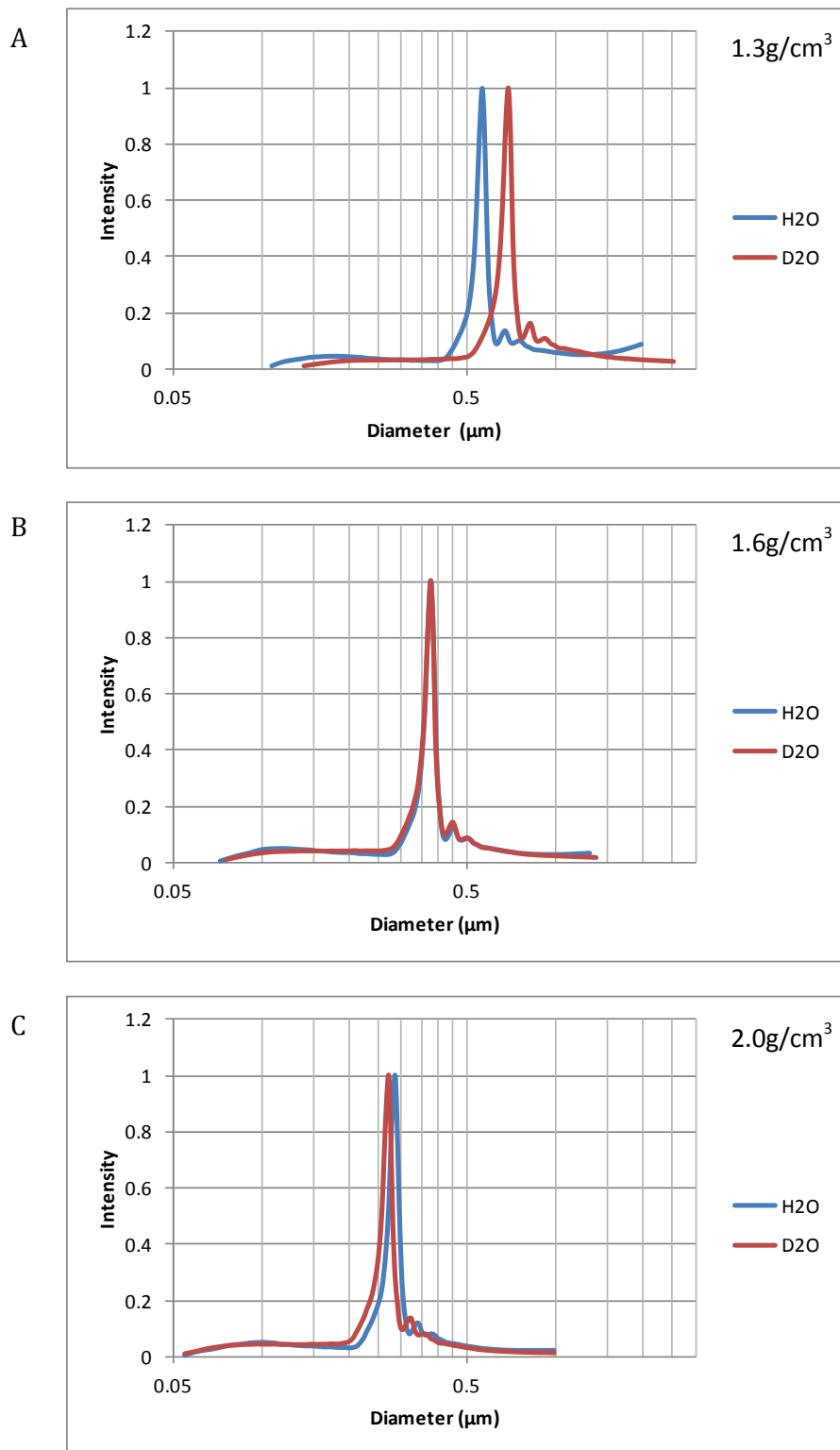


Figure 3.18: Diameter of silica nanoparticles in water and D₂O calculated at different densities: (A) 1.3g/cm³, (B) 1.6g/cm³, (C) 2.0g/cm³.

Similarly, the density of polyacrylamide nanoparticles has also been calculated using a 4-12% sucrose gradient in water and D₂O, and the density was found to be approximately 2.3g/cm³, which was higher than had been expected given the density of similar materials such as polyacrylamide gels (Figure 3.19)²¹⁸. The separation between peaks for the polyacrylamide nanoparticles was less pronounced than for silica nanoparticles, therefore only an approximation of the density is given.

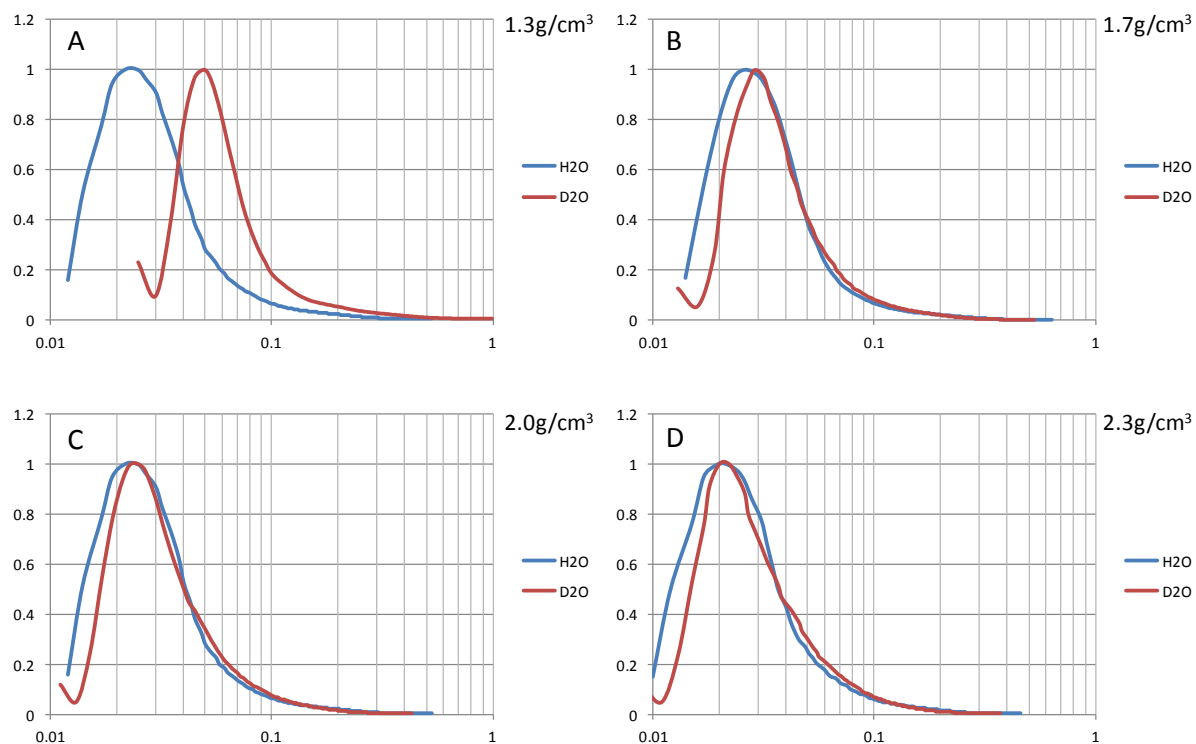


Figure 3.19: Diameter of polyacrylamide nanoparticles in water and D₂O calculated at different densities (A) 1.3g/cm³, (B) 1.7g/cm³, (C) 2.0g/cm³ and (D) 2.3g/cm³.

3.2.4 Fluorescence

A fluorescent dye, Alexa 488, was incorporated into the nanoparticle matrix in order to allow tracking of nanoparticle uptake into cells using fluorescence microscopy.

3.2.4.1 Polyacrylamide nanoparticle fluorescence

There was no correlation between polyacrylamide nanoparticle charge and the intensity of fluorescence emission from the particles when measured at pH 7.4 using both the fluorimeter and the microscope although the pattern of fluorescence emission intensity was different (Figure 3.20 and 3.21). There was an approximately 2.5 fold difference between the most and least fluorescent nanoparticles when measured using the fluorimeter (Figure 3.20). However, when measured using the microscope, most particles had similar fluorescence intensity (Figure 3.21). The nanoparticles containing 5% N-acryloxysuccinimide and those conjugated to Tat peptide displayed a lower intensity of fluorescence emission but this was accounted for in quantitative measurements of nanoparticle uptake. Only one set of particles were significantly different in the intensity of emission when measured on the microscope, those containing 10% ACTA (Figure 3.21). The results indicate that the charge on the particle or functionalisation with different groups to enable conjugation did not affect the incorporation of dye into the matrix, therefore any difference in emission intensity can be attributed to experimental variation.

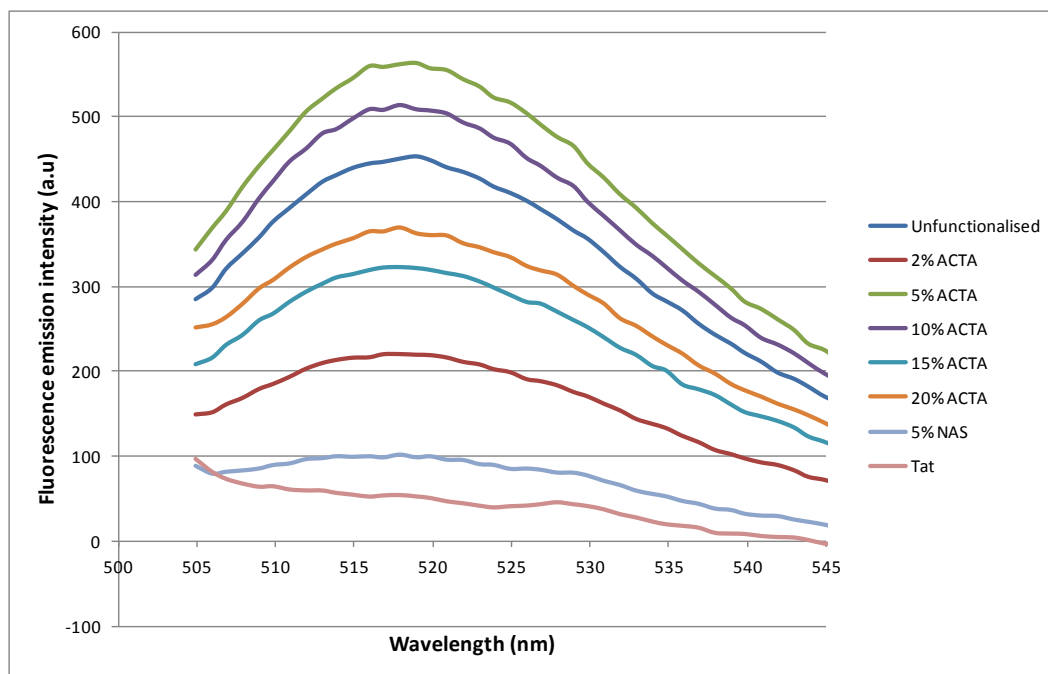


Figure 3.20: Fluorescence intensity of polyacrylamide nanoparticles with different charge measured on fluorimeter.

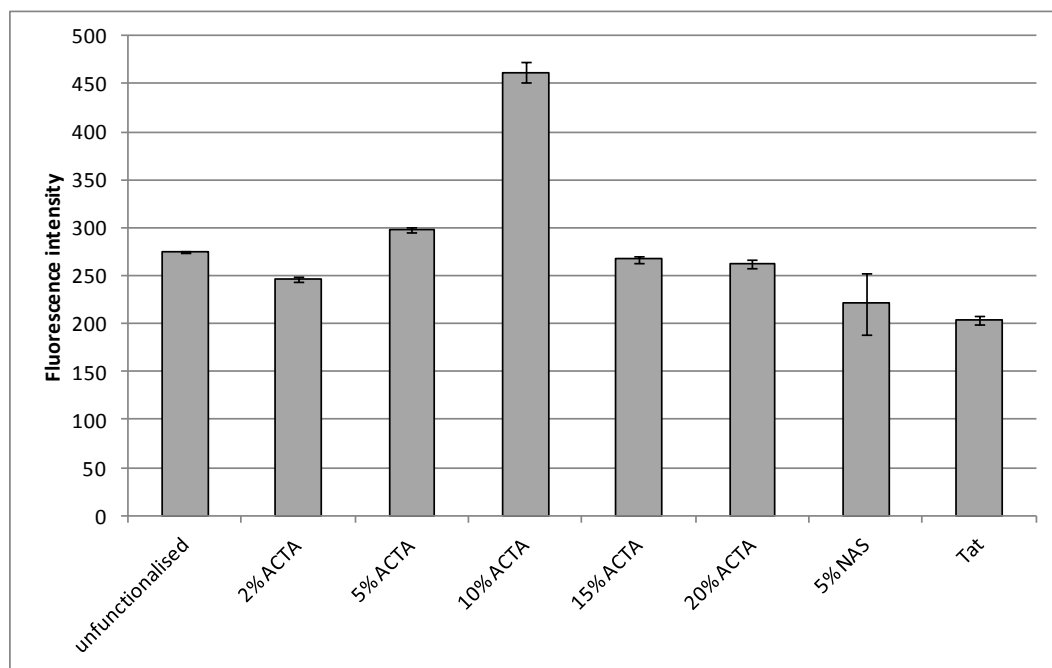


Figure 3.21: Fluorescence intensity of polyacrylamide nanoparticles on widefield microscope.

3.2.4.2 Silica nanoparticle fluorescence

Fluorescence intensity at pH 7.4 for positively charged silica nanoparticles was found to be approximately three times that of the negatively charged silica nanoparticles when measured using the fluorimeter with an excitation wavelength of 495nm (Figure 3.22). This has previously been reported and is thought to be related to the properties of Alexa Fluor dyes, since the dyes frequently carry a negative charge, therefore may be attracted to the positive charge in the particle and enhanced entrapment into the nanoparticle may occur^{185, 219}.

To investigate this further, the fluorescence of silica nanoparticle was also measured on the microscope that cellular uptake measurements were performed on. However, this produced very different results to the fluorimeter and indicated that both types of silica nanoparticle had similar fluorescence emission intensity (Figure 3.23). This could be due to the use of a different excitation sources and the use of bandwidth filters and a dichromatic mirror in the microscope.

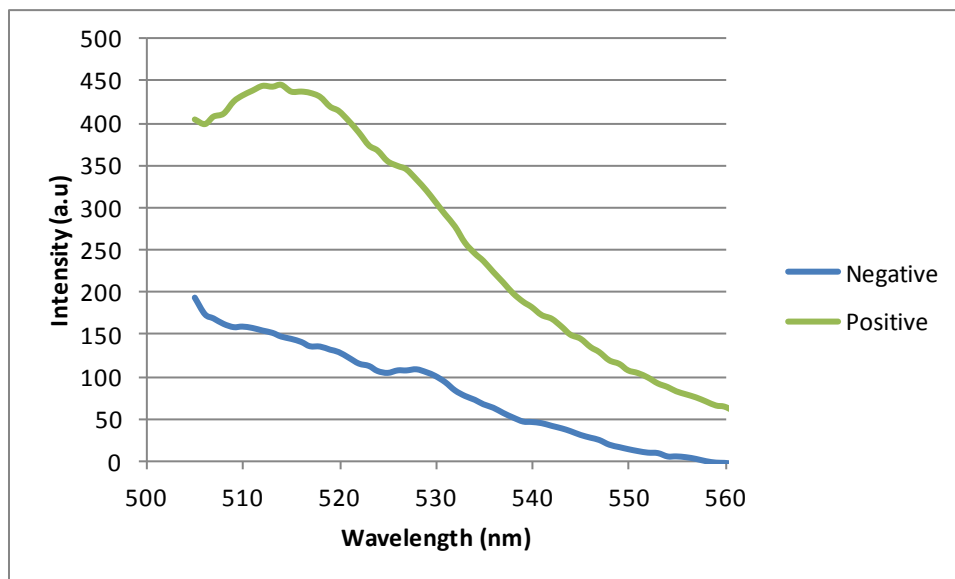


Figure 3.22: Fluorescence intensity of silica nanoparticles on fluorimeter.

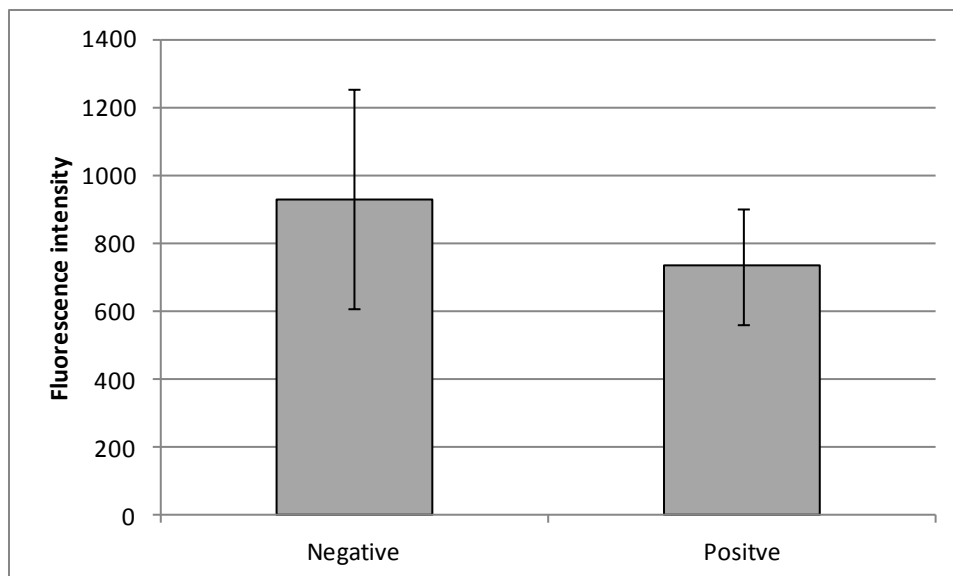


Figure 3.23: Fluorescence intensity of silica nanoparticles on widefield fluorescent microscope.

Both the CPS disc centrifuge and DLS have been demonstrated to be useful techniques to use to investigate polyacrylamide and silica nanoparticle size and size distribution. In general they appear to produce complementary data but the CPS disc centrifuge has the added advantage that it has better resolving power for similarly sized populations due to the way in which it measures size. Since sedimentation varies with square of particle diameter, similarly sized populations are more easily resolved when using the disc centrifuge than when using DLS. The disc centrifuge was particularly useful when measuring the size of silica nanoparticles and resolving populations, but it was often more problematic to use when characterising polyacrylamide nanoparticles because their small size required a long run time causing some problems with background noise towards the end of the experimental run

The reverse microemulsion technique of polyacrylamide nanoparticle synthesis technique was found to reliably and repeatedly produce nanoparticles of 30-60nm but the incorporation of additional monomers was found to affect particle size as observed following the incorporation of 20% ACTA. The synthesis of the silica nanoparticles was more troublesome and it proved to be difficult to produce

nanoparticles of the same size and charge repeatedly. Further investigation is required in this area in order to identify a reliable method of production.

		Diameter (nm) in PBS		Diameter (nm) in SF DMEM	
		DLS	CPS	DLS	CPS
Polyacrylamide	Unfunctionalised	36.5 ± 1.7	33.8 ± 0.8	38.1 ± 1.0	32.5 ± 0.3
	2% ACTA	32.2 ± 1.1	(-)	33.0 ± 0.5	(-)
	5% ACTA	38.0 ± 0.3	(-)	38.3 ± 0.7	(-)
	10% ACTA	39.3 ± 1.3	(-)	40.0 ± 0.1	(-)
	15% ACTA	41.2 ± 0.9	33.2 ± 1.0	42.4 ± 0.3	30.4 ± 1.0
	20% ACTA	53.4 ± 1.5	39.8 ± 0.8	54.7 ± 0.2	39.8 ± 0.8
Silica	Negative	290.9 ± 5.4	360.9 ± 0.1	315.5 ± 32.0	360.4 ± 2.0
	Positive	291.8 ± 2.9	293.0 ± 1.8	293.6 ± 20.9	290.2 ± 0.7

Table 3.1: Summary table of polyacrylamide and silica nanoparticle diameter (nm) in PBS and serum free DMEM (SF DMEM) measured using Dynamic Light Scattering (DLS) and the CPS Disc Centrifuge. (-) indicates batches of nanoparticles not measured using the CPS Disc Centrifuge.

		Zeta Potential (mV)		
		PBS	DMEM	SF DMEM
Polyacrylamide	Unfunctionalised	-3.5 ± 0.1	-5.2 ± 0.7	-3.3 ± 0.7
	2% ACTA	-2.3 ± 1.5	-3.2 ± 0.6	1.8 ± 0.7
	5% ACTA	5.6 ± 0.8	-0.1 ± 0.5	6.9 ± 1.7
	10% ACTA	12.3 ± 1.3	5.9 ± 0.5	13.2 ± 0.6
	15% ACTA	15.0 ± 0.7	6.4 ± 0.5	17.6 ± 2.3
	20% ACTA	19.0 ± 0.7	3.9 ± 0.3	18.6 ± 1.9
Silica	Negative	-29.4 ± 2.0	-10.7 ± 0.8	-25.0 ± 1.5
	Positive	25.4 ± 0.9	-8.9 ± 0.2	26.5 ± 2.7

Table 3.2: Summary table of the zeta potential (mV) of polyacrylamide and silica nanoparticles in PBS, DMEM and serum free DMEM (SF DMEM).

3.3 Conclusion

Silica and polyacrylamide nanoparticles with varying charge and surface functionalisation have been synthesised and their size and charge have been well characterised using a number of methods. The density of the nanoparticles has been calculated using the CPS disc centrifuge. Nanoparticle fluorescence has been characterised using two methods in order to be able to eliminate any differences in

particle fluorescence from the measurement of nanoparticle uptake which was calculated using the measured fluorescence intensity within cells.

Chapter 4 - Scanning Probe Microscopy

Atomic Force Microscopy and Scanning Ion Conductance Microscopy

4.1 Introduction

The first step in the uptake of nanoparticles into cells involves their interaction with the cell membrane and this interaction is an important factor in the route of uptake of the nanoparticles. In addition, the subsequent subcellular trafficking of nanoparticles can be influenced by their interaction with intracellular components. There are many factors that govern this interaction and these have been discussed in the introduction but briefly, they include nanoparticle size, shape, surface chemistry and charge, along with cell dependent factors including cell type and membrane components. Increasing the understanding of how nanoparticles interact with cell membranes on the nano and micron scale will help to increase understanding of the uptake processes and may be useful in the development of more efficient drug delivery systems.

The development of scanning probe microscopy techniques such as AFM and SICM have enabled this interaction to be visualized in real time at the nanoscale. AFM has been used extensively to investigate how nanoparticles and peptides interact with supported lipid bilayers. These results have often been shown to correlate well with *in vitro* studies of nanoparticle uptake into cells. New technology is beginning to enable the imaging of cells using AFM, which has previously been extremely difficult due to the force applied to the cell membrane by the AFM tip. More recently, the development of the non contact scanning probe technique, SICM, has enabled the visualization of the interaction of nanoparticles with a real cell membrane both on cells that have been chemically fixed as uptake occurs, and also on live cells¹⁶³.

In this work, two scanning probe techniques were used to image the interaction of polyacrylamide and silica nanoparticles with model and real cell membranes. SICM, combined with fluorescence microscopy in a technique known as Scanning Surface Confocal Microscopy (SSCM), was used to investigate the interaction of silica nanoparticles with cell membranes of MRC-5 cells. It was not possible to repeat this

work using polyacrylamide nanoparticles since the resolution of the SSCM was not high enough. Instead, the interaction of polyacrylamide nanoparticles was investigated using supported lipid bilayers (SLBs) composed of dipalmitoylphosphatidylcholine (DPPC), which were imaged using tapping mode atomic force microscopy (AFM) in liquid.

4.1.1 Cell membranes

Cell membranes are complex structures that surround cells, and components of the membrane play a crucial role in maintaining the intracellular environment. They contribute to many of the processes that cells undergo, including transport of molecules, signalling and migration^{11, 220}. The membrane is composed of a number of molecules including phospholipids, sphingolipids, cholesterol and proteins¹⁷. Phospholipids are amphiphilic lipids that form the majority of the cell membrane through their association into a lipid bilayer. They consist of hydrophilic head groups and hydrophobic fatty acid chains. These lipids spontaneously form the membrane bilayer when the hydrophobic chains of two phospholipids associate and face each other leading to the exclusion of water. Differences in these fatty acid chains such as level of saturation and length can affect the structure of the membrane and influence parameters such as the packing of lipids, affecting the fluidity of the bilayer. There are a number of different phospholipids that can be found in cell membranes and these include phosphatidylcholine and phosphatidylethanolamine. The different head groups on these lipids give them specific properties, which therefore influence the properties and functions of the bilayer they reside in. The upper and lower leaflets of the bilayer are usually asymmetric in terms of their lipid and protein composition, and the presence of these different molecules confers different functions to these parts of the bilayer^{150, 221}.

The cell membrane is not a static structure, it is fluid and can move and change shape depending on conditions. It has been suggested that unlike previously thought, this movement is not random but that the membrane consists of defined regions that have a distinct protein and lipid composition e.g. caveolae rich regions and lipid 'rafts' composed of sphingolipids and cholesterol²²². In addition to lateral movement in one half of the bilayer, proteins and lipids can flip between the upper

and lower leaflets of the bilayer^{150, 221, 222}. Bilayers are sensitive to temperature and also to the effects of molecules such as cell penetrating peptides and these interactions can lead to changes in the phase of the bilayer. The bilayer can exist in a number of different phases including a fluid, liquid state and a more rigid gel-like state²²³⁻²²⁵.

4.1.2 Supported lipid bilayers

AFM studies of cell membranes are difficult due to their delicate nature and the force that is applied by the AFM tip during imaging. This force can lead to deformation of the cell, damage to the membrane and the transfer of components from the membrane onto the tip which affects imaging resolution. Studies that use AFM to investigate the interaction of molecules with cell membranes therefore generally use model membranes^{150, 157}. Supported lipid bilayers (SLBs) are model cell membranes that can be produced by a number of methods that result in the formation of a phospholipid bilayer on a solid surface. These bilayers can then be imaged using AFM^{156, 157, 159, 223, 226-229}. SLBs are a useful tool for investigating the interaction of molecules with cell membranes since information about changes in surface topography and bilayer thickness can be obtained^{53, 93, 230-232}.

The vesicle fusion technique is a simple technique that can be used to form bilayers and involves the formation of small, unilamellar lipid vesicles via freeze-thawing and extrusion. These vesicles adsorb to a mica support and over time, they collapse and fuse to form a symmetrical bilayer. When bilayers are formed by this method, other molecules such as proteins can be included if required but one drawback is that only symmetrical bilayers can be produced^{146, 156, 157}. The composition of the membrane chosen is important because nanoparticles have been found to interact differently with bilayers composed of a single phospholipid compared to a more complex model endothelial cell membrane²³³.

4.1.3 Atomic Force Microscopy

AFM has proved to be a very useful technique for the study of interactions of different substances with SLBs. It has been used to investigate the effect of a wide range of molecules and particles such as dendrimers, cell penetrating peptides and nanoparticles^{95, 231, 234}. The interaction of these molecules with the bilayer can lead to effects such as changes in the height of the membrane, changes in the phase of the

bilayer between fluid and gel phases, and changes in topography such as the formation and expansion of holes in the bilayer which can be observed and measured^{234, 235}. Measurement of changes in height can be particularly useful for identifying changes in the phase of the bilayer.

4.1.3.1 Investigating the effects of nanoparticles using AFM

AFM has been used to assess the interaction of many different nanoparticles with SLBs. A variety of cationic nanoparticles, cell penetrating peptides and polymers have been shown to enter cells, and AFM studies have indicated that these nanoparticles lead to varying degrees of bilayer disruption (Figure 4.1)^{97, 234}.

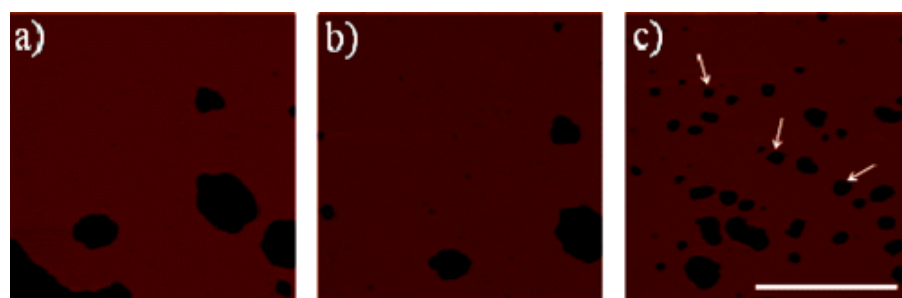


Figure 4.1: The effect of the cationic polymer poly-L-lysine on a DMPC supported lipid bilayer. The addition of the polymer caused the appearance of defects in the bilayer which are indicated by the white arrows²³⁴.

Cationic nanomaterials may interact with bilayers via insertion into the bilayer if their size is very small, or more commonly via electrostatic interactions between the material and the head groups of phospholipids in the bilayer^{53, 233}. In contrast, neutral and negatively charged molecules appear to induce minimal bilayer disruption²³⁴. Changes that can be observed following exposure to cationic particles include the formation and/or expansion of holes in the bilayer and changes in the height of the bilayer. Membrane thinning and erosion, and hole formation in lipid bilayers due to cationic nanoparticles is commonly observed regardless of the size, chemical composition or shape of the nanoparticle^{86, 97, 236, 237}. In addition to the formation of holes, changes in the phase of the bilayer, for example fluidisation, have also been observed following interactions with nanoparticles. These changes can be caused by the interaction of molecules with the head groups of lipids, leading to a change in the tilt angle of the lipid in the membrane^{97, 235}. To demonstrate the

importance of using multiple different lipids in a SLB to imitate the different regions observed in a cell membrane, Peetla *et al.* used a model endothelial cell membrane. They found that cationic nanoparticles interacted to a greater extent with the liquid phase region leading to condensation of the regions via insertion into the membrane or electrostatic interaction⁵³.

Relating the changes observed in SLBs using AFM to *in vitro* cell studies can help to explain what may be happening during uptake, for example, the formation of holes in a model membrane may explain the cytotoxicity of some nanoparticles. It has been shown that the degree of SLB disruption correlates well with *in vitro* studies of enzyme leakage, nanoparticle uptake and cytotoxicity⁹⁷. The nanoscale nature of AFM also means that the subtle nature of differences in these interactions can be observed, for example Leroueil *et al.* found that more highly charged polymers have been found to expand pre-existing defects and form new defects, whilst polymers with a lower charge accumulated around the edge of pre-existing defects⁹⁷.

In addition to topography imaging of model cell membranes with AFM, it can also be used to investigate the forces of interactions between molecules, e.g. ligands and receptors or protein interaction and unfolding²³⁸. AFM has been used to measure the force of attraction between nanoparticles and the cell membrane, and to correlate this force to the cellular uptake of nanoparticles. Vasir *et al.* used AFM to look at the internalization of nanoparticles over time and the effect on membrane height and general topography. Additionally, it was used to measure the force of interaction using nanoparticle functionalised tips. PLGA nanoparticles functionalised with the cationic peptide poly-L-lysine were found to display a five-fold greater force of adhesion with the cell membrane and their internalization was rapid compared to unmodified nanoparticles. Time lapse images of live cells imaged using tapping mode AFM showed rapid uptake of the poly-L-lysine functionalised nanoparticles whereas cell surfaces remained covered with unfunctionalised nanoparticles since they were not internalized. The nanoparticles used in the study were negatively charged under the experimental conditions, indicating that electrostatic interactions were not important, adhesion was more likely to be due to nonspecific interactions such as hydrogen bonding⁶¹.

4.1.3.2 Investigating the effects of cell penetrating peptides using AFM

As discussed in the main introduction, cell penetrating peptides are a class of molecules that have been shown to effectively transport cargo including nanoparticles across the cell membrane. They include Tat, an arginine and lysine rich peptide derived from the HIV-1 protein^{192, 239, 240}. The mechanism by which Tat transports cargo molecules across the cell membrane has been a subject of much debate, although it is now believed that macropinocytosis may play a role^{50, 108}. By using AFM to visualize the interaction of Tat peptide with cell membranes on the nanoscale, this may help to increase the level of understanding about the processes involved.

Tat (transactivating transcriptional activator) peptide is derived from the HIV-1 Tat protein, an 86 amino acid protein involved in replication of the HIV-1 virus. It consists of an acidic N terminal region involved in transactivation, a DNA binding domain and a basic region containing a nuclear localization signal²⁴¹. Tat peptide is the most well studied CPP and it is popular because it has a short sequence and is very efficient at crossing membranes^{11, 105, 242}. Only a small region of the full protein is required for its cell penetrating ability. This small peptide contains a basic region of amino acids with a highly cationic cluster comprising 6 arginine and 2 lysine residues (GRKKRRQRRRQ)^{45, 48, 101, 217}.

The interaction of Tat peptide with model cell membranes has been extensively studied using AFM. The mechanism by which Tat peptide interacts with model membranes is a subject of controversy with some groups suggesting that it can insert into the bilayer causing the formation of raised regions as the bilayer reorganises to accommodate it. In one study on model membranes composed of a liquid and gel phase lipids to model the lipid rafts in cell membranes, Tat peptide was found to cause expansion of the taller, gel-phase regions via insertion into the bilayer²⁴³. Other work indicates that it does not insert into the bilayer, but interacts with the negatively charged head groups of lipids in the bilayer, causing a change in the tilt angle of the lipids and reorganisation of the bilayer⁴⁵.

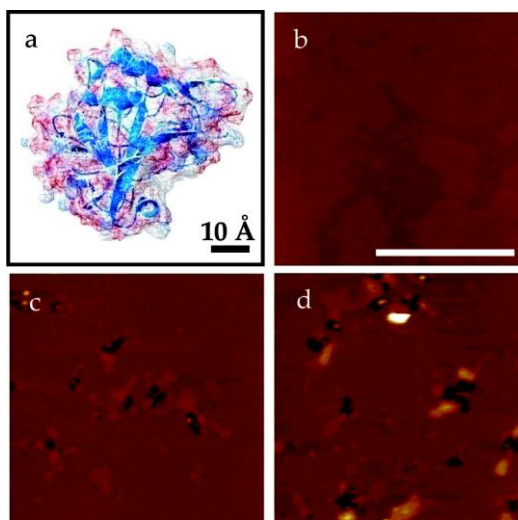


Figure 4.2: (a) Space filling model of Tat, (b) DMPC bilayer before addition of Tat, (c) and (d) are subsequent images taken over 20mins showing the formation and expansion of defects in the bilayer⁹⁷.

Although Tat peptide is cationic and therefore may be expected to interact through electrostatic interactions with the head groups of lipids, it has few hydrophobic residues compared to many other CPPs, and this may decrease the likelihood of it inserting into bilayers^{192, 243}.

4.1.3.3 Peptide conjugated nanoparticles

Cell penetrating peptides such as Tat have been shown to be able to transport a wide range of cargos into cells including gold⁶⁴, polymeric nanoparticles^{244, 245} and lipoplexes²⁴⁶. The cationic nature of Tat and the presence of a nuclear localization signal make it an attractive molecule for potentially enhancing the delivery of molecules such as DNA that need to reach the nucleus to be effective²⁴⁶.

It is generally observed that provided the peptide maintains its conformation upon attachment to the nanoparticle, the presence of the peptide leads to enhanced uptake into cells when compared to nanoparticles alone, even if they are cationic or amine functionalised^{93, 217}. The addition of a conjugated cargo to the Tat protein transduction domain has been shown to lead to association of the cargo with cell membrane lipids and increased association of the Tat peptide with the membrane. The presence of the cargo may therefore affect the way in which the peptide is presented to the membrane, leading to a different interaction. Alternatively, the

cargo itself may have some effects on the bilayer which subsequently affect the interaction of the peptide with the membrane²³⁹.

Peetla *et al.* investigated the effect of Tat peptide conjugation to nanoparticles, the Tat peptide sequence and the amount of peptide on the nanoparticle. They showed that these factors significantly affected the biophysical interaction of the nanoparticles with a model endothelial cell membrane. It was found that the Tat peptide conjugated to poly(L-lactide) nanoparticles had a greater effect on the membrane, measured using surface pressure than the peptide alone. This indicated that the conjugate was interacting with the membrane to a greater extent than either of the components alone, either via insertion into the membrane or electrostatic interactions. Tat conjugated nanoparticles became embedded in the membrane and caused fluidisation of the endothelial cell membrane. It was suggested that this may be due to the interaction of the hydrophobic tyrosine residue on the Tat peptide with the bilayer, along with electrostatic interactions with the anionic phospholipids in the membrane. Since Tat peptide and nanoparticles alone did not display the same interaction despite similar cationic charges, the way in which the nanoparticles interact with cell membrane lipids when conjugated to the CPP must play a role in their internalization. The AFM studies corresponded well with *in vitro* work showing increased uptake of the nanoparticles when conjugated to Tat. However, the peptide sequence was important since when the same experiment was repeated with scrambled Tat peptide that exposed different residues to the bilayer, the interaction was comparable to that of unconjugated nanoparticles⁹³.

4.1.4 Scanning Ion Conductance Microscopy

The use of SICM increases the range of experimental techniques that can be performed to investigate nanoparticle uptake. The non contact nature of the technique means that it is better suited to the imaging of cells than AFM since it will not cause damage to the cell. In addition, it is more suited to relatively high and rough samples such as cells due to a greater z range, and it can be used to image larger areas of a membrane. SICM has been used to look at delicate, eukaryotic cells that have proven to be difficult to image using other scanning probe techniques such as AFM. The hopping mode of SICM has been used to image neuronal cells with fine

processes such as axons at high resolution without damage¹⁶⁴. As well as imaging, the hollow pipette used in SICM allows for the delivery of molecules to specific areas of the sample. SICM has been used to image ion channels on the surface of cells and to investigate the interaction of various particles with cells^{168, 172, 176, 177}. In addition to topography imaging, the development of SSCM has enabled the simultaneous imaging of changes in topography and fluorescence, allowing tracking of nanoparticles during cellular uptake. However, despite these advantages, the resolution and imaging speed of SICM is generally lower than AFM, meaning that live cell studies can be difficult¹⁶¹.

4.1.4.1 Investigating the effects of nanoparticles using SSCM

Gorelik *et al.* used SSCM to image the uptake of virus like particles into COS-7 cells and showed that SSCM could combine high resolution topography imaging with fluorescence imaging in order to identify the location of the nanoparticles on the cell surface and to monitor them during internalization (Figure 4.3).

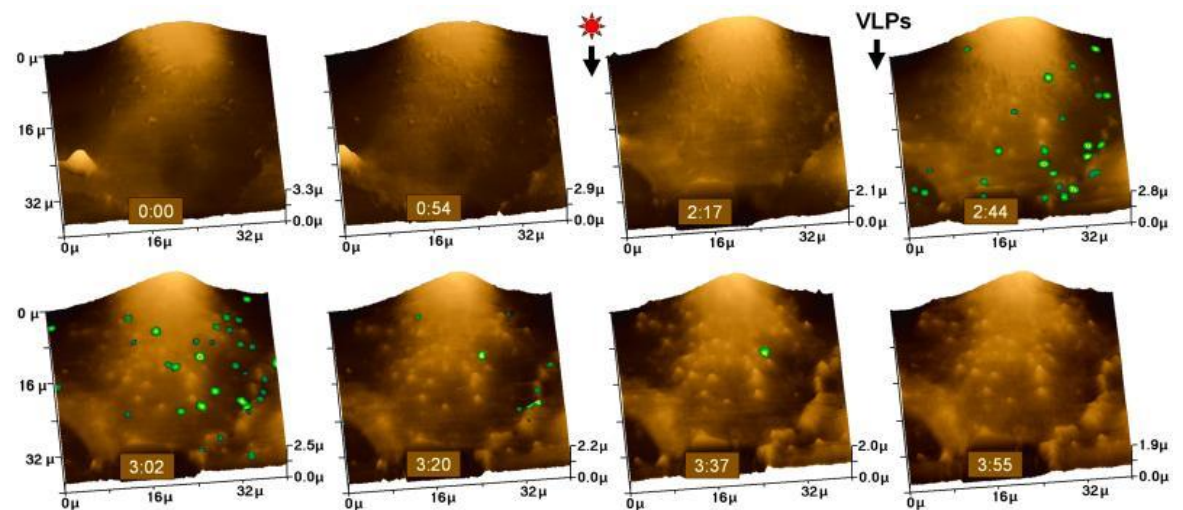


Figure 4.3: COS-7 cells exposed to virus like particles (green fluorescence) showing uptake of the particles over a four hour time period. The red star indicates the beginning of the scanning for fluorescence and VLPs indicates when the fluorescent virus like particles (VLPs) were added¹⁷⁷.

SICM has also been used to investigate the effect of amine functionalised polystyrene nanoparticle size, surface chemistry and charge on the topography of the cell membrane of human alveolar epithelial type 1-like cells (AT1). It was found

that exposure to the amine modified nanoparticles caused damage to the cell membrane, characterized by the appearance of holes in the membrane. The nanoparticles were also found to lead to some disruption of the contacts between cells, and it was suggested that nanoparticle inhalation therefore has the potential to cause damage to lung cells. These effects on the cell were not observed with other types of nanoparticles (unmodified and carboxyl modified) which, following incubation with the cells showed that they retained a flat, mainly featureless membrane. The effects of the nanoparticles on the cell membrane correlated well with complementary studies that were performed looking at cytotoxicity⁵⁴.

SSCM has also been used to investigate latex nanoparticle uptake in primary human alveolar type 2 (AT2) cells and immortalized AT2 cells that showed an AT1-like phenotype. It was found that charge, rather than size was the key factor in nanoparticle uptake and that negatively charged particles were internalized to a greater degree by AT1 cells, which form the majority of the alveolar surface. SSCM demonstrated that internalization of the 50nm particles occurred in areas enriched with microvilli¹.

Recently, the use of SSCM to investigate clathrin mediated endocytosis has shown that uptake by this route may involve additional protrusions and processes on the cell membrane than those previously identified. This highlights the benefits of scanning probe techniques such as AFM and SICM which help to reveal the nanoscale nature of the interactions of nanoparticles and cells¹⁶³.

4.1.5 Comparison between AFM and SICM

Whilst both AFM and SICM are undoubtedly useful techniques for imaging the interaction and uptake of nanoparticles with model membranes and cells, there are limitations to both techniques and one or the other may be better suited for a particular experiment. In a study that compared the ability of both AFM and SICM to image MRC-5 cells, the height of the cell was underestimated using AFM due to the force applied by the AFM tip during imaging. A lateral force was also applied by the AFM tip, and this was observed as a shift in the trace and re-trace of the AFM profile. In contrast, SICM enabled the visualization of protruding features on the cell surface which were dislodged by the AFM tip. Using AFM, more subcellular features such as the cytoskeleton were visible although this was also influenced by the fixation

procedure. Both AFM and SICM face difficulties when imaging structures with large height differences such as the step up from the cell culture dish to the edge of the cell¹⁶¹.

SICM has also been used to image various samples including collagen fibres and HeLa cells and the images were compared to those obtained using AFM. SICM was found to produce high resolution images indicating the presence of delicate surface features on HeLa cells and enabled the real time monitoring of changes in the cell surface over time. Although AFM produces images with a better resolution than SICM, the restriction in the Z range of AFM means that the hopping mode of SICM may produce better images of samples with sudden, steep changes in height and may cause less damage to the sample than the AFM tip. In addition, AFM is often restricted in the size of sample it can image before it encounters problems with lateral forces and restrictions at the edge of the imaging area²⁴⁷.

4.2 Results and Discussion

4.2.1 AFM results

4.2.1.1 Characterisation of liposomes

Suspensions of liposomes used to form SLBs were analysed using the low density disc on the CPS Disc Centrifuge (see section 2.6.1). A 1mg/ml suspension of liposomes was analysed on a 4-12% sucrose in D₂O gradient. The diameter of DPPC liposomes was 118nm.

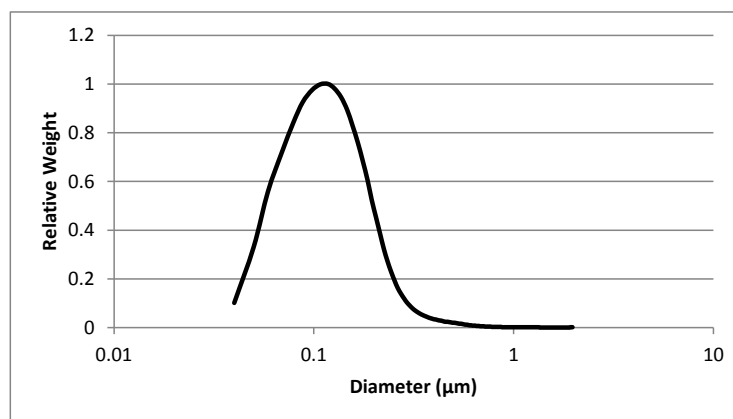


Figure 4.4: Diameter of DPPC liposomes obtained using the low density disc.

4.2.1.2 Interactions of nanoparticles with SLBs

SLBs composed of the gel phase lipid DPPC were imaged following exposure to a range of polyacrylamide nanoparticles. In Figure 4.5 darker areas represent the mica surface whilst lighter coloured areas represent areas covered by the bilayer. Lipids can exist in different phases depending on their composition and temperature. The behaviour of the lipid is determined by the main gel-fluid transition and a number of transient intermediate states can also be formed^{159, 235}. DPPC is in the gel phase at room temperature since it has a transition temperature of around 41°C. In AFM imaging, this was identified by examining bilayer thickness since gel phase bilayers are approximately one nanometre higher than fluid phase bilayers. Literature reports indicate that a height of 4.5 – 5.8nm is characteristic of a DPPC bilayer¹⁵⁹. The results from this work show a rather wide range in bilayer thickness of 5.9 – 6.9nm. However, a thin water layer is known to exist between the

mica and the lower surface of the bilayer and may account for this^{232, 248}. The DPPC gel phase bilayer formed regions of continuous bilayer with defects exposing the underlying mica and was stable when imaged over time.

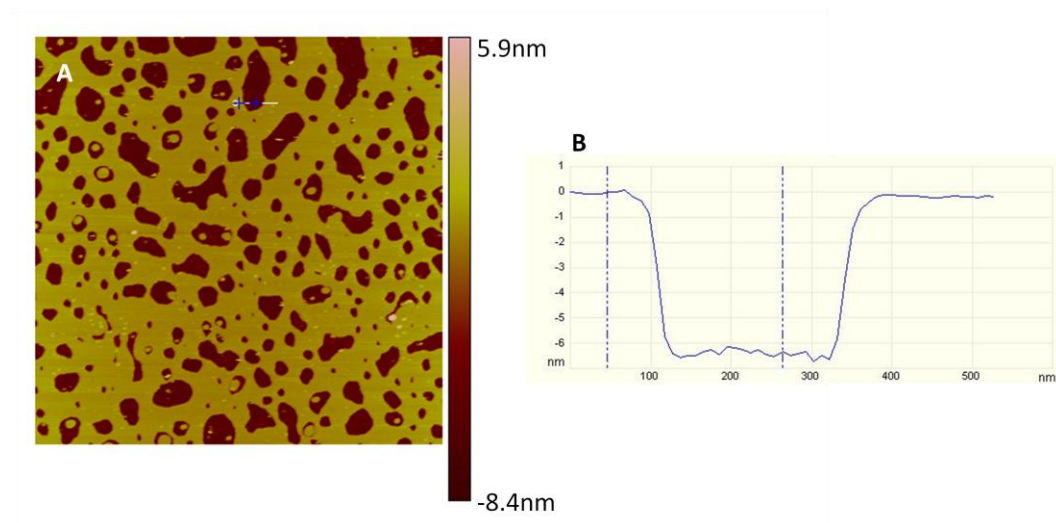


Figure 4.5: (A) DPPC bilayer, (B) cross section of DPPC bilayer as indicated by white line in (A). Bilayer height is 6.3nm.

4.2.1.3 Interactions of polyacrylamide nanoparticles with SLBs

Unfunctionalised polyacrylamide nanoparticles (37nm) with a charge of -6mV did not change the appearance or height of the bilayer and adsorbed to the mica surface (Figure 4.6). This is consistent with data obtained from cellular uptake experiments discussed in Chapter 5.2.1, which show that unfunctionalised polyacrylamide nanoparticles with a slightly negative zeta potential were not significantly taken up by MRC-5 fibroblasts.

Positively charged polyacrylamide nanoparticles containing 5% ACTA (6.9mV) were imaged on mica (Figure 4.6). Nanoparticle size was analysed using the particle analysis function in the Nanoscope software which indicated that the particles had a mean diameter of 32nm with a range between 22 and 64nm. This correlated well with the nanoparticle size data obtained using DLS and the CPS disc centrifuge presented in Chapter 3.2.2.1 and 3.2.2.3.

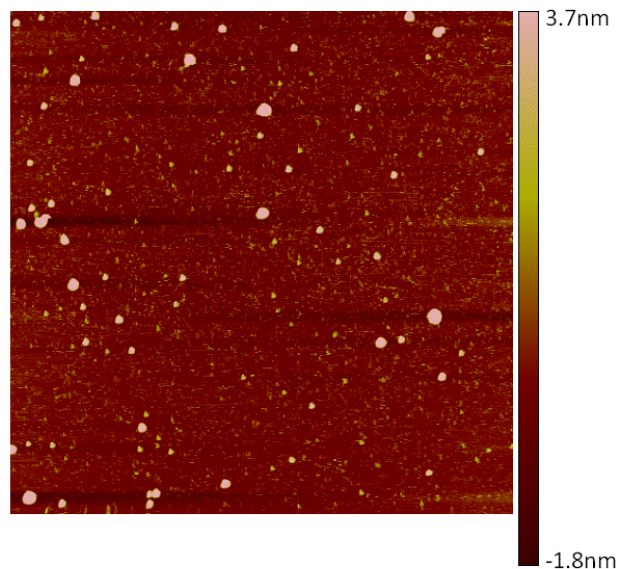


Figure 4.6: AFM image of 100 μ g/ml suspension of positively charged polyacrylamide nanoparticles in water on a mica surface. Scan size 2 x 2 μ m.

Positively charged polyacrylamide nanoparticles were found to cause limited reorganization of the DPPC lipid bilayer. This was only observed at relatively high nanoparticle concentrations and was characterized by changes in topography such as the fusion of some bilayer defects. However, the majority of the nanoparticles were again found to be present on the mica surface and around the edge of defects in the bilayer (Figure 4.7). At the highest concentration of 25 μ g/ml, the positively charged nanoparticles caused several bilayer defects to merge and form larger holes in the DPPC bilayer. However, these events were isolated and the widespread formation of new holes was not observed.

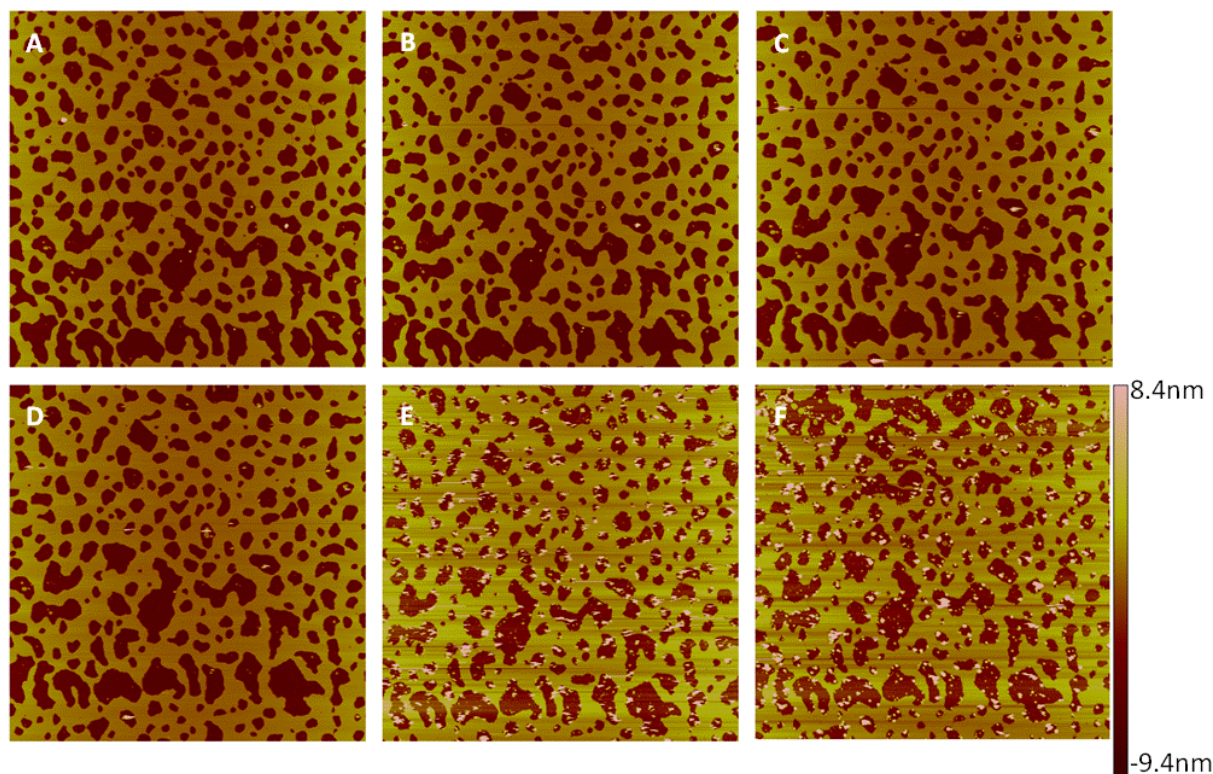


Figure 4.7: AFM images of a DPPC lipid bilayer exposed to increasing concentrations of positively charged polyacrylamide nanoparticles. (A) The DPPC bilayer was relatively stable over time and when exposed to 20 µl of HPLC grade water (B). Images C to F show the effect of exposure to increasing concentrations of positively charged nanoparticles (C) 1 µg/ml, (D) 10 µg/ml and (E) 25 µg/ml. (F) was taken 30 minutes after (E). Scan size 5 x 5 µm.

The slightly reduced height of the nanoparticle observed in the cross section (Figure 4.8 B1) is likely to be due to tip deformation of the nanoparticle and the nanoparticle being pushed into the soft bilayer surface by the AFM tip.

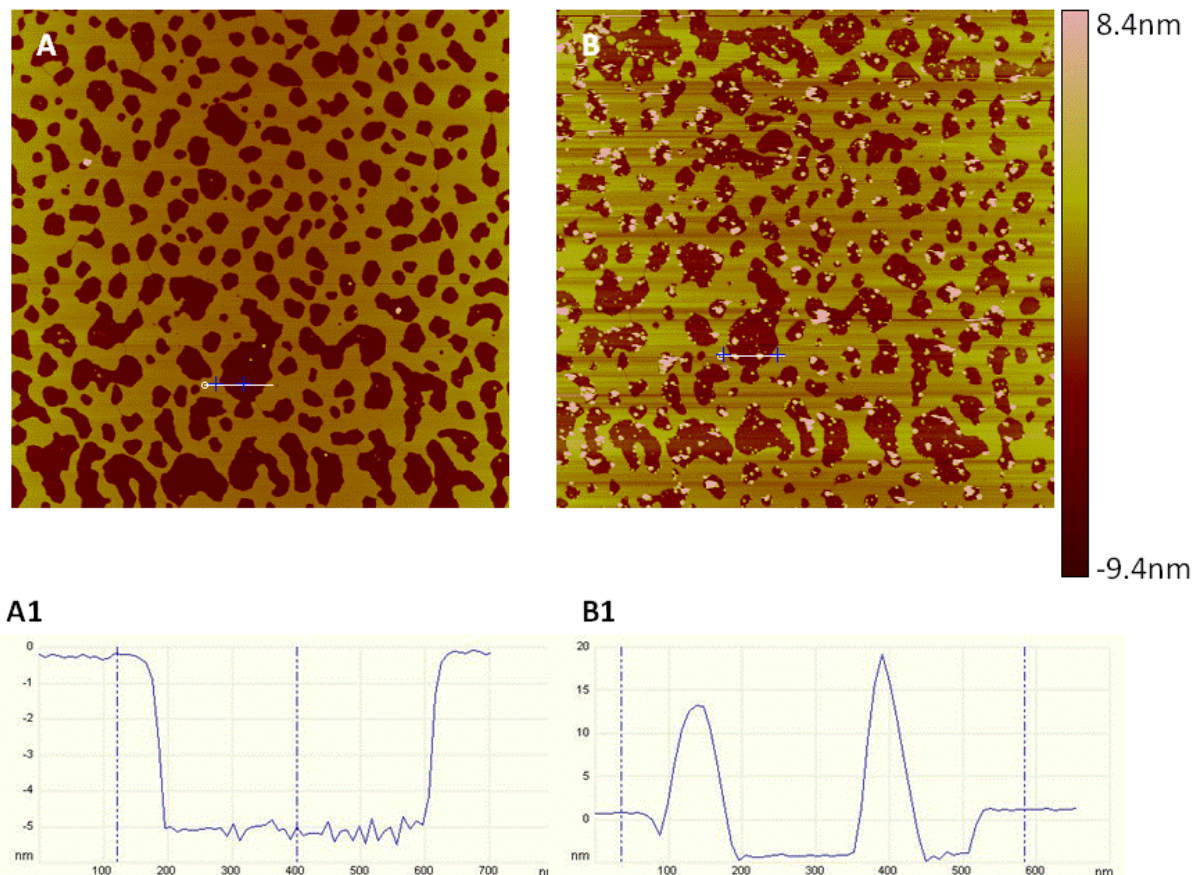


Figure 4.8: Cross sections of DPPC bilayer exposed to positively charged nanoparticles demonstrate the nanoparticle addition had no effect on bilayer thickness. (A) DPPC bilayer before particle addition, height is 4.8nm. (B) DPPC bilayer following the addition of 25µg/ml positively charged nanoparticles, height is 5.0nm.. Scan size 5µm x 5µm.

Figure 4.9 shows an enlarged area of a small section of Figure 4.8 to show in detail the association of the positively charged nanoparticles with the edge of the bilayer and with the mica surface. This is consistent with the results of Leroueil *et al.* who showed that cationic entities with a relatively low degree of positive charge tended to accumulate at the edge of bilayers without causing many defects. The mica surface and bilayer itself often carry a slight negative charge, causing the nanoparticles to be attracted to these regions of the bilayer⁹⁷. The elongated shape of the nanoparticles and the slight ‘tail’ seen on some of the nanoparticles suggests that the tip can drag the nanoparticle across the bilayer surface due to the presence

of only a weak attraction between the bilayer and the particle. This can lead to the tip depositing the particle at the edge of the bilayer or on the mica surface.

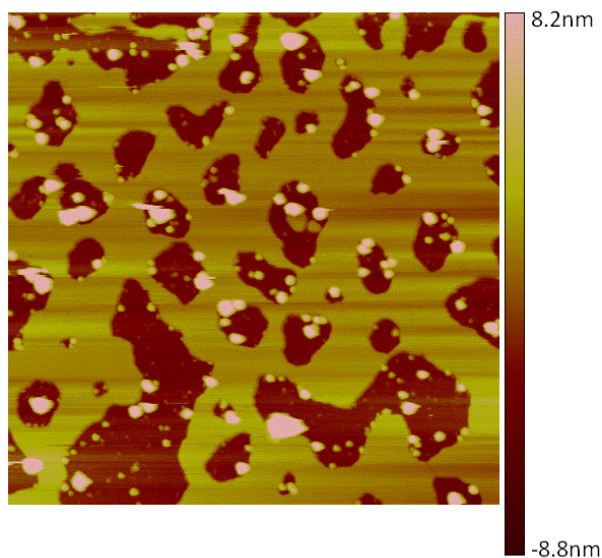


Figure 4.9: Enlarged area of Figure 4.8B to show detail of positively charged polyacrylamide nanoparticles associated with the edge of membrane defects and mica. Scan size 2 x 2 μm .

Bearing analysis to look at the coverage of the bilayer was performed using the Nanoscope software. It showed that the area of mica covered by the bilayer was not significantly affected by the addition of the nanoparticles, indicating that no solubilisation of the bilayer occurred due to nanoparticles. This again shows that the positively charged nanoparticles had limited effects on the structure of the DPPC bilayer. Initial bilayer area in Fig 4.7A was 60% whilst in Fig 4.7F the area covered by the bilayer was 59%.

The interaction of positively charged polyacrylamide nanoparticles with a model cell membrane composed of DPPC therefore appeared limited when the particles possessed a low level of charge. This correlates well with *in vitro* studies presented in Chapter 5 that show limited uptake of the same positively charged particles into MRC-5 cells. The effect of the polyacrylamide nanoparticles produced with a higher level of charge on SLBs was not investigated due to time constraints. However, it would be expected that they would cause increased effects on the structure of the bilayer such as increased fusion of holes and the formation of new defects. The

nanoparticles are unlikely to insert into the bilayer due to their size, therefore the effects are more likely to occur via the interaction of the charged groups on the nanoparticle with the head groups of the lipid causing some change in the organisation of the lipids forming the bilayer²³⁵.

4.2.1.4 Interactions of Tat peptide with SLBs

Initially, the addition of low concentrations of Tat peptide did not cause dramatic changes in surface topography, but led to a small change in the height of the bilayer. Following exposure to higher concentrations of Tat, the formation of raised regions around bilayer defects was observed. In addition, Tat catalysed the formation of holes in the bilayer and enlargement of existing defects (Figure 4.10).

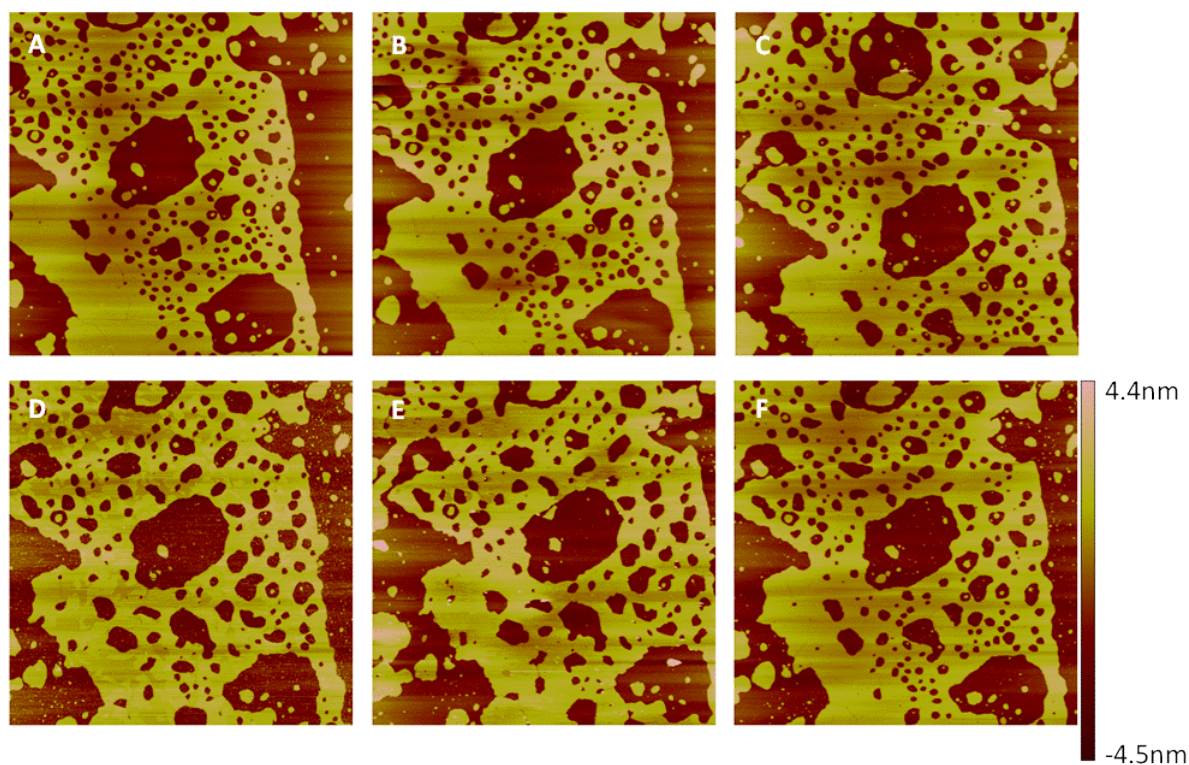


Figure 4.10: AFM images of the effects of Tat peptide on a lipid bilayer. (A) DPPC bilayer and (B) following addition of 20µl HPLC grade water shows some mobility but few changes in bilayer structure. Images C to F show the bilayer following exposure to increasing concentrations of Tat peptide. (C) 1µM, (D) 2.5µM, (E) 5µM and (F) 10µM. The formation of higher domains is observed around the edge of bilayer defects. Scan size 5 x 5µm.

Figure 4.11 shows a smaller scale area ($2 \times 2\mu\text{m}$) showing in detail the effect of Tat peptide on the DPPC bilayer. In Figure 4.11 E especially, it can be clearly be seen that there are distinct regions of different height within the bilayer which can be identified by different shades of colour.

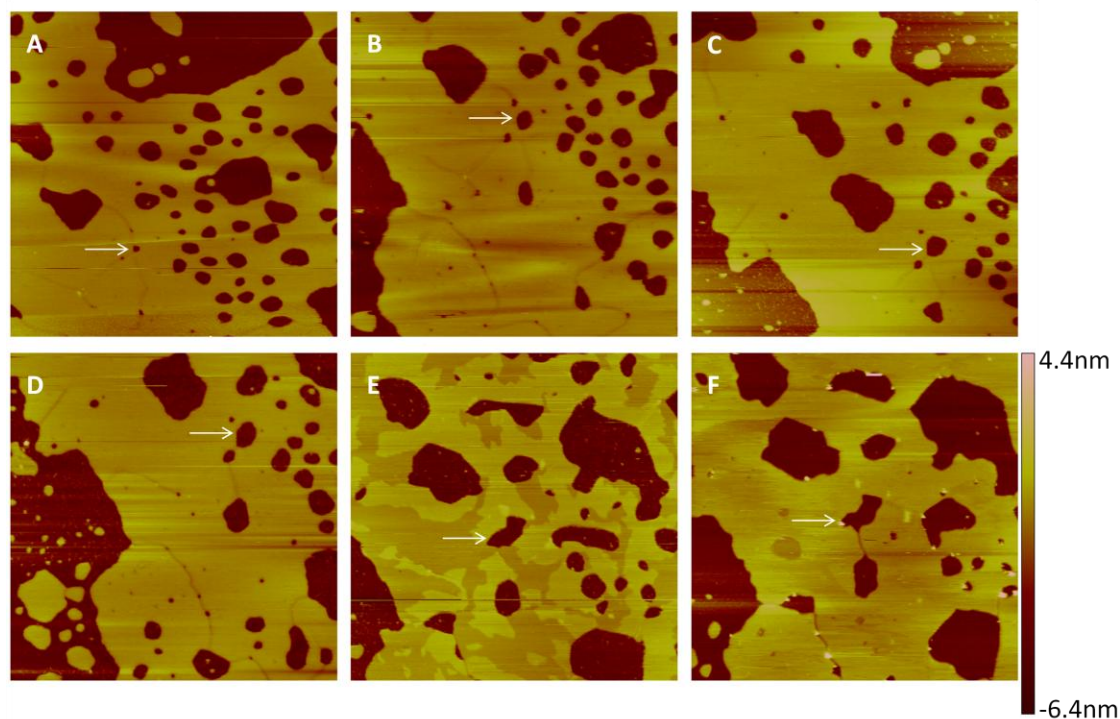


Figure 4.11: AFM images of a smaller area of the same DPPC bilayer as in Figure 4.10. (A) DPPC bilayer, (B) following addition of $20\mu\text{l}$ HPLC grade water, (C) $1\mu\text{M}$ Tat, (D) $2.5\mu\text{M}$ Tat, (E) $5\mu\text{M}$ Tat showing raised domains around edge of defect. (F) $10\mu\text{M}$ Tat with further coverage of raised domains. White arrows indicate the same defect in the bilayer which gradually expands along with the merging of other defects. Scan size $2 \times 2\mu\text{m}$.

In Figure 4.12 the white lines are cross sections of the bilayer showing that the height of the bilayer increased by approximately one nanometre following Tat exposure at $5\mu\text{M}$. A1 shows a 4.2nm bilayer, which is representative of a DPPC gel phase bilayer. B1 shows an increase in bilayer height with a raised region at the edge of the bilayer defect, approximately 0.8nm above the bilayer.

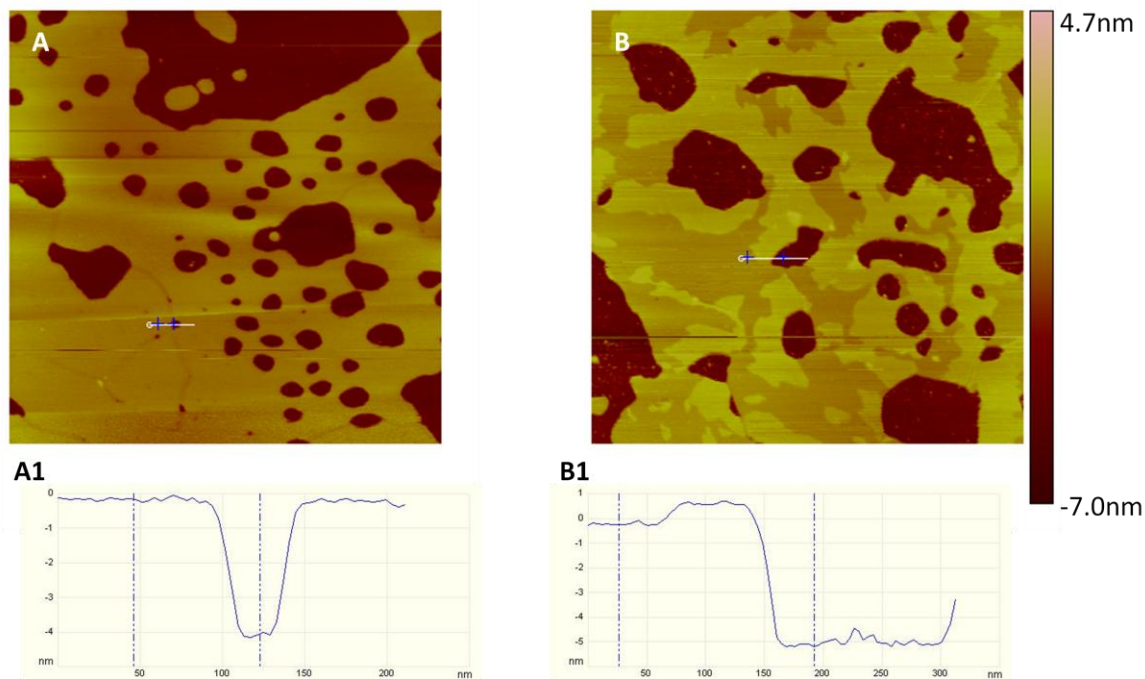


Figure 4.12: Cross sections of DPPC before (A) and after exposure (B) to 5 μ M Tat peptide. Original height of bilayer is 3.6nm, in B1, bilayer height is 4.6nm and the height of the bilayer where Tat peptide acts is 5.7nm, approximately 1nm higher. Scan size 2 x 2 μ m.

Bearing analysis of bilayer area was also performed on these images. Overall, bilayer area was again not affected to a great extent by the addition of Tat peptide, similarly to that observed for the positively charged nanoparticles. Initial bilayer area in Figure 4.10A was 55% whilst in Figure 4.10F, the area was 53%. The average measurement of bilayer coverage produced from all images (not shown) at each concentration of Tat shows that bilayer coverage on average decreased from $54 \pm 1.6\%$ to $53 \pm 1.1\%$. Similarly in Figure 4.11A, area covered by the bilayer was 84% which decreased to 74% in Figure 4.11F but the average decrease for the whole series of images was from $79 \pm 7.7\%$ to $71 \pm 1.0\%$. However, it was interesting to see that although the overall coverage of the bilayer was only marginally changed, the area of the raised regions in Figure 4.10E and Figure 4.11E could be easily measured using the bearing analysis function. In Figure 4.10E this was 21.2% and in Figure 4.11E the area was 37.3%, providing a quantitative

measurement of the area of the bilayer that changed in height following the addition of Tat peptide.

The increases in bilayer height caused by the addition of Tat peptide may be attributed to the insertion of the peptide into the bilayer, causing reorganisation and condensation of lipids^{45, 48}. However, some groups argue that this is unlikely due to the lack of hydrophobic residues on the peptide and the densely packed acyl chains of the phospholipids present in the bilayer²⁴³. If Tat does interact with the membrane in this manner, as it inserts into the bilayer, there is less space for the lipid molecules, so they become more ordered to accommodate the presence of the peptide leading to an increase in bilayer thickness. However, there may also be a decrease in bilayer thickness caused by solubilisation of the lipid. This would be expected as the lipid reorders following insertion of the Tat peptide. An alternative explanation for the effect of Tat peptide is through surface adsorption via electrostatic interactions that may result in the formation of raised domains via membrane restructuring or lipid tilt. Tat is a basic cationic peptide carrying multiple positive charges and may therefore be expected to interact with the zwitterionic lipid head groups of the phospholipids. The raised regions could therefore represent aggregates of peptide on the bilayer or a change in the way the lipids pack in the bilayer due to the interaction of the peptide with the head groups^{192, 239, 242}.

4.2.1.5 Interaction of Tat peptide conjugated nanoparticles with SLBs

Tat peptide conjugated polyacrylamide nanoparticles have been shown to cross the cell membrane and do not require any additional techniques to be delivered into cells^{10, 186}. Following exposure of the bilayer to a 1µg/ml suspension of Tat conjugated nanoparticles with a charge of 5.5mV, no changes were observed in the topography of the bilayer. Increasing the concentration of Tat conjugated nanoparticles to 10µg/ml led to the appearance of small holes in the bilayer. Exposure to a higher concentration (25µg/ml) resulted in significant changes in the bilayer including the formation of new holes, expansion of pre-existing defects and solubilisation of the bilayer over time (Figure 4.12).

Significantly more lipid reorganisation was observed to be caused by the Tat peptide conjugated nanoparticles than by Tat peptide alone or positively charged polyacrylamide nanoparticles alone. Although some catalysis of pore coalescence was observed using positively charged nanoparticles, this was limited and the widespread formation of new defects was not observed. Both types of nanoparticle caused some solubilisation of the bilayer and enlargement of pre-existing defects, but this was much more pronounced with the peptide conjugated nanoparticles in localised areas of the DPPC bilayer (Figures 4.7 and 4.13).

The presence of the nanoparticle conjugated to Tat peptide may affect the way in which Tat interacts with the bilayer, leading to more pronounced effects on the bilayer structure. For instance, nanoparticles may cause fluidisation of the bilayer, leading to a greater interaction with Tat due to the fluid nature of the bilayer, or the conjugation of the nanoparticle may affect the conformation in which Tat is presented to the bilayer. Alternatively, the presence of the peptide may cause changes in the bilayer itself as the peptide inserts into or interacts with the bilayer. This change in bilayer structure may then allow for a greater interaction of the nanoparticle with the bilayer. The results obtained using AFM correlate well with the *in vitro* fluorescence uptake studies which demonstrated enhanced uptake of Tat conjugated nanoparticles (Chapter 5.2.2.).

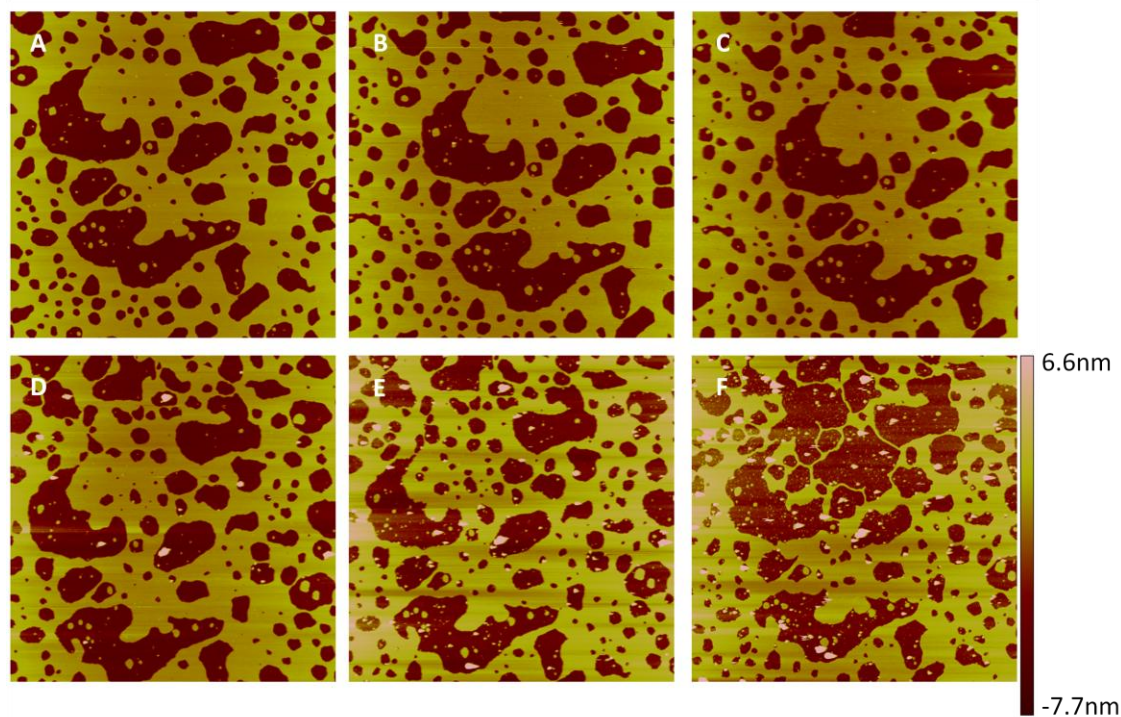


Figure 4.13: AFM images of the interaction between Tat conjugated polyacrylamide nanoparticles and a DPPC lipid bilayer. (A) DPPC, (B) following addition of 20µl HPLC grade water, (C) 1µg/ml Tat conjugated nanoparticles, (D) 10µg Tat conjugated nanoparticles caused the appearance of small holes in the bilayer and exposure to higher concentrations such as 25µg/ml (E) led to the formation of new defects and solubilisation of the bilayer over time. Image (F) was taken one hour after (E) Scan size 5 x 5 µm.

Exposure of a DPPC bilayer to Tat conjugated nanoparticles also led to a change in the height of the bilayer (Figure 4.14). Initially, the cross section shows the bilayer to have a height typical of a DPPC bilayer of 5.7nm. Following exposure to the Tat conjugated nanoparticles, some raised regions can be observed around the edge of bilayer defects as was seen using Tat peptide alone (Figure 4.11 and Figure 4.14 B1 circled). In addition, particles can be observed and the height of the bilayer was reduced to 4.8nm.

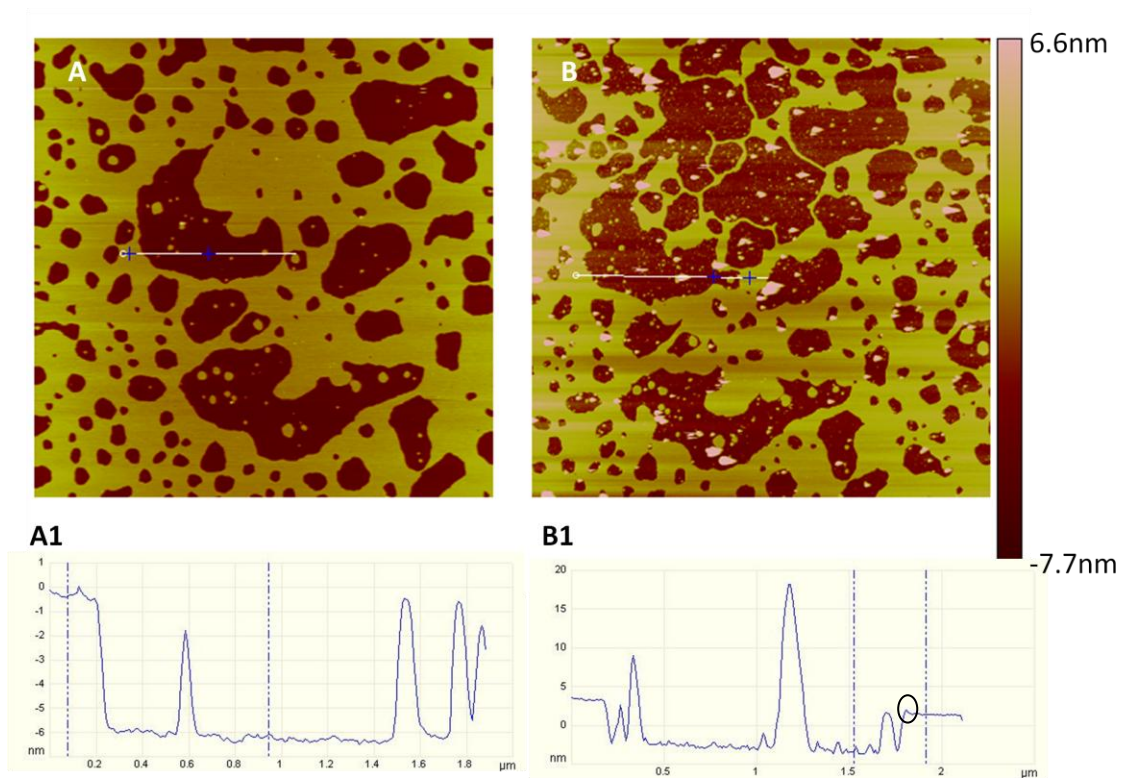


Figure 4.14: (A) DPPC bilayer before exposure to Tat conjugated nanoparticles, (A1) cross section indicated by white line on (A). (B) DPPC bilayer following exposure to 25 μ g/ml Tat conjugated nanoparticles, (B1) Cross section indicated by white line on (B) showing particles and changes in bilayer height. Original bilayer height in (A) is 5.7nm and following exposure to Tat peptide conjugated nanoparticles, bilayer height reduces to 4.8nm and particle height is 21.5nm (B1).

Figure 4.15 clearly shows the dramatic change in the bilayer in a region significantly altered by the addition of Tat conjugated nanoparticles. It can again be observed that although the nanoparticles do not appear to be associated with the bilayer as was the case with the positively charged nanoparticles, there is a much greater effect on the bilayer than with the positively charged nanoparticles alone. This suggests that the presence of the Tat peptide, which is too small to be observed using AFM in these images, is having an additional effect on the bilayer as the particles move over the bilayer surface.

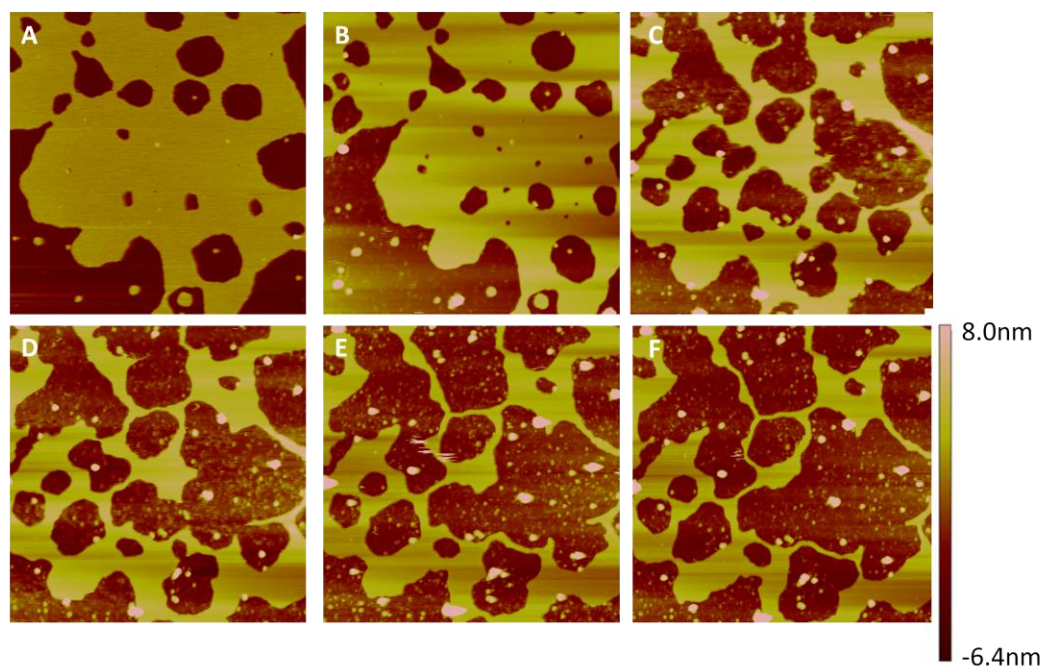


Figure 4.15: AFM images of the interaction between Tat conjugated polyacrylamide nanoparticles and a DPPC lipid bilayer. (A) DPPC, (B) following addition of 20 μ l HPLC grade water, (C) 1 μ g/ml Tat conjugated nanoparticles, (D) 10 μ g Tat conjugated nanoparticles caused the appearance of small holes in the bilayer and exposure to higher concentrations such as 25 μ g/ml (E) led to the formation of new defects and solubilisation of the bilayer over time. Image (F) was taken one hour after (E) Scan size 2 x 2 μ m.

Bearing analysis of the area covered by the bilayer confirmed what can be observed in Figures 4.13-15. In Figure 4.13A the bilayer covers 60% of the image and this value decreases to 55% in Figure 4.13F. This decrease is relatively small because some regions of the bilayer are dramatically altered by the addition of the Tat conjugated nanoparticles whilst other areas are left relatively intact, for instance the bottom third of the images in Figure 4.13 remains relatively constant. The average change in bilayer coverage in these images was from $59 \pm 0.1\%$ to $52 \pm 0.2\%$. However, when an area that is obviously affected by the addition of the nanoparticles is analysed, there is a more significant change in surface coverage. In Figure 4.15, the solubilisation of the bilayer as the concentration of the Tat peptide conjugated increases is much more apparent, and bilayer area decreases from 64% in Figure 4.15A to 32% in Figure 4.15F.

In summary, negatively charged polyacrylamide nanoparticles were found to adhere to the mica surface and did not insert into the bilayer. Positively charged polyacrylamide nanoparticles led to small changes in the bilayer characterised by the fusion and enlargement of bilayer defects. Tat peptide alone caused some changes in the bilayer including the formation of raised regions around bilayer defects and solubilisation of some areas along with fusion of small defects. In contrast, nanoparticles functionalised with Tat peptide caused significant rearrangement in the bilayer through the formation of new holes, expansion of previous defects in the bilayer and the acceleration of the coalescence of smaller pores into larger ones. This work correlates well with *in vitro* studies indicating the uptake of positively charged and Tat conjugated nanoparticles into cells. It suggests that AFM studies of SLBs on mica can be a good model for predicting the effects of nanoparticles on more complex cell systems.

4.2.2 SICM Results

The interaction of positively and negatively charged 300nm silica nanoparticles was imaged using SSCM. In addition, the effect of larger, 1 μ m positively charged nanoparticles was also briefly investigated. The use of SSCM enabled the simultaneous gathering of topography and fluorescence imaging with the fluorescence images in focus at the pipette tip. This enabled detection of the nanoparticles on or near the cell membrane via fluorescence. It had previously proven to be very difficult to detect the nanoparticles via topography imaging alone, due to the presence of nanoscale features on the membrane. Once identified, high resolution imaging of smaller areas of the membrane where the nanoparticles had been identified was used in order to visualize the nanoscale interaction between the particles and the cell membrane. This imaging was done using topography alone since the resolution of the fluorescence microscope was too low at this point.

4.2.2.1 Control images of MRC-5 cells

Control samples of fixed MRC-5 cells not exposed to nanoparticles showed that the cells possessed a relatively flat membrane with a few raised surface features and no visible holes or defects in the cell membrane (Figure 4.16). The cytoskeleton was often visible under the cell membrane and this was probably due to the dehydrating fixation process of ice cold methanol that was used¹⁶¹.

Although it initially appeared that it would be possible to identify the nanoparticles using topography alone given the relatively flat and featureless membrane of the membrane on a large scale, it was later found that this was not possible, hence the need to use SSCM. This may be because the addition of the nanoparticles induced some response in the cell leading to changes in the membrane structure which then complicated the imaging of small areas of the membrane. For example, if membrane blebbing occurred, it may be difficult to distinguish this from the nanoparticles.

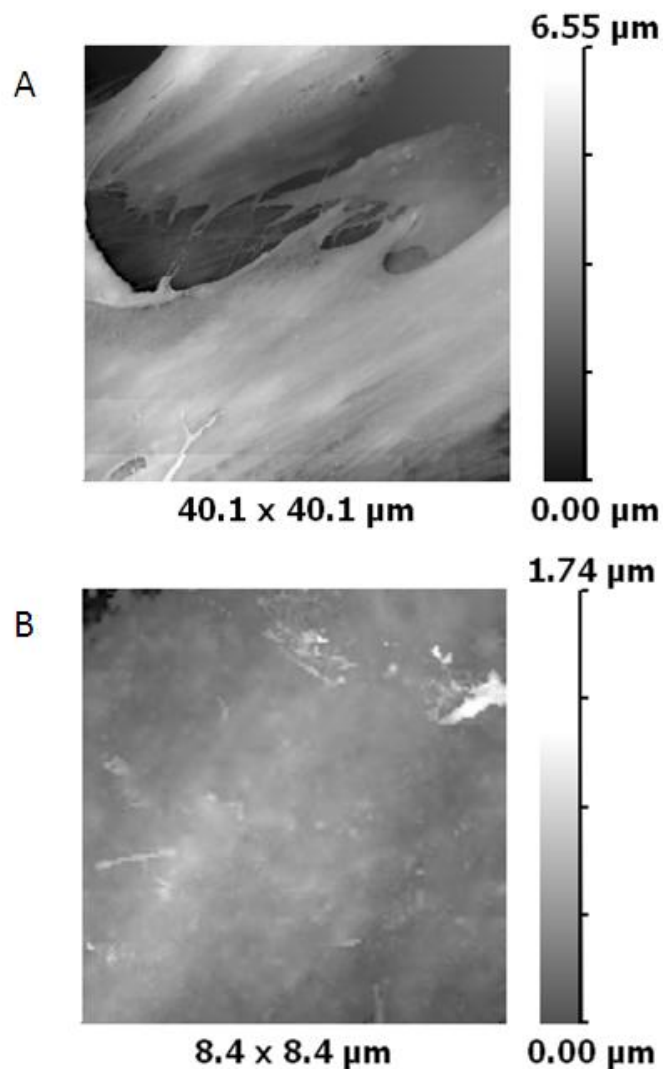


Figure 4.16: MRC-5 cells control samples (A) large area of multiple MRC-5 cells and (B) a smaller area both showing relatively flat membrane. The cytoskeleton can be observed in (A).

4.2.2.2 300nm negatively charged silica nanoparticles

Negatively charged silica nanoparticles containing Alexa 488 with a zeta potential of -25 mV in serum free DMEM and a size of 290 nm were easily located by their fluorescence using SSCM (Figure 4.17). Since the cells were fixed after a relatively short incubation time (30 mins), some nanoparticles were captured as they crossed the cell membrane, whilst some had already entered the cell. Nanoparticles on the membrane could be seen as discrete spots whilst those that had already been taken up by the cell produced diffuse areas of fluorescence, since the fluorescence image

was in focus at the pipette tip. The nanoparticles were very difficult to identify by topography alone because extensions of the cell membrane were found to envelop the nanoparticles as they were taken up by the cell, making them difficult to identify and resolve. In addition, some of the cell membrane features had a similar size to the nanoparticles. The nanoparticles appeared to be present mainly as aggregates of approximately 1-5 μm on the cell membrane.

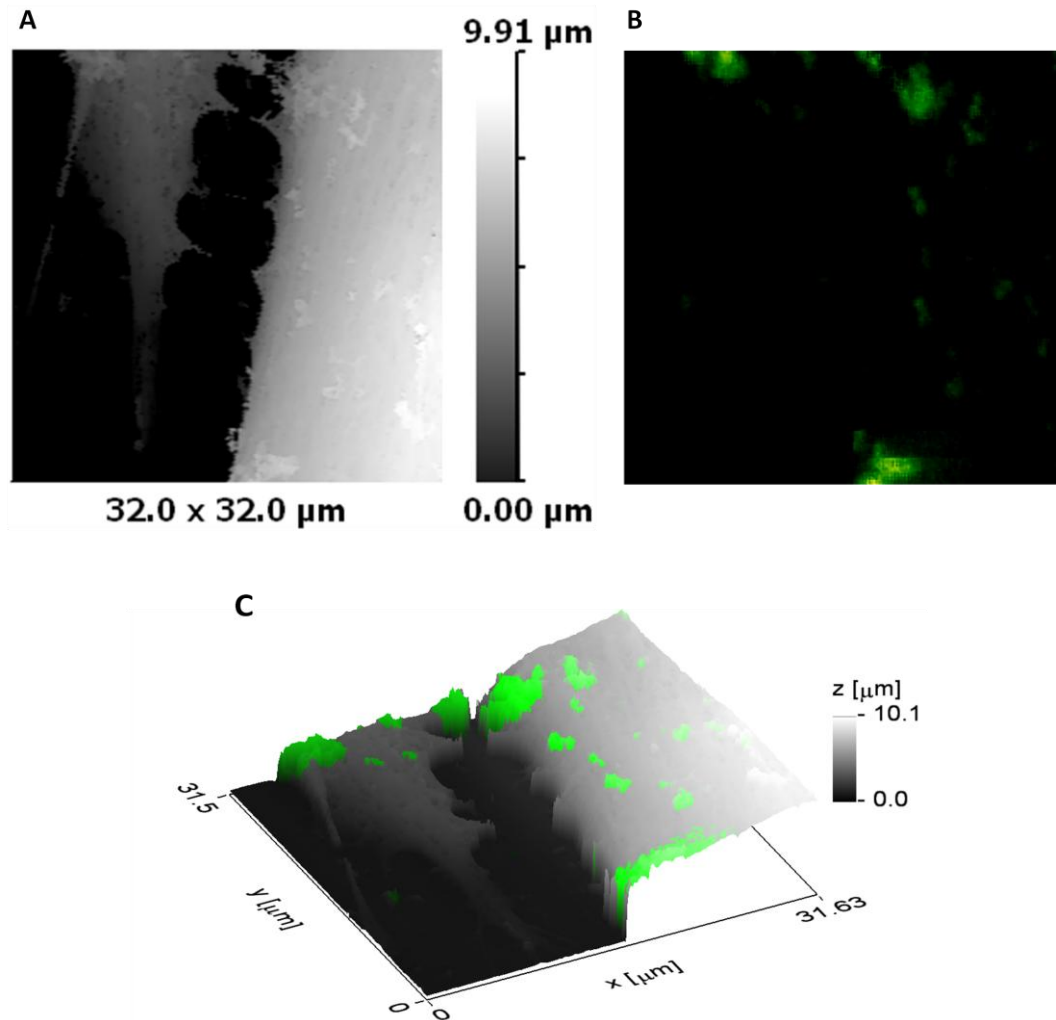


Figure 4.17: (A) Topography image of MRC-5 cell exposed to negatively charged silica nanoparticles, (B) Corresponding fluorescence images showing nanoparticles and aggregates of nanoparticles (green). (C) Overlaid image of fluorescence and topography.

Higher resolution scans of a smaller area of the cell membrane revealed a number of features including aggregates of nanoparticles which were detected by their fluorescence. A number of possible holes or defects in the membrane could also be observed along with some features of the cytoskeleton. It appeared that most of the negatively charged silica nanoparticles were associated with extensions of the cell membrane (Figure 4.18). Due to their size, which excludes their uptake by clathrin and caveolae mediated endocytosis, this could suggest that the negatively charged silica nanoparticles may enter cells by a route of endocytosis such as macropinocytosis. Macropinocytosis is associated with the formation of projections on the cell membrane that encapsulate extracellular fluid and any surrounding particles, and it has been suggested in the literature as a possible route of uptake for 500nm silica nanoparticles¹⁹¹.

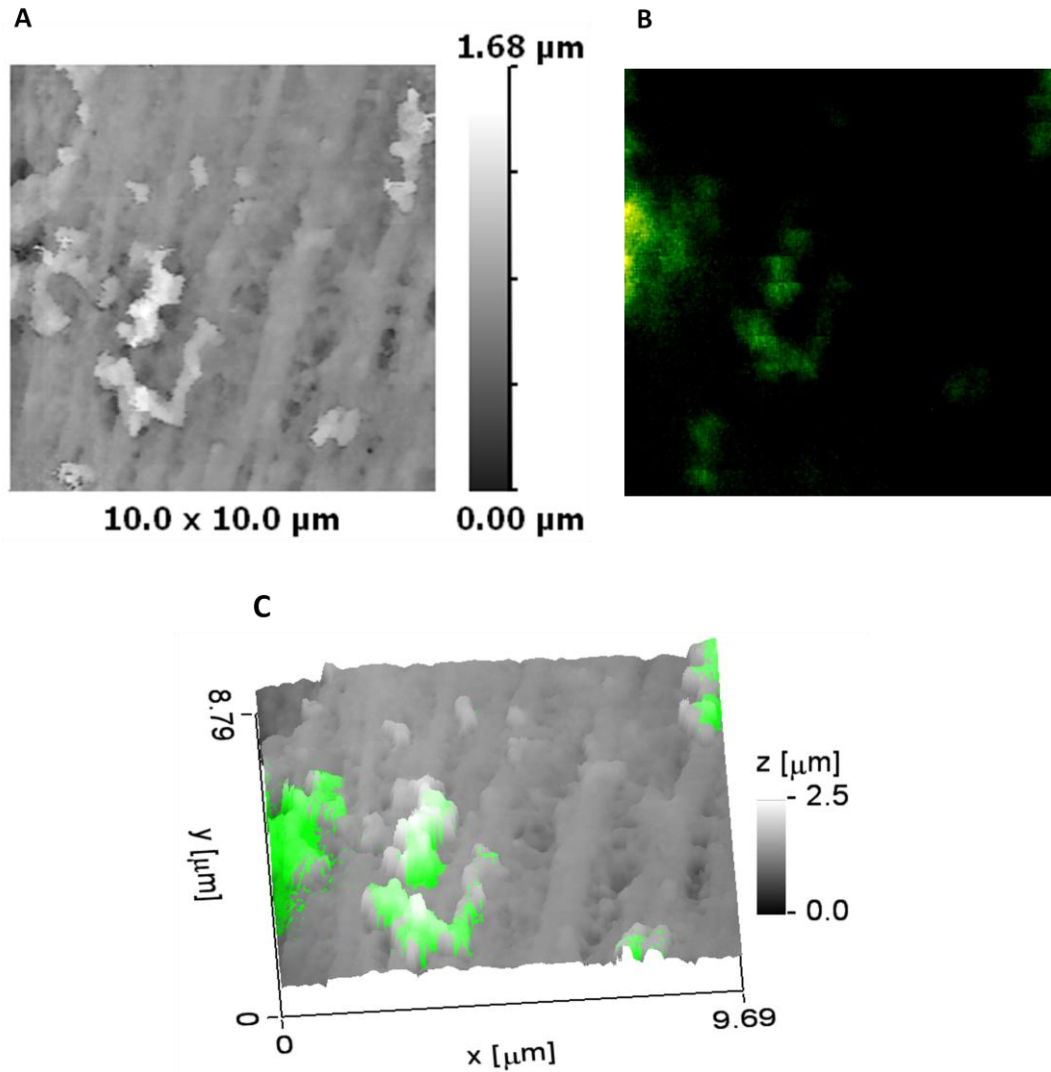


Figure 4.18: Smaller area scan of MRC-5 cell exposed to negatively charged silica nanoparticles (A) Topography, (B) corresponding fluorescence and (C) overlaid image of fluorescence and topography showing multiple negatively charged silica nanoparticles (green) associated with the cell membrane.

Figure 4.19 shows a smaller area of membrane highlighting the interaction of a single negatively charged silica nanoparticle with a protrusion of the cell membrane.

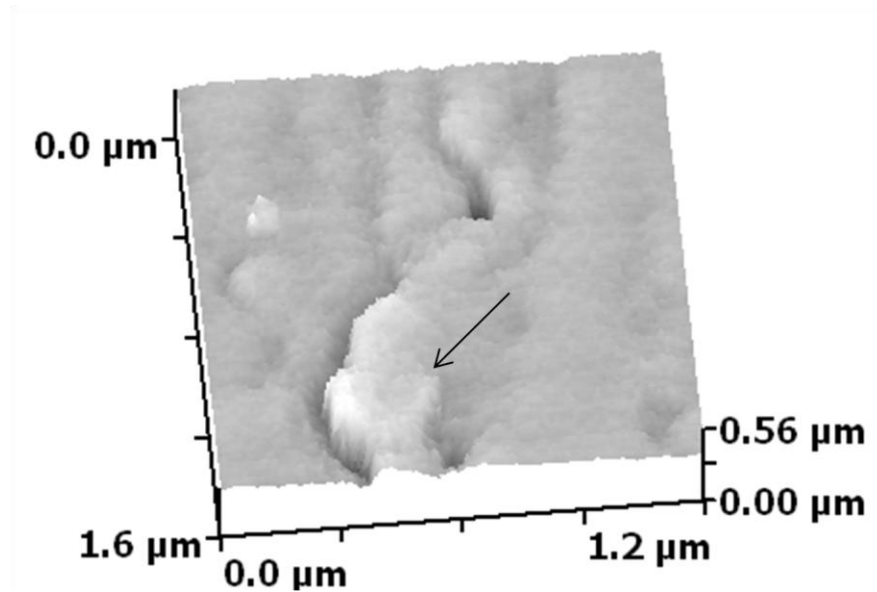


Figure 4.19: A topography image that indicates the interaction of a single negatively charged silica nanoparticle with the cell membrane. The nanoparticle is indicated by the arrow.

4.2.2.3 Positively charged silica nanoparticles

1.3μm Positively charged silica nanoparticles

1.3μm silica nanoparticles created a discrete area of damage in the cell membrane but left surrounding areas of the membrane largely undamaged (Figure 4.20). Although not extensively investigated in this work by other techniques due to their size, this data is included since it was interesting to note the different effects of the large, micron sized particles compared to the nanoparticles.

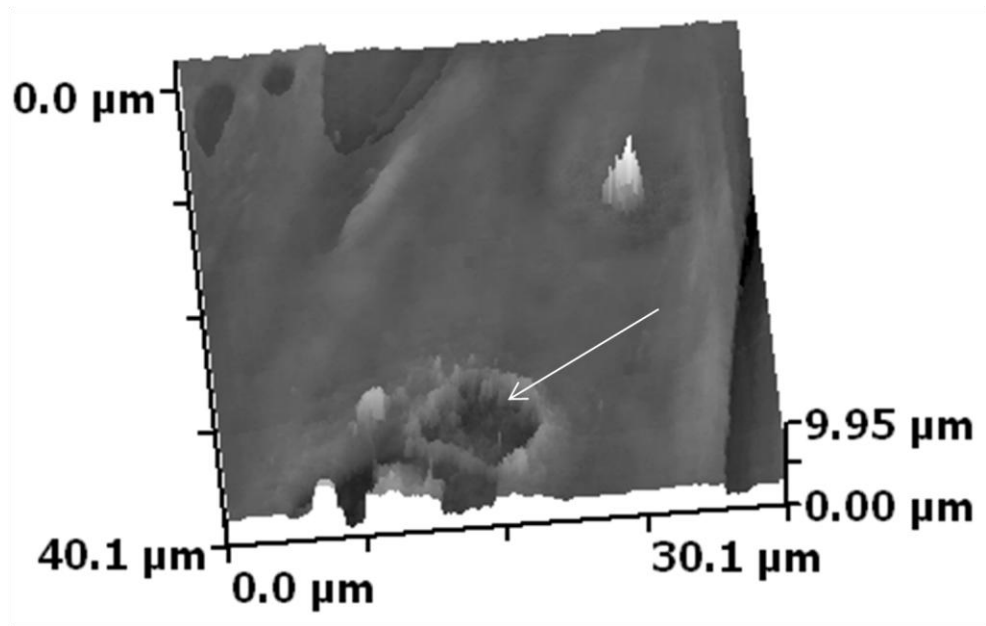


Figure 4.20: Effect of 1.3µm silica nanoparticles on MRC-5 cells. This image was taken using hopping mode only at Nottingham. The arrow indicates the damaged area of the cell membrane.

300nm positively charged silica nanoparticles

Positively charged silica nanoparticles appeared to induce more changes in the topography of the cell surface membrane of MRC-5 cells than the negatively charged silica nanoparticles. Unlike negatively charged silica nanoparticles, positively charged nanoparticles (27mV) with a similar size of 292nm led to the formation of multiple large holes in the cell membrane (Figure 4.21). This indicated that the interaction of the nanoparticles with the bilayer caused damage to the cell membrane. These holes were clearly visible on the topography image, whilst diffuse intracellular fluorescence indicated that some nanoparticles had already entered the cell (Figure 4.21).

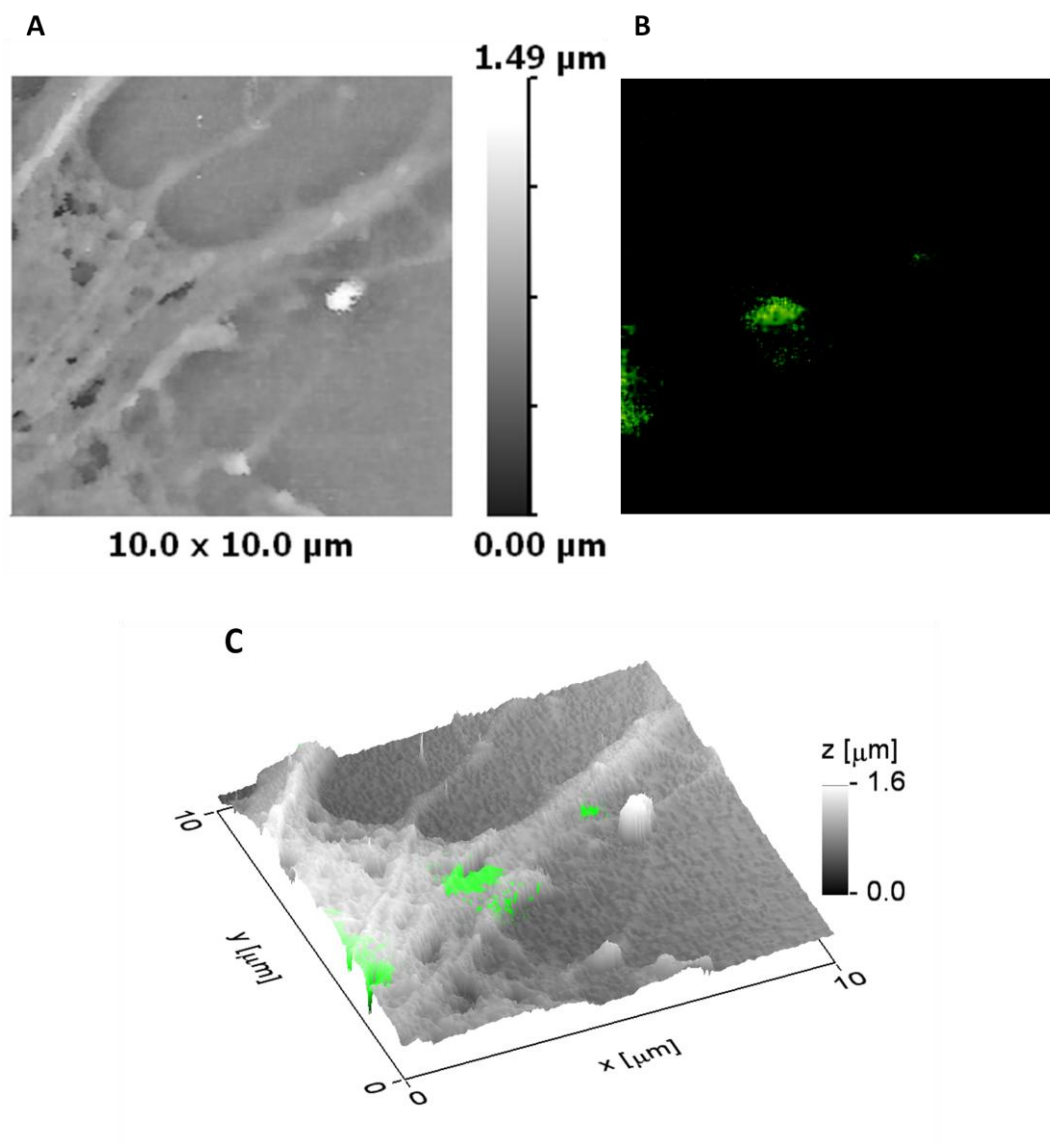


Figure 4.21: (A) Topography image of MRC-5 cells exposed to positively charged silica nanoparticles, (B) corresponding fluorescence image. (C) is the overlaid image showing holes visible in the cell membrane plus diffuse fluorescence from positively charged silica nanoparticles.

Although positively charged silica nanoparticles were also found associated with extensions of the cell membrane to some extent (Figure 4.22), they were also frequently found isolated on the membrane (Figure 4.23). The presence of isolated positively charged nanoparticles may suggest an alternative uptake mechanism to the negatively charged particles. For instance, direct translocation across the membrane via the formation of holes by the particles may play a role along with

other mechanisms such as macropinocytosis. However, the relatively large size of the nanoparticle makes a mechanism of direct translocation unlikely, although if it did occur it would be potentially damaging to the cell and produce holes such as those seen in Figure 4.21. Macropinocytosis may be suggested by Figure 4.22 since the nanoparticle is clearly associated with an extension of the cell membrane as it enters the cell.

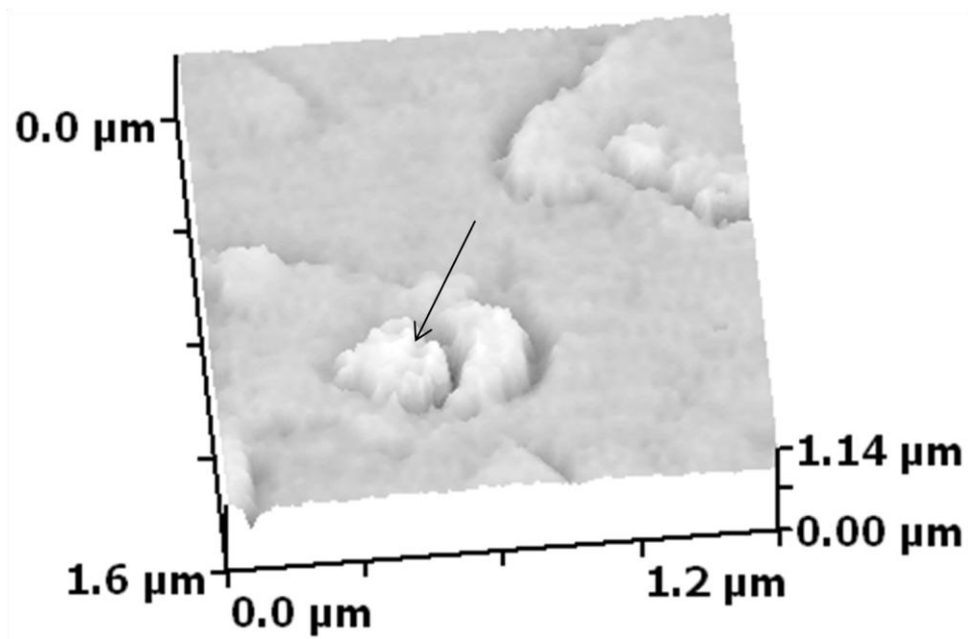


Figure 4.22: Positively charged silica nanoparticle (indicated by the arrow) partially embedded in membrane and also associated with a region of the membrane.

Figure 4.23 shows a single positively charged silica nanoparticle that is embedded in the cell membrane but it is not associated with any extensions of the cell membrane. This may indicate that an active uptake process is not required or the nanoparticle may have been captured at a different stage in the uptake process, perhaps when any extensions of the cell membrane have rejoined the membrane and are no longer visible.

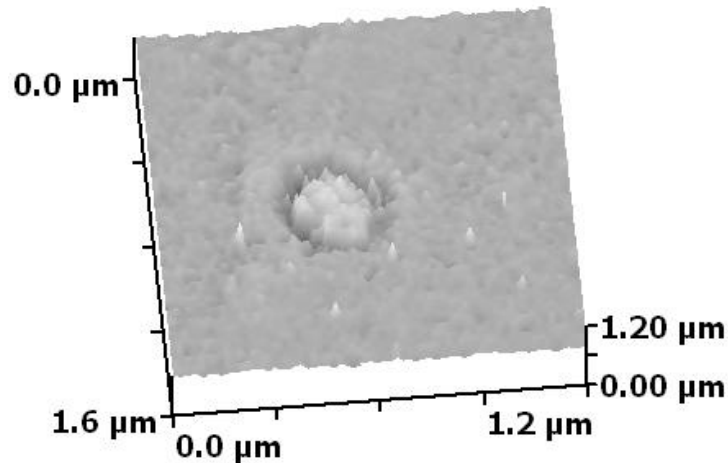


Figure 4.23: Isolated positively charged silica nanoparticle partially embedded in the cell membrane.

It appears that regardless of charge, silica nanoparticles of approximately 300nm caused some damage to the cell membrane of MRC-5 cells as demonstrated by the formation of defects in the membrane structure. Positively charged nanoparticles caused more extensive damage which could be observed as an increased number of holes in the membrane (Figure 4.21). The size of the nanoparticles appeared to be important since larger, micron sized particles caused discrete areas of damage (Figure 4.20). In general, negatively charged nanoparticles were more often associated with extensions of the membrane. In contrast, positively charged nanoparticles, whilst also associated with membrane processes to some extent were also found isolated and embedded into the membrane. The results indicate that extremes of both positive and negative charge on silica nanoparticles lead to interaction with the cell membrane and subsequent cellular uptake, which correlates well with the results of the fluorescence uptake experiments described in the following chapter.

4.3 Conclusion

Both AFM and SSCM proved to be useful techniques to image the interaction of nanoparticles with either a real or model cell membrane. Both techniques were suitable for the nanoparticles used and could resolve both the individual nanoparticles and features of the membrane or bilayer. Changes in the structure and height of the bilayer or membrane could be observed following interaction with

nanoparticles and the results gained help to provide more information about the initial stages of the interaction of nanoparticles with cell membranes. Advances in both techniques could enable improvements in the range of samples that can be imaged. Improving the resolution and speed of imaging would enable the processes to be investigated on live cells in real time. These developments are discussed in Chapter 6.

Chapter 5 - Fluorescence microscopy

5.1 Fluorescence microscopy and nanoparticle uptake

5.1.1 Imaging nanoparticle uptake with fluorescence

Nanoparticles can be labelled with a range of fluorescent dyes by a variety of methods. These include physical entrapment within the nanoparticle matrix or conjugation to the monomers used to form the nanoparticles. This labelling enables the cellular uptake route of the nanoparticles to be monitored using fluorescence microscopy. It also allows further investigation of the subsequent subcellular localization of nanoparticles, via colocalization studies. These can be performed following the fluorescent labelling of intracellular organelles such as endosomes, lysosomes, mitochondria and the nucleus²⁸. In addition to imaging, fluorescent dyes sensitive to certain analytes such as hydrogen, calcium or oxygen can be encapsulated in the nanoparticle. For example, FITC can be used to measure changes in pH. Changes in the fluorescence emission of these dyes in response to alterations in the level of the analyte enable intracellular measurements of the analytes to be performed^{219, 249}. Future applications of this technology may enable the development of real time monitoring systems, for example, a glucose sensitive system for diabetes²⁵⁰⁻²⁵².

In this work, the fluorescent dye Alexa 488 was encapsulated within polyacrylamide and silica nanoparticles and their uptake into MRC-5 cells was investigated and quantified using widefield fluorescence microscopy.

5.1.2 Cellular uptake of polyacrylamide nanoparticles

Polyacrylamide nanoparticles have the potential for a number of biological applications including diagnostic measurements of intracellular analytes, imaging and measurement of intracellular processes, and they are also being investigated for use as a delivery system for photodynamic therapy⁷⁶. The polyacrylamide nanoparticle matrix can be used to trap dyes, protecting cells from any potentially toxic effects of the dye, and also protecting the dye from any interference by cellular components. Despite their small size, they can contain multiple dyes, enabling ratiometric and simultaneous measurements of different analytes to be performed^{200, 219}. In addition to dyes, they have also been used to entrap other

molecules such as aptamers²⁰⁰. The size, charge and chemistry of polyacrylamide nanoparticles can be readily modified via the incorporation of different monomers in order to improve their uptake and targeting^{83,219}. Their small size causes minimal cell perturbation and therefore negligible biological effects and they have been shown to be biocompatible with a range of cells^{186,253}. Another benefit of their small size is that they have a high surface area to volume ratio which allows changes in the environment to be measured rapidly. as analytes only need to diffuse a small distance through the nanoparticle²¹⁹.

Polyacrylamide nanoparticles may enter cells by a variety of routes depending on their surface chemistry and the presence of any targeting molecules e.g. cell penetrating peptides. Their size means that they are likely to be taken into cells via some form of pinocytosis mechanism such as receptor independent clathrin or caveolae mediated endocytosis or macropinocytosis, since their size should help them to evade uptake and clearance by phagocytosis⁷⁶. The mechanism of cellular uptake will also depend on cell type, for example only some cells perform phagocytosis. In the body, nanoparticles have the potential to accumulate in tumours via the enhanced permeability and retention effect. This effect is when nanoparticles of a similar size to polyacrylamide (<200nm) have been shown to escape blood vessels with increased permeability in tumours, leading to potential applications in targeted drug delivery to tumours^{76, 254}. Besides uptake by endocytosis, polyacrylamide nanoparticles can also be delivered into cells using specific delivery techniques such as cationic liposomes (Lipofectamine), picoinjection, gene gun and conjugation to cell penetrating peptides¹⁸⁶.

Previous work investigating the uptake of polyacrylamide nanoparticles into cells is relatively limited. A number of studies have investigated measurement of the concentration of intracellular analytes using fluorescent dyes trapped within the polyacrylamide matrix but most do not investigate the uptake mechanism and interaction of the nanoparticles with the cell membrane. Literature reports suggest that following internalization into cells, polyacrylamide nanoparticles generally display fluorescence within cells as punctate spots, suggesting they are not dispersed throughout the cytoplasm but may reside in an intracellular compartment, for example endosomes^{10, 76, 186}. This indicates that uptake occurs by

a route that delivers nanoparticles to the endolysosomal pathway and these include the major pinocytosis pathways. Kuruppuarachchi *et al.* synthesised a range of polyacrylamide nanoparticles for use as a delivery system for photodynamic therapy. They studied the uptake of unfunctionalised polyacrylamide nanoparticles, polylysine bound tetrasulfonato-aluminium phthalocyanine entrapped polyacrylamide nanoparticles and the same nanoparticles conjugated to a porphyrin based photosensitizer into HT29 cells. It was found that all three types of nanoparticles readily entered the cells without any additional delivery vehicle. The punctate, granular appearance of the fluorescence from the nanoparticles indicated that they were encapsulated in endocytic vesicles within the cell, although further investigations to identify the route of uptake were not performed⁷⁶.

Some studies have looked at the effects of positive charge and Tat peptide conjugation on the internalization of polyacrylamide nanoparticles. Sun *et al.* synthesised cationic polyacrylamide nanoparticles containing the positively charged monomer 3-(acrylamidopropyl)-trimethylammonium chloride (ACTA). The cationic nanoparticles were found to be internalized into HepG2 cells without the need for any special delivery vehicle. It was suggested that the presence of the quaternary ammonium ion in ACTA led to an electrostatic interaction between the nanoparticles and the cell membrane, leading to enhanced uptake of the nanoparticles into cells¹⁸⁷. In two studies by Coupland *et al.* into the uptake of Tat conjugated polyacrylamide nanoparticles, flow cytometry and confocal microscopy were used to show that the nanoparticles entered mesenchymal stem cells and CHO-K1 cells without leading to effects on cell morphology or viability. The appearance of granular areas of fluorescence indicated that the nanoparticles were present in endosomes or lysosomes. pH measurements using FITC, and colocalization studies performed also suggested a lysosomal location for the nanoparticles. Unfunctionalised polyacrylamide nanoparticles with no surface conjugation did not appear to enter the cells^{10, 186}. Conjugation of the nanoparticle cargo to the peptide appeared to alter its uptake, since when the peptide was conjugated to FITC alone, the subcellular localization of the conjugate was different to that of the peptide conjugated nanoparticles¹⁰.

5.1.3 Cellular uptake of silica nanoparticles

Much more literature is available on investigations into the cellular uptake of silica nanoparticles of varying size, shape and charge, and they have been more extensively investigated as drug delivery tools. However, the results are complicated by the wide variety of methods used to produce the nanoparticles, their composition, surface chemistry and size^{191, 255, 256}. Silica nanoparticles are biocompatible and have also been used for intracellular sensing²⁵⁷. The encapsulation of fluorescent dyes inside silica nanoparticles is useful since they are hydrophilic, biocompatible and optically transparent. In addition, their chemistry can be readily modified with various different fluorescent probes and other molecules to impart a charge or provide conjugation to molecules such as cell penetrating peptides^{209, 214}. Multiple studies have found that silica nanoparticles rapidly enter many different cell types including HeLa, 3T3 and stem cells via an actin dependent active uptake mechanism such as clathrin or caveolae mediated endocytosis or macropinocytosis. Uptake has been shown to be significantly reduced when the experiments were performed at 4°C compared to 37°C and in the presence of actin destabilising agents such as cytochalasin D^{26, 214, 256, 258-260}. Begum *et al.* found that 90nm silica nanoparticles entered HeLa cells by clathrin dependent endocytosis²⁶. Slowing *et al.* suggested that the functionalisation of silica nanoparticles with different surface groups led to uptake by different routes. They suggested that unfunctionalised 150nm (-35mV) and N-folate-3-aminopropyl functionalised (+13mV) silica nanoparticles entered cells by clathrin mediated endocytosis whilst 3-aminopropyl (-5mV) and guanidinopropyl (-3mV) functionalised nanoparticles were internalized by a caveolae mediated mechanism²⁵⁶.

The effect of size on silica nanoparticle internalization has been investigated and silica nanoparticles with different sizes (80nm and 500nm) have been shown to enter human dermal fibroblast cells to different extents. This suggests that the rate and amount of uptake of silica nanoparticles is dependent on size to some extent, and that particles of different sizes may use different uptake mechanisms. Figure 5.1 shows that the 80nm nanoparticles were found colocalized with lysosomes to some extent but did not enter the cell nucleus. This exclusion from the nucleus is

expected due to the presence of the nuclear envelope which prevents many molecules accessing the nucleus¹⁹¹.

Genistein, an inhibitor of clathrin independent endocytosis, was shown to reduce the uptake of 80nm silica particles but not 500nm particles, again suggesting that different mechanisms of uptake are involved for differently sized particles. Uptake of 500nm silica particles was found to depend more on the macropinocytosis pathway, a result that may be expected due to the size limits of the clathrin and caveolae mediated mechanisms of endocytosis¹⁹¹. A study by Lu *et al.* found that uptake of silica nanoparticles into HeLa cells was greatest for particles with a diameter of 50nm and uptake decreased at both smaller and larger diameters (30nm and 110nm)⁷⁴. This finding was in agreement with the literature in general which demonstrates a rapid uptake of small nanoparticles and a decrease in uptake of larger nanoparticles as size increases. A number of literature reports have also concluded that very small nanoparticles can display a decrease in cellular uptake^{4, 82, 91, 261}. The use of silica nanoparticles has also been investigated as a drug delivery tool to help to enhance the delivery of poorly soluble drugs. It was found that the use of silica nanoparticles in a tablet formulation for oral delivery resulted in enhanced drug permeability and a higher release rate of the drug compared to a tablet composed of silica microparticles. Cellular uptake studies on Caco-2 cells, used as a model of intestinal absorption, showed that silica nanoparticles could be internalized but uptake of microparticles was not observed²⁶².

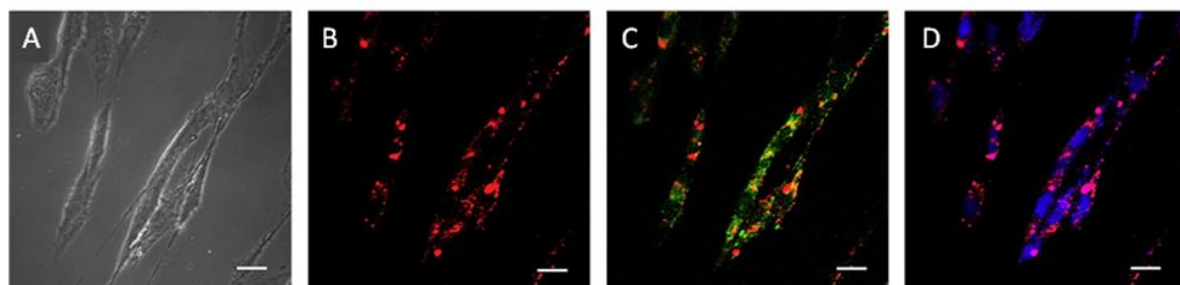


Figure 5.1: 80nm silica nanoparticles in human dermal fibroblasts cells (A) bright field, (B) RITC-silica nanoparticles (red) (C) Merge of RITC-silica particles and LysoTracker Green, (D) Merge of RITC-silica particles and DAPI (blue)¹⁹¹.

Literature reports in general suggest that positively charged silica nanoparticles show enhanced uptake into cells^{26, 214}. 100nm silica nanoparticle uptake into 3T3-

L1 and hMSCs cells was shown to be increased by the presence of a positive surface charge and endocytosis occurred via a clathrin and an actin dependent mechanism. However, the effect of blocking a particular route of uptake using phenylarsine oxide to inhibit clathrin and cytochalasin D to inhibit macropinocytosis, was different between the cells, indicating that each type of cell internalized the particles by a different mechanism²¹⁴. Similarly to polyacrylamide and other nanoparticles and polymers, some studies have suggested that the presence of a positive surface charge can lead to escape of the particles from endosomes into the cytoplasm, which has implications for enhancing drug delivery applications^{263, 264}. A number of studies have indicated this pattern of increased uptake of nanoparticles with increasing positive charge and the possible reasons for this have been discussed previously. However, a number of studies investigating the uptake of unfunctionalised silica nanoparticles, which naturally carry a high degree of negative charge, have indicated that they can also enter cells. It has been suggested that this uptake occurs via non specific pinocytosis uptake mechanisms since the nanoparticles have also been shown to reside in endosomes^{98, 255}. Graf *et al.* synthesised silica nanoparticles with a range of zeta potential from highly negative to positive values. Positively charged particles were found to enter HeLa cells and it was suggested that this occurred following their increased association with the negatively charged cell membrane. However, positive charge in itself was found to be inadequate for the uptake of silica nanoparticles synthesised with an alternative monomer and containing a different functional group that caused aggregation⁹⁹. These results indicate that one parameter, i.e. size or charge cannot be considered in isolation in regard to cellular uptake. The presence of polyethylene glycol (PEG), which confers neutrality onto many nanoparticles, was found to inhibit uptake. PEG is often used to stabilise nanoparticles since it helps to maintain colloidal stability and minimise biological interactions. However, it has often been found to inhibit the cellular uptake of nanoparticles due to these reduced interactions with the environment around the particle^{11, 99}.

200nm silica nanoparticles have also been conjugated to Tat peptide and flow cytometry studies have shown that internalization of Tat conjugated particles occurred at a faster rate and to a greater degree than nanoparticles not conjugated to the peptide^{102, 217}. Internalization of both unfunctionalised and Tat conjugated

nanoparticles was inhibited by low temperature, indicating an active uptake mechanism was involved. With more Tat peptide present on the particle surface, it was found that a larger number of particles were internalized²¹⁷. In addition, Pan *et al.* found that conjugation of the peptide to the nanoparticle is required for uptake and that simultaneous incubation of free nanoparticles and peptide does not lead to enhanced uptake²⁶⁵. Although it is clear that Tat delivers cargo such as silica nanoparticles to cells, the mechanism by which this occurs is unclear. Again, there may be different mechanisms depending on the cargo. For example small cargo may be able to enter cells via energy independent electrostatic interactions or size limited clathrin or caveolae mediated endocytosis, whilst larger cargos may require a mechanism such as macropinocytosis^{10, 217}.

5.2 Results and Discussion

5.2.1 Polyacrylamide nanoparticles

Polyacrylamide nanoparticles with a size of 40-50nm and a range of charges between -3mV and 18mV were internalized into MRC-5 cells within a six hour time period. A strong positive correlation was observed between the degree of positive charge on the nanoparticles and the level of uptake into cells which was measured using the green fluorescence intensity from the nanoparticles within the cells. Cells exposed to unfunctionalised polyacrylamide nanoparticles and nanoparticles containing 2-5% ACTA displayed low levels of fluorescence, indicating minimal cellular uptake. In cells exposed to polyacrylamide nanoparticles containing between 10% and 20% ACTA and with a charge greater than 13mV, bright areas of green fluorescence could be observed within the cells (Figure 5.2).

Although the resolution of the fluorescent microscope used does not allow observation of the individual nanoparticles, fluorescence from the particles was observed throughout the cell and generally appeared as a punctate, granular distribution. This distribution pattern has previously been observed in other studies and it suggests that the nanoparticles are not dispersed throughout the cytoplasm, but may be present within intracellular compartments such as endosomes or lysosomes^{10, 186}. At high levels of positive charge, the nanoparticles were often found to be particularly concentrated in endosomes or lysosomes in the perinuclear region of the cell. However, in no cases did the nanoparticles cross the nuclear membrane and enter the nucleus itself. Uptake of the nanoparticles was generally observed to be similar across all the cells in a sample, although in some cases where nanoparticles with a higher charge were used, more differences were observed between cells.

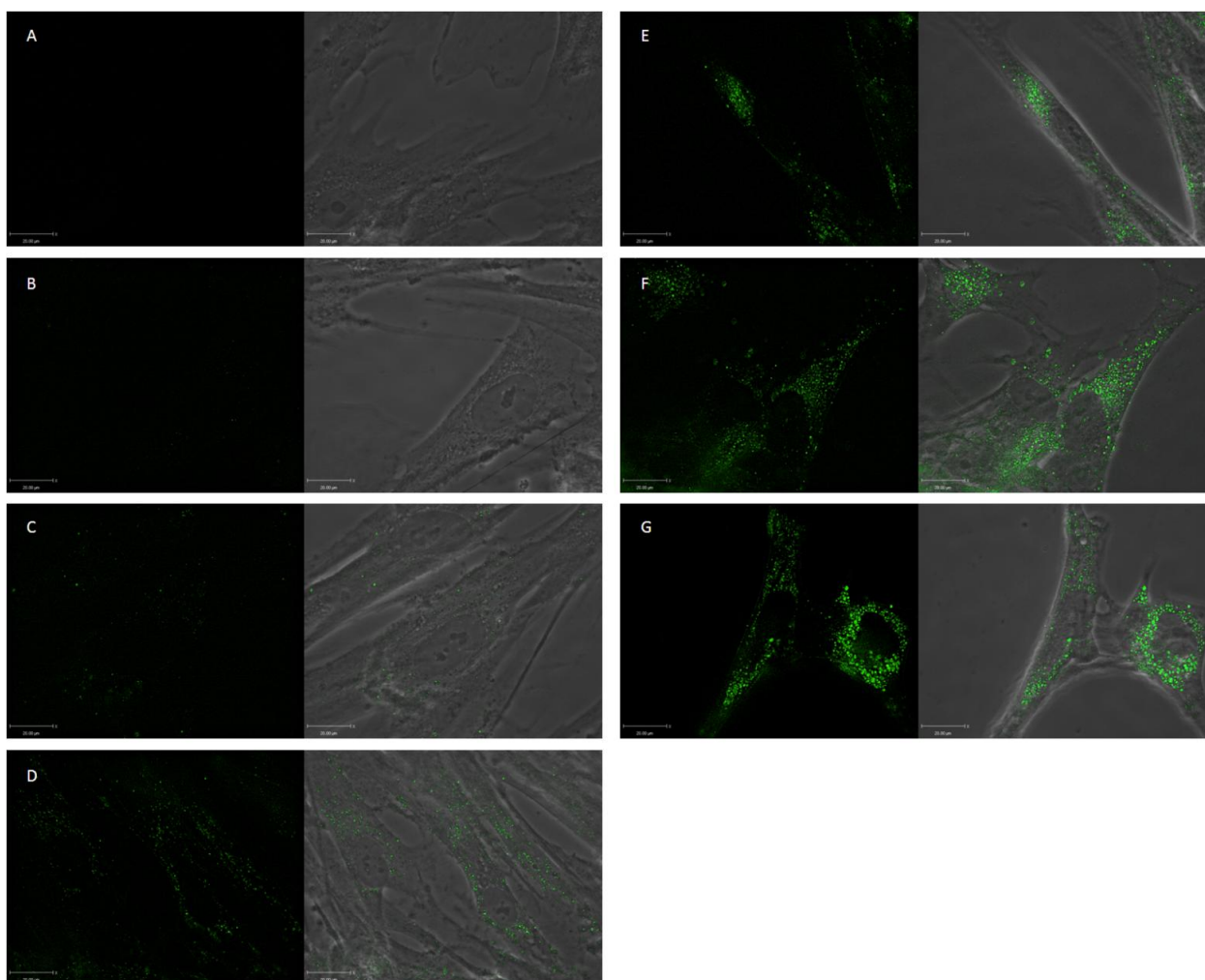


Figure 5.2: Representative images showing polyacrylamide nanoparticles (green) with increasing positive charge in MRC-5 cells. Images are shown in pairs of green fluorescence alone beside the green fluorescence and brightfield merged images. (A) Control, (B) Unfunctionalised (-3.3mV), (C) 2% ACTA (1.8mV), (D) 5% ACTA (6.9mV), (E) 10% ACTA (13.2mV), (F) 15% ACTA (17.6mV) (G) 20% ACTA (18.6mV).

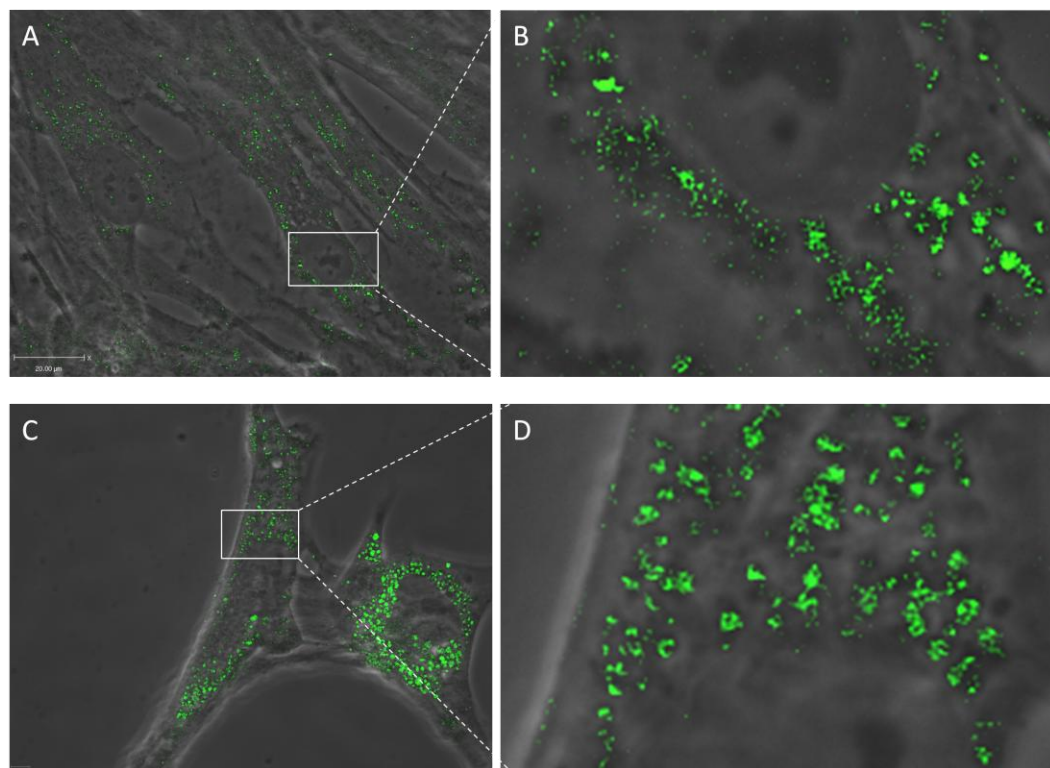


Figure 5.3: Example images of MRC-5 cells exposed to polyacrylamide nanoparticles to show perinuclear, punctate distributions of nanoparticles (green) indicating an endocytic route of uptake. (A) 5% ACTA containing polyacrylamide particles and (B) enlarged area from white box in (A). (C) 20% ACTA containing polyacrylamide nanoparticles and (D) enlarged area from white box in (C).

Green fluorescence intensity measurements within the cells displayed an overall trend of an increase in fluorescence intensity as positive charge on the nanoparticles increased. This trend was retained following correction to account for differences in the batch to batch fluorescence emission of the nanoparticles, indicating that increasing the positive charge on the nanoparticle increased uptake into cells (Figure 5.4). The effect was especially pronounced for nanoparticles containing 15% and 20% ACTA, suggesting that the correlation was non linear and that increasing charge beyond a threshold level had even greater effects on enhancing uptake. As mentioned previously, the uptake of nanoparticles containing 20% ACTA was not as uniform across different cells as for the other particles, leading to a high standard deviation for the sample.

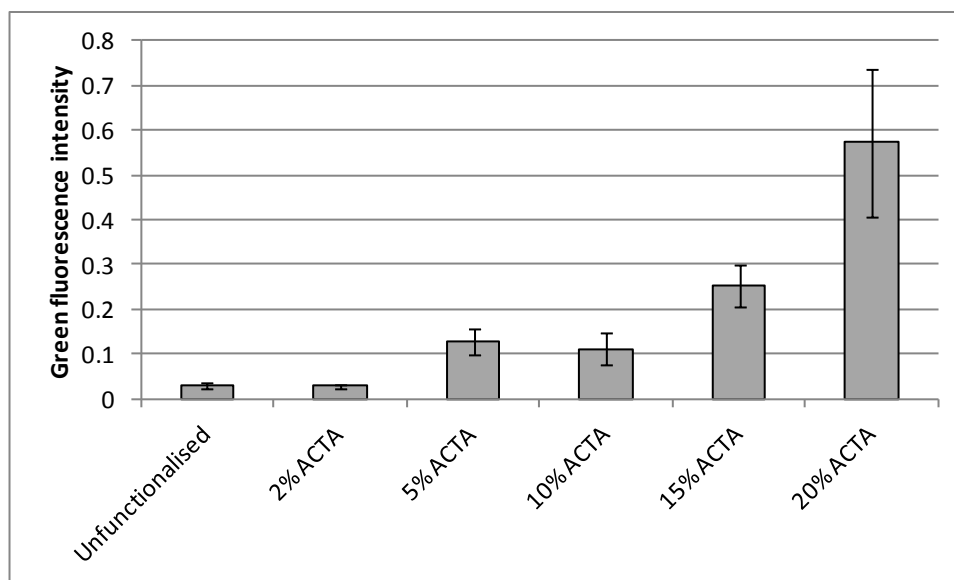


Figure 5.4: Increase in cellular uptake of polyacrylamide nanoparticles with increasing charge. N= 50.

The results correlate well with many studies in the literature that show that positive charge leads to enhanced uptake of a variety of molecules^{2, 14, 54, 62, 85, 98}. This increase in uptake is probably due to increased affinity and interaction of the positively charged nanoparticles with the cell membrane. This enhanced interaction may increase the opportunity for nanoparticle uptake into the cell via endocytosis. The size range of polyacrylamide nanoparticles produced means that they could enter cells by any of the main routes of endocytosis. They may be able to interact with areas of the membrane involved in clathrin or caveolae mediated endocytosis and their increased association with the membrane would increase the likelihood of their encapsulation into a macropinosome as it formed on the cell membrane. Since the nanoparticles appeared to be localized to intracellular vesicles following uptake, this also supports an endocytic uptake mechanism such as clathrin mediated endocytosis or macropinocytosis. This is because these routes of uptake direct the substances they transport into endosomes and lysosomes. Alternatively, as suggested by some literature reports, the positive charge on the nanoparticles and their small size may also mean that they can enter the cell without the need for a specific route of uptake by forming transient holes in the cell membrane^{11, 86, 97}. This is supported by the results discussed in Chapter 4.2.1.3 using AFM. However it would be expected that if the nanoparticles did enter cells by this route then the

appearance of fluorescence from the particles may be more diffuse and spread throughout the cytoplasm.

The enhanced uptake observed with some highly cationic nanoparticles is also linked to an increase in cytotoxicity. If the nanoparticles do cause increased permeabilization of the membrane in order to enter the cell, this can lead to leakage of intracellular fluid and molecules which can lead to cell death. This may have been the case for the nanoparticles containing 20% ACTA since the particles appeared to have effects on cell morphology and the high variation in uptake that was observed may have been caused by damage to the cell by the nanoparticles. This could be investigated further through the use of cell viability and cytotoxicity studies⁵⁵.

Limited internalization of slightly negatively charged and near neutral polyacrylamide nanoparticles into MRC-5 cells was observed. This correlates well with literature reports that indicate that nanoparticles with a neutral and near neutral charge, or those functionalised with neutral molecules such as PEG, show limited biological interactions and reduced uptake into cells¹¹.

Following this observation that a positive charge of around 18mV increased uptake of the nanoparticles, it was decided to try and investigate the effects of imparting a greater negative charge onto the nanoparticle. However, it proved to be difficult to obtain nanoparticles with the charge required so uptake studies were performed using the most negatively charged nanoparticles that could be produced. The aim of the experiment was to try and identify whether a high degree of positive charge was required to enhance uptake, or whether extremes of charge, either positive or negative could influence nanoparticle uptake.

Polyacrylamide nanoparticles containing 5% N-acryloxysuccinimide with a charge of -5.5mV in serum free DMEM entered cells to a small extent over the time course of the experiment. The level of uptake was less than that of the unfunctionalised polyacrylamide nanoparticles with a charge of -3.3mV. The intracellular distribution of the few nanoparticles that could be observed within MRC-5 cells following uptake displayed a similar pattern to the other polyacrylamide nanoparticles investigated (Figure 5.5). They showed a punctate appearance indicating localization into an intracellular vesicle and were again excluded from the

nucleus. The nanoparticles appeared to be distributed throughout the cell within these intracellular vesicles, although some were still found in the perinuclear region. No nanoparticles were found to adhere to the cell membrane.

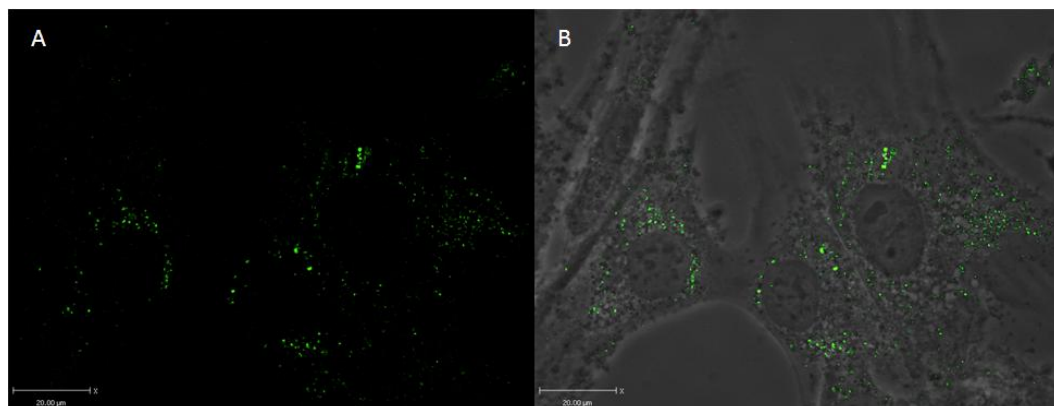


Figure 5.5: (A) Green fluorescence from Alexa 488 containing nanoparticles within MRC-5 cells, (B) Brightfield and green fluorescence overlaid image showing intracellular localization of polyacrylamide nanoparticles containing 5% N-acryloxysuccinimide.

Measurements of the green fluorescence intensity within cells following incubation with polyacrylamide nanoparticles containing 5% N-acryloxysuccinimide showed that these cells displayed a lower fluorescence than those incubated with unfunctionalised nanoparticles (Figure 5.6). The slightly higher level of negative charge therefore appeared to inhibit the internalization of the nanoparticles. This effect may have been caused by a decrease in the association of the nanoparticles with the cell membrane due to the unfavourable charge interaction, reducing the likelihood of uptake. In addition, the negative charge may reduce the rate of uptake significantly so that over the short time course of the experiment, overall uptake of the negatively charged nanoparticles appeared reduced. It would be interesting to observe in future whether an increased incubation period may increase internalization of the negatively charged polyacrylamide nanoparticles.

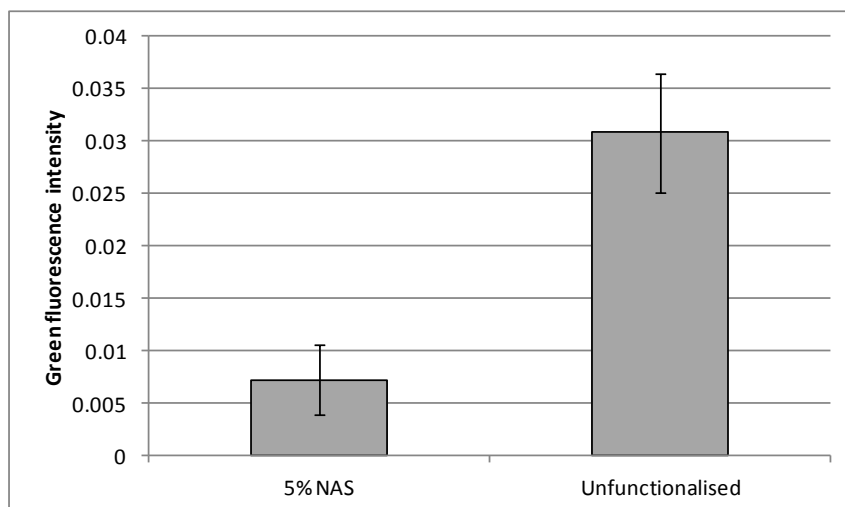


Figure 5.6: Comparison of the green fluorescence intensity of 5% N-acryloxysuccinimide (NAS) polyacrylamide nanoparticles (-5.5mV) and unfunctionalised polyacrylamide nanoparticles (-3.3mV) in MRC-5 cells. N=55.

5.2.2 *Tat conjugated polyacrylamide nanoparticles*

Tat conjugated polyacrylamide nanoparticles with a charge of 5.2mV entered cells to a greater degree than positively charged polyacrylamide nanoparticles with a similar or higher charge. Only the nanoparticles containing 20% ACTA entered cells to a greater extent (Figure 5.7). Similarly to the other polyacrylamide nanoparticles investigated, the Tat conjugated nanoparticles displayed a punctate intracellular appearance indicating encapsulation into endosomes or lysosomes. These were again often found to be concentrated in the perinuclear region but did they not enter the nucleus itself (Figure 5.8).

Despite the aggregation of the Tat conjugated nanoparticles which produced a population of 500-600nm particles in addition to the typical polyacrylamide nanoparticle population at 30-50nm, no nanoparticles were observed adhered to the cell membrane.

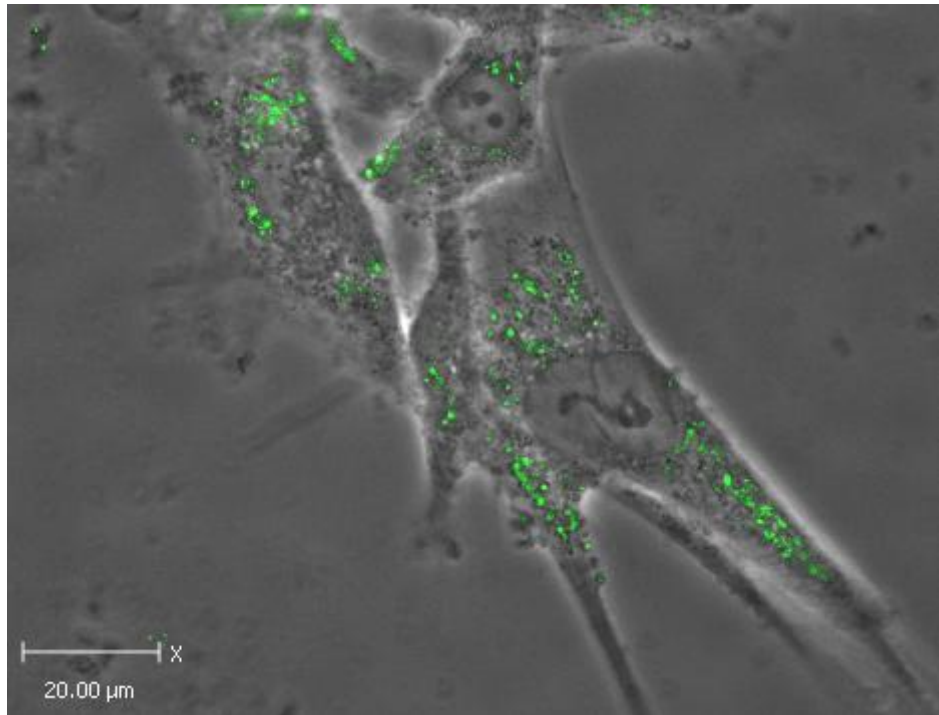


Figure 5.7: Representative image of MRC-5 cells containing Tat conjugated polyacrylamide nanoparticles (5.2mV).

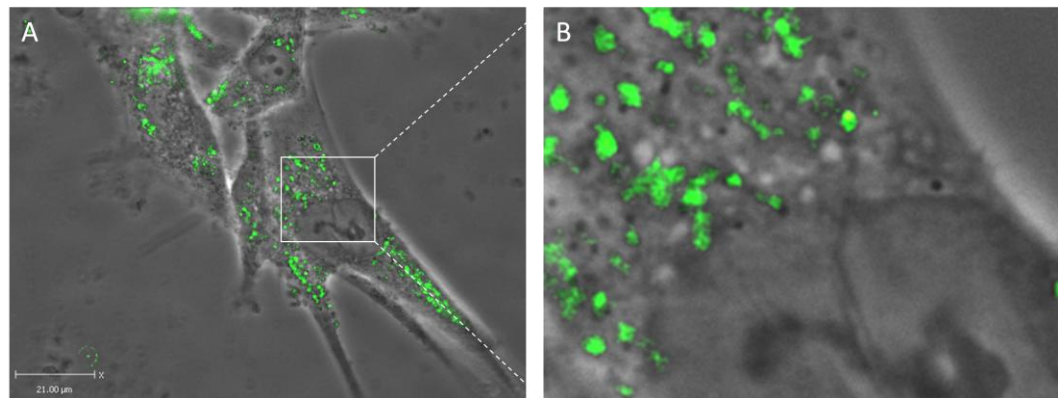


Figure 5.8: (A) MRC-5 cells with Tat conjugated nanoparticles and (B) enlarged area from (A) to show intracellular distribution of nanoparticles close to the nucleus.

Compared to positively charged polyacrylamide nanoparticles containing 5% and 15% ACTA which had a similar and higher positive charge (6.9mV and 17mV respectively), more Tat conjugated nanoparticles were internalized into MRC-5 cells (Figure 5.9). Only the nanoparticles containing 20% ACTA were found to display a

higher level of uptake. However, the increased size due to aggregation of the Tat conjugated polyacrylamide nanoparticles complicates the analysis of the results to some extent. This is because size has also been shown to affect the internalization of many different types of nanoparticles. Despite this, the increased size of the Tat conjugated nanoparticles did not appear to, in this study, inhibit uptake of the particles. This may have been expected since previous studies in the literature have identified a reduced rate and overall uptake of larger nanoparticles. The effect of the peptide may therefore be significant in enhancing the uptake of larger nanoparticle aggregates.

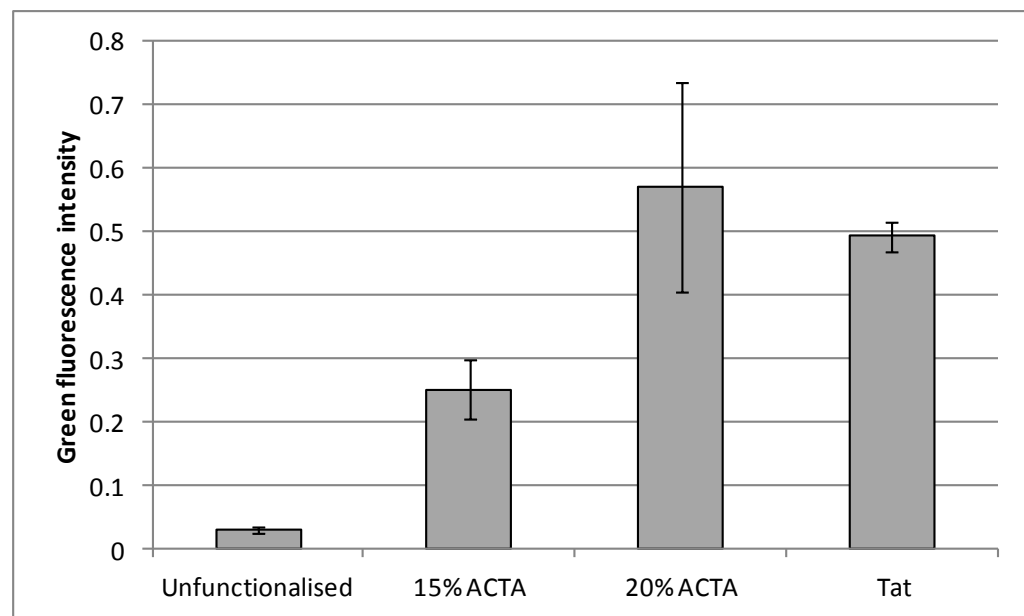


Figure 5.9: Comparison of the green fluorescence intensity in cells after exposure to nanoparticles containing increasing amounts of ACTA or conjugated to Tat peptide. Unfunctionalised (-3.3mV), 15% ACTA (17.6mV), 20% ACTA (18.6mV), Tat peptide conjugated (5.2mV). N=35.

The enhanced uptake of nanoparticles upon conjugation to cell penetrating peptides such as Tat has been demonstrated in the literature^{93, 217}. The presence of the peptide on the nanoparticle surface must in some way influence the interaction of the nanoparticles with the cell membrane. This could occur either by effects on the way the nanoparticle is presented to the membrane or from effects on the membrane by the peptide, which then influences how the membrane interacts with the nanoparticles. This could include changes in the phase of the membrane such as

fluidisation and increased permeability following interaction with the peptide. Tat peptide has previously been shown to induce the formation of holes in a model lipid bilayer and this increased permeability of the membrane has been shown to lead to translocation of the peptide and associated cargo across the membrane^{45, 48}. The results presented in Chapter 4.1.3.3 indicate that Tat peptide conjugated nanoparticles can lead to significant changes in the structure of a lipid bilayer and this would support the suggestion of a mechanism of direct translocation across the membrane. However, this route of uptake is potentially cytotoxic at high concentrations and again, it would be expected that nanoparticle fluorescence would be more widespread and diffuse than that observed in the fluorescence uptake studies. Alternatively, it has previously been indicated that Tat peptide may enter cells via routes of endocytosis especially macropinocytosis^{50, 108}. Conjugation of a cargo to Tat peptide may be able to influence the endocytic pathway used for internalization and this is believed to be due to the difference in size between the peptide alone and the nanoparticle-peptide conjugate¹⁰. This was also demonstrated in this work using AFM as discussed in Chapter 4.1.3.3 where it was observed that Tat conjugated nanoparticles had much greater effects on a model cell membrane than the peptide alone. Since the Tat peptide conjugated polyacrylamide nanoparticles used in this work were prone to significant aggregation, it is possible that they entered cells via a different or additional uptake mechanism than that observed for the positively charged polyacrylamide nanoparticles. For instance, the monodisperse population of approximately 40-50nm positively charged polyacrylamide nanoparticles could enter cells by mechanisms such as receptor independent clathrin or caveolae mediated uptake. Larger aggregates of Tat conjugated nanoparticles are unable to enter cells by this route but their cationic nature and the presence of the peptide on the surface, along with their increased size may mean that they have a high degree of association and subsequent interaction with the cell membrane, possibly via the Tat peptide. These nanoparticles are unlikely to rapidly dissociate from the membrane which has been observed with some smaller nanoparticles. This, in theory, could increase the chance of the internalization of an aggregate, composed of multiple nanoparticles into a cell via a route such as macropinocytosis and account for the enhanced uptake that was observed^{266, 267}.

5.2.3 Silica nanoparticles

Unlike polyacrylamide nanoparticles, which showed a clear dependence on positive charge for internalization into MRC-5 cells, both negatively charged (-25mV) and positively charged silica (27mV) nanoparticles entered MRC-5 cells within three hours (see Chapter 3.2.1.3 for details). Both types of silica nanoparticle had a similar diameter of 290nm, and 292nm respectively. Negatively and positively charged silica nanoparticles displayed a similar intracellular distribution and the nanoparticles were not dispersed throughout the cytoplasm but were observed as punctate spots in the perinuclear region (Figure 5.10 and 5.11). This granular appearance of the nanoparticles within the cells again indicated that they were present in intracellular vesicles such as endosomes or lysosomes. Neither the negatively or positively charged silica nanoparticles were found to cross the nuclear membrane since no fluorescence was observed in the cell nucleus. In addition, even with a high level of positive or negative charge present on the particles, no changes in cell morphology were observed in contrast to the polyacrylamide nanoparticles. This indicates that the silica nanoparticles may be biocompatible with MRC-5 cells at this concentration and this could be confirmed using cell viability and toxicity studies.

Initial studies to try and quantify the uptake of the silica nanoparticles into cells were complicated by a high degree of association of the nanoparticles with the cell membrane and the glass bottom of the cell culture dish. This remained even after repeated and extensive washing of the cells. It was necessary to find a way to remove these excess nanoparticles in order to be able to perform accurate measurements of internalization of the nanoparticles. This was achieved by the incorporation of some additional steps in the sample preparation procedure where trypsin was used to remove the cells from the dish following incubation with the nanoparticles. The cells were resuspended in media and then centrifuged to create a pellet and the supernatant containing the excess nanoparticles could then be removed. Following replating of the cells onto new dishes, it was observed that the excess nanoparticles had been removed. This enabled clearer images to be obtained of the nanoparticles internalized into the cells, therefore allowing measurements to be performed. However, during the analysis of the results, it must be noted that although it was assumed that when the cells were replated there were no

nanoparticles adhered to the membrane, if this was the case and nanoparticles were still attached, the actual time course of the experiment for both types of silica nanoparticle would be 27 hours.

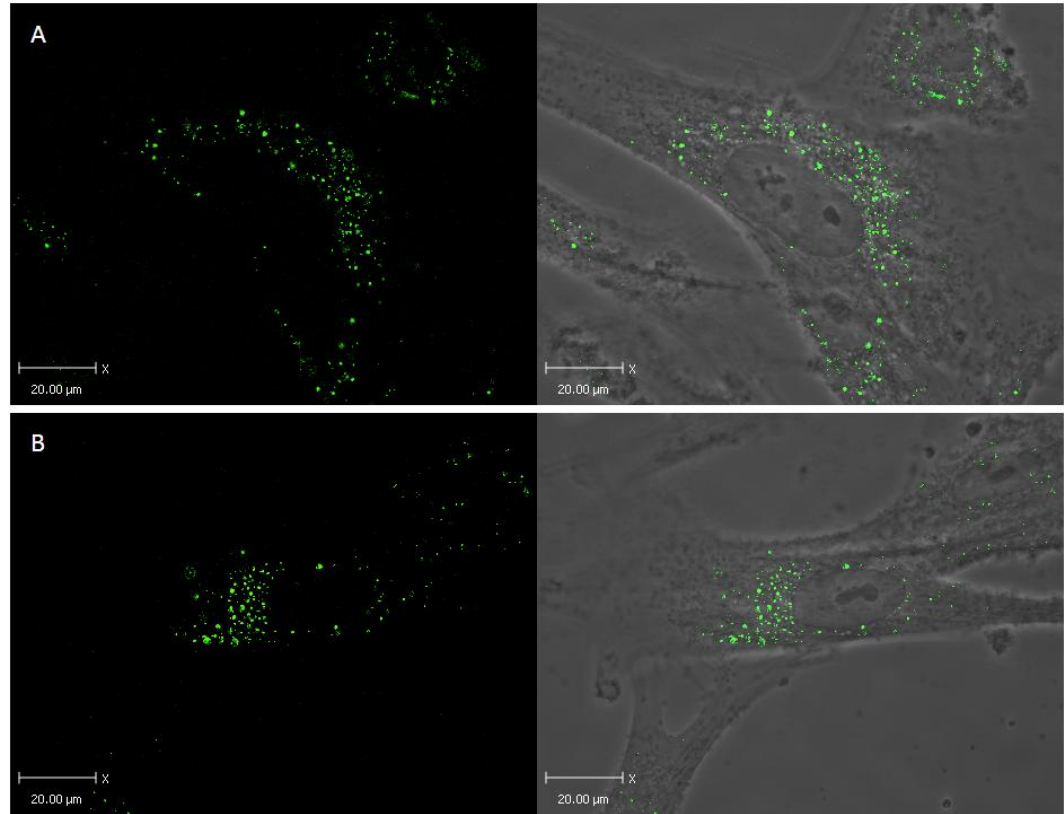


Figure 5.10: (A) Pair of images showing green fluorescence from negatively charged silica nanoparticles (-25mV) in MRC-5 cells and the merged green fluorescence and brightfield image. (B) Green fluorescence from positively charged silica nanoparticles (27mV) in MRC-5 cells and merged green fluorescence and brightfield image.

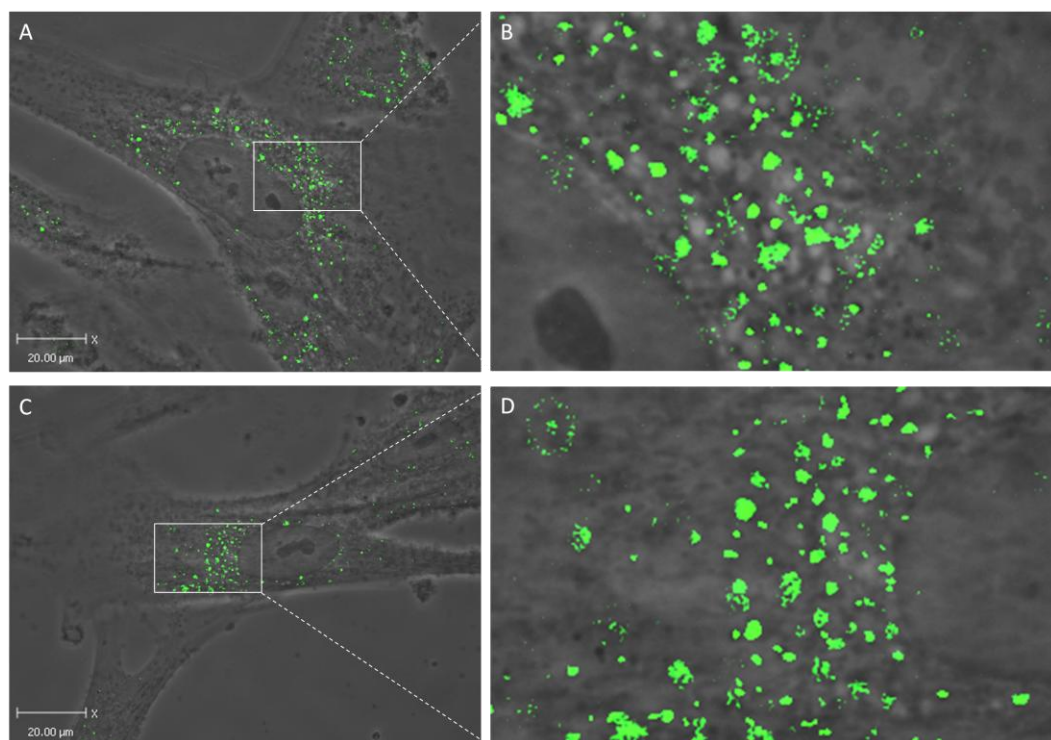


Figure 5.11: Images showing in greater detail the intracellular localization of silica nanoparticles in MRC-5 cells. (A) Negative silica nanoparticles and (B) enlarged image of region in (A) showing perinuclear localization of nanoparticles. (C) Positive nanoparticles and (D) enlarged region of (C) again showing a perinuclear distribution.

Quantification of the uptake of silica nanoparticles was performed by measurement of the green fluorescence intensity from the nanoparticles within cells as explained in Chapter 2.6.3.4. This showed that both the negatively and positively charged nanoparticles entered cells to a similar degree during the time course of the experiment (Figure 5.12). This is in contrast to the results obtained for polyacrylamide nanoparticles which showed a dependence on positive charge for internalization.

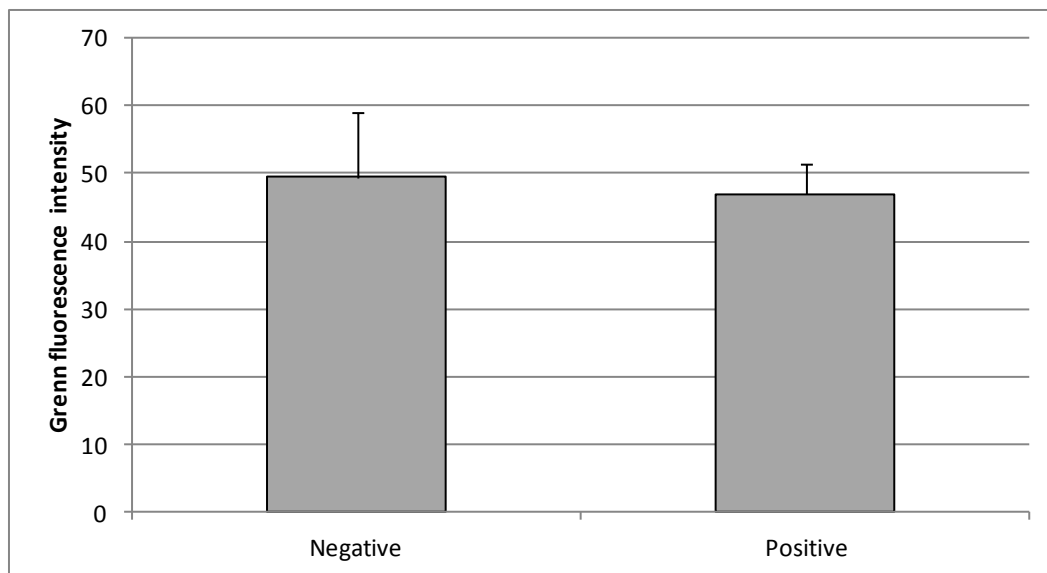


Figure 5.12 Green fluorescence intensity within cells incubated with negative and positively charged silica nanoparticles. N=45

A similar effect of charge on the internalization of silica nanoparticles has been observed previously although the monomers used to impart charge were different to those used in this work, and the size of the nanoparticles was approximately 50nm. Chen *et al.* demonstrated that negatively and positively charged silica nanoparticles with a similar zeta potential to those used in these experiments showed roughly equivalent internalization into HeLa cells. However, they also suggested that the differently charged nanoparticles were found in different intracellular locations, whilst in this work it appears that the nanoparticles display similar intracellular destinations. They found that whilst the positively charged nanoparticles were found in the cytosol, negatively charged nanoparticles were found in endosomes, leading them to conclude that the positively charged nanoparticles entered cells via direct translocation across the membrane, or were able to escape endosomes following uptake resulting in their cytosolic location⁹⁸.

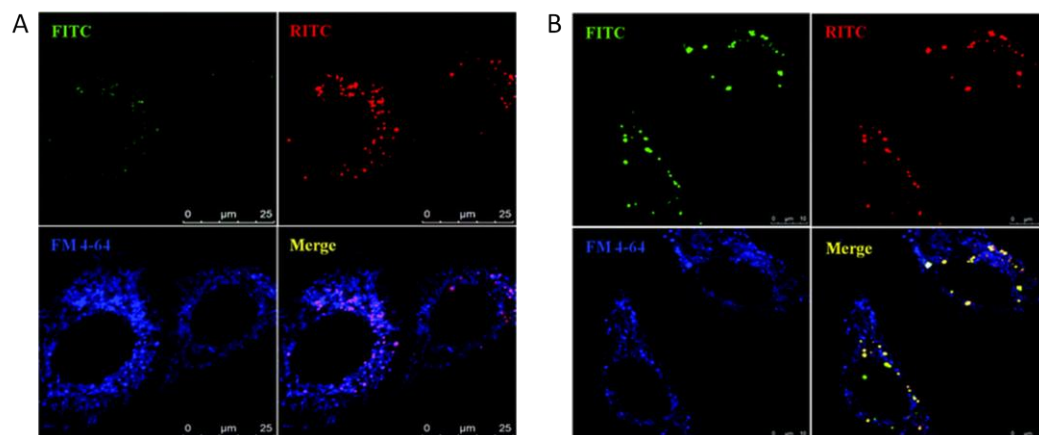


Figure 5.13: Confocal microscope images of (A) negatively charged phosphate functionalised and (B) positively charged quaternary ammonium functionalised silica nanoparticles in HeLa cells showing the nanoparticles (containing FITC and RITC), FM4-64 is a marker for endosomes and the merged imaged shows colocalization of the negatively charged but not the positively charged nanoparticles with endosomes⁹⁸.

The similar levels of uptake observed in this work may indicate that both types of silica nanoparticle were internalized into cells via the same route of uptake. The route used is unlikely to be influenced by charge since unlike polyacrylamide nanoparticles, it did not appear that the presence of the negative charge inhibited the rate or overall extent of uptake of the silica nanoparticles. A non specific route of uptake such as macropinocytosis may be indicated for these nanoparticles since their size of approximately 300nm means they are unlikely to be internalized through either of the common routes of clathrin or caveolae mediated endocytosis. Uptake of a variety of negatively charged nanoparticles, whilst less commonly reported than uptake of positively charged nanoparticles, has been observed by a number of groups^{17, 25, 27, 55, 98, 99}. Both positive and negatively charged nanoparticles can interact with components of a cell membrane, for example proteins and lipids. The heterogeneity of cell membranes means that in different regions, nanoparticles may be able to interact to a greater or lesser extent. Any association with the membrane can increase the chance of internalization, for instance it could interact with a region rich in proteins used for clathrin mediated uptake or just by virtue of its association with the membrane it could be encapsulated by macropinocytosis. In addition, if the excess nanoparticles were not fully removed from the cell membrane

during the trypsin treatment, they could continue to be internalized into cells during the following 24 hour period. This may mean that even if one type of nanoparticle was internalized at a slower rate than the other, overall uptake levels would be equivalent once all the remaining particles had been internalized.

5.3 Conclusion

An increase in the positive surface charge on polyacrylamide nanoparticles via incorporation of ACTA was found to lead to an increase in the uptake of the nanoparticles into MRC-5 cells. This may be due to increased interactions of the nanoparticles with the membrane or direct translocation of small, highly charged particles across the membrane. Negatively charged and near neutral polyacrylamide nanoparticles entered cells to a very limited extent, and this may be due to a reduced association with the membrane due to an unfavourable charge interaction. It would be interesting in future to synthesise polyacrylamide nanoparticles with a higher level of negative charge in order to investigate whether an extreme of negative charge has the same effect on polyacrylamide nanoparticle uptake as it did for silica nanoparticles. The hypothesis that high levels of charge lead to increased internalization is also supported to some extent by the results observed with polyacrylamide nanoparticles. Cell uptake at low levels of positive and negative charge was limited and only at higher charges, over 15mV, did the uptake begin to increase significantly.

Both negative and positively charged silica nanoparticles were taken up into MRC-5 fibroblasts to a similar level, indicating that extremes of charge may lead to enhanced cellular uptake, but the mechanism by which this uptake occurs is uncertain. In addition to the effects of extreme positive and negative charge observed in this work, it would have been interesting to observe the effect of neutralising the charge on silica nanoparticles on their uptake. Nanoparticles with a neutral surface charge often display reduced cellular interaction and internalization due to limited interactions with their biological environment.

It is possible that although similar intracellular distributions were observed for polyacrylamide and silica nanoparticles, different mechanisms of uptake may be employed. This is because of the size difference between the nanoparticles and the

fact that a dependence on charge for uptake was only observed for the polyacrylamide nanoparticles.

Chapter 6 – Conclusions and Future Perspectives

6.1 Conclusion

The work presented in this thesis aimed to investigate the uptake of nanoparticles into cells and to visualize the initial stages of this process using scanning probe techniques. AFM and SSCM were used to image the interaction on the nanoscale, before progressing to look at uptake of the nanoparticles on a whole cell scale. The results from the fluorescence microscopy studies of cellular uptake correlate well with the observations gained using the model and fixed cell membranes imaged using the scanning probe techniques of AFM and SSCM.

Polyacrylamide nanoparticles displayed a clear dependence on positive charge for uptake into cells. Negatively charged polyacrylamide nanoparticles entered cells to a very small extent, indicating that the presence of a negative surface charge inhibited internalization and/or slowed the rate of uptake significantly. A low level of positive charge (6.9mV) on nanoparticles containing 5% ACTA showed a small increase in the level of uptake into cells compared to unfunctionalised polyacrylamide nanoparticles. This correlated well with AFM studies which showed that these particles caused some changes in the model cell membrane including some limited reorganisation of the bilayer along with the fusion of small defects to form larger holes in the bilayer. This might suggest that these particles could directly cross the membrane without any additional endocytosis machinery via the formation of transient holes in the membrane.

Tat conjugated polyacrylamide nanoparticles displayed enhanced uptake into cells compared to positively charged polyacrylamide nanoparticles with a similar or higher surface charge. This was again supported by the AFM studies which demonstrated significant effects of these particles on the bilayer including changes in the height of the bilayer, possibly caused by the insertion of the peptide or electrostatic interactions. In addition, catalysis of the fusion of small holes in the bilayer, and the formation of new defects was observed, which occurred to a much greater extent than with the positively charged particles alone. The presence of the peptide on the surface of the nanoparticle must therefore play a role in the interaction of the conjugate with the membrane and the subsequent uptake of the

nanoparticles, other than just carrying a positive charge as discussed in detail in Chapters 4 and 5.

In contrast, silica nanoparticles with a high degree of both positive and negative charge entered cells to a similar extent and displayed a similar intracellular localization. This was supported by the results obtained using SSCM which showed that both negative and positive silica nanoparticles had significant effects on the membrane of MRC-5 cells observed as the development of multiple holes in the membrane. However, the use of SSCM provided additional information about the possible route of uptake since the association of the particles with the membrane was sometimes different. Negatively charged particles were found to be mainly associated with projections of the cell membrane that were wrapped around the nanoparticles, whereas positively charged nanoparticles, although associated with membrane projections to some extent were also found isolated on the membrane. This could indicate that both types of silica nanoparticle can be internalized by a mechanism such as macropinocytosis where projections of the cell membrane encapsulate extracellular fluid and membrane associated molecules, leading to their internalization.

Both scanning probe techniques therefore seem to be good methods to use to image the nanoparticle – cell interaction on the nanoscale and they correlate well with the results of *in vitro* cell uptake studies. However, the model membrane used for AFM experiments requires significant enhancement, for example by the use of combinations of different lipids and other components to produce a more realistic biological membrane. SICM is currently limited by the imaging speed and resolution of the pipette tip therefore advances in SICM that could enable faster imaging would provide better monitoring of fast processes such as endocytosis and will widen the range of experiments to which it could be applied.

Fluorescence imaging of nanoparticle uptake into cells enabled visualization of the intracellular localization of the nanoparticles and quantitative measurements of nanoparticle uptake were performed. Advances in fluorescent microscopy technology may help to improve the resolution of images obtained allowing better colocalization studies of particles and intracellular organelles to be performed and

more precise quantitative data to be obtained. These, and further possible advances in all the techniques used in this thesis are discussed in the next section.

6.2 Technical limitations of equipment and future advances

Difficulties in this work arose from the fact that some of the instruments were used at the limits of their resolution. For instance, both SICM and fluorescence microscopy cannot resolve individual polyacrylamide nanoparticles. All the techniques used have the potential to be improved in order to increase resolution, speed of imaging, and conditions for cells in order to enable better imaging of the nanoscale interactions in real time on live cells.

6.2.1 Scanning Ion Conductance Microscopy

SICM is a relatively new technique for imaging cellular uptake processes and therefore there are a number of limitations which affect the ability of the equipment to achieve the desired results. Initially it was intended to use SICM to image cellular uptake of nanoparticles in live cells, however, due to a number of limitations, this was not possible within this project and some adjustments had to be made in order to achieve the most out of the equipment within the limitations present.

One of the major limitations was the rate of imaging achievable with the equipment in the hopping mode. Two factors limit this rate - the settling time of the XY piezo scanner and the rate at which the Z piezo brings the pipette towards the sample surface (fall rate). If the fall rate is too high it creates a large amount of background noise, and therefore the hopping mode technique requires dampening of the mechanical vibrations caused by the motion of the piezo. Faster, more stable piezos may help to reduce noise and increase imaging speed. This limitation in imaging speed means that it can take a relatively long time to image a small area of a cell membrane at the high level of resolution required. This may mean that the cell begins to die, since there was no incubator available on the equipment used in this thesis, and also that the uptake processes may be missed as they often occur within minutes. Recently, the development of a heating unit that can be incorporated into the SICM stage that can maintain cells at 37°C has been reported. Morphological studies of cell spreading at 22°C and 37°C using SICM demonstrated significant differences, highlighting the importance of temperature in live cell experiments²⁶⁸.

It was not possible to carry out the desired imaging on the equipment available in Nottingham since the MRC-5 cells used had a number of features on the cell membrane that were of a similar size to the nanoparticles being investigated. The only way to identify the particles of interest was by the use of the combined Scanning Surface Confocal Microscope (SSCM) located at Imperial College, London. This group has used SSCM for similar work and are one of the pioneers of the SICM technique. They have been able to image the uptake of fluorescent nanoparticles into live AT1 cells but this was only possible because the cells have a very smooth surface meaning imaging times are fast and nanoparticles are easy to identify¹.

A limitation of SICM that was not investigated in this work is that of the resolution of the pipette tip and the material it is made from. Decreasing the inner diameter of the glass pipette used for imaging leads to an increase in resolution since the resolution of the system is directly related to the internal radius of the pipette. Quartz pipettes have been used to try and obtain very small diameters. However, at very small inner diameters, problems can occur which means that the resolution will eventually be limited to a level where the problems caused by the narrow pipette opening outweigh the benefits of a potentially higher resolution image. Imaging with nanopipettes with an internal diameter of 13nm has been reported but imaging with these very small diameter pipettes can be difficult²⁶⁹. One of the reasons for this is that the ion current flowing through these smaller pipettes is low, around 100pA compared to approximately 0.7nA for pipettes with an internal diameter of 70nm. The pipette to sample imaging distance is also reduced since the change in ion current flow will only be detected when the pipette is much closer to the surface. The use of these pipettes therefore requires a SICM design with a high degree of mechanical stability in order to decrease the effects of noise. Since the ion current flow is much lower and the pipette is much closer to the sample, mechanical or acoustic noise could lead to reduced feedback control which may cause the pipette to come into contact with the sample¹⁴².

6.2.2 Advances in Atomic Force Microscopy

AFM has previously been very limited when it comes to imaging live cells because of the nature of the contact between the tip and the soft cell surface. To achieve the best images, the tip must be scanned very gently over the surface of the cell using

the tapping mode technique with a soft, flexible cantilever in order to minimise damage to the tip and sample. Sharp tips are not particularly useful since they can puncture the cell membrane. Imaging of cells using AFM also requires the imaging of a larger sample area than for many other AFM samples which can lead to problems with drift, or non-linearity, in the piezoelectric scanner¹⁵⁰.

Although AFM is primarily known as a contact technique, non contact AFM (NC AFM) modes have been developed that have extended the range of samples that can be investigated. NC AFM was first developed in 1987 and was designed in order to maintain tip sharpness since the AFM tip is often quickly blunted as it moves over the sample and to obtain the best resolution for most samples, the tip needs to be as sharp as possible. Along with imaging, NC AFM can also be used for quantifying tip-sample forces and interaction potentials and also to manipulate individual atoms. As well as protecting the tip, NC AFM is also particularly useful for soft biological samples such as cells since normal AFM studies of cells are often damaging to the sample and difficult due to the deforming effects of the AFM tip on the sample^{270, 271}.

NC AFM works via the principle of 'amplitude modulation' detection. Instead of contact AFM, where the tip is in contact with the sample surface and repulsive interactions dominate, in NC AFM, the tip is oscillated at a frequency slightly above its resonant frequency and the amplitude of oscillation is typically only a few nanometres. At this point above the surface of the sample, attractive Van der Waals forces dominate the interaction and these forces cause a decrease in the resonant frequency of the cantilever. These deflections are too small to be observed using traditional direct current detection methods so an alternating current detection method is used which is more sensitive, increasing the resolution of NC AFM^{150, 270, 271}.

In addition to NC AFM, living cells have also been imaged using fast scanning AFM and 'Trolling' mode AFM. Fast-scanning AFM was developed to be able to image processes such as the movement of motor proteins which occur at a faster rate than standard AFM technology can image at the required resolution. It also uses a sharp probe and a high sensitivity of feedback control, minimising the force applied to the cell²⁷². 'Trolling' mode AFM uses a nanoneedle grown on a standard AFM cantilever to overcome the decreased resolution that can be encountered when performing

AFM imaging in a liquid environment. By immersing the sample in a minimal level of liquid, the nanoneedle can reach the sample whilst the cantilever remains in air and its sensitivity is maximised. The nanoneedle can have a diameter as low as 20nm. It has been shown to produce AFM images of cells without deformation or imaging of the cytoskeleton²⁷³.

Other developments of AFM have involved the combination of an AFM with another form of microscopy such as SICM, SNOM, Raman or electron microscopy¹⁵⁰. These combinations help to increase the data that can be obtained about a sample, enabling better characterisation. The combination of AFM with other microscopy techniques would, in a similar way to the use of SSCM in this work, allow for the simultaneous tracking of topography and fluorescence during particle interaction and uptake.

6.2.3 Fluorescence microscopy

Although there have been many advances in fluorescent microscopy since it was first developed, further improvements could be made that would improve the imaging capability further. These include increasing the resolution, enabling the observation of small objects that are beyond the resolution of current systems. Other areas where improvements could be made are on how the laser affects cells in order to try and reduce phototoxicity. This would help to keep cells alive longer, allowing long term imaging and thereby avoiding the need to fix cells and removing the associated artefacts.

Despite the advances achieved in fluorescent microscopy, the commonly used techniques such as widefield and CLSM are limited in their resolution by the diffraction limit of light, which restricts the information that can be captured using standard equipment, mainly the objective. Resolution is defined as the largest distance at which the image of two point shaped objects seems to amalgamate. The diffraction limit of light means that optical techniques cannot distinguish between two objects that are separated by a distance which is less than half the wavelength of the light used to image the sample. For confocal microscopy, this means that the maximum resolution is limited to half the wavelength of blue light, approximately 200nm. The maximum resolution is rarely obtained since there are interfering factors from the environment and sample. Electron microscopy has a higher

resolution since it uses electrons rather than photons and the wavelength is 10^5 times smaller, but it is limited by the conditions required for the sample, removing the ability to image live cells¹³⁶.

A wide range of new fluorescent microscopy techniques have been developed such as Total Internal Reflectance Microscopy (TIRF) which has a good signal to noise ratio but only looks at the area of the cell close to the membrane. Near-field scanning optical microscopy (NSOM) avoids the diffraction limit of light by scanning samples with small probes. Both of these techniques work close to the cell surface but other techniques have been developed, known as far-field methods which have a greater range of applications and can be used alongside existing techniques for sample preparation. These techniques, such as STED and STORM have been developed since Stefan Hell first published a concept for overcoming Abbe's diffraction barrier based on stimulated emission to inhibit fluorescence for molecules at the edge of the excitation point spread function ²⁷⁴. They have the potential for much higher resolution than standard CLSM, enabling visualization of processes such as caveolae mediated uptake which has been difficult to image using conventional techniques (Figure 6.1)^{30, 136, 275}.

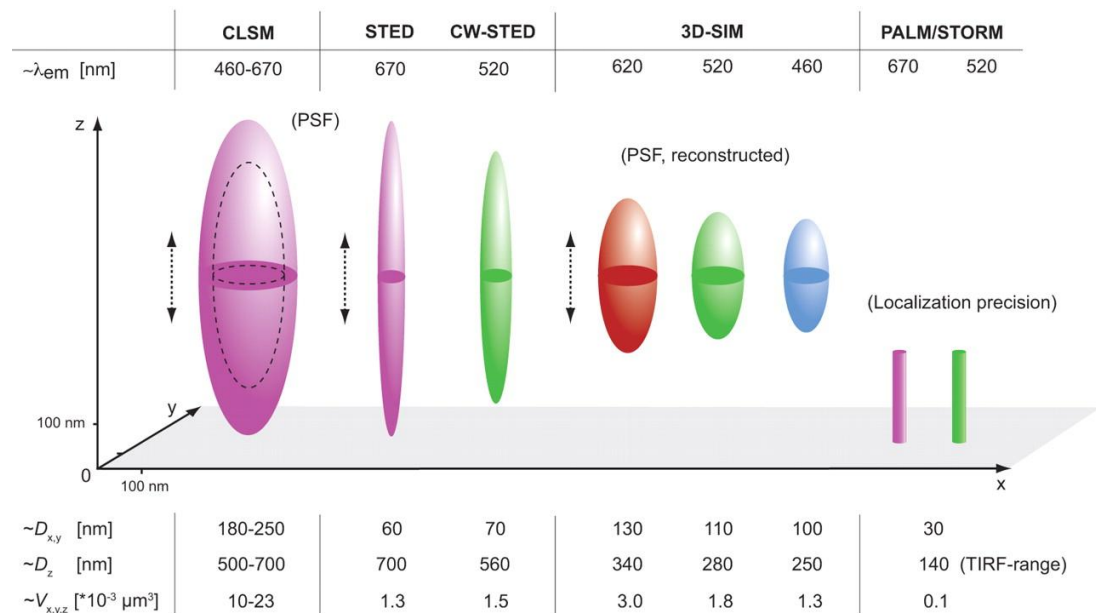


Figure 6.1: Resolution of different microscopy techniques.

6.2.3.1 Stimulated Emission Depletion Microscopy (STED)

STED is a form of super resolution fluorescent microscopy that uses the process of de-excitation, or suppression of fluorescent dyes, in order to overcome the resolution limit imposed by the diffraction of light. By doing this it effectively decreases the diameter of the laser spot and increases resolution²⁷⁴⁻²⁷⁶. Instead of the spontaneous relaxation which is usually used to produce fluorescence emission, a molecule can also be returned to its ground state by a process known as stimulated emission. If a fluorophore in the excited state is irradiated with light of a similar wavelength to the fluorescence light, known as a red-shifted de-excitation beam, electrons can immediately return to the ground state. During this process a photon of exactly the same wavelength and momentum of the light used is emitted, preventing the spontaneous emission of a fluorescence photon. To separate the light originating from the spontaneous decay and the stimulated emission, filters are used.

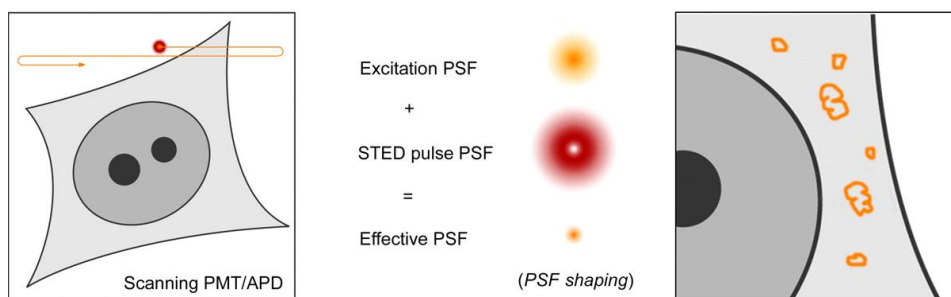


Figure 6.2: Diagram to show basic principle of STED¹³⁶.

A STED microscope therefore uses a pair of synchronised laser pulses. Initially, the laser is raster scanned over the sample, in a similar way to CLSM, and excitation light is provided by a short laser pulse at the required wavelength for the dye in the sample¹³⁶. The excitation pulse produces an ordinary diffraction limited spot of excited molecules similar to that observed using CLSM. However, in STED microscopy, the excitation pulse is immediately followed by the red-shifted, lower energy laser pulse, known as the depletion or STED pulse. This leads to quenching of the fluorophores to their ground state²⁷⁷. The overall effect of the STED pulse is that the excited molecules that the STED pulse acts on cannot fluoresce because their energy is lost. STED achieves greater resolution than CLSM by arranging the

STED pulse in a ring or doughnut shape which is generated by a phase plate in the light path of the laser (Figure 6.2)^{275, 277}. This means that fluorescence is selectively inhibited for the molecules at the periphery of the spot. In the centre of the doughnut or ring shape, where the STED pulse is absent, fluorescence remains unaffected. As the intensity of the STED pulse increases, the size of the central region where molecules can still fluoresce becomes smaller, whilst the inhibition of fluorescence around the edge of the ring is increased. Therefore, by increasing the intensity of the STED pulse, the fluorescent spot can be progressively narrowed down, potentially to the molecular level although currently, a resolution of less than 20nm can be achieved^{136, 276, 277}.

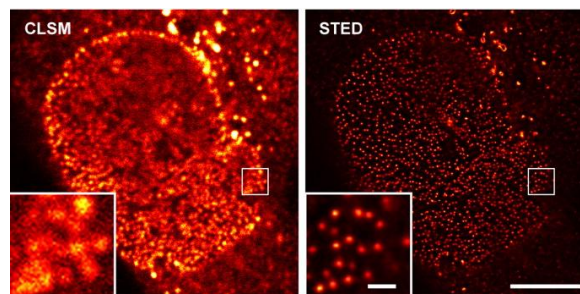


Figure 6.3: HeLa cells stained with antibodies against the nuclear pore complex protein Nup153 and secondary antibodies conjugated with ATT0647N on a standard confocal (CLSM) and a TCS STED Confocal microscope (Leica)¹³⁶.

6.2.3.2 Stochastic Optical Reconstruction Microscopy (STORM)

STORM microscopy is a localization based super resolution microscopy technique and has also been shown to achieve a resolution of 20nm. It is part of a family of related techniques including Photoactivated Localization Microscopy (PALM) and Fluorescence Photoactivation Localization Microscopy (FPALM), all of which are based on very similar theories and modes of operation. They work based on the principle of limiting the number of particles that are simultaneously excited, to avoid detecting particles with overlapping signals^{131, 132, 278}. Following excitation, a point source function is applied to the images.

This process is known as stochastic activation and it activates small numbers of fluorescent molecules that are optically resolvable using low intensity light, and this is used to obtain localization information in 3D. Multiple cycles of exposure are

used and in each exposure a unique set of fluorophores are excited^{275, 276}. Over time, as the images are combined, this enables a complete image to be constructed with the positions of many different fluorophores reported. Photobleaching is used in between exposures to enable separation (Figure 6.4)¹³⁶.

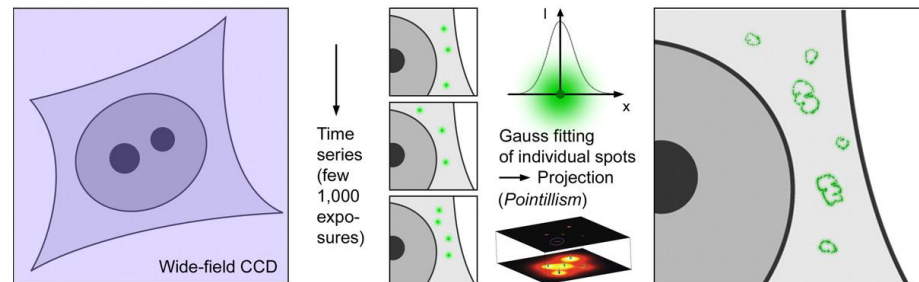


Figure 6.4: Diagram of the basic principle of STORM¹³⁶.

Although STORM uses a basic widefield microscope setup, it requires the use of specialised dyes, some of the most commonly used ones are cyanine dyes since they are photoswitchable or phototactivatable so that only some are visible at any time in a single frame^{131, 275}. This means they can be made to both fluoresce and deactivate using light of different wavelengths. Dedicated fluorescent dye pairings containing an activator (short wavelength) and a reporter (long wavelength) are used, enabling various colour combinations to be observed. These dyes are used as probes to separate overlapping images of individual molecules in order to improve resolution since the activated fluorescent molecules must be separated by a distance that exceeds the Abbe diffraction limit of around 250nm. Images of each subset of fluorescent molecules activated are captured rapidly until they spontaneously photobleach or re-enter a dark state²⁷⁸.

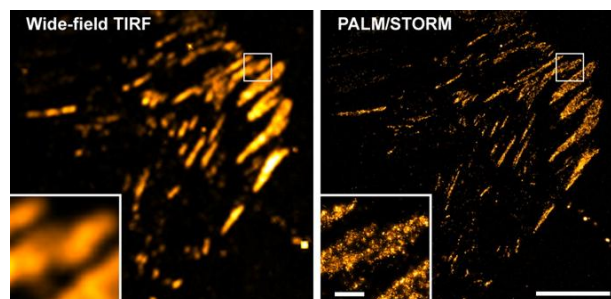


Figure 6.5: TdEosFP-Pallaxin expressed in Hep G2 cells to label adhesion complexes on lower surface using TIRF and TIRF/STORM combined¹³⁶.

Both STED and STORM require special fluorophores and STED requires a high laser power, therefore live cell imaging is currently restricted but in future, as the techniques develop, there is the potential that nanoparticles such as small, 50nm polyacrylamide particles could be observed within live cells and better colocalization studies could be performed to further investigate their intracellular localization^{131, 276}.

6.3 Future work

Much of this work in this thesis requires further investigations in order to be able to draw definitive conclusions about the effects of some of the parameters investigated on cellular uptake.

It would be interesting to extend the current work in order to further investigate the effects of nanoparticle charge on uptake. This could be achieved by creating a larger library of both polyacrylamide and silica nanoparticles with a wider range of both positive and negative charges, possibly via the incorporation of different functional groups to those used in this work. Additionally, the effects of conjugation to cell penetrating peptides could be further investigated by using a number of different cell penetrating peptides with different sequences and structures.

Another important area of research that may aid the future design of the nanoparticle systems would be to investigate in much greater detail the specific routes of endocytosis that are employed by the different nanoparticles. This requires the use of specific pharmacological inhibitors of different endocytic pathways in order to try and identify the effects on cellular uptake of blocking pathways. Alternatively, in more recent studies that block specific endocytic pathways, some groups have moved more towards the development of siRNA probes that can deplete intracellular endocytic proteins. These probes may prove to be a more specific and suitable method for investigating endocytosis since some pharmacological inhibitors can have multiple effects on the cell via the inhibition of molecules involved in more than one endocytic pathway⁵⁰. More advanced studies could also be carried out into colocalization of the nanoparticles with intracellular compartments such as endosomes and lysosomes and also with markers of certain uptake pathways such as transferrin (clathrin) or dextran (macropinocytosis).

The use of some of the more advanced imaging techniques that are described in this chapter would help to improve the quality of the images obtained. This applies to both the topography and fluorescence imaging of the nanoparticle-cell interaction. Improving the imaging and hence the quality of data obtained would help to provide more detail of this interaction on the nanoscale. One of the best ways to get the most out of the imaging techniques is to combine a number of techniques, for example, as was done using SICM combined with confocal microscopy in SSCM. Many manufacturers are now moving towards combined systems as demand for better images increases and there are now numerous combinations of scanning probe and fluorescent microscopy techniques that can be employed depending on the specific experiment being performed.

Other techniques that could have been used in this work to support the data obtained include fluorescence activated cell sorting (FACS) which would give a more global view of the uptake of the nanoparticles into cells. It measures the fluorescence of many cells in a sample and would provide measurements much faster than doing individual measurements using images obtained from a widefield microscope. Electron microscopy techniques such as transmission electron microscopy (TEM) could also have been performed for silica nanoparticles in order to investigate intracellular localization of the nanoparticles since it can produce high resolution images of subcellular structures.

With the use of better imaging techniques, it may be easier to perform quantitative measurements of analytes within cells. This can be achieved by the use of combinations of dyes entrapped in the nanoparticles, some sensitive to analytes such as H^+ , Ca^{2+} or O_2 , and others insensitive to the same analytes. These enable intracellular measurements to be performed via the measurement of changes in fluorescence. The use of an analyte insensitive dye means that ratiometric measurements can be taken which remove any inaccuracies associated with uneven particle or dye distribution within the cell. It would have been interesting to use a pH sensitive nanoparticle system to investigate the change in pH during the uptake process and to link these images to topography changes.

Finally, cytotoxicity studies need to be performed in order to investigate the effect of the internalization of the nanoparticles on the cells. Many studies in the literature

link increased uptake of highly charged nanoparticles and cell penetrating peptides with increased cell death. If any of these systems were ever to be developed for a biological use, this effect would need consideration and the nanoparticles may need to be adapted in order to ensure cell survival.

Chapter 7 - References

1. Kemp, S. J.; Thorley, A. J.; Gorelik, J.; Seckl, M. J.; O'Hare, M. J.; Arcaro, A.; Korchev, Y.; Goldstraw, P.; Tetley, T. D., Immortalization of Human Alveolar Epithelial Cells to Investigate Nanoparticle Uptake. *American Journal of Respiratory Cell and Molecular Biology* **2008**, 39, (5), 591-597.
2. Zhao, F.; Zhao, Y.; Liu, Y.; Chang, X.; Chen, C.; Zhao, Y., Cellular Uptake, Intracellular Trafficking, and Cytotoxicity of Nanomaterials. *Small* **2011**, 7, (10), 1322-1337.
3. Cheng, M. M. C.; Cuda, G.; Bunimovich, Y. L.; Gaspari, M.; Heath, J. R.; Hill, H. D.; Mirkin, C. A.; Nijdam, A. J.; Terracciano, R.; Thundat, T.; Ferrari, M., Nanotechnologies for biomolecular detection and medical diagnostics. *Current Opinion in Chemical Biology* **2006**, 10, (1), 11-19.
4. Chithrani, B. D.; Ghazani, A. A.; Chan, W. C. W., Determining the size and shape dependence of gold nanoparticle uptake into mammalian cells. *Nano Letters* **2006**, 6, (4), 662-668.
5. O'Riordan, T. C.; Fitzgerald, K.; Ponomarev, G. V.; Mackrill, J.; Hynes, J.; Taylor, C.; Papkovsky, D. B., Sensing intracellular oxygen using near-infrared phosphorescent probes and live-cell fluorescence imaging. *American Journal of Physiology-Regulatory Integrative and Comparative Physiology* **2007**, 292, (4), R1613-R1620.
6. Si, D.; Epstein, T.; Lee, Y. E. K.; Kopelman, R., Nanoparticle PEBBLE Sensors for Quantitative Nanomolar Imaging of Intracellular Free Calcium Ions. *Analytical Chemistry* **2012**, 84, (2), 978-986.
7. Slowing, II; Vivero-Escoto, J. L.; Wu, C. W.; Lin, V. S. Y., Mesoporous silica nanoparticles as controlled release drug delivery and gene transfection carriers. *Advanced Drug Delivery Reviews* **2008**, 60, (11), 1278-1288.
8. Yacobi, N. R.; Malmstadt, N.; Fazlollahi, F.; DeMaio, L.; Marchelletta, R.; Hamm-Alvarez, S. F.; Borok, Z.; Kim, K.-J.; Crandall, E. D., Mechanisms of Alveolar Epithelial Translocation of a Defined Population of Nanoparticles. *American Journal of Respiratory Cell and Molecular Biology* **2010**, 42, (5), 604-614.
9. Labhasetwar, V., Nanotechnology for drug and gene therapy: the importance of understanding molecular mechanisms of delivery. *Current Opinion in Biotechnology* **2005**, 16, (6), 674-680.
10. Coupland, P. G.; Briddon, S. J.; Aylott, J. W., Using fluorescent pH-sensitive nanosensors to report their intracellular location after Tat-mediated delivery. *Integrative Biology* **2009**, 1, (4), 318-323.
11. Verma, A.; Stellacci, F., Effect of Surface Properties on Nanoparticle-Cell Interactions. *Small* **2010**, 6, (1).
12. Schulz, A.; Wotschadlo, J.; Heinze, T.; Mohr, G. J., Fluorescent nanoparticles for ratiometric pH-monitoring in the neutral range. *Journal of Materials Chemistry* **2010**, 20, (8), 1475-1482.
13. Conner, S. D.; Schmid, S. L., Regulated portals of entry into the cell. *Nature* **2003**, 422, (6927), 37-44.
14. Harush-Frenkel, O.; Rozentur, E.; Benita, S.; Altschuler, Y., Surface charge of nanoparticles determines their endocytic and transcytotic pathway in polarized MDCK cells. *Biomacromolecules* **2008**, 9, (2), 435-443.
15. Doherty, G. J.; McMahon, H. T., Mechanisms of Endocytosis. *Annual Review of Biochemistry* **2009**, 78, 857-902.

16. Mosesson, Y.; Mills, G. B.; Yarden, Y., Derailed endocytosis: an emerging feature of cancer. *Nature Reviews Cancer* **2008**, 8, (11), 835-850.
17. Canton, I.; Battaglia, G., Endocytosis at the nanoscale. *Chemical Society Reviews* **2012**, 41, (7), 2718-2739.
18. Hillaireau, H.; Couvreur, P., Nanocarriers' entry into the cell: relevance to drug delivery. *Cellular and Molecular Life Sciences* **2009**, 66, (17), 2873-2896.
19. Schmid, E. M.; Ford, M. G. J.; Burtley, A.; Praefcke, G. J. K.; Peak-Chew, S. Y.; Mills, I. G.; Benmerah, A.; McMahon, H. T., Role of the AP2 beta-appendage hub in recruiting partners for clathrin-coated vesicle assembly. *Plos Biology* **2006**, 4, (9), 1532-1548.
20. Praefcke, G. J. K.; McMahon, H. T., The dynamin superfamily: Universal membrane tubulation and fission molecules? *Nature Reviews Molecular Cell Biology* **2004**, 5, (2), 133-147.
21. Eisenberg, E.; Greene, L. E., Multiple roles of auxilin and Hsc70 in clathrin-mediated endocytosis. *Traffic* **2007**, 8, (6), 640-646.
22. Xing, Y.; Bocking, T.; Wolf, M.; Grigorieff, N.; Kirchhausen, T.; Harrison, S. C., Structure of clathrin coat with bound Hsc70 and auxilin: mechanism of Hsc70-facilitated disassembly. *Embo Journal* **2010**, 29, (3), 655-665.
23. Marks, M. S.; Woodruff, L.; Ohno, H.; Bonifacino, J. S., Protein targeting by tyrosine- and di-leucine-based signals: Evidence for distinct saturable components. *Journal of Cell Biology* **1996**, 135, (2), 341-354.
24. Sorkin, A., Cargo recognition during clathrin-mediated endocytosis: a team effort. *Current Opinion in Cell Biology* **2004**, 16, (4), 392-399.
25. Sahay, G.; Alakhova, D. Y.; Kabanov, A. V., Endocytosis of nanomedicines. *Journal of Controlled Release* **2010**, 145, (3), 182-195.
26. Begum, G.; Singh, S.; Rangaraj, N.; Srinivas, G.; Rana, R. K., Cellular permeation with nuclear infiltration capability of biomimetically synthesised fluorescent monodisperse mesoporous silica nanospheres in HeLa and human stem cells. *Journal of Materials Chemistry* **2010**, 20, (39), 8563-8570.
27. Mailander, V.; Landfester, K., Interaction of Nanoparticles with Cells. *Biomacromolecules* **2009**, 10, (9), 2379-2400.
28. Vercauteren, D.; Vandenbroucke, R. E.; Jones, A. T.; Rejman, J.; Demeester, J.; De Smedt, S. C.; Sanders, N. N.; Braeckmans, K., The Use of Inhibitors to Study Endocytic Pathways of Gene Carriers: Optimization and Pitfalls. *Molecular Therapy* **2010**, 18, (3), 561-569.
29. Richter, T.; Floetenmeyer, M.; Ferguson, C.; Galea, J.; Goh, J.; Lindsay, M. R.; Morgan, G. P.; Marsh, B. J.; Parton, R. G., High-resolution 3D quantitative analysis of caveolar ultrastructure and caveola-cytoskeleton interactions. *Traffic* **2008**, 9, (6), 893-909.
30. Wang, Z. J.; Tiruppathi, C.; Minshall, R. D.; Malik, A. B., Size and Dynamics of Caveolae Studied Using Nanoparticles in Living Endothelial Cells. *Acs Nano* **2009**, 3, (12), 4110-4116.
31. Parton, R. G.; Hanzal-Bayer, M.; Hancock, J. F., Biogenesis of caveolae: a structural model for caveolin-induced domain formation. *Journal of Cell Science* **2006**, 119, (5), 787-796.
32. Parton, R. G.; Simons, K., The multiple faces of caveolae. *Nature Reviews Molecular Cell Biology* **2007**, 8, (3), 185-194.

33. Sargiacomo, M.; Scherer, P. E.; Tang, Z. L.; Kubler, E.; Song, K. S.; Sanders, M. C.; Lisanti, M. P., OLIGOMERIC STRUCTURE OF CAVEOLIN - IMPLICATIONS FOR CAVEOLAE MEMBRANE ORGANIZATION. *Proceedings of the National Academy of Sciences of the United States of America* **1995**, 92, (20), 9407-9411.
34. Fra, A. M.; Masserini, M.; Palestini, P.; Sonnino, S.; Simons, K., A PHOTO-REACTIVE DERIVATIVE OF GANGLIOSIDE GM1 SPECIFICALLY CROSS-LINKS VIP21-CAVEOLIN ON THE CELL-SURFACE. *Febs Letters* **1995**, 375, (1-2), 11-14.
35. Pelkmans, L.; Burli, T.; Zerial, M.; Helenius, A., Caveolin-stabilized membrane domains as multifunctional transport and sorting devices in endocytic membrane traffic. *Cell* **2004**, 118, (6), 767-780.
36. Glebov, O. O.; Bright, N. A.; Nichols, B. J., Flotillin-1 defines a clathrin-independent endocytic pathway in mammalian cells. *Nature Cell Biology* **2006**, 8, (1), 46-U16.
37. Frick, M.; Bright, N. A.; Riento, K.; Bray, A.; Merrified, C.; Nichols, B. J., Coassembly of flotillins induces formation of membrane microdomains, membrane curvature, and vesicle budding. *Current Biology* **2007**, 17, (13), 1151-1156.
38. Lundmark, R.; Doherty, G. J.; Howes, M. T.; Cortese, K.; Vallis, Y.; Parton, R. G.; McMahon, H. T., The GTPase-Activating Protein GRAF1 Regulates the CLIC/GEEC Endocytic Pathway. *Current Biology* **2008**, 18, (22), 1802-1808.
39. Payne, C. K.; Jones, S. A.; Chen, C.; Zhuang, X. W., Internalization and trafficking of cell surface proteoglycans and proteoglycan-binding ligands. *Traffic* **2007**, 8, (4), 389-401.
40. Mercer, J.; Helenius, A., Virus entry by macropinocytosis. *Nature Cell Biology* **2009**, 11, (5), 510-520.
41. Sandvig, K.; Torgersen, M. L.; Raa, H. A.; Van Deurs, B., Clathrin-independent endocytosis: from nonexisting to an extreme degree of complexity. *Histochemistry and Cell Biology* **2008**, 129, (3), 267-276.
42. Grimmer, S.; van Deurs, B.; Sandvig, K., Membrane ruffling and macropinocytosis in A431 cells require cholesterol. *Journal of Cell Science* **2002**, 115, (14), 2953-2962.
43. Dharmawardhane, S.; Schurmann, A.; Sells, M. A.; Chernoff, J.; Schmid, S. L.; Bokoch, G. M., Regulation of macropinocytosis by p21-activated kinase-1. *Molecular Biology of the Cell* **2000**, 11, (10), 3341-3352.
44. Jones, A. T., Gateways and tools for drug delivery: Endocytic pathways and the cellular dynamics of cell penetrating peptides. *International Journal of Pharmaceutics* **2008**, 354, (1-2), 34-38.
45. Herce, H. D.; Garcia, A. E., Cell Penetrating Peptides: How Do They Do It? *Journal of Biological Physics* **2007**, 33, (5-6), 345-356.
46. Rydstrom, A.; Deshayes, S.; Konate, K.; Crombez, L.; Padari, K.; Boukhaddaoui, H.; Aldrian, G.; Pooga, M.; Divita, G., Direct Translocation as Major Cellular Uptake for CADY Self-Assembling Peptide-Based Nanoparticles. *Plos One* **2011**, 6, (10).
47. Yacobi, N. R.; DeMaio, L.; Xie, J.; Hamm-Alvarez, S. F.; Borok, Z.; Kim, K.-J.; Crandall, E. D., Polystyrene nanoparticle trafficking across alveolar epithelium. *Nanomedicine-Nanotechnology Biology and Medicine* **2008**, 4, (2), 139-145.
48. Herce, H. D.; Garcia, A. E., Molecular dynamics simulations suggest a mechanism for translocation of the HIV-1 TAT peptide across lipid membranes. *Proceedings of the National Academy of Sciences of the United States of America* **2007**, 104, (52), 20805-20810.

49. Ivanov, A. I., Pharmacological inhibition of endocytic pathways: Is it specific enough to be useful? *Methods in Molecular Biology* **2008**, 15-33.
50. Al Soraj, M.; He, L.; Peynshaert, K.; Cousaert, J.; Vercauteren, D.; Braeckmans, K.; De Smedt, S. C.; Jones, A. T., siRNA and pharmacological inhibition of endocytic pathways to characterize the differential role of macropinocytosis and the actin cytoskeleton on cellular uptake of dextran and cationic cell penetrating peptides octaarginine (R8) and HIV-Tat. *Journal of Controlled Release* **2012**, 161, (1), 132-141.
51. Lorenz, M. R.; Holzapfel, V.; Musyanovych, A.; Nothelfer, K.; Walther, P.; Frank, H.; Landfester, K.; Schrezenmeier, H.; Mailander, V., Uptake of functionalized, fluorescent-labeled polymeric particles in different cell lines and stem cells. *Biomaterials* **2006**, 27, (14), 2820-2828.
52. Nel, A. E.; Maedler, L.; Velegol, D.; Xia, T.; Hoek, E. M. V.; Somasundaran, P.; Klaessig, F.; Castranova, V.; Thompson, M., Understanding biophysicochemical interactions at the nano-bio interface. *Nature Materials* **2009**, 8, (7), 543-557.
53. Peetla, C.; Labhasetwar, V., Biophysical characterization of nanoparticle-endothelial model cell membrane interactions. *Molecular Pharmaceutics* **2008**, 5, (3), 418-429.
54. Ruenraroengsak, P.; Novak, P.; Berhanu, D.; Thorley, A. J.; Valsami-Jones, E.; Gorelik, J.; Korchev, Y. E.; Tetley, T. D., Respiratory epithelial cytotoxicity and membrane damage (holes) caused by amine-modified nanoparticles. *Nanotoxicology* **2012**, 6, (1), 94-108.
55. He, C. B.; Hu, Y. P.; Yin, L. C.; Tang, C.; Yin, C. H., Effects of particle size and surface charge on cellular uptake and biodistribution of polymeric nanoparticles. *Biomaterials* **2010**, 31, (13), 3657-3666.
56. Georgieva, J. V.; Kalicharan, D.; Couraud, P.-O.; Romero, I. A.; Weksler, B.; Hoekstra, D.; Zuhorn, I. S., Surface Characteristics of Nanoparticles Determine Their Intracellular Fate in and Processing by Human Blood-Brain Barrier Endothelial Cells In Vitro. *Molecular Therapy* **2011**, 19, (2), 318-325.
57. Rejman, J.; Oberle, V.; Zuhorn, I. S.; Hoekstra, D., Size-dependent internalization of particles via the pathways of clathrin- and caveolae-mediated endocytosis. *Biochemical Journal* **2004**, 377, 159-169.
58. Vacha, R.; Martinez-Veracochea, F. J.; Frenkel, D., Receptor-Mediated Endocytosis of Nanoparticles of Various Shapes. *Nano Letters* **2011**, 11, (12), 5391-5395.
59. Li, X., Size and shape effects on receptor-mediated endocytosis of nanoparticles. *Journal of Applied Physics* **2012**, 111, (2).
60. Harush-Frenkel, O.; Debotton, N.; Benita, S.; Altschuler, Y., Targeting of nanoparticles to the clathrin-mediated endocytic pathway. *Biochemical and Biophysical Research Communications* **2007**, 353, (1), 26-32.
61. Vasir, J. K.; Labhasetwar, V., Quantification of the force of nanoparticle-cell membrane interactions and its influence on intracellular trafficking of nanoparticles. *Biomaterials* **2008**, 29, (31), 4244-4252.
62. Xia, T.; Kovochich, M.; Liang, M.; Zink, J. I.; Nel, A. E., Cationic polystyrene nanosphere toxicity depends on cell-specific endocytic and mitochondrial injury pathways. *ACS Nano* **2008**, 2, (1), 85-96.
63. Escriou, V.; Carriere, M.; Scherman, D.; Wils, P., NLS bioconjugates for targeting therapeutic genes to the nucleus. *Advanced Drug Delivery Reviews* **2003**, 55, (2), 295-306.

64. Tkachenko, A. G.; Xie, H.; Coleman, D.; Glomm, W.; Ryan, J.; Anderson, M. F.; Franzen, S.; Feldheim, D. L., Multifunctional gold nanoparticle-peptide complexes for nuclear targeting. *Journal of the American Chemical Society* **2003**, *125*, (16), 4700-4701.
65. Katz, E.; Willner, I., Integrated nanoparticle-biomolecule hybrid systems: Synthesis, properties, and applications. *Angewandte Chemie-International Edition* **2004**, *43*, (45), 6042-6108.
66. Safi, M.; Courtois, J.; Seigneuret, M.; Conjeaud, H.; Berret, J. F., The effects of aggregation and protein corona on the cellular internalization of iron oxide nanoparticles. *Biomaterials* **2011**, *32*, (35), 9353-9363.
67. Lesniak, A.; Fenaroli, F.; Monopoli, M. R.; Aberg, C.; Dawson, K. A.; Salvati, A., Effects of the Presence or Absence of a Protein Corona on Silica Nanoparticle Uptake and Impact on Cells. *Acs Nano* **2012**, *6*, (7), 5845-5857.
68. Laurent, S.; Burtea, C.; Thirifays, C.; Rezaee, F.; Mahmoudi, M., Significance of cell "observer" and protein source in nanobiosciences. *Journal of Colloid and Interface Science* **2013**, *392*, 431-445.
69. Lesniak, A.; Salvati, A.; Santos-Martinez, M. J.; Radomski, M. W.; Dawson, K. A.; Aberg, C., Nanoparticle Adhesion to the Cell Membrane and Its Effect on Nanoparticle Uptake Efficiency. *Journal of the American Chemical Society* **2013**, *135*, (4), 1438-1444.
70. Monopoli, M. P.; Aberg, C.; Salvati, A.; Dawson, K. A., Biomolecular coronas provide the biological identity of nanosized materials. *Nature Nanotechnology* **2012**, *7*, (12), 779-786.
71. Prapainop, K.; Witter, D. P.; Wentworth, P., A Chemical Approach for Cell-Specific Targeting of Nanomaterials: Small-Molecule-Initiated Misfolding of Nanoparticle Corona Proteins. *Journal of the American Chemical Society* **2012**, *134*, (9), 4100-4103.
72. Sandin, P.; Fitzpatrick, L. W.; Simpson, J. C.; Dawson, K. A., High-Speed Imaging of Rab Family Small GTPases Reveals Rare Events in Nanoparticle Trafficking in Living Cells. *Acs Nano* **2012**, *6*, (2), 1513-1521.
73. Fisichella, M.; Dabboue, H.; Bhattacharyya, S.; Lelong, G.; Saboungi, M. L.; Warmont, F.; Midoux, P.; Pichon, C.; Guerin, M.; Hevor, T.; Salvat, J. P., Uptake of Functionalized Mesoporous Silica Nanoparticles by Human Cancer Cells. *Journal of Nanoscience and Nanotechnology* **2010**, *10*, (4), 2314-2324.
74. Lu, F.; Wu, S. H.; Hung, Y.; Mou, C. Y., Size Effect on Cell Uptake in Well-Suspended, Uniform Mesoporous Silica Nanoparticles. *Small* **2009**, *5*, (12), 1408-1413.
75. Win, K. Y.; Feng, S. S., Effects of particle size and surface coating on cellular uptake of polymeric nanoparticles for oral delivery of anticancer drugs. *Biomaterials* **2005**, *26*, (15), 2713-2722.
76. Kurupparachchi, M.; Savoie, H.; Lowry, A.; Alonso, C.; Boyle, R. W., Polyacrylamide Nanoparticles as a Delivery System in Photodynamic Therapy. *Molecular Pharmaceutics* **2011**, *8*, (3), 920-931.
77. Mitragotri, S.; Lahann, J., Physical approaches to biomaterial design. *Nature Materials* **2009**, *8*, (1).
78. Jin, Y. H.; Lohstreter, S.; Pierce, D. T.; Parisien, J.; Wu, M.; Hall, C.; Zhao, J. X. J., Silica nanoparticles with continuously tunable sizes: Synthesis and size effects on cellular contrast Imaging. *Chemistry of Materials* **2008**, *20*, (13), 4411-4419.
79. Orr, G.; Panther, D. J.; Phillips, J. L.; Tarasevich, B. J.; Dohnalkova, A.; Hu, D. H.; Teeguarden, J. G.; Pounds, J. G., Submicrometer and nanoscale inorganic particles exploit the actin machinery to be propelled along microvilli-like structures into alveolar cells. *Acs Nano* **2007**, *1*, (5), 463-475.

80. dos Santos, T.; Varela, J.; Lynch, I.; Salvati, A.; Dawson, K. A., Quantitative Assessment of the Comparative Nanoparticle-Uptake Efficiency of a Range of Cell Lines. *Small* **2011**, *7*, (23), 3341-3349.
81. Clift, M. J. D.; Rothen-Rutishauser, B.; Brown, D. M.; Duffin, R.; Donaldson, K.; Proudfoot, L.; Guy, K.; Stone, V., The impact of different nanoparticle surface chemistry and size on uptake and toxicity in a murine macrophage cell line. *Toxicology and Applied Pharmacology* **2008**, *232*, (3), 418-427.
82. Jiang, W.; Kim, B. Y. S.; Rutka, J. T.; Chan, W. C. W., Nanoparticle-mediated cellular response is size-dependent. *Nature Nanotechnology* **2008**, *3*, (3), 145-150.
83. Gao, D.; Agayan, R. R.; Xu, H.; Philbert, M. A.; Kopelman, R., Nanoparticles for two-photon photodynamic therapy in living cells. *Nano Letters* **2006**, *6*, (11), 2383-2386.
84. Desai, M. P.; Labhsetwar, V.; Walter, E.; Levy, R. J.; Amidon, G. L., The mechanism of uptake of biodegradable microparticles in Caco-2 cells is size dependent. *Pharmaceutical Research* **1997**, *14*, (11), 1568-1573.
85. Harush-Frenkel, O.; Altschuler, Y.; Benita, S., Nanoparticle-Cell Interactions: Drug Delivery Implications. *Critical Reviews in Therapeutic Drug Carrier Systems* **2008**, *25*, (6), 485-544.
86. Chen, J.; Hessler, J. A.; Putschakayala, K.; Panama, B. K.; Khan, D. P.; Hong, S.; Mullen, D. G.; DiMaggio, S. C.; Som, A.; Tew, G. N.; Lopatin, A. N.; Baker, J. R., Jr.; Holl, M. M. B.; Orr, B. G., Cationic Nanoparticles Induce Nanoscale Disruption in Living Cell Plasma Membranes. *Journal of Physical Chemistry B* **2009**, *113*, (32), 11179-11185.
87. Chen, L. A.; McCrate, J. M.; Lee, J. C. M.; Li, H., The role of surface charge on the uptake and biocompatibility of hydroxyapatite nanoparticles with osteoblast cells. *Nanotechnology* **2011**, *22*, (10).
88. Dausend, J.; Musyanovych, A.; Dass, M.; Walther, P.; Schrezenmeier, H.; Landfester, K.; Mailander, V., Uptake Mechanism of Oppositely Charged Fluorescent Nanoparticles in HeLa Cells. *Macromolecular Bioscience* **2008**, *8*, (12), 1135-1143.
89. Li, Y.; Wang, J.; Gao, Y.; Zhu, J.; Wientjes, M. G.; Au, J. L. S., Relationships between Liposome Properties, Cell Membrane Binding, Intracellular Processing, and Intracellular Bioavailability. *Aaps Journal* **2011**, *13*, (4), 585-597.
90. Fenart, L.; Casanova, A.; Dehouck, B.; Duhem, C.; Slupek, S.; Cecchelli, R.; Betbeder, D., Evaluation of effect of charge and lipid coating on ability of 60-nm nanoparticles to cross an in vitro model of the blood-brain barrier. *Journal of Pharmacology and Experimental Therapeutics* **1999**, *291*, (3), 1017-1022.
91. Gratton, S. E. A.; Ropp, P. A.; Pohlhaus, P. D.; Luft, J. C.; Madden, V. J.; Napier, M. E.; DeSimone, J. M., The effect of particle design on cellular internalization pathways. *Proceedings of the National Academy of Sciences of the United States of America* **2008**, *105*, (33).
92. Zhu, Z. J.; Ghosh, P. S.; Miranda, O. R.; Vachet, R. W.; Rotello, V. M., Multiplexed Screening of Cellular Uptake of Gold Nanoparticles Using Laser Desorption/Ionization Mass Spectrometry. *Journal of the American Chemical Society* **2008**, *130*, (43), 14139-14143.
93. Peetla, C.; Rao, K. S.; Labhsetwar, V. In *Relevance of Biophysical Interactions of Nanoparticles with a Model Membrane in Predicting Cellular Uptake: Study with TAT Peptide-Conjugated Nanoparticles*, NanoMedicine Summit on Nanoparticles for Imaging, Diagnosis and Therapeutics, Cleveland, OH, Sep 25, 2008; Cleveland, OH, 2008; pp 1311-1320.

94. Verma, A.; Uzun, O.; Hu, Y.; Han, H.-S.; Watson, N.; Chen, S.; Irvine, D. J.; Stellacci, F., Surface-structure-regulated cell-membrane penetration by monolayer-protected nanoparticles. *Nature Materials* **2008**, *7*, (7), 588-595.
95. Mecke, A.; Majoros, I. J.; Patri, A. K.; Baker, J. R.; Holl, M. M. B.; Orr, B. G., Lipid bilayer disruption by polycationic polymers: The roles of size and chemical functional group. *Langmuir* **2005**, *21*, (23), 10348-10354.
96. Zhao, Y. N.; Vivero-Escoto, J. L.; Slowing, II; Trewyn, B. C.; Lin, V. S. Y., Capped mesoporous silica nanoparticles as stimuli-responsive controlled release systems for intracellular drug/gene delivery. *Expert Opinion on Drug Delivery* **2010**, *7*, (9), 1013-1029.
97. Leroueil, P. R.; Berry, S. A.; Duthie, K.; Han, G.; Rotello, V. M.; McNerny, D. Q.; Baker, J. R.; Orr, B. G.; Holl, M. M. B., Wide varieties of cationic nanoparticles induce defects in supported lipid bilayers. *Nano Letters* **2008**, *8*, (2), 420-424.
98. Chen, Y.-P.; Chen, H.-A.; Hung, Y.; Chien, F.-C.; Chen, P.; Mou, C.-Y., Surface charge effect in intracellular localization of mesoporous silica nanoparticles as probed by fluorescent ratiometric pH imaging. *Rsc Advances* **2012**, *2*, (3), 968-973.
99. Graf, C.; Gao, Q.; Schutz, I.; Noufele, C. N.; Ruan, W. T.; Posselt, U.; Korotianskiy, E.; Nordmeyer, D.; Rancan, F.; Hadam, S.; Vogt, A.; Lademann, J.; Haucke, V.; Ruhl, E., Surface Functionalization of Silica Nanoparticles Supports Colloidal Stability in Physiological Media and Facilitates Internalization in Cells. *Langmuir* **2012**, *28*, (20), 7598-7613.
100. Gan, Q.; Dai, D. W.; Yuan, Y.; Qian, J. C.; Sha, S.; Shi, J. L.; Liu, C. S., Effect of size on the cellular endocytosis and controlled release of mesoporous silica nanoparticles for intracellular delivery. *Biomedical Microdevices* **2012**, *14*, (2), 259-270.
101. Kaplan, I. M.; Wadia, J. S.; Dowdy, S. F., Cationic TAT peptide transduction domain enters cells by macropinocytosis. *Journal of Controlled Release* **2005**, *102*, (1), 247-253.
102. Santra, S.; Yang, H.; Dutta, D.; Stanley, J. T.; Holloway, P. H.; Tan, W. H.; Moudgil, B. M.; Mericle, R. A., TAT conjugated, FITC doped silica nanoparticles for bioimaging applications. *Chemical Communications* **2004**, (24), 2810-2811.
103. Jones, A. T.; Sayers, E. J., Cell entry of cell penetrating peptides: tales of tails wagging dogs. *Journal of Controlled Release* **2012**, *161*, (2), 582-591.
104. Johnson, R. M.; Harrison, S. D.; Maclean, D., Therapeutic Applications of Cell-Penetrating Peptides. *Cell-Penetrating Peptides: Methods and Protocols* **2011**, *683*, 535-551.
105. Zhao, M.; Kircher, M. F.; Josephson, L.; Weissleder, R., Differential conjugation of tat peptide to superparamagnetic nanoparticles and its effect on cellular uptake. *Bioconjugate Chemistry* **2002**, *13*, (4), 840-844.
106. Koren, E.; Torchilin, V. P., Cell-penetrating peptides: breaking through to the other side. *Trends in Molecular Medicine* **2012**, *18*, (7), 385-393.
107. Zhang, Y. A.; Xu, D.; Li, W. Q.; Yu, J.; Chen, Y., Effect of Size, Shape, and Surface Modification on Cytotoxicity of Gold Nanoparticles to Human HEp-2 and Canine MDCK Cells. *Journal of Nanomaterials* **2012**, *7*.
108. Jones, A. T., Macropinocytosis: searching for an endocytic identity and role in the uptake of cell penetrating peptides. *Journal of Cellular and Molecular Medicine* **2007**, *11*, (4), 670-684.

109. Vives, E.; Brodin, P.; Lebleu, B., A truncated HIV-1 Tat protein basic domain rapidly translocates through the plasma membrane and accumulates in the cell nucleus. *Journal of Biological Chemistry* **1997**, 272, (25), 16010-16017.
110. Derossi, D.; Joliot, A. H.; Chassaing, G.; Prochiantz, A., THE 3RD HELIX OF THE ANTENNAPEDIA HOMEODOMAIN TRANSLOCATES THROUGH BIOLOGICAL-MEMBRANES. *Journal of Biological Chemistry* **1994**, 269, (14), 10444-10450.
111. Rothbard, J. B.; Garlington, S.; Lin, Q.; Kirschberg, T.; Kreider, E.; McGrane, P. L.; Wender, P. A.; Khavari, P. A., Conjugation of arginine oligomers to cyclosporin A facilitates topical delivery and inhibition of inflammation. *Nature Medicine* **2000**, 6, (11), 1253-1257.
112. Elmquist, A.; Lindgren, M.; Bartfai, T.; Langel, U., VE-cadherin-derived cell-penetrating peptide, pVEC, with carrier functions. *Experimental Cell Research* **2001**, 269, (2), 237-244.
113. Morris, M. C.; Deshayes, S.; Heitz, F.; Divita, G., Cell-penetrating peptides: from molecular mechanisms to therapeutics. *Biology of the Cell* **2008**, 100, (4), 201-217.
114. Oehlke, J.; Scheller, A.; Wiesner, B.; Krause, E.; Beyermann, M.; Klauschenz, E.; Melzig, M.; Bienert, M., Cellular uptake of an alpha-helical amphipathic model peptide with the potential to deliver polar compounds into the cell interior non-endocytically. *Biochimica Et Biophysica Acta-Biomembranes* **1998**, 1414, (1-2), 127-139.
115. Crombez, L.; Aldrian-Herrada, G.; Konate, K.; Nguyen, Q. N.; McMaster, G. K.; Brasseur, R.; Heitz, F.; Divita, G., A New Potent Secondary Amphipathic Cell-penetrating Peptide for siRNA Delivery Into Mammalian Cells. *Molecular Therapy* **2009**, 17, (1), 95-103.
116. Wender, P. A.; Mitchell, D. J.; Pattabiraman, K.; Pelkey, E. T.; Steinman, L.; Rothbard, J. B., The design, synthesis, and evaluation of molecules that enable or enhance cellular uptake: Peptoid molecular transporters. *Proceedings of the National Academy of Sciences of the United States of America* **2000**, 97, (24), 13003-13008.
117. Bode, S. A.; Thevenin, M.; Bechara, C.; Sagan, S.; Bregant, S.; Lavielle, S.; Chassaing, G.; Burlina, F., Self-assembling mini cell-penetrating peptides enter by both direct translocation and glycosaminoglycan-dependent endocytosis. *Chemical Communications* **2012**, 48, (57), 7179-7181.
118. Ziegler, A., Thermodynamic studies and binding mechanisms of cell-penetrating peptides with lipids and glycosaminoglycans. *Advanced Drug Delivery Reviews* **2008**, 60, (4-5), 580-597.
119. Ross, M. F.; Filipovska, A.; Smith, R. A. J.; Gait, M. J.; Murphy, M. P., Cell-penetrating peptides do not cross mitochondrial membranes even when conjugated to a lipophilic cation: evidence against direct passage through phospholipid bilayers. *Biochemical Journal* **2004**, 383, 457-468.
120. Merhi, M.; Dombu, C. Y.; Brient, A.; Chang, J.; Platel, A.; Le Curieux, F.; Marzin, D.; Nessler, F.; Betbeder, D., Study of serum interaction with a cationic nanoparticle: Implications for in vitro endocytosis, cytotoxicity and genotoxicity. *International journal of pharmaceutics* **2012**, 423, (1), 37-44.
121. Fazlollahi, F.; Angelow, S.; Yacobi, N. R.; Marchelletta, R.; Yu, A. S. L.; Hamm-Alvarez, S. F.; Borok, Z.; Kim, K.-J.; Crandall, E. D., Polystyrene nanoparticle trafficking across MDCK-II. *Nanomedicine-Nanotechnology Biology and Medicine* **2011**, 7, (5), 588-594.
122. LabatMoleur, F.; Steffan, A. M.; Brisson, C.; Perron, H.; Feugeas, O.; Furstenberger, P.; Oberling, F.; Brambilla, E.; Behr, J. P., An electron microscopy study

- into the mechanism of gene transfer with lipopolyamines. *Gene Therapy* **1996**, 3, (11), 1010-1017.
123. Couzinet, S.; Cejas, E.; Schittny, J.; Deplazes, P.; Weber, R.; Zimmerli, S., Phagocytic uptake of Encephalitozoon cuniculi by nonprofessional phagocytes. *Infection and Immunity* **2000**, 68, (12), 6939-6945.
124. Ng, C. T.; Li, J. J.; Perumalsamy, R.; Watt, F.; Yung, L. Y. L.; Bay, B. H., Localizing cellular uptake of nanomaterials in vitro by transmission electron microscopy. *Microscopy: Science, Technology, Applications and Education* **2010**, 1, 316-320.
125. Li, J. J.; Zou, L.; Hartono, D.; Ong, C. N.; Bay, B. H.; Yung, L. Y. L., Gold nanoparticles induce oxidative damage in lung fibroblasts in vitro. *Advanced Materials* **2008**, 20, (1), 138.
126. Belade, E.; Armand, L.; Martinon, L.; Kheuang, L.; Fleury-Feith, J.; Baeza-Squiban, A.; Lanone, S.; Billon-Galland, M. A.; Pairon, J. C.; Boczkowski, J., A comparative transmission electron microscopy study of titanium dioxide and carbon black nanoparticles uptake in human lung epithelial and fibroblast cell lines. *Toxicology in Vitro* **2012**, 26, (1), 57-66.
127. Radu, M.; Munteanu, M. C.; Petrache, S.; Serban, A. K.; Dinu, D.; Hermenean, A.; Sima, C.; Dinischiotu, A., Depletion of intracellular glutathione and increased lipid peroxidation mediate cytotoxicity of hematite nanoparticles in MRC-5 cells. *Acta Biochimica Polonica* **2010**, 57, (3), 355-360.
128. Munteanu, M. C.; Radu, M.; Hermenean, A.; Sima, C.; Dinu, D.; Costache, M.; Grigoriu, C.; Dinischiotu, A., Antioxidative response induced by SiO₂ nanoparticles in MRC5 cell line. *Romanian Biotechnological Letters* **2010**, 15, (1), 5000-5007.
129. Rinne, J.; Albarran, B.; Jylhava, J.; Ihalainen, T. O.; Kankaanpaa, P.; Hytonen, V. P.; Stayton, P. S.; Kulomaa, M. S.; Vihinen-Ranta, M., Internalization of novel non-viral vector TAT-streptavidin into human cells. *Bmc Biotechnology* **2007**, 7.
130. North, A. J., Seeing is believing? A beginners' guide to practical pitfalls in image acquisition. *Journal of Cell Biology* **2006**, 172, (1), 9-18.
131. Ball, G.; Parton, R. M.; Hamilton, R. S.; Davis, I., A CELL BIOLOGIST'S GUIDE TO HIGH RESOLUTION IMAGING. *Imaging and Spectroscopic Analysis of Living Cells: Optical and Spectroscopic Techniques* **2012**, 504, 29-55.
132. Henriques, R.; Griffiths, C.; Rego, E. H.; Mhlanga, M. M., PALM and STORM: Unlocking Live-Cell Super-Resolution. *Biopolymers* **2011**, 95, (5), 322-331.
133. Spring, K. R.; Davidson, M. W. Introduction to Fluorescence Microscopy. www.microscopyu.com/articles/fluorescence/fluorescenceintro.html. (26th July),
134. Waters, J. C., Live-Cell Fluorescence Imaging. In *Methods in Cell Biology: Digital Microscopy*, 3rd ed.; Wolf, D. E.; Sluder, G., Eds. Academic Press: 2007; Vol. 81.
135. Waters, J. C., Accuracy and precision in quantitative fluorescence microscopy. *Journal of Cell Biology* **2009**, 185, (7), 1135-1148.
136. Schermelleh, L.; Heintzmann, R.; Leonhardt, H., A guide to super-resolution fluorescence microscopy. *Journal of Cell Biology* **2010**, 190, (2), 165-175.
137. Greb, C. Deconvolution - Image Processing for Widefield Microscopy. www.leica-microsystems.com/science-lab/deconvolution/. (26th July),
138. Eaton, P.; West, P., *Atomic Force Microscopy*. Oxford University Press: 2010.
139. Binnig, G.; Rohrer, H., SCANNING TUNNELING MICROSCOPY. *Helvetica Physica Acta* **1983**, 56, (1-3), 481-482.
140. Binnig, G.; Rohrer, H., SCANNING TUNNELING MICROSCOPY. *Surface Science* **1985**, 152, (APR), 17-26.

141. Binnig, G.; Rohrer, H., SCANNING TUNNELING MICROSCOPY. *Ibm Journal of Research and Development* **1986**, 30, (4), 355-369.
142. Rheinlaender, J.; Schaffer, T. E., Scanning Ion Conductance Microscopy. In *Scanning Probe Microscopy of Functional Materials*, 1 ed.; Kalinin, S. V.; Gruverman, A., Eds. Springer: 2011.
143. Binnig, G.; Quate, C. F.; Gerber, C., ATOMIC FORCE MICROSCOPE. *Physical Review Letters* **1986**, 56, (9), 930-933.
144. Hansma, P. K.; Drake, B.; Marti, O.; Gould, S. A. C.; Prater, C. B., THE SCANNING ION-CONDUCTANCE MICROSCOPE. *Science* **1989**, 243, (4891), 641-643.
145. Korchev, Y. E.; Bashford, C. L.; Milovanovic, M.; Vodyanoy, I.; Lab, M. J., Scanning ion conductance microscopy of living cells. *Biophysical Journal* **1997**, 73, (2), 653-658.
146. Dufrene, Y. F.; Lee, G. U., Advances in the characterization of supported lipid films with the atomic force microscope. *Biochimica Et Biophysica Acta-Biomembranes* **2000**, 1509, (1-2), 14-41.
147. Rezende, C. A.; Lee, L. T.; Galembeck, F., Surface Mechanical Properties of Thin Polymer Films Investigated by AFM in Pulsed Force Mode. *Langmuir* **2009**, 25, (17), 9938-9946.
148. Hansma, H. G., Surface biology of DNA by atomic force microscopy. *Annual Review of Physical Chemistry* **2001**, 52, 71-92.
149. Willemsen, O. H.; Snel, M. M. E.; Cambi, A.; Greve, J.; De Grooth, B. G.; Figdor, C. G., Biomolecular interactions measured by atomic force microscopy. *Biophysical Journal* **2000**, 79, (6), 3267-3281.
150. Morris, V.; Kirby, A.; Gunning, A., *Atomic Force Microscopy for Biologists*. 2nd ed.; Imperial College Press: 2010.
151. de Pablo, P. J., Introduction to Atomic Force Microscopy. *Single Molecule Analysis: Methods and Protocols* **2011**, 783.
152. Basak, S.; Raman, A., Dynamics of tapping mode atomic force microscopy in liquids: Theory and experiments. *Applied Physics Letters* **2007**, 91, (6).
153. Baro, A. M.; Reifengerger, R. G., *Atomic Force Microscopy in Liquid: Biological Applications*. Wiley-VCH: 2012.
154. Braga, P. C.; Ricci, D., Atomic Force Microscopy in Biomedical Research: Methods and Protocols. *Atomic Force Microscopy in Biomedical Research: Methods and Protocols* **2011**, 736.
155. Geisse, N. A., AFM and combined optical techniques. *Materials Today* **2009**, 12, (7-8), 40-45.
156. Egawa, H.; Furusawa, K., Liposome adhesion on mica surface studied by atomic force microscopy. *Langmuir* **1999**, 15, (5), 1660-1666.
157. Brasseur, R.; Deleu, M.; Mingeot-Leclercq, M. P.; Francius, G.; Dufrene, Y. F., Probing peptide-membrane interactions using AFM. *Surface and Interface Analysis* **2008**, 40, (3-4), 151-156.
158. Chim, Y. T. A.; Lam, J. K. W.; Ma, Y.; Armes, S. P.; Lewis, A. L.; Roberts, C. J.; Stolnik, S.; Tandler, S. J. B.; Davies, M. C., Structural study of DNA condensation induced by novel phosphorylcholine-based copolymers for gene delivery and relevance to DNA protection. *Langmuir* **2005**, 21, (8), 3591-3598.
159. Leonenko, Z. V.; Finot, E.; Ma, H.; Dahms, T. E. S.; Cramb, D. T., Investigation of temperature-induced phase transitions in DOPC and DPPC phospholipid bilayers using temperature-controlled scanning force microscopy. *Biophysical Journal* **2004**, 86, (6), 3783-3793.

160. Schaus, S. S.; Henderson, E. R., Cell viability and probe-cell membrane interactions of XR1 glial cells imaged by atomic force microscopy. *Biophysical Journal* **1997**, *73*, (3), 1205-1214.
161. Rheinlaender, J.; Geisse, N. A.; Proksch, R.; Schaeffer, T. E., Comparison of Scanning Ion Conductance Microscopy with Atomic Force Microscopy for Cell Imaging. *Langmuir* **2011**, *27*, (2), 697-704.
162. Henderson, E.; Haydon, P. G.; Sakaguchi, D. S., ACTIN FILAMENT DYNAMICS IN LIVING GLIAL-CELLS IMAGED BY ATOMIC FORCE MICROSCOPY. *Science* **1992**, *257*, (5078), 1944-1946.
163. Shevchuk, A. I.; Novak, P.; Taylor, M.; Diakonov, I. A.; Ziyadeh-Isleem, A.; Bitoun, M.; Guicheney, P.; Lab, M. J.; Gorelik, J.; Merrifield, C. J.; Klenerman, D.; Korchev, Y. E., An alternative mechanism of clathrin-coated pit closure revealed by ion conductance microscopy. *Journal of Cell Biology* **2012**, *197*, (4), 499-508.
164. Novak, P.; Li, C.; Shevchuk, A. I.; Stepanyan, R.; Caldwell, M.; Hughes, S.; Smart, T. G.; Gorelik, J.; Ostanin, V. P.; Lab, M. J.; Moss, G. W. J.; Frolenkov, G. I.; Klenerman, D.; Korchev, Y. E., Nanoscale live-cell imaging using hopping probe ion conductance microscopy. *Nature Methods* **2009**, *6*, (4), 279-281.
165. Zhang, Y. J.; Gorelik, J.; Sanchez, D.; Shevchuk, A.; Lab, M.; Vodyanoy, I.; Klenerman, D.; Edwards, C.; Korchev, Y., Scanning ion conductance microscopy reveals how a functional renal epithelial monolayer maintains its integrity. *Kidney International* **2005**, *68*, (3), 1071-1077.
166. Duclohier, H., Neuronal sodium channels in ventricular heart cells are localized near T-tubules openings. *Biochemical and Biophysical Research Communications* **2005**, *334*, (4), 1135-1140.
167. Gorelik, J.; Zhang, Y. J.; Shevchuk, A. I.; Frolenkov, G. I.; Sanchez, D.; Lab, M. J.; Vodyanoy, I.; Edwards, C. R. W.; Klenerman, D.; Korchev, Y. E., The use of scanning ion conductance microscopy to image A6 cells. *Molecular and Cellular Endocrinology* **2004**, *217*, (1-2), 101-108.
168. Shevchuk, A. I.; Hobson, P.; Lab, M. J.; Klenerman, D.; Krauzewicz, N.; Korchev, Y. E., Imaging single virus particles on the surface of cell membranes by high-resolution scanning surface confocal microscopy. *Biophysical Journal* **2008**, *94*, (10), 4089-4094.
169. Gorelik, J.; Yang, L.; Zhang, Y.; Lab, M.; Korchev, Y. E.; del Monte, F.; Harding, S. E., A novel Z-groove index characterizing myocardial surface structure and its modification in failing human heart. *Journal of Molecular and Cellular Cardiology* **2007**, *42*, S153-S153.
170. Boecker, M.; Muschter, S.; Schmitt, E. K.; Steinem, C.; Schaeffer, T. E., Imaging and Patterning of Pore-Suspending Membranes with Scanning Ion Conductance Microscopy. *Langmuir* **2009**, *25*, (5), 3022-3028.
171. Bruckbauer, A.; Zhou, D. J.; Ying, L. M.; Korchev, Y. E.; Abell, C.; Klenerman, D., Multicomponent submicron features of biomolecules created by voltage controlled deposition from a nanopipet. *Journal of the American Chemical Society* **2003**, *125*, (32), 9834-9839.
172. Bruckbauer, A.; James, P.; Zhou, D. J.; Yoon, J. W.; Excell, D.; Korchev, Y.; Jones, R.; Klenerman, D., Nanopipette delivery of individual molecules to cellular compartments for single-molecule fluorescence tracking. *Biophysical Journal* **2007**, *93*, 3120-3131.
173. Nikolaev, V. O.; Moshkov, A.; Lyon, A. R.; Miragoli, M.; Novak, P.; Paur, H.; Lohse, M. J.; Korchev, Y. E.; Harding, S. E.; Gorelik, J., beta(2)-Adrenergic Receptor

- Redistribution in Heart Failure Changes cAMP Compartmentation. *Science* **2010**, 327, (5973), 1653-1657.
174. Takahashi, Y.; Shevchuk, A. I.; Novak, P.; Murakami, Y.; Shiku, H.; Korchev, Y. E.; Matsue, T., Simultaneous Noncontact Topography and Electrochemical Imaging by SECM/SICM Featuring Ion Current Feedback Regulation. *Journal of the American Chemical Society* **2010**, 132, (29), 10118-10126.
175. Proksch, R.; Lal, R.; Hansma, P. K.; Morse, D.; Stucky, G., Imaging the internal and external pore structure of membranes in fluid: TappingMode scanning ion conductance microscopy. *Biophysical Journal* **1996**, 71, (4), 2155-2157.
176. Korchev, Y. E.; Negulyaev, Y. A.; Edwards, C. R. W.; Vodyanoy, I.; Lab, M. J., Functional localization of single active ion channels on the surface of a living cell. *Nature Cell Biology* **2000**, 2, (9), 616-619.
177. Gorelik, J.; Shevchuk, A.; Ramalho, M.; Elliott, M.; Lei, C.; Higgins, C. F.; Lab, M. J.; Klenerman, D.; Krauzewicz, N.; Korchev, Y., Scanning surface confocal microscopy for simultaneous topographical and fluorescence imaging: Application to single virus-like particle entry into a cell. *Proceedings of the National Academy of Sciences of the United States of America* **2002**, 99, (25), 16018-16023.
178. Shevchuk, A. I.; Hobson, P.; Lab, M. J.; Klenerman, D.; Krauzewicz, N.; Korchev, Y. E., Endocytic pathways: combined scanning ion conductance and surface confocal microscopy study. *Pflugers Archiv-European Journal of Physiology* **2008**, 456, (1), 227-235.
179. MalvernInstruments Dynamic Light Scattering - An Introduction in 30 minutes. [http://www.malvern.com/malvern/kbase.nsf/allbyno/KB000792/\\$file/MRK656-01 An Introduction to DLS.pdf](http://www.malvern.com/malvern/kbase.nsf/allbyno/KB000792/$file/MRK656-01%20An%20Introduction%20to%20DLS.pdf) (24th May 2012),
180. MalvernInstruments Zeta Potential - An introduction in 30 minutes. [http://www.malvern.com/malvern/kbase.nsf/allbyno/KB000734/\\$file/MRK654-01%20An%20Introduction%20to%20Zeta%20Potential%20v3.pdf](http://www.malvern.com/malvern/kbase.nsf/allbyno/KB000734/$file/MRK654-01%20An%20Introduction%20to%20Zeta%20Potential%20v3.pdf) (24th May 2012),
181. MalvernInstruments Simplifying the measurement of zeta potential using M3-PALS. [http://www.malvern.com/malvern/kbase.nsf/allbyno/KB000411/\\$file/Simplifying%20zeta%20potential%20with%20M3-PALS%20MRK512-01.pdf](http://www.malvern.com/malvern/kbase.nsf/allbyno/KB000411/$file/Simplifying%20zeta%20potential%20with%20M3-PALS%20MRK512-01.pdf) (24th May 2012),
182. CPSInstruments CPS Disc Centrifuge General Brochure: Nanoparticle size analysis. <http://www.cpsinstruments.eu/pdf/General%20Brochure.pdf> (27th May 2012),
183. Scott, D. J.; Harding, S. E.; Rowe, A. J., *Analytical Ultracentrifugation. Techniques and Methods*. RSC Publishing: 2005.
184. CPSInstruments, Developing New Operating Procedures. In CPS Instruments Technical Note.
185. Panchuk-Voloshina, N.; Haugland, R. P.; Bishop-Stewart, J.; Bhalgat, M. K.; Millard, P. J.; Mao, F.; Leung, W. Y., Alexa dyes, a series of new fluorescent dyes that yield exceptionally bright, photostable conjugates. *Journal of Histochemistry & Cytochemistry* **1999**, 47, (9), 1179-1188.
186. Coupland, P. G.; Fisher, K. A.; Jones, D. R. E.; Aylott, J. W., Internalisation of polymeric nanosensors in mesenchymal stem cells: Analysis by flow cytometry and confocal microscopy. *Journal of Controlled Release* **2008**, 130, (2), 115-120.
187. Sun, H. H.; Andresen, T. L.; Benjaminsen, R. V.; Almdal, K., Polymeric Nanosensors for Measuring the Full Dynamic pH Range of Endosomes and Lysosomes in Mammalian Cells. *Journal of Biomedical Nanotechnology* **2009**, 5, (6), 676-682.

188. Hermanson, G. T., Heterobifunctional Crosslinkers. In *Bioconjugate techniques*, Second ed.; Hermanson, G. T., Ed. Academic Press: 2008; pp 276-335.
189. ThermoScientific Sulfo SMCC : A water soluble amine to sulfhydryl crosslinker with a medium length cyclohexane spacer.
<http://www.piercenet.com/browse.cfm?fldID=02030378> (26th July 2012),
190. Stober, W.; Fink, A.; Bohn, E., CONTROLLED GROWTH OF MONODISPERSE SILICA SPHERES IN MICRON SIZE RANGE. *Journal of Colloid and Interface Science* **1968**, 26, (1), 62-&
191. Zhang, Y. Y.; Hu, L.; Yu, D. H.; Gao, C. Y., Influence of silica particle internalization on adhesion and migration of human dermal fibroblasts. *Biomaterials* **2010**, 31, (32), 8465-8474.
192. Afonin, S.; Frey, A.; Bayerl, S.; Fischer, D.; Wadhvani, P.; Weinkauff, S.; Ulrich, A. S., The cell-penetrating peptide TAT(48-60) induces a non-lamellar phase in DMPC membranes. *Chemphyschem* **2006**, 7, (10), 2134-2142.
193. Macdonald, R. C.; Macdonald, R. I.; Menco, B. P. M.; Takeshita, K.; Subbarao, N. K.; Hu, L. R., SMALL-VOLUME EXTRUSION APPARATUS FOR PREPARATION OF LARGE, UNILAMELLAR VESICLES. *Biochimica Et Biophysica Acta* **1991**, 1061, (2), 297-303.
194. Clark, H. A.; Hoyer, M.; Philbert, M. A.; Kopelman, R., Optical nanosensors for chemical analysis inside single living cells. 1. Fabrication, characterization, and methods for intracellular delivery of PEBBLE sensors. *Analytical Chemistry* **1999**, 71, (21), 4831-4836.
195. Clark, H. A.; Kopelman, R.; Tjalkens, R.; Philbert, M. A., Optical nanosensors for chemical analysis inside single living cells. 2. Sensors for pH and calcium and the intracellular application of PEBBLE sensors. *Analytical Chemistry* **1999**, 71, (21), 4837-4843.
196. Song, A.; Parus, S.; Kopelman, R., High-performance fiber optic pH microsensors for practical physiological measurements using a dual-emission sensitive dye. *Analytical Chemistry* **1997**, 69, (5), 863-867.
197. Buck, S. M.; Xu, H.; Brasuel, M.; Philbert, M. A.; Kopelman, R., Nanoscale probes encapsulated by biologically localized embedding (PEBBLEs) for ion sensing and imaging in live cells. *Talanta* **2004**, 63, (1), 41-59.
198. Buck, S. M.; Koo, Y. E. L.; Park, E.; Xu, H.; Philbert, M. A.; Brasuel, M. A.; Kopelman, R., Optochemical nanosensor PEBBLEs: photonic explorers for bioanalysis with biologically localized embedding. *Current Opinion in Chemical Biology* **2004**, 8, (5), 540-546.
199. Giuntini, F.; Dumoulin, F.; Daly, R.; Ahsen, V.; Scanlan, E. M.; Lavado, A. S. P.; Aylott, J. W.; Rosser, G. A.; Beeby, A.; Boyle, R. W., Orthogonally bifunctionalised polyacrylamide nanoparticles: a support for the assembly of multifunctional nanodevices. *Nanoscale* **2012**, 4, (6), 2034-2045.
200. Nielsen, L. J.; Olsen, L. F.; Ozalp, V. C., Aptamers Embedded in Polyacrylamide Nanoparticles: A Tool for in Vivo Metabolite Sensing. *Acs Nano* **2010**, 4, (8), 4361-4370.
201. Green, D. L.; Lin, J. S.; Lam, Y. F.; Hu, M. Z. C.; Schaefer, D. W.; Harris, M. T., Size, volume fraction, and nucleation of Stober silica nanoparticles. *Journal of Colloid and Interface Science* **2003**, 266, (2), 346-358.
202. Wang, X.-D.; Shen, Z.-X.; Sang, T.; Cheng, X.-B.; Li, M.-F.; Chen, L.-Y.; Wang, Z.-S., Preparation of spherical silica particles by Stober process with high concentration of tetra-ethyl-orthosilicate. *Journal of Colloid and Interface Science* **2010**, 341, (1).

203. Trewyn, B. G.; Nieweg, J. A.; Zhao, Y.; Lin, V. S. Y., Biocompatible mesoporous silica nanoparticles with different morphologies for animal cell membrane, penetration. *Chemical Engineering Journal* **2008**, *137*, (1), 23-29.
204. Folling, J.; Polyakova, S.; Belov, V.; van Blaaderen, A.; Bossi, M. L.; Hell, S. W., Synthesis and characterization of photoswitchable fluorescent silica nanoparticles. *Small* **2008**, *4*, (1), 134-142.
205. Zhao, X. J.; Bagwe, R. P.; Tan, W. H., Development of organic-dye-doped silica nanoparticles in a reverse microemulsion. *Advanced Materials* **2004**, *16*, (2), 173-+.
206. Wencel, D.; Barczak, M.; Borowski, P.; McDonagh, C., The development and characterisation of novel hybrid sol-gel-derived films for optical pH sensing. *Journal of Materials Chemistry* **2012**, *22*, (23), 11720-11729.
207. Nozawa, K.; Gailhanou, H.; Raison, L.; Panizza, P.; Ushiki, H.; Sellier, E.; Delville, J. P.; Delville, M. H., Smart control of monodisperse silica particles: Effect of reactant addition rate on growth process. *Langmuir* **2005**, *21*, (4), 1516-1523.
208. Vanblaaderen, A.; Vangeest, J.; Vrij, A., MONODISPERSE COLLOIDAL SILICA SPHERES FROM TETRAALKOXYSILANES - PARTICLE FORMATION AND GROWTH-MECHANISM. *Journal of Colloid and Interface Science* **1992**, *154*, (2).
209. Vanblaaderen, A.; Vrij, A., SYNTHESIS AND CHARACTERIZATION OF MONODISPERSE COLLOIDAL ORGANO-SILICA SPHERES. *Journal of Colloid and Interface Science* **1993**, *156*, (1), 1-18.
210. Matsoukas, T.; Gulari, E., DYNAMICS OF GROWTH OF SILICA PARTICLES FROM AMMONIA-CATALYZED HYDROLYSIS OF TETRA-ETHYL-ORTHOSILICATE. *Journal of Colloid and Interface Science* **1988**, *124*, (1).
211. Matsoukas, T.; Gulari, E., MONOMER-ADDITION GROWTH WITH A SLOW INITIATION STEP - A GROWTH-MODEL FOR SILICA PARTICLES FROM ALKOXIDES. *Journal of Colloid and Interface Science* **1989**, *132*, (1).
212. Bogush, G. H.; Zukoski, C. F., STUDIES OF THE KINETICS OF THE PRECIPITATION OF UNIFORM SILICA PARTICLES THROUGH THE HYDROLYSIS AND CONDENSATION OF SILICON ALKOXIDES. *Journal of Colloid and Interface Science* **1991**, *142*, (1).
213. Bogush, G. H.; Zukoski, C. F., UNIFORM SILICA PARTICLE-PRECIPITATION - AN AGGREGATIVE GROWTH-MODEL. *Journal of Colloid and Interface Science* **1991**, *142*, (1).
214. Chung, T. H.; Wu, S. H.; Yao, M.; Lu, C. W.; Lin, Y. S.; Hung, Y.; Mou, C. Y.; Chen, Y. C.; Huang, D. M., The effect of surface charge on the uptake and biological function of mesoporous silica nanoparticles 3T3-L1 cells and human mesenchymal stem cells. *Biomaterials* **2007**, *28*, (19), 2959-2966.
215. Beaudet, L.; Pitre, R.; Robillard, L.; Mercier, L., Structural Perturbations in Mesoporous Silica Microspheres Prepared Using Cationic Organosilanes. *Chemistry of Materials* **2009**, *21*, (22), 5349-5357.
216. Kneuer, C.; Sameti, M.; Bakowsky, U.; Schiestel, T.; Schirra, H.; Schmidt, H.; Lehr, C. M., A nonviral DNA delivery system based on surface modified silica-nanoparticles can efficiently transfect cells in vitro. *Bioconjugate Chemistry* **2000**, *11*, (6), 926-932.
217. Mao, Z.; Wan, L.; Hu, L.; Ma, L.; Gao, C., Tat peptide mediated cellular uptake of SiO₂ submicron particles. *Colloids and Surfaces B-Biointerfaces* **2010**, *75*, (2), 432-440.
218. Lira, L. M.; Martins, K. A.; de Torresi, S. I. C., Structural parameters of polyacrylamide hydrogels obtained by the Equilibrium Swelling Theory. *European Polymer Journal* **2009**, *45*, (4), 1232-1238.
219. Lee, Y. E. K.; Smith, R.; Kopelman, R., Nanoparticle PEBBLE Sensors in Live Cells and In Vivo. *Annual Review of Analytical Chemistry* **2009**, *2*, 57-76.

220. Muller, D. J., AFM: a nanotool in membrane biology. *Biochemistry* **2008**, *47*, (31), 7986-7998.
221. Goodman, S. R., *Medical Cell Biology*. 3rd ed.; Lippincott Williams and Wilkins.
222. Somerharju, P.; Virtanen, J. A.; Cheng, K. H., Lateral organisation of membrane lipids - The superlattice view. *Biochimica Et Biophysica Acta-Molecular and Cell Biology of Lipids* **1999**, *1440*, (1), 32-48.
223. Garcia-Manyes, S.; Oncins, G.; Sanz, F., Effect of pH and ionic strength on phospholipid nanomechanics and on deposition process onto hydrophilic surfaces measured by AFM. *Electrochimica Acta* **2006**, *51*, (24), 5029-5036.
224. Nagle, J. F.; Tristram-Nagle, S., Lipid bilayer structure. *Current Opinion in Structural Biology* **2000**, *10*, (4), 474-480.
225. Nagle, J. F.; Tristram-Nagle, S., Structure of lipid bilayers. *Biochimica Et Biophysica Acta-Reviews on Biomembranes* **2000**, *1469*, (3), 159-195.
226. Tokumasu, F.; Jin, A. J.; Feigenson, G. W.; Dvorak, J. A., Atomic force microscopy of nanometric liposome adsorption and nanoscopic membrane domain formation. *Ultramicroscopy* **2003**, *97*, (1-4), 217-227.
227. Milhiet, P. E.; Giocondi, M. C.; Baghdadi, O.; Ronzon, F.; Le Grimellec, C.; Roux, B., AFM detection of GPI protein insertion into DOPC/DPPC model membranes. *Single Molecules* **2002**, *3*, (2-3), 135-140.
228. Shaw, J. E.; Slade, A.; Yip, C. M., Simultaneous in situ total internal reflectance fluorescence/atomic force microscopy studies of DPPC/dPOPC microdomains in supported planar lipid bilayers. *Journal of the American Chemical Society* **2003**, *125*, (39), 11838-11839.
229. Reviakine, I.; Brisson, A., Formation of supported phospholipid bilayers from unilamellar vesicles investigated by atomic force microscopy. *Langmuir* **2000**, *16*, (4), 1806-1815.
230. Lincopan, N.; Espindola, N. M.; Vaz, A. J.; Carmona-Ribeiro, A. M., Cationic supported lipid bilayers for antigen presentation. *International Journal of Pharmaceutics* **2007**, *340*, (1-2), 216-222.
231. Leroueil, P. R.; Hong, S. Y.; Mecke, A.; Baker, J. R.; Orr, B. G.; Holl, M. M. B., Nanoparticle interaction with biological membranes: Does nanotechnology present a janus face? *Accounts of Chemical Research* **2007**, *40*, (5), 335-342.
232. Himmelhaus, M.; Takei, H., Self-assembly of polystyrene nano particles into patterns of random-close-packed monolayers via chemically induced adsorption. *Physical Chemistry Chemical Physics* **2002**, *4*, (3), 496-506.
233. Peetla, C.; Labhasetwar, V., Effect of Molecular Structure of Cationic Surfactants on Biophysical Interactions of Surfactant-Modified Nanoparticles with a Model Membrane and Cellular Uptake. *Langmuir* **2009**, *25*, (4), 2369-2377.
234. Hong, S. P.; Leroueil, P. R.; Janus, E. K.; Peters, J. L.; Kober, M. M.; Islam, M. T.; Orr, B. G.; Baker, J. R.; Holl, M. M. B., Interaction of polycationic polymers with supported lipid bilayers and cells: Nanoscale hole formation and enhanced membrane permeability. *Bioconjugate Chemistry* **2006**, *17*, (3), 728-734.
235. Wang, B.; Zhang, L. F.; Bae, S. C.; Granick, S., Nanoparticle-induced surface reconstruction of phospholipid membranes. *Proceedings of the National Academy of Sciences of the United States of America* **2008**, *105*, (47), 18171-18175.
236. Parimi, S.; Barnes, T. J.; Prestidge, C. A., PAMAM Dendrimer Interactions with Supported Lipid Bilayers: A Kinetic and Mechanistic Investigation. *Langmuir* **2008**, *24*, (23), 13532-13539.

237. Zhang, Z. Y.; Smith, B. D., High-generation polycationic dendrimers are unusually effective at disrupting anionic vesicles: Membrane bending model. *Bioconjugate Chemistry* **2000**, 11, (6), 805-814.
238. Jena, B. P.; Heinrich Horber, J. K., *Atomic Force Microscopy in Cell Biology*. Academic Press: 2002.
239. Dennison, S. R.; Baker, R. D.; Nicholl, I. D.; Phoenix, D. A., Interactions of cell penetrating peptide Tat with model membranes: A biophysical study. *Biochemical and Biophysical Research Communications* **2007**, 363, 178-182.
240. Takechi, Y.; Tanaka, H.; Kitayama, H.; Yoshii, H.; Tanaka, M.; Saito, H., Comparative study on the interaction of cell-penetrating polycationic polymers with lipid membranes. *Chemistry and Physics of Lipids* **2012**, 165, (1), 51-58.
241. Lindgren, M.; Hallbrink, M.; Prochiantz, A.; Langel, U., Cell-penetrating peptides. *Trends in Pharmacological Sciences* **2000**, 21, (3), 99-103.
242. Brooks, H.; Lebleu, B.; Vives, E., Tat peptide-mediated cellular delivery: back to basics. *Advanced Drug Delivery Reviews* **2005**, 57, (4), 559-577.
243. Shaw, J. E.; Epand, R. F.; Hsu, J. C. Y.; Mo, G. C. H.; Epand, R. M.; Yip, C. M., Cationic peptide-induced remodeling of model membranes: Direct visualization by in situ atomic force microscopy. *Journal of Structural Biology* **2008**, 162, (1), 121-138.
244. Nori, A.; Jensen, K. D.; Tijerina, M.; Kopeckova, P.; Kopecek, J., Subcellular trafficking of HPMA copolymer-Tat conjugates in human ovarian carcinoma cells. *Journal of Controlled Release* **2003**, 91, (1-2), 53-59.
245. Sethuraman, V. A.; Bae, Y. H., TAT peptide-based micelle system for potential active targeting of anti-cancer agents to acidic solid tumors. *Journal of Controlled Release* **2007**, 118, (2), 216-224.
246. Hyndman, L.; Lemoine, J. L.; Huang, L.; Porteous, D. J.; Boyd, A. C.; Nan, X. S., HIV-1 Tat protein transduction domain peptide facilitates gene transfer in combination with cationic liposomes. *Journal of Controlled Release* **2004**, 99, (3), 435-444.
247. Ushiki, T.; Nakajima, M.; Choi, M.; Cho, S.-J.; Iwata, F., Scanning ion conductance microscopy for imaging biological samples in liquid: A comparative study with atomic force microscopy and scanning electron microscopy. *Micron (Oxford, England : 1993)* **2012**, 43, (12).
248. Sek, S.; Pawlowski, J., Supported Lipid Bilayers: AFM Imaging of Lipid Vesicles Fusion and Spreading. *Imaging and Microscopy 2012*, p 3.
249. Veerananarayanan, S.; Poulouse, A. C.; Mohamed, S.; Aravind, A.; Nagaoka, Y.; Yoshida, Y.; Maekawa, T.; Kumar, D. S., FITC Labeled Silica Nanoparticles as Efficient Cell Tags: Uptake and Photostability Study in Endothelial Cells. *Journal of Fluorescence* **2012**, 22, (2), 537-548.
250. Koschinsky, T.; Heinemann, L., Sensors for glucose monitoring: technical and clinical aspects. *Diabetes-Metabolism Research and Reviews* **2001**, 17, (2), 113-123.
251. Koschwanez, H. E.; Reichert, W. M., In vitro, in vivo and post explantation testing of glucose-detecting biosensors: Current methods and recommendations. *Biomaterials* **2007**, 28, (25), 3687-3703.
252. Clark, H. A.; Hoyer, M.; Parus, S.; Philbert, M. A.; Kopelman, M., Optochemical nanosensors and subcellular applications in living cells. *Mikrochimica Acta* **1999**, 131, (1-2), 121-128.
253. Webster, A.; Coupland, P.; Houghton, F. D.; Leese, H. J.; Aylott, J. W. In *The delivery of PEBBLE nanosensors to measure the intracellular environment*, Conference

- on Bionanotechnology - From Self-Assembly to Cell Biology, Cambridge, ENGLAND, Jan 03-05, 2007; Cambridge, ENGLAND, 2007; pp 538-543.
254. Sinha, R.; Kim, G. J.; Nie, S. M.; Shin, D. M., Nanotechnology in cancer therapeutics: bioconjugated nanoparticles for drug delivery. *Molecular Cancer Therapeutics* **2006**, 5, (8), 1909-1917.
255. Botella, P.; Abasolo, I.; Fernandez, Y.; Muniesa, C.; Miranda, S.; Quesada, M.; Ruiz, J.; Schwartz, S., Jr.; Corma, A., Surface-modified silica nanoparticles for tumor-targeted delivery of camptothecin and its biological evaluation. *Journal of Controlled Release* **2011**, 156, (2), 246-257.
256. Slowing, I.; Trewyn, B. G.; Lin, V. S. Y., Effect of surface functionalization of MCM-41-type mesoporous silica nanoparticles on the endocytosis by human cancer cells. *Journal of the American Chemical Society* **2006**, 128, (46), 14792-14793.
257. Hu, L.; Mao, Z.; Zhang, Y.; Gao, C., Influences of size of silica particles on the cellular endocytosis, exocytosis and cell activity of HepG2 cells. *Journal of Nanoscience Letters* **2011**, 1, (1), 16.
258. Huang, X. L.; Teng, X.; Chen, D.; Tang, F. Q.; He, J. Q., The effect of the shape of mesoporous silica nanoparticles on cellular uptake and cell function. *Biomaterials* **2010**, 31, (3), 438-448.
259. Lin, Y. S.; Tsai, C. P.; Huang, H. Y.; Kuo, C. T.; Hung, Y.; Huang, D. M.; Chen, Y. C.; Mou, C. Y., Well-ordered mesoporous silica nanoparticles as cell markers. *Chemistry of Materials* **2005**, 17, (18), 4570-4573.
260. Blumen, S. R.; Cheng, K.; Ramos-Nino, M. E.; Taatjes, D. J.; Weiss, D. J.; Landry, C. C.; Mossman, B. T., Unique uptake of acid-prepared mesoporous spheres by lung epithelial and mesothelioma cells. *American Journal of Respiratory Cell and Molecular Biology* **2007**, 36, (3), 333-342.
261. Osaki, F.; Kanamori, T.; Sando, S.; Sera, T.; Aoyama, Y., A quantum dot conjugated sugar ball and its cellular uptake on the size effects of endocytosis in the subviral region. *Journal of the American Chemical Society* **2004**, 126, (21), 6520-6521.
262. Zhang, Y. Z.; Wang, J. C.; Bai, X. Y.; Jiang, T. Y.; Zhang, Q.; Wang, S. L., Mesoporous Silica Nanoparticles for Increasing the Oral Bioavailability and Permeation of Poorly Water Soluble Drugs. *Molecular Pharmaceutics* **2012**, 9, (3), 505-513.
263. Panyam, J.; Zhou, W. Z.; Prabha, S.; Sahoo, S. K.; Labhasetwar, V., Rapid endo-lysosomal escape of poly(DL-lactide-co-glycolide) nanoparticles: implications for drug and gene delivery. *Faseb Journal* **2002**, 16, (10).
264. Konan, Y. N.; Chevallier, J.; Gurny, R.; Allemann, E., Encapsulation of p-THPP into nanoparticles: Cellular uptake, subcellular localization and effect of serum on photodynamic activity. *Photochemistry and Photobiology* **2003**, 77, (6), 638-644.
265. Pan, L. M.; He, Q. J.; Liu, J. N.; Chen, Y.; Ma, M.; Zhang, L. L.; Shi, J. L., Nuclear-Targeted Drug Delivery of TAT Peptide-Conjugated Monodisperse Mesoporous Silica Nanoparticles. *Journal of the American Chemical Society* **2012**, 134, (13), 5722-5725.
266. Vranic, S.; Boggetto, N.; Contremoulins, V.; Mornet, S.; Reinhardt, N.; Marano, F.; Baeza-Squiban, A.; Boland, S., Deciphering the mechanisms of cellular uptake of engineered nanoparticles by accurate evaluation of internalization using imaging flow cytometry. *Particle and Fibre Toxicology* **2013**, 10, (2).
267. Gyenge, E. B.; Darphin, X.; Wirth, A.; Piele, U.; Walt, H.; Bredell, M.; Maake, C., Uptake and fate of surface modified silica nanoparticles in head and neck squamous cell carcinoma. *Journal of Nanobiotechnology* **2011**, 9.

268. Pollard, A., Scanning Ion Conductance Microscopy: Variable Temperature Live Cell Morphological Studies. *Imaging and Microscopy* 2012, p 3.
269. Shevchuik, A. I.; Frolenkov, G. I.; Sanchez, D.; James, P. S.; Freedman, N.; Lab, M. J.; Jones, R.; Klenerman, D.; Korchev, Y. E., Imaging proteins in membranes of living cells by high-resolution scanning ion conductance microscopy. *Angewandte Chemie-International Edition* **2006**, 45, (14), 2212-2216.
270. Schwarz, U. D., Noncontact atomic force microscopy. *Beilstein Journal of Nanotechnology* **2012**, 3, 172-173.
271. Perez, R.; Garcia, R.; Schwarz, U., High-resolution noncontact atomic force microscopy. *Nanotechnology* **2009**, 20, (26).
272. Takeyasu, K.; Suzuki, Y.; Yoshida, A., Fast-scanning AFM: Combined AFM - Inverted Optical Microscope for Wet Cell Imaging. *Imaging and Microscopy* 2012, p 3.
273. Minary, M., 'Trolling'-Mode Atomic Force Microscopy: High Resolution Imaging of Single Cells. *Imaging and Analysis* 2012, p 2.
274. Hell, S. W.; Wichmann, J., BREAKING THE DIFFRACTION RESOLUTION LIMIT BY STIMULATED-EMISSION - STIMULATED-EMISSION-DEPLETION FLUORESCENCE MICROSCOPY. *Optics Letters* **1994**, 19, (11), 780-782.
275. Huang, B., Super-resolution optical microscopy: multiple choices. *Current Opinion in Chemical Biology* **2010**, 14, (1), 10-14.
276. Klenerman, D.; Korchev, Y. E.; Davis, S. J., Imaging and characterisation of the surface of live cells. *Current Opinion in Chemical Biology* **2011**, 15, (5), 696-703.
277. Wessels, J. T.; Yamauchi, K.; Hoffman, R. M.; Wouters, F. S., Advances in Cellular, Subcellular, and Nanoscale Imaging In Vitro and In Vivo. *Cytometry Part A* **2010**, 77A, (7), 667-676.
278. Metcalf, D.; Erdelyi, M., Single Molecule Pointillism: Challenges in Localization Based Super-Resolution Microscopy. *Imaging and Microscopy* 2012, p 3.